# A MACHINE LEARNING METHOD FOR THE SUPPORT DESIGN IN UNDERGROUND MINE HAUL ROADS

A THESIS SUBMITTED TO
THE GRADUATE SCHOOL OF NATURAL AND APPLIED SCIENCES
OF
MIDDLE EAST TECHNICAL UNIVERSITY

BY

GÖKHAN KUTLUBAY

IN PARTIAL FULFILLMENT OF THE REQUIREMENTS
FOR
THE DEGREE OF MASTER OF SCIENCE
IN
MINING ENGINEERING

JULY 2023

Approval of the thesis:

**THESIS TITLE**

submitted by **GÖKHAN KUTLUBAY** in partial fulfillment of the requirements for the degree of **Master of Science** i**n Mining Engineering, Middle East Technical University** by,

Prof. Dr. Halil Kalıpçılar
Dean, Graduate School of **Natural and Applied Sciences** _____

Prof. Dr. N. Emre Altun
Head of the Department, **Mining Engineering** _____

Asst. Prof. Dr. Ahmet Güneş Yardımcı
Supervisor, **Mining Engineering, METU** _____

**Examining Committee Members:**

Assoc. Prof. Dr. Mehmet Ali Hindistan
Mining Engineering, Hacettepe University _____

Asst. Prof. Dr. Ahmet Güneş Yardımcı
Mining Engineering, METU _____

Assoc. Prof. Dr. Onur Gölbaşı
Mining Engineering, METU _____

**Date**: 18.07.2023

**I hereby declare that all information in this document has been obtained and presented in accordance with academic rules and ethical conduct. I also declare that, as required by these rules and conduct, I have fully cited and referenced all material and results that are not original to this work.**

Name, Last Name : Gökhan, Kutlubay

Signature :

# ABSTRACT

## A MACHINE LEARNING METHOD FOR THE SUPPORT DESIGN IN UNDERGROUND MINE HAUL ROADS

Kutlubay, Gökhan
Master of Science, Mining Engineering
Supervisor : Asst. Prof. Dr. Ahmet Güneş Yardımcı

July 2023, 190 pages

Permanent openings in underground mines require extensive geomechanical and geological investigation to determine the excavation dimensions and the support configuration assuring the long-term stability.Empirical systems have been adopted in underground excavation design due to their advantages in terms of matching the rock mass quality with the potential support configuration.Geomechanical classification system and Q-tunneling index are the most commonly accepted techniques for the preliminary support analysis. However, they cover only the significant conditions and they require to specify the intermediate conditions by field observations or numerical analyses. Computational geomechanics makes use of computational power to simulate the various excavation and support designs well-before the implementation. This research carries out a parametric study to examine the support requirements for underground mine haul roads excavated in various geomechanical conditions at different depths and field loadings. Performance of the empirically recommended support systems were checked with the finite element models relying on stress and deformation analyses. Finally, an artificial neural network model was trained using the numerical simulation outputs.

Predictions of the model approve a good correlation computational outputs, which implies the proposed method can be considered for certain conditions.

Keywords: Underground Mining, Main Haul Roads, Support Design, Numerical Analysis, Machine Learning

# ÖZ

## YER ALTI MADEN NAKLİYE YOLLARINDA TAHKİMAT TASARIMI İÇİN MAKİNE ÖĞRENMESİ YÖNTEMİ

Kutlubay, Gökhan
Yüksek Lisans, Maden Mühendisliği
Tez Yöneticisi: Dr. Ahmet Güneş Yardımcı

Temmuz 2023, 190 sayfa

Yer altı maden ocaklarında yer alan kalıcı açıklıkların, uzun vadeli duraylılığının sağlanması için kazı boyutlarını ve tahkimat konfigürasyonunu belirlemek amacıyla kapsamlı jeomekanik ve jeolojik araştırmalar gerekmektedir. Potansiyel tahkimat konfigürasyonunu kaya kütlesi kalitesiyle eşleştirmek açısından ampirik sistemler yer altı kazı tasarımında tercih edilmektedir. Jeomekanik sınıflandırma sistemi ve Q-tünel indeksi, ön tahkimat analizi için en yaygın kabul edilen tekniklerdir. Ancak bunlar yalnızca önemli koşulları kapsamakta ve ara koşulların belirlenmesi için saha gözlemleri veya sayısal analizlere ihtiyaç duymaktadırlar. Sayısal jeomekanik ise uygulamadan çok önce çeşitli kazı ve tahkimat tasarımlarını simüle etmek için sayısal yetisinden yararlanmaktadır. Bu araştırma, farklı derinliklerde ve saha koşullarında oluşturulmuş yer altı maden nakliye yolları için tahkimat gereksinimlerini incelemek amacıyla parametrik bir çalışma gerçekleştirmektedir. Ampirik olarak önerilen tahkimat sistemlerinin verimliliği, gerilme ve deformasyon analizlerine dayanan sonlu eleman modelleriyle kontrol edilmiştir. Son olarak, sayısal simülasyon çıktılarını kullanarak bir yapay sinir ağı modeli eğitilmiştir. Modelin tahminleri, hesaplamalı çıktılar ile iyi bir uyum

gösterdiğinden, önerilen yöntemin belirli koşullar için kullanılabileceği öngörülmektedir.

Anahtar Kelimeler: Yer altı Madenciliği, Ana Nakliye Yolları, Tahkimat Tasarımı, Sayısal Çözümleme, Makine Öğrenmesi

To my beloved family

## ACKNOWLEDGMENTS

I'd like to express my sincere gratitude to my esteemed Supervisor, Asst. Prof. Dr. Ahmet Güneş Yardımcı, whose commitment to academic achievement, vast knowledge, and essential guidance have all played a role in the accomplishment of this thesis. His guidance and resolute insights have not only extended my understanding of the subject but have also motivated me to push beyond my capabilities.

I sincerely appreciate his dedication, patience and encouragement throughout the entire process of this thesis. From the inception of this thesis to its completion, he has been a pillar of support, always there to provide critical comments and expert guidance, inspiring me to overcome obstacles and refine my thinking.

I extend my gratitude to my thesis defense committee members, Assoc. Prof. Dr. Mehmet Ali Hindistan and Assoc. Prof. Dr. Onur Gölbaşı, for making my defense a remarkable experience, and for their valuable feedback and recommendations.

I would also like to thank my beloved family: my father Ali Yaser Kutlubay, my mother Birten Kutlubay, and my sister Neslihan Kutlubay. Their unconditional support, constant encouragement, and faith have been the driving forces behind the completion of this study, making each step more fulfilling and valuable.

Last but not least, I am grateful to my amazing friends, Ece Boyacıoğlu Özbaş, Yılgün Gürcan, Murat Taşer, Selin Çatana, and Mehmet Ali İncücük for their ongoing encouragement, moral support, and companionship.

## TABLE OF CONTENTS

ABSTRACT.....v

ÖZ.....vii

ACKNOWLEDGMENTS.....x

TABLE OF CONTENTS.....xi

LIST OF TABLES.....xiv

LIST OF FIGURES.....xvi

LIST OF ABBREVIATIONS.....xxii

LIST OF SYMBOLS.....xxiv

CHAPTERS

1 INTRODUCTION.....1

1.1 General Remarks ..... 1

1.2 Problem Statement ..... 2

1.3 Research Objectives and Methodology..... 3

1.4 Thesis Outline ..... 5

1.5 Contributions to Literature ..... 6

2 LITERATURE SURVEY.....7

2.1 Rock Mass Classification Systems..... 7

2.2 Premises of Rock Mass Classification System.....10

2.2.1 Terzaghi's Rock Load System.....11

2.2.2 Rock Quality Designation Index (RQD).....13

2.2.3 Lauffer Classification- Stand up Time.....14

2.2.4 Rock Structure Rating.....15

2.3 Commonly Used Rock Mass Classification Systems ..... 16

2.3.1 The Geomechanical Classification System: Rock Mass Rating (RMR).....17
2.3.2 Q-Tunneling Index System.....25
2.3.3 Limitations of the RMR and Q Systems.....29
2.3.4 Correlations between RMR and Q systems.....31
2.3.5 Geological Strength Index (GSI).....33
2.4 Estimation of Geomechanical Properties of Rock Mass .....37
2.4.1 Estimation of the Uniaxial Compressive Strength.....38
2.4.2 Estimation of the Tensile Strength.....41
2.4.3 Estimation of Elastic Modulus.....44
2.5 Rock Support Design .....47
2.5.1 Common Support Types used in Underground Mining Openings....47
2.5.2 Shotcrete/Concrete Support Systems.....53
2.5.3 Rock Reinforcement Systems/ Rock Bolts.....55
2.5.4 Steel Sets/Ribs Support System.....60
2.6 Underground Mining Transport, Haulage and Materials Handling Systems.....61
2.7 Numerical Modelling Methods Used in Support Analyses of Underground Openings.....66
2.7.1 Numerical Modelling/Finite Element Method (FEM).....69
2.8 Artificial Neural Networks (ANN) .....71
3 PARAMETRIC ANALYSIS OF STABILITY IN A TYPICAL UNDERGROUND MINE HAUL ROAD.....75
3.1 Determination of the Representative Geomechanical Properties for Different Rock Mass Quality Classes.....75

3.2 Determination of the Representative Support System Properties for Numerical Modeling ..... 79

3.3 Numerical Models: Geometry, Boundary Conditions and Parametric Study .....80

3.4 Interpretations of the Numerical Modelling..... 83

3.5 A Proposed System Based on Machine Learning for Support Decision.. 87

4 RESULTS AND DISCUSSION.....93

5 CONCLUSIONS AND RECOMMENDATIONS.....117

REFERENCES.....121

APPENDICES

A. Vertical Displacements at Roof for K Values 0.5, 1.0, 1.5 and Different Rock Mass Properties at 200, 400, 600 Meters Depths ..... 139

B. Roof Major Principal Strain for K Values 0.5, 1.0, 1.5 and Different Rock Mass Properties at 200, 400, 600 Meters Depths..... 145

C. Roof Minimum Principal Stresses for K Values 0.5, 1.0, 1.5 and Different Rock Mass Properties at 200, 400, 600 Meters Depths ..... 151

D. Horizontal Displacements at Wall for K Values 0.5, 1.0, 1.5 and Different Rock Mass Properties at 200, 400, 600 Meters Depth..... 160

E. Wall Major Principal Strain for K Values 0.5, 1.0, 1.5 and Different Rock Mass Properties at 200, 400, 600 Meters Depths..... 169

F. Wall Maximum Principal Stresses for K Values 0.5, 1.0, 1.5 and Different Rock Mass Properties at 200, 400, 600 Meters Depths ..... 178

G. Results After Computation and Interpretation of The Supported Model in Terms of Vertical and Horizontal Displacements, Maximum and Minimum Stresses..... 187

## LIST OF TABLES

TABLES

Table 2.1 Rock mass classification systems ..... 8
Table 2.2 Rock Load Classification of Terzaghi (1946) ..... 12
Table 2.3 Rock mass quality classes according to RMR (Bieniawski, 1989) ..... 18
Table 2.4 Guidelines for excavation and support of rock tunnels according to RMR (Bieniawski, 1989) ..... 20
Table 2.5 Modifications in the rating system of RMR (modified from Rehman et al. (2018)) ..... 21
Table 2.6 Empirical correlations between the RMR and Q scores ..... 32
Table 2.7 Formulas that describe the relationships between $RMR_{89}$ and GSI (from (Somodi et al., 2021) ..... 37
Table 2.8 Empirical relations to estimate the Uniaxial Compressive Strength (UCS) ..... 39
Table 2.9 Prediction of the rock tensile strength ..... 42
Table 2.10 Empirical relations between the rock mass quality and the elastic modulus of rock mass ..... 46
Table 2.11 Overview of primary support methods utilized in mining excavations (Hoek, 2007; Jovičić et al., 2009; Whittaker, 1986) ..... 48
Table 2.12 Ultimate strength and load deformation characteristics of typical rockbolts (modified from Brown & Hoek, 1980) ..... 58
Table 2.13 Comparison of key parameters for driving tunnels and underground mine openings in terms of configuration (Tatiya, 2013) ..... 65
Table 2.14 Frequently used numerical techniques in Rock Engineering (Barla, 2016) ..... 67
Table 3.1 Rock mass properties used in the numerical models ..... 76
Table 3.2 Rock bolt and liner parameters used in FEM analyses ..... 80
Table 3.3 The range of parameters used in FEM models ..... 81

Table 3.4 Mechanical readings and their locations on the FEM models of a typical underground mine haul road opening ..... 83
Table 4.1 Equivalent rock mass quality scores of the hypothetical cases ..... 102
Table 4.2 Recommended rock support systems for the hypothetic cases..... 105
Table 4.3 Comparison of the yielded span on the roof from the numerical analysis and the ANN model ..... 115
Table 4.4 Comparison of the yielded length on the wall from the numerical analysis and the ANN model ..... 116

## LIST OF FIGURES

FIGURES

Figure 1.1 Process Methodology Flowchart of the Fundamental Elements ..... 5
Figure 2.1. The diagram indicating the loading of a rock tunnel (Terzaghi, 1946) 12
Figure 2.2. RQD Calculation and Measurement Procedure (Deere, 1989) ..... 14
Figure 2.3. For various classes of rock mass, Lauffer's relationship between active span and stand-up (1958), A Very good rock, G Very Poor Rock ..... 15
Figure 2.4. Correlation between RSR index and support requirements for a 7.3 m diameter circular tunnel (Wickham et al., 1972) ..... 16
Figure 2.5. Stand-up time versus unsupported span for various rock mass classes according to RMR (Bieniawski, 1984). ..... 19
Figure 2.6. Comparison of the determined and predicted $RMR_b$ scores for various types of prediction models (Jalalifar et al., 2011). ..... 24
Figure 2.7. Support recommendations table of Q system (NGI, 2015) ..... 27
Figure 2.8. The correlations among rock mass quality, seismic velocity, and modulus of deformation (Barton, 1995) ..... 28
Figure 2.9. Correlation between the RMR and Q scores (Bieniawski, 1989) ..... 32
Figure 2.10. Geological Strength Index (GSI) chart (Hoek & Marinos, 2000) ..... 35
Figure 2.11. Correlation between the elastic modulus of rock mass and RMR score (Bieniawski, 1984) ..... 45
Figure 2.12. Principles of rock support (Hudson & Harrison, 1997) ..... 55
Figure 2.13. A sample ungrouted mechanical-anchored bolt (Hoek, 2008) where $d_b$ is the diameter and $s_c$ is the spacing between the bolts or cables installed in the cross-section. ..... 56
Figure 2.14. Results of a pull-out test performed on a mechanically anchored bolt (Stillborg, 1994). ..... 57
Figure 2.15. The experiments involved using high strength reinforced concrete blocks with a uniaxial compressive strength of 60 MPa. To simulate real rock conditions, the holes were drilled using a percussion rig. (Stillborg, 1994) ..... 59

Figure 2.16. Example of steel rib support configurations (dsi underground, 2023) 60
Figure 2.17. Steel reinforced support in direct contact with the rock (Hoek et al., 2008) ..... 61
Figure 2.18. The layout of an underground mine showing different haul road types (Atlas Copco, 2007) ..... 63
Figure 2.19. A sample haul road profile in an underground mine (Atkinson, 1992) ..... 66
Figure 2.20. A sample continuum models of twin tunnels in RS2, a) model generated, b) after computing the model, interpretation tab view (Rocscience, 2023) ..... 69
Figure 2.21. A continuum model and finite-element discretization (Bobet et al., 2009) ..... 70
Figure 2.22. (A) Human neuron; (B) artificial neuron or hidden unity; (C) biological synapse; (D) ANN synapses (Suzuki, 2013)..... 72
Figure 2.23. Different activation functions for a unit. ..... 74
Figure 3.1. A sample FEM model of a typical underground mine haul road with no support, 400m. depth, hydrostatic loading conditions, excavated in $MP_3$ type rock mass..... 82
Figure 3.2. A sample FEM model of a typical underground mine haul road with liner and pattern bolts, 400 m depth, hydrostatic loading conditions and excavated in $MP_3$ type rock mass..... 82
Figure 3.3. The major principal strain and the span of yielded elements for the unsupported case where the excavation is 400 m deep in MP3 and under hydrostatic loading..... 85
Figure 3.4. The major principal strain and the span of yielded elements for the supported case where the excavation is 400 m deep in $MP_3$ and under hydrostatic loading..... 86
Figure 3.5. A sample plot showing the vertical displacements (m) at the roof of haul road opening excavated in various rock mass quality conditions vs. depth (m) when k=0.5..... 88

Figure 3.6. Schematic of the feedforward artificial neural network model.....90
Figure 3.7. The block diagram of the artificial neural network created in the Matlab neural net fitting toolbox .....91
Figure 4.1. Simulated major principal strain at roof (%) vs. depth (m) for k=1.0 for $MP_2$.....94
Figure 4.2. Simulated major principal strain at roof (%) vs. depth (m) for k=1.0 for $MP_3$.....95
Figure 4.3. Simulated major principal strain at roof (%) vs. depth (m) for k=1.0 for $MP_4$.....96
Figure 4.4. Simulated vertical displacement at roof (m) vs. depth (m) for k=1.0 for $MP_2$.....97
Figure 4.5. Simulated vertical displacement at roof (m) vs. depth (m) for k=1.0 for $MP_3$.....98
Figure 4.6. Simulated vertical displacement at roof (m) vs. depth (m) for k=1.0 for $MP_4$.....99
Figure 4.7. Six randomly generated hypothetical cases to compare the performance of support recommendations of empirical systems with the numerical benchmarks .....101
Figure 4.8. Unsupported stand-up time for the six hypothetical cases.....103
Figure 4.9. Correlation of the numerical simulation outputs with the training, validation, and test data of the ANN model predicting the yielded span in the roof .....111
Figure 4.10. Correlation of the numerical simulation outputs with the training, validation, and test data of the ANN model predicting the yielded span in the wall .....112
Figure 4.11. Comparison of the yielded span on the roof obtained from the numerical analysis and the ANN model.....113
Figure 4.12. Comparison of the yielded span on the wall obtained from the numerical analysis and the ANN model.....113
Figure A.1 Vertical displacement at roof (m) vs. depth (m) for k=0.5 for $MP_2$....139

Figure A.2 Vertical displacement at roof (m) vs. depth (m) for k=0.5 for $MP_3$ ... 140
Figure A.3 Vertical displacement at roof (m) vs. depth (m) for k=0.5 for $MP_4$ ... 141
Figure A.4 Vertical displacement at roof (m) vs. depth (m) for k=1.5 for $MP_2$ ... 142
Figure A.5 Vertical displacement at roof (m) vs. depth (m) for k=1.5 for $MP_3$ ... 143
Figure A.6 Vertical displacement at roof (m) vs. depth (m) for k=1.5 for $MP_4$ ... 144
Figure B.1 Major principal strain at roof (%) vs. depth (m) for k=0.5 for $MP_2$ ... 145
Figure B.2 Major principal strain at roof (%) vs. depth (m) for k=0.5 for $MP_3$ ... 146
Figure B.3 Major principal strain at roof (%) vs. depth (m) for k=0.5 for $MP_4$ ... 147
Figure B.4 Major principal strain at roof (%) vs. depth (m) for k=1.5 for $MP_2$ ... 148
Figure B.5 Major principal strain at roof (%) vs. depth (m) for k=1.5 for MP3 .. 149
Figure B.6 Major principal strain at roof (%) vs. depth (m) for k=1.5 for $MP_4$ ... 150
Figure C.1 Minimum principal stress at roof (MPa) vs. depth (m) for k=0.5 for $MP_2$ ..... 151
Figure C.2 Minimum principal stress at roof (MPa) vs. depth (m) for k=0.5 for $MP_3$ ..... 152
Figure C.3 Minimum principal stress at roof (MPa) vs. depth (m) for k=0.5 for $MP_4$ ..... 153
Figure C.4 Minimum principal stress at roof (MPa) vs. depth (m) for k=1.0 for $MP_2$ ..... 154
Figure C.5 Minimum principal stress at roof (MPa) vs. depth (m) for k=1.0 for $MP_3$ ..... 155
Figure C.6 Minimum principal stress at roof (MPa) vs. depth (m) for k=1.0 for $MP_4$ ..... 156
Figure C.7 Minimum principal stress at roof (MPa) vs. depth (m) for k=1.5 for $MP_2$ ..... 157
Figure C.8 Minimum principal stress at roof (MPa) vs. depth (m) for k=1.5 for $MP_3$ ..... 158
Figure C.9 Minimum principal stress at roof (MPa) vs. depth (m) for k=1.5 for $MP_4$ ..... 159
Figure D.1 Horizontal displacement at wall (m) vs. depth (m) for k=0.5 for $MP_2$160

Figure D.2 Horizontal displacement at wall (m) vs. depth (m) for k=0.5 for $MP_3$161
Figure D.3 Horizontal displacement at wall (m) vs. depth (m) for k=0.5 for $MP_4$162
Figure D.4 Horizontal displacement at wall (m) vs. depth (m) for k=1.0 for $MP_2$163
Figure D.5 Horizontal displacement at wall (m) vs. depth (m) for k=1.0 for $MP_3$164
Figure D.6 Horizontal displacement at wall (m) vs. depth (m) for k=1.0 for $MP_4$165
Figure D.7 Horizontal displacement at wall (m) vs. depth (m) for k=1.5 for $MP_2$166
Figure D.8 Horizontal displacement at wall (m) vs. depth (m) for k=1.5 for $MP_3$167
Figure D.9 Horizontal displacement at wall (m) vs. depth (m) for k=1.5 for $MP_4$168
Figure E.1 Major principal strain (%) at wall (m) vs. depth (m) for k=0.5 for $MP_2$ .....169
Figure E.2 Major principal strain (%) at wall (m) vs. depth (m) for k=0.5 for $MP_3$ .....170
Figure E.3 Major principal strain (%) at wall (m) vs. depth (m) for k=0.5 for $MP_4$ .....171
Figure E.4 Major principal strain (%) at wall (m) vs. depth (m) for k=1.0 for $MP_2$ .....172
Figure E.5 Major principal strain (%) at wall (m) vs. depth (m) for k=1.0 for $MP_3$ .....173
Figure E.6 Major principal strain (%) at wall (m) vs. depth (m) for k=1.0 for $MP_4$ .....174
Figure E.7 Major principal strain (%) at wall (m) vs. depth (m) for k=1.5 for $MP_2$ .....175
Figure E.8 Major principal strain (%) at wall (m) vs. depth (m) for k=1.5 for $MP_3$ .....176
Figure E.9 Major principal strain (%) at wall (m) vs. depth (m) for k=1.5 for $MP_4$ .....177
Figure F.1 Maximum principal stress (MPa) at wall (m) vs. depth (m) for k=0.5 for $MP_2$ .....178
Figure F.2 Maximum principal stress (MPa) at wall (m) vs. depth (m) for k=0.5 for $MP_3$ .....179

Figure F.3 Maximum principal stress (MPa) at wall (m) vs. depth (m) for k=0.5 for $MP_4$ ..... 180
Figure F.4 Maximum principal stress (MPa) at wall (m) vs. depth (m) for k=1.0 for $MP_2$ ..... 181
Figure F.5 Maximum principal stress (MPa) at wall (m) vs. depth (m) for k=1.0 for $MP_3$ ..... 182
Figure F.6 Maximum principal stress (MPa) at wall (m) vs. depth (m) for k=1.0 for $MP_4$ ..... 183
Figure F.7 Maximum principal stress (MPa) at wall (m) vs. depth (m) for k=1.5 for $MP_2$ ..... 184
Figure F.8 Maximum principal stress (MPa) at wall (m) vs. depth (m) for k=1.5 for $MP_3$ ..... 185
Figure F.9 Maximum principal stress (MPa) at wall (m) vs. depth (m) for k=1.5 for $MP_4$ ..... 186
Figure G.1 Results after computation and interpretation of the unsupported model in terms of vertical displacement (m) ..... 187
Figure G.2 Results after computation and interpretation of the supported model in terms of vertical displacement (m)..... 187
Figure G.3 Results after computation and interpretation of the unsupported model in terms of horizontal displacement (m) ..... 188
Figure G.4 Results after computation and interpretation of the supported model in terms of horizontal displacement (m) ..... 188
Figure G.5 Results after computation and interpretation of the unsupported model in terms of maximum principal stress ($\sigma_1$)..... 189
Figure G.6 Results after computation and interpretation of the supported model in terms of Maximum Principal Stress ($\sigma_1$)..... 189
Figure G.7 Results after computation and interpretation of the unsupported model in terms of minimum principal stress ($\sigma_3$) ..... 190
Figure G.8 Results after computation and interpretation of the supported model in terms of minimum principal stress ($\sigma_3$)..... 190

## LIST OF ABBREVIATIONS

| | |
|---|---|
| ANFIS | Adaptive neuro-fuzzy inference system |
| ANN | Artificial neural network |
| BEM | Boundary element method |
| BTS | Brazilian tensile strength |
| c | Cohesion |
| $E_{rm}$ | Rock mass modulus |
| ESR | Excavation support ratio |
| FDM | Finite difference method |
| FEM | Finite element method |
| GPa | Gigapascal |
| GSI | Geological strength index |
| $G_w$ | Groundwater condition |
| $I_S$ (50) | Point load test index |
| $J_a$ | Joint alteration number |
| $J_c$ | Discontinuity condition |
| $J_n$ | Joint set number |
| $J_r$ | Joint roughness number |
| $J_s$ | Discontinuity spacing |
| $J_w$ | Joint water reduction number |
| kPA | Kilopascal |
| MN | Meganewton |
| MPa | Megapascal |
| M-RMR | Modified rock mass rating |
| Q | Rock mass quality |
| RMR | Rock mass rating |
| RQD | Rock quality designation |
| RSR | Rock structure rating |
| SRF | Stress reduction number |

| | |
|---|---|
| SRH | Schmidt rebound hammer |
| $T_{bf}$ | Ultimate strength |
| TBM | Tunnel boring machine |
| UCS | Uniaxial compressive strength |

## LIST OF SYMBOLS

| | |
|---|---|
| $\sigma_{ci}$ | Uniaxial compressive strength of intact rock |
| $\sigma_t$ | Tensile strength |
| $\gamma$ | Unit weight |
| $\gamma_w$ | Unit weight of water |
| $\sigma_3$ | Minimum principal stress |
| $\emptyset$ | Internal friction angle |
| $\sigma_1$ | Maximum principal stress |
| $\varepsilon$ | Strain |

# CHAPTER 1

# INTRODUCTION

## 1.1 General Remarks

In underground mining, main haul roads not only involve the critical infrastructure such as power and communication lines but also provide access to personnel, equipment, and materials to and from the production regions. Design and construction of permanent openings require extensive geological and geomechanical assessments to ensure the long-term stability. Considering the access roads serve throughout the mine life, determination of the viable opening dimensions and the support configuration is an essential part of rock mechanics surveys.

The field and laboratory studies are commonly used for gathering comprehensive information about the intact and mass scale properties like strength, stiffness, and diggability as well as seismicity and hydrogeological features like groundwater flow nets for the rocks or soils surrounding the underground access roads. Empirical, analytical and numerical assesments rely on this background and lead to a decision on the support system that can withstand the induced stresses. The rock mass classification systems offer an empirical workflow to design the stable underground openings regarding the structural and mechanical properties. They match an overall indicator for the rock mass quality with the state of stability in significant case histories to provide an understanding about the potential challenges. The most widely used systems in underground excavations are the 'Rock Mass Rating (RMR)' of Bieniawski (1973) and the Q-tunnelling index (Barton et al, 1974). The RMR correlates the opening dimensions, time dependent behavior, various support configurations and recommendations on the excavation advance. On the other hand, the Q-tunneling index was specifically developed for

underground excavations and it provides a more detailed guidance for the support configurations and excavation dimensions. The analytical methods are mathematical expressions to calculate the stress and deformation for a simple geometry and mechanical conditons. The Kirsch (1898) solution is an example that provides the induced stresses around circular openings based on the assumption of continuous, isotropic and linear elastic material behavior. Alternatively, the numerical methods may provide a more comprehensive outview for the opening stability relying on the powerful computational framework.

This research determines the support configurations recommended by the commonly used empirical methods and investigates their performance by numerical simulations. Following the specification of geomechanical inputs representing various quality rock masses, a common haul road opening was analyzed with a Finite Element Method based numerical code to reveal the mechanical performance of the empirical support recommendations. Finally, a machine learning based design tool was developed to provide an alternative design scheme that relies on a comprehensive database generated with the geomechanical simulations. The study intends to provide a practical and reliable tool for the design of stable underground haul roads.

## 1.2 Problem Statement

The empirical methods, such as the rock mass classification systems and design charts, provide a guideline for the required support system in underground openings. However, they offer solutions relying on the particular case histories representing some distinct geological, geomechanical and structural conditions and lacks in the global solution for various circumstances. The predictions should be expected to be more accurate for similar conditions and the database requires to be updated with new case histories to be valid for various conditions. Considering the difficulties in generating and observing the data points, which represent significant geomechanical events, it is not practical to expand the case history database

covering any potential condition. Specifically, the Q tunneling index relies on the expert view and case histories to make useful support recommendations for the preliminary stage of design. However, it has several limitations in the interpretation of support performance with regard to depth, deformations, and stress concentrations. The yielded zone around the opening is dependent on the induced stresses, the opening depth, the mechanical properties, the structural condition and the excavation type. Although 'stress reduction factor' adjusts the rock mass quality score conforming to various field loadings, the support performance remains to be questionable in anisotropic rock mass.

In another aspect, the computational advantages and accuracy offered by the analytical solutions cannot be used globally for determination of the support system as they are valid only under some distinct circumstances. Development of an analytical solution is an exhaustive procedure involving mathematical complexities and experimental validation. On the other hand, the numerical methods can produce geomechanical simulations in a realistic manner relying on some mathematical models that imitate the behavior of the rock mass and its supporting structures exposed to various boundary conditions. The solution scheme allows for parametric and scenario-based analyses of various support systems and determine any necessary alterations or adjustments to ensure the stability and safety of the underground excavation.

## 1.3 Research Objectives and Methodology

This study aims to examine the performance of the support configurations suggested by the Q-system for a typical underground mine haul road using numerical simulations. Initial attempts focused on determination of support categories matching with different rock mass quality conditions and opening depth. Later, the numerical modeling approach was used to check the performance of the support system. The analyses led to the necessary modifications or adjustments to the current scheme of the empirical support design.

Various support configurations were implemented on different rock mass quality conditions ranging from poor to good, and numerical analysis were carried out using the Rocscience RS2 code, which is a finite element method software for geomechanical simulations. The stress and deformation analyses provided the patterns and trends of the investigated support configurations. The computational analyses allowed for the parametric study of a typical mine access road under different conditions. Comparing some significant cases generated from the Q system support recommendation table with the simulation results the conventional scheme of empirical support design was discussed and the potential for auxiliary design tools were investigated.

In addition, this study aimed to develop a practical tool that can be used without extensive knowledge of geomechanical modeling to obtain reliable and detailed information about the support performance. The mechanical indicators of stability collected from the numerical models were used to create a database to train an 'Artificial Neural Network (ANN)'. Using this trained machine, the stability of an underground haul road was investigated under different circumstances. Model validation was performed to ensure that the ANN makes plausible predictions for the opening stability and support configuration. Figure 1.1 summarizes the process methodology flowchart of this study, depicting the fundamental elements involved.

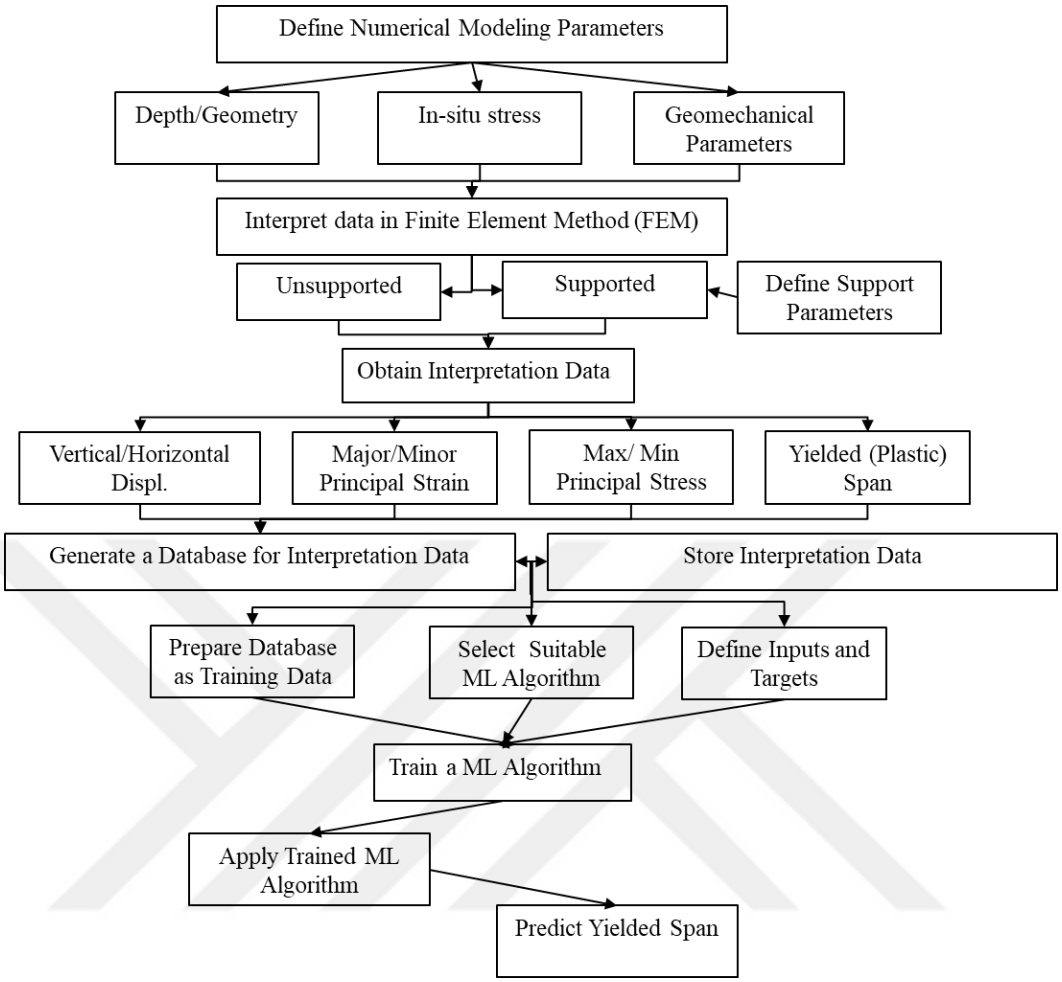


Figure 1.1 Process Methodology Flowchart of the Fundamental Elements

## 1.4 Thesis Outline

This dissertation involves five chapters and seven appendices that presents the study outcomes. Chapter 1 explains the weaknesses of the commonly used empirical support design methods for permanent underground openings like haul roads and presents the potential of the numerical analyses to obtain a comprehensive understanding about the support performance.

Chapter 2 reviews the existing literature related to rock mass classification systems by discussing the previous research and studies conducted on the support design. Finite Element Method

The concluding chapter summarizes the key findings drawn from the study. It presents recommendations for a reliable support design in underground mine haul roads based on the research outcomes. Additionally, the chapter suggests potential areas for further research and improvement in the field. It concludes with closing remarks and final thoughts on the significance of the study's results.

## 1.5 Contributions to Literature

This study contributes to the literature on the design of support configuration for mine access roads by presenting a user-friendly method that requires no experience in numerical modeling but relies on a database obtained from the mechanical outputs of proper numerical simulations. The proposed method replaces the old-fashioned scatter plots by an ANN model to accurately assess the performance of the support system in mine access roads. It provides a comprehensive understanding of the support behavior under various field loading and rock mass geomechanical conditions. Another aspect of the developed method is its potential to improve the empirical support design methodology by including a reliable database showing the mechanical performance of the support system.

# CHAPTER 2

# LITERATURE SURVEY

This study's literature review may provide a basic overview of rock mass engineering in underground openings. It discusses various critical topics, such as rock mass classification, geomechanical property estimation, rock support design principles, underground mining transport and materials handling systems, and numerical modeling approaches for support analysis in underground openings. The survey delves into multiple key areas, aiming to explore and understand the intricacies involved in rock mass behavior and its impact on underground openings.

## 2.1 Rock Mass Classification Systems

Rock mass classification systems are developed relying on engineering experience and observations gathered during the construction of surface or underground rock structures. The data obtained from the exploratory work are evaluated by statistical methods to come up with an understanding of the rock mass quality. The purpose of rock classification is to perceive the mechanical, geological and structural characteristics of rocks in the field scale. As their simple framework is suitable even for non-experts, the classification systems are widely used in the preliminary stage of design in rock constructions. Some of the systems intends to describe the rock mass quality in a descriptive manner. On the other hand, quantitative systems are also available for determining the fundamental design parameters. Modifications have potential to provide more insight about the impact of field loadings and the type of excavation. The comprehensive understanding about the rock mass quality may lead to the anticipation of rock behavior under various circumstances, which provides a useful background for the design of support systems.

The commonly used classification systems are the Rock Mass Rating (RMR) (Bieniawski, 1973; Bieniawski, 1989), Q-Tunneling Index (Barton et al., 1974) and Geological Strength Index (GSI) (Hoek, 1994; Hoek, Kaiser and Bawden, 1995; Hoek and Brown, 1997; Hoek, Marinos and Benissi, 1998; Marinos and Hoek, 2001). There are more than 30 different rock mass classification systems and even more in number involving the modifications of the major systems that have been developed so far (Table 2.1). The RMR and Q-Tunneling Index are two of the popular systems that have various modifications for specific purposes. For instance, Ünal and Özkan (1990) developed the M-RMR (Modified Rock Mass Rating-Reorganized Rock Mass Index) classification system for weak-layered-anisotropic rocks with clay content.

Table 2.1 Rock mass classification systems

| **Name of the system** | **Author(s)** | **Origin of Country** | **Application** |
|---|---|---|---|
| Rock Load | Terzaghi, 1946 | USA | Tunnels with steel Support |
| Stand- up Time | Lauffer, 1958 | Australia | Tunneling |
| Rock Quality Designation (RQD) | Deere et al., 1963 | USA | Core logging, tunneling |
| New Austrian Tunneling Method (NATM) | Pacher et al., 1964 | Austria | Tunneling |
| Rock Structure Rating (RSR) | Wickham et al., 1972 | USA | Tunneling |
| Rock Mass Rating (RMR) | Bieniawski et al, 1973 (modification 1989-USA) | South Africa | Tunnels, mines (slopes, foundations) |

Table 2.1 (continued)

| | | | |
|---|---|---|---|
| Rock Mass Quality (Q) | Barton et al, 1974 (modification 1974, 2014) | Norway | Tunnels, mines, foundations |
| Strength Block Size | Franklin, 1975 | Canada | Tunneling |
| Basic Geotechnical Classification | ISRM, 1981 | International | General |
| Rock Mass Strength (RMS) | Stille et al., 1982 | Sweden | Metal Mining |
| Unified Rock Mass Classification System (URCS) | Williamson, 1984 | USA | General |
| Slope Mass Rating | Romana, 1985 | Spain | Slopes |
| Weakening Coefficient System (WCS) | Singh, 1986 | India | Coal Mining |
| Modified Rock Mass Rating (M-RMR) | Ünal and Özkan, 1990 | Türkiye | Mining |
| Coal Mine Roof Rating (CMRR) | Molinda and Mark, 1994 | USA | Coal Mining |
| Rock Mass Index (RMi) | Palmström, 1996 | Sweden | Tunneling |
| Geological Strength Index (GSI) | Hoek and Brown, 1997 | Canada | General |
| Anisotropy Index (Heterogeneous Rock Masses, (modification of GSI) | Marinos and Hoek, 2000 | Canada | General |

Table 2.1 (continued)

| | | | |
|---|---|---|---|
| Continuous rock mass rating | Sen and Sadagah, 2003 | International | General |
| Rock mass quality rating | Aydan et al., 2014 | International | General |

Each of these systems has their own strengths and limitations regarding the complexity, and level of detail. Although some of them have been widely adopted and used in geotechnical engineering practice, the research is still going on for most of them for the minor improvements. Selection of an appropriate system matching with the design considerations is an important stage to obtain a reliable insight about the rock mass quality.

## 2.2 Premises of Rock Mass Classification System

The premises of rock mass classification system dates back to the first half of the $20^{th}$ century. Although the initial attempts involved the soil material, later, the classification of rock and soil mass is separated. Following rise of rock constructions that require advanced engineering practice and sophisticated design procedures relying on mechanical simulations, determination of rock mass parameters became a significant challenge. Although field scale testing can provide useful data, operational and economic restrictions led to alternative methods for assessment of the rock mass quality and extraction of field scale parameters from laboratory testing. Additionally, user-friendly tools for assessment of the interactions between the rock mass and support systems were required for the preliminary stability analyses. Developments in the empirical systems led to more efficient analysis of geomechanical conditions. This section presents some of the early developments in rock mass characterization.

### 2.2.1 Terzaghi's Rock Load System

Terzaghi's (1946) study to estimate the support requirements for various rock conditions based on the general character of the rock mass may appear to have been the first attempt. However, the system only considers the usage of steel sets and does not involve the shotcrete and rock bolting. It is based on the simplified loading scheme as shown in Figure 2.1 and assumes that the opening depth is sufficient to lead to the full earth arching effect.

Terzaghi defines the arching effect as the transmission of roof loads to the side walls due to excavation. The ground arch is used to refer to the mass of rock that distributes the load. Friction forces around the disturbed region (acdb) will resist towards failure, and the stress will concentrate on the side walls. The Terzaghi's system doesn't allow for a quantitative assessment of the rock mass characteristics. Another drawback was noted to be overdesign in terms of the support capacity. Various researchers conducted follow up studies to improve the Terzaghi's concept.

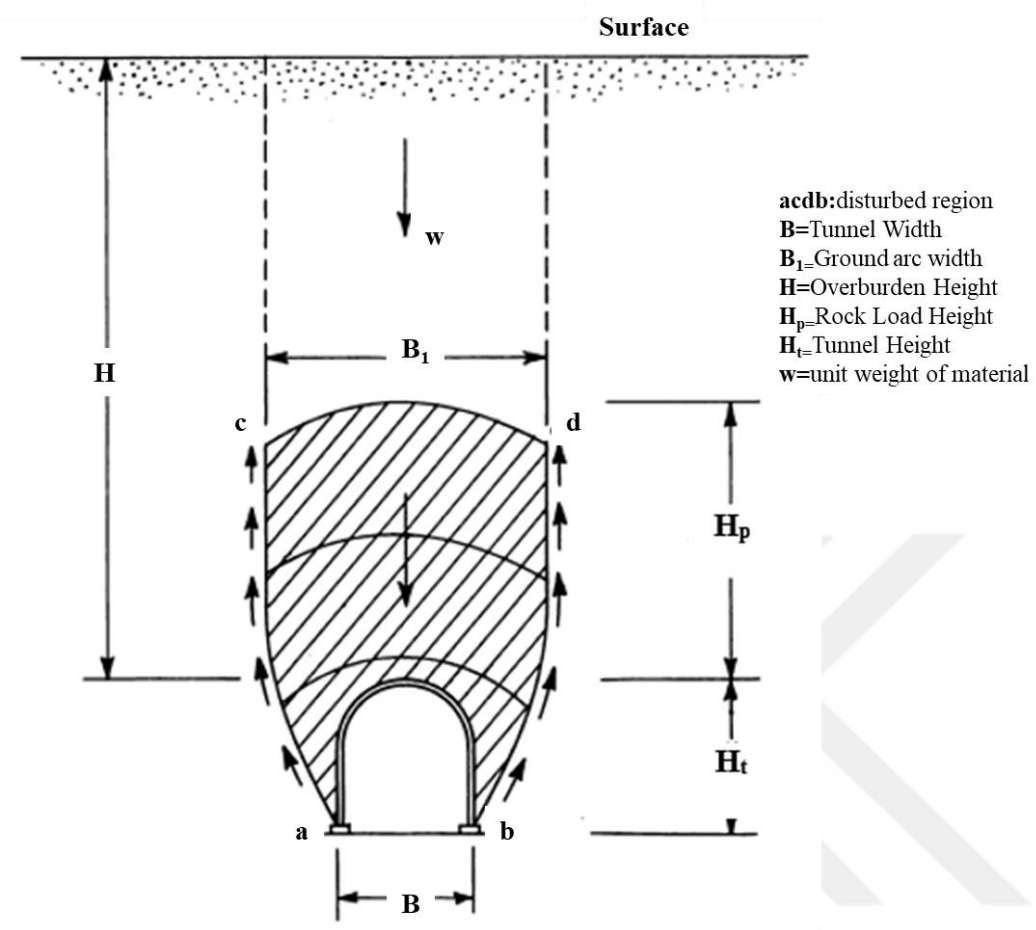


Figure 2.1. The diagram indicating the loading of a rock tunnel (Terzaghi, 1946)

Table 2.2 shows the classification of the rock mass and the required support categories according to Terzaghi.

Table 2.2 Rock Load Classification of Terzaghi (1946)

| No | Rock Condition | Rock Loading Height ($H_p$) | Comments |
|---|---|---|---|
| 1 | Hard and intact | Zero | Light lining only if spalling or popping occurs |
| 2 | Hard, stratified or schistose | 0 – 0.5 B | Light support, mainly against spalling, |
| 3 | Massive, moderately jointed | 0 – 0.25 B | Loading changes likely |

Table 2.2 (continued)

| | | | |
|---|---|---|---|
| 4 | Moderately blocky and seamy | 0.25 B – 0.35 $(B+H_t)$ | Negligible side pressure |
| 5 | Very blocky and seamy | (0.35- 1.10) $(B+H_t)$ | Little to negligible side pressure |
| 6 | Completely Crushed | 1.10 $(B+H_t)$ | Significant side pressure, softening from seepage in lower part of the tunnel requires continuous support |
| 7 | Squeezing rock, moderate depth | (1.10 – 2.10) $(B+H_t)$ | Heavy side pressure, with need for invert struts, circular ribs recommended |
| 8 | Squeezing rock, significant depth | (2.10 – 4.5) $(B+H_t)$ | Heavy side pressure, with need for invert struts, circular ribs recommended |
| 9 | Swelling Rock | Up to 76m, irrespective of $(B+H_t)$ | Circular ribs required and yielding support possible |

### 2.2.2 Rock Quality Designation Index (RQD)

The Rock Quality Designation Index (RQD) (Deere et al., 1967) was developed to make a quantitative assessment of the inherent discontinuities in the rock mass based on drill core samples. RQD is an expression of the ratio of fractures that divide the rock blocks into pieces greater than 10 cm (xi). Sum of this core length is divided by the total drill length to find the RQD score as shown in Figure 2.2. and Equation 2.1.

$$RQD = \frac{\sum xi}{L} \qquad \text{Equation 2.1}$$

where, $x_i$= rock cores greater than 10 cm

L= total drill length

According to Deere (1967), the RQD can be utilized in conjunction with a thorough understanding of the geology and geotechnical factors. It cannot be used as a design parameter on its own because of the insufficient structural insight. RQD can only provide a limited understanding of the inherent fractures in the rock mass. The RMR and Q tunneling index systems make use of RQD as an input parameter.

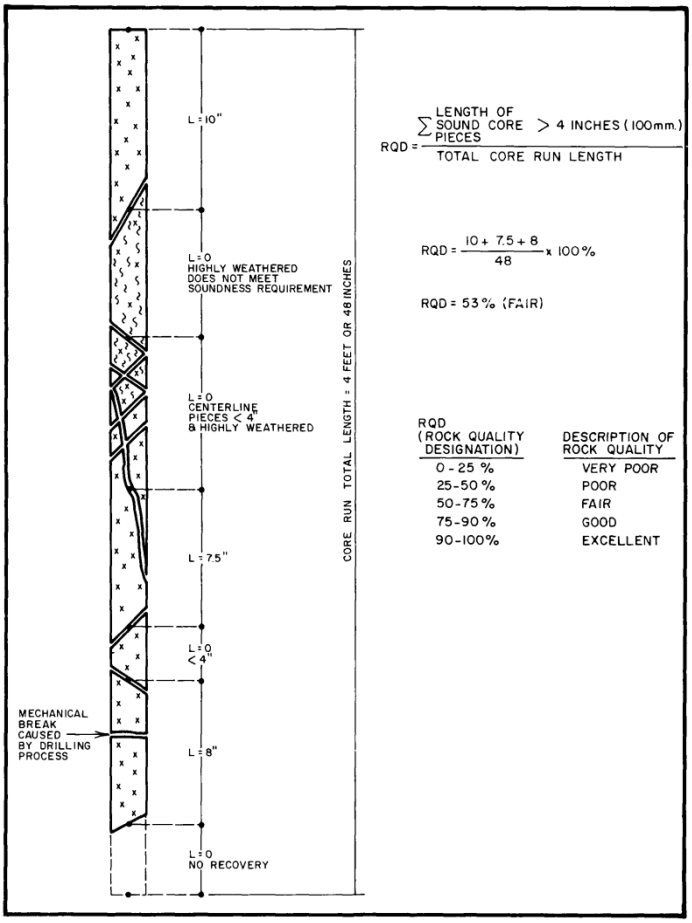


Figure 2.2. RQD Calculation and Measurement Procedure (Deere, 1989)

### 2.2.3 Lauffer Classification- Stand up Time

The Lauffer's classification system was published in 1958 and later, it was improved with NATM, bringing the idea that the span and stand-up time are important characteristics in support design. Stand up time is the average amount of time it takes for an unsupported span to collapse. It has a considerable impact on the development of most of the recent rock mass classification system. However, it doesn't provide a rating system or design parameters. As shown in Figure 2.3, Lauffer's system correlates the stand-up time for each active, unsupported rock span with different rock mass quality classes.

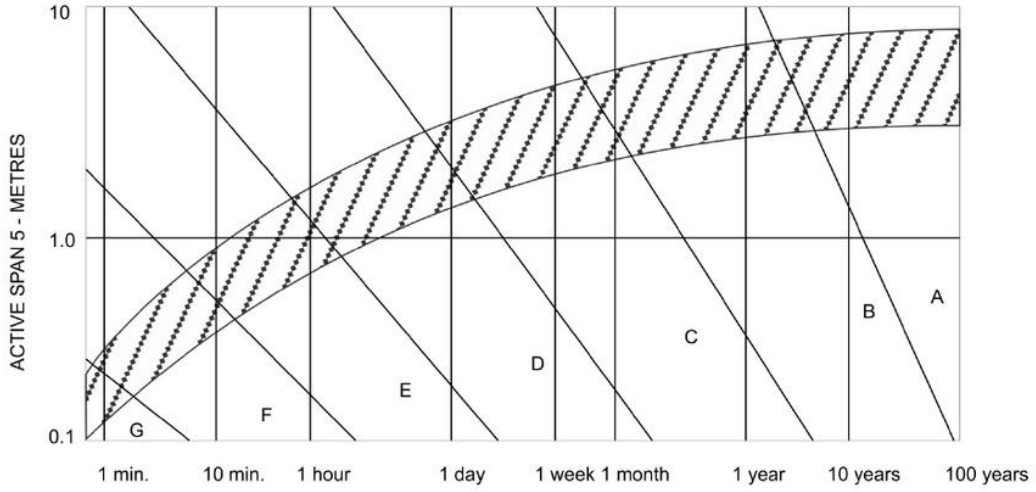


Figure 2.3. For various classes of rock mass, Lauffer's relationship between active span and stand-up (1958), A Very good rock, G Very Poor Rock

### 2.2.4 Rock Structure Rating

The Rock Structure Rating (RSR) was proposed by Wickham et al. in 1972 as a quantitative method for describing the quality of a rock mass and selecting the appropriate support systems for underground excavations

The RSR concept considered three general categories of factors that influence the behavior of rock masses in tunneling: geologic parameters, construction parameter and groundwater and joint condition parameters. However, the authors pointed out that in some cases, it might be challenging to accurately define these factors, and only general approximations can be made. Therefore, the classification system provides a standardized method for evaluating the rock mass quality and predicting its behavior under different loading conditions.

The construction, groundwater, and joint condition parameters, on the other hand, are related to the tunneling and include the size of the tunnel, the direction of drive,

the method of excavation, groundwater inflow and joint conditions such as poor, fair and good. These factors can also affect the rock mass behavior, and the appropriate support system should be selected based on both geologic and construction parameters. Based on the RSR, a support system can be proposed as indicated Figure 2.4.

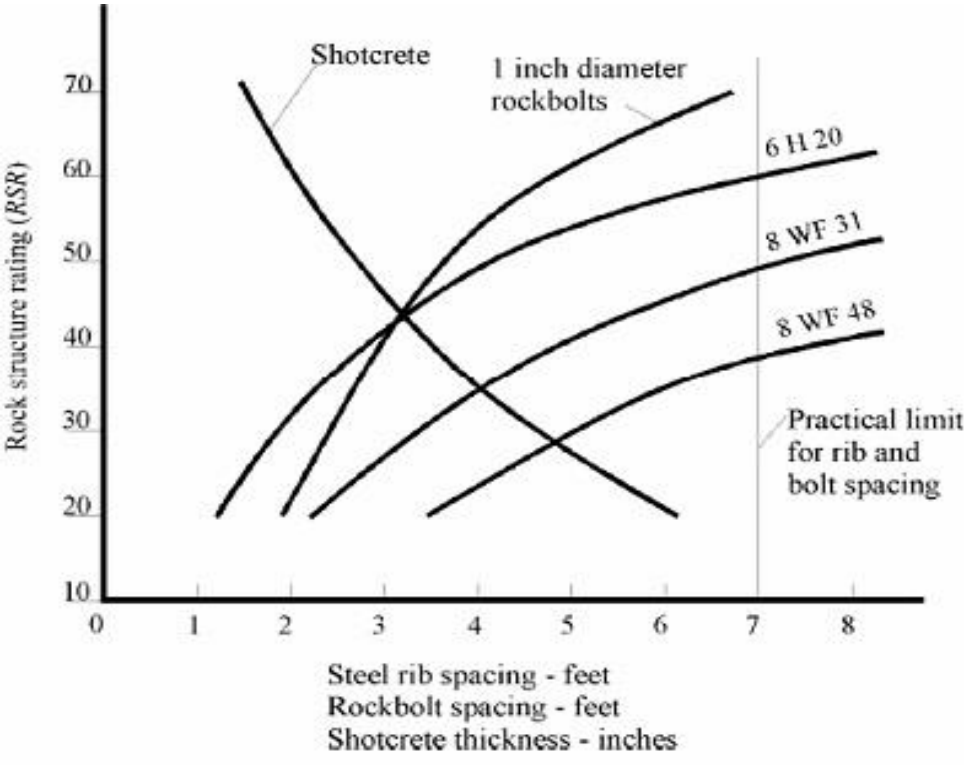


Figure 2.4. Correlation between RSR index and support requirements for a 7.3 m diameter circular tunnel (Wickham et al., 1972)

## 2.3 Commonly Used Rock Mass Classification Systems

Among many alternatives some of the rock mass quality characterization systems are more popular with a superior reliability ensured by an extensive use in surface and underground rock constructions, easy framework and viability for modification regarding specific purposes. The Geomechanical Classification System (RMR), Q-Tunneling Index System and Geological Strength Index (GSI) are the most

remarkable ones. This section presents the characteristic features and limitations of the widely used rock mass classification systems.

### 2.3.1 The Geomechanical Classification System: Rock Mass Rating (RMR)

Bieniawski (1973; 1989) proposed one of the widely used rock mass classification systems that is viable to select an appropriate support system for tunnels, foundations, slopes and other underground openings. The system has undergone various improvements with further studies and observations and the most commonly used version is the one developed in 1989. It was first used in 1973 under the name of South African Council of Scientific and Industrial Research (CSIR). The RMR system offers advantages in terms of ease of collecting data representing the rock mass and allows a quick evaluation of the rock mass quality. The input parameters of the system are given below;

1. Strength of intact rock material ($\sigma_{ci}$)
2. Rock quality designation (RQD)
3. Discontinuity spacing ($J_s$)
4. Discontinuity condition ($J_c$)
    a) Persistence
    b) Aperture
    c) Roughness
    d) Infilling
    e) Weathering
5. Groundwater condition (Gw)
6. Discontinuity orientation

To minimize the error in subjective evaluations of rock properties, it is useful to provide a range of values for different parameters instead of a single value. This approach is embraced also in the RMR system. Field observations and experience of the skilled experts provided a useful background to match the linguistic definitions of rock mass quality with the numerical identifiers. Table 2.3 presents the interpretation table of RMR that associates the empirical rock mass quality with the mechanical properties and a useful understanding of the stand-up time without any support.

Table 2.3 Rock mass quality classes according to RMR (Bieniawski, 1989)

| **Rating** | 100-81 | 80-61 | 60-41 | 40-21 | <20 |
|---|---|---|---|---|---|
| **Class No** | I | II | II | IV | V |
| **Description** | Very good | Good | Fair | Poor | Very Poor |
| **Average Stand Up Time** | 10 years for 15 m span | 6 months for 6 m span | 1 week for 5 m span | 10 hours for 2.5 m span | 30 minutes for 1 m span |
| **Cohesion (kPa)** | >400 | 300-400 | 200-300 | 100-200 | <100 |
| **Internal Friction Angle** | >45° | 45-35° | 35-25° | 25-15° | <15° |

The RMR method's stand-up time and maximum stable unsupported span for underground excavations including tunnels, chambers, and mines are its other primary outputs.

For each of the five RMR rock classes, the approach gives an unsupported span versus stand-up time chart (Figure 2.5). By combining this chart with the RMR score, it is possible to estimate the amount of time that initial support needs to be installed.

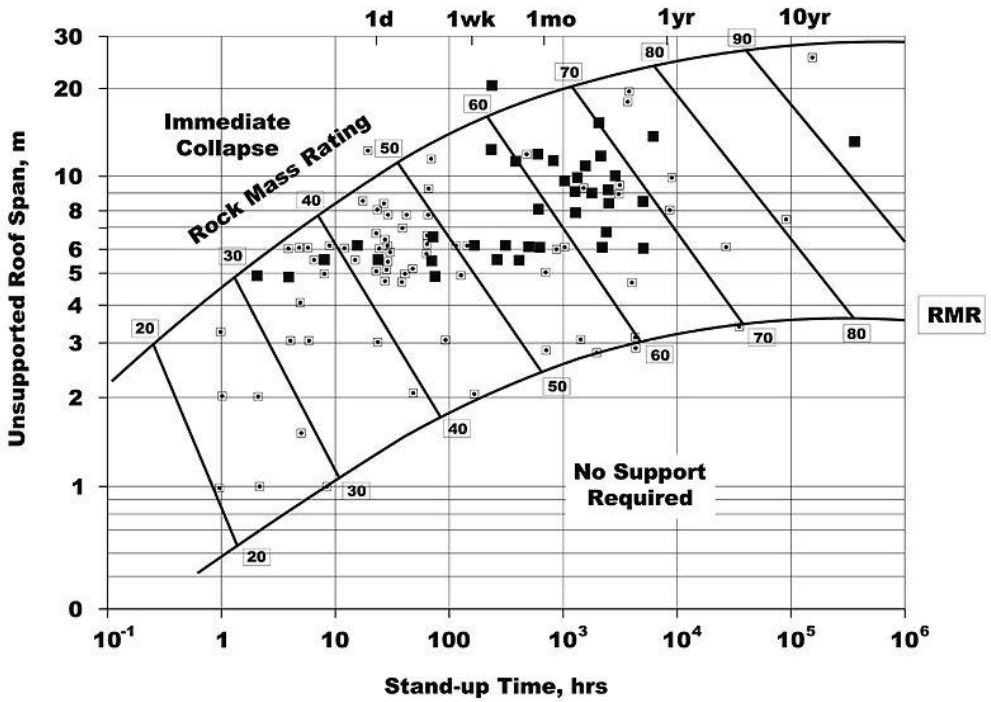


Figure 2.5. Stand-up time versus unsupported span for various rock mass classes according to RMR (Bieniawski, 1984).

Bieniawski (1984) also proposed a set of guidelines for choosing the appropriate support configuration for underground openings that are excavated using conventional drilling and blasting technique (see Table 2.4). The decision criteria involves several factors including the depth of the opening (which takes into account the overburden pressure and in situ stress), as well as the dimensions, shape, and method of excavation. The recommended support measures are presented in Table 2.4.

Table 2.4 Guidelines for excavation and support of rock tunnels according to RMR (Bieniawski, 1989)

| Rock Mass Quality Class | Excavation | Support | | |
|---|---|---|---|---|
| | | **Rock bolts (20 mm diameter fully grouted)** | **Conventional Shotcrete** | **Steel Sets** |
| **Very good**<br><br>**RMR=81-100** | Full face, 3m advance | Generally no support required except for occasional spot bolting | | |
| **Good rock**<br><br>**RMR=61-80** | Full face 1-1.5 m advance, complete support 20 m from face | Locally, bolts in crown 3 m long, spaced 2.5 m, with occasional wire mesh | 50 mm in crown where required | None |
| **Fair rock**<br><br>**RMR=41–60** | Heading and bench; 1.5–3 m advance in heading; commence support after each blast; complete support 10 m from face | Systematic bolts 4 m long, spaced 1.5–2 m in crown and walls with wire mesh in crown | 50–100 mm in crown and 30 mm in sides | None |
| **Poor rock**<br><br>**RMR=21–40** | Top heading and bench; 1.0–1.5 m advance in top heading; install support concurrently with excavation 10 m from face | Systematic bolts 4–5 m long, spaced 1–1.5 m in crown and wall with wire mesh | 100–150 mm in crown and 100 mm in sides | Light to medium ribs spaced 1.5 m where required |
| **Very poor rock**<br><br>**RMR <20** | Multiple drifts; 0.5–1.5 m advance in top heading; install support concurrently with excavation; shotcrete as soon as possible after blasting | Systematic bolts 5–6 m long, spaced 1–1.5 m in crown and walls with wire mesh; bolt invert | 150–200 mm in crown, 150 mm in sides, and 50 mm on face | Medium to heavy ribs spaced 0.75 m with steel lagging forepoling if required; close invert |

Shape: Horseshoe; width:10 m; vertical stress <25 MPa

Based on common knowledge until now, the RMR system has been used in over 350 remarkable applications in various underground openings, tunnels, underground mines, and open-pit slope designs. Since the initial version in 1973 researchers continued to offer major and minor improvements. One of the most significant one was published until 1989. Besides, the rating scales and parameters have undergone changes between 1973 and 2014 (Bieniawski 1973; 1974; 1975; 1979; 1989; 2011; 2013 and 2014). Table 2.5 provides detailed information about the modified parameters.

Table 2.5 Modifications in the rating system of RMR (modified from Rehman et al. (2018))

| **Parameter** | **1973** | **1974** | **1975** | **1979** | **1989** | **2011** | **2013** | **2014** |
|---|---|---|---|---|---|---|---|---|
| **Intact Rock Strength (MPa)** | 0-10 | 0-10 | 0-15 | 0-15 | 0-15 | 0-15 | 0-15 | 0-15 |
| **RQD** | 3-16 | 3-20 | 3-20 | 3-20 | 3-20 | 3-20 | - | - |
| **Joint Spacing (mm, $J_s$)** | 5-30 | 5-30 | 5-30 | 5-20 | 5-20 | 5-20 | - | - |
| **Separation of joints (mm)** | 1-5 | | | | | | | |
| **Continuity of joints (m)** | 0-5 | | | | | | | |
| **Weathering** | 1-9 | | | | | | | |
| **Conditions of joints (m, $J_c$)** | - | 0-15 | 0-25 | 0-30 | 0-30 | 0-30 | 0-30 | 0-20 |
| **Discontinuity density (j/m, RQD + joint spacing)** | - | - | - | - | - | - | 0-40 | 0-40 |
| **Groundwater (Gw)** | 2-10 | 2-10 | 0-10 | 0-15 | 0-15 | 0-15 | 0-15 | 0-15 |
| **Alterability (%)** | | | | | | | | 0-10 |
| **Rating Adjustment** | $F_o$ | 3-15 | 3-15 | 0-(-12) | 0-(-12) | 0-(-12) | 0-(-12) | 0-(-12) |
| | $F_e$ | | | | | | | 1.32-1 |
| | $F_s$ | | | | | | | 1.3-1 |

$F_o$= adjustment factor for the orientation, $F_e$= adjustment for a particular excavation method, $F_s$= adjustment factor for the stress-strain behavior

The RMR version of 1973 involved eight parameters. Later in 1974, the parameters were reduced to six by embedding the joint separation, continuity, and weathering into a new parameter called the joint condition ($J_c$). Between 1974 and 1975, the ratings for $J_c$ and 'Intact Rock Strength' were raised by 10 and 5 points, respectively.

The 'Rating Adjustment' parameter was rated positively on a scale of 3 to 15, with 3 indicating the least favorable orientation and 15 indicating the most favorable orientation in the versions of 1973 and 1974. However, starting from 1975, the rating for this parameter was set to negative values, with 0 representing the most favorable and -12 representing the least favorable orientation.

On 1975 and 1976, the rating scales in the RMR system remained the same, but there were minor changes in the scores indicating rock mass quality class. In 1979 version, the maximum rating for the $J_s$ term was decreased by 10 points, and the impact of both $J_c$ and Gw was raised by 5 points each. The 1989 version introduced a modification in the evaluation of sub-horizontal joints. The range of rating varies between very favorable to very unfavorable for tunnel stability. This change led to a five-point difference in the overall RMR scores.

The major improvements were published in 1989, resulting in new graphs and tables for evaluating the scores of strength of intact rock material, RQD, spacing, and the condition of discontinuities. This enhanced version of the system was named $RMR_{89}$. In $RMR_{89}$, the basic RMR score was calculated as the sum of the scores for five parameters, including strength of intact rock material ($R_1$), RQD (R2), discontinuity spacing ($R_3$), joint condition ($R_4$), and groundwater condition ($R_5$). Furthermore, the rating of joint orientation in relation to the tunnel strike ($R_6$) was adjusted to obtain the final RMR score. The overall statement is given in Equation 2.3. The new $RMR_{89}$ system was noted to improve the reliability in determination of the rock mass quality.

$$RMR_{89} = R_1 + R_2 + R_3 + R_4 + R_5 + R_6 \qquad \text{Equation 2.3}$$

Previously in $RMR_{73}$, the minimum values of $R_2$ and $R_3$ were 3 and 5, respectively. However, later modifications (Bieniawski, 2011) of $RMR_{89}$ changed the range for $R_2$ and $R_3$ from 0 to 20.

In historical order, RQD has always been a part of RMR and Q systems. However, due to certain limitations, RQD was supported with the joint frequency in rock core or excavation face analysis (Pells et al., 2017; Pells & Pells, 2018). Koutsoftas (2018) conducted an analysis of the discrepancies in RQD definitions across different regions and the use of rock exposures to determine RQD were determined as the major source of error. The modified equation of $RMR_{89}$ with five basic parameters is expressed in Equation 2.4

$$RMR_{89} = R_1 + R_{2-3} + R_4 + R_5 + R_6. \qquad \text{Equation 2.4}$$

Here, $R_{2-3}$ shows the rating for fracture frequency.

An improved version of $RMR_{89}$, called $RMR_{14}$, was proposed after 25 years. It includes new parameters, a modified rating, and an updated interpretation table (Celada et al., 2014). Equation 2.5 presents the formulation of the $RMR_{14}$ structure.

$$RMR_{14} = (RMR_b + F_o) \times F_s \times F_e \qquad \text{Equation 2.5}$$

where $RMR_b$ = basic RMR score without the effect of excavation,

$F_0$ = A factor used to adjust for the orientation of a tunnel's axis in relation to the primary discontinuity set in the rock mass, is invariably negative.

$F_e$ = A factor is used to adjust for a particular excavation method.

$F_s$ = A factor is used to adjust for the stress-strain behavior of the rock mass at the tunnel faces.

Besides, there has been an increasing trend towards the use of artificial intelligence (AI), such as fuzzy logic, machine learning and neural networks in rock mass

classification. These techniques allow for more accurate and efficient classification based on a wider range of input parameters. Jalalifar et al., (2011) asserted that findings of their study on the use of neuro-fuzzy algorithms to estimate the rock mass rating provide more accurate predictions than the conventional rating system. They used three different simulation processes to calculate RMR with ANFIS (adaptive neuro-fuzzy inference system) based on grid partitioning, subtractive clustering, and fuzzy c-means clustering. Figure 2.6 represents the actual and predicted RMR from the three types of ANFIS models.

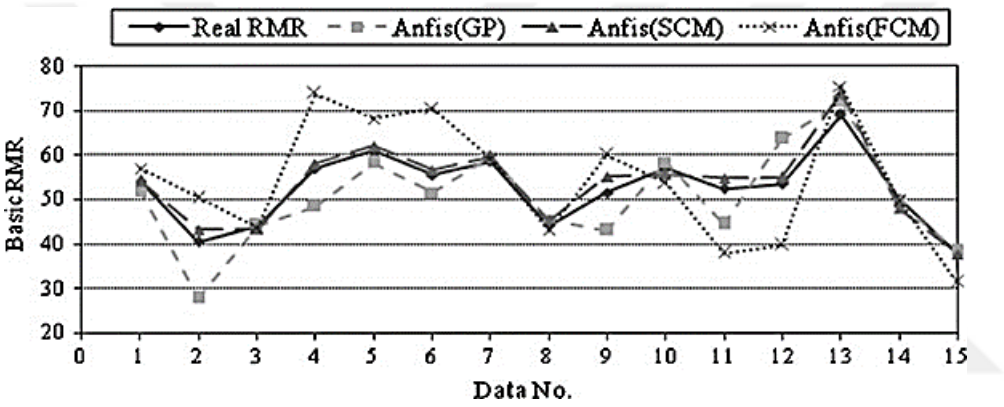


Figure 2.6. Comparison of the determined and predicted $RMR_b$ scores for various types of prediction models (Jalalifar et al., 2011).

W. Chen et al., (2022) designed a new RMR prediction model using an optimized neural network (NN). The system was considered improvement of the performance of tunnel boring machines. The model makes use of optimization logic to train the optimized neural network by updating the weight. The self-adaptive rider optimization (SA-ROA) is then proposed as a new hybrid algorithm in which the updated evaluation is redefined with a new condition and lastly, the performance of the implemented work is validated using state-of-the-art error analysis models.

Gholami et al., (2013) compared RMR scores obtained from the conventional scheme with the machine-learning models. The proposed methods were validated using two case studies from northern Iran. Two robust machine-learning methodologies called relevance vector regression (RVR) and support vector regression (SVR), were used to estimate the RMR for tunnel host rocks. (Martins & Miranda, 2012) used data mining tools to generate new models for estimating the rock deformation modulus and the Rock Mass Rating (RMR). The R programming was used to implement the sophisticated methods and several algorithms such as Regression Trees (RT), Multiple Regression (MR), Artificial Neural Networks (ANN), Support Vector Machines (SVM) and k-Nearest Neighbors (k-NN).

### 2.3.2 Q-Tunneling Index System

Q-Tunneling Index is another widely used classification system for assessing the quality of rock mass specifically in underground openings excavated for mining and tunneling. The system was first proposed in Norwegian Geotechnical Institute in 1974 by Barton et al. The system was created based on approximately 200 tunnel case studies from Norway and Sweden. It is a quantitative classification system and viable to offer support recommendations for underground openings.

Some of the remarkable contributions that the Q system provides in any rock construction are listed below:

1. Identification of the rock mass quality
2. Determination of the stable opening dimensions
3. Estimation of the suitable support configuration.

The Q-tunneling index system is an empirical method that provides more detailed analyses of structural and geological features. The Q score, which is a numerical value in logarithmic scale provides guideline for determination of the design parameters of various support elements. Although the system has a wide

background in underground rock excavations, it may be misleading under different rock mass conditions as it relies on previous case histories. The Q-system comprises of six factors as given in equation 2.2.

$$Q = \frac{RQD}{J_n} \times \frac{J_r}{J_a} \times \frac{J_w}{SRF} \qquad \text{Equation 2.2}$$

where RQD is the Rock Quality Designation; $J_n$ is the joint set number; $J_r$ is the joint roughness number; $J_a$ is the joint alteration number; $J_w$ is the joint water reduction number, and SRF is the stress reduction number.

The Q index and equivalent dimension are two of the factors in determining the support type. Figure 2.7 shows the interpretation chart where Q-values are plotted on the horizontal axis and equivalent dimension is on the vertical axis. The chart is based on empirical data from various cases. The chart represents a range of support classes on a continuous scale for bolt spacing and shotcrete thickness. The support chart also provides detailed information such as the energy absorption, bolt length, and reinforced ribs. In challenging geotechnical conditions, it may be necessary to increase the amount or change the type of support beyond the table's recommendations (NGI, 2015).

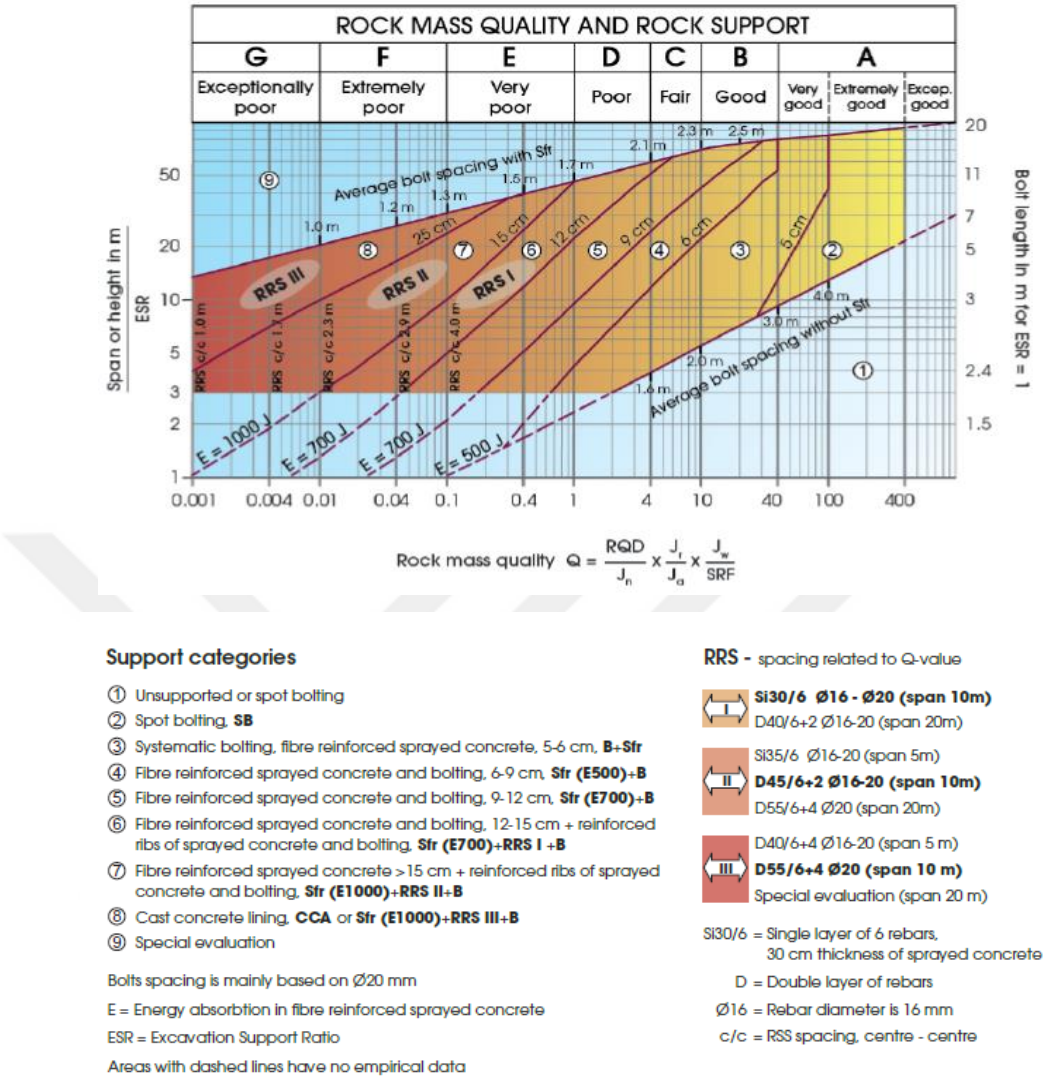


Figure 2.7. Support recommendations table of Q system (NGI, 2015)

Since its introduction, the Q system has not undergone as much significant updates as RMR in the range of rates. The major novelties were proposed with regard to $\sigma_c$ and SRF (Barton, 1995; Grimstad & Barton, 1993). Therefore, Equation 2.6 is adjusted with a normalization factor to calculate a modified $Q_c$.

$$Q_c = \left(\frac{\mathrm{RQD}}{\mathrm{J_n}} \times \frac{\mathrm{J_r}}{\mathrm{J_a}} \times \frac{\mathrm{J_w}}{\mathrm{SRF}}\right) \frac{\sigma_c}{100} \qquad \text{Equation 2.6.}$$

Barton's (1995) further examination of outcomes from various regions worldwide, involving weak and permeable rocks as well as deep samples, has led to the proposed correlations among rock mass quality, seismic velocity, and modulus of deformation as indicated in Figure 2.8.

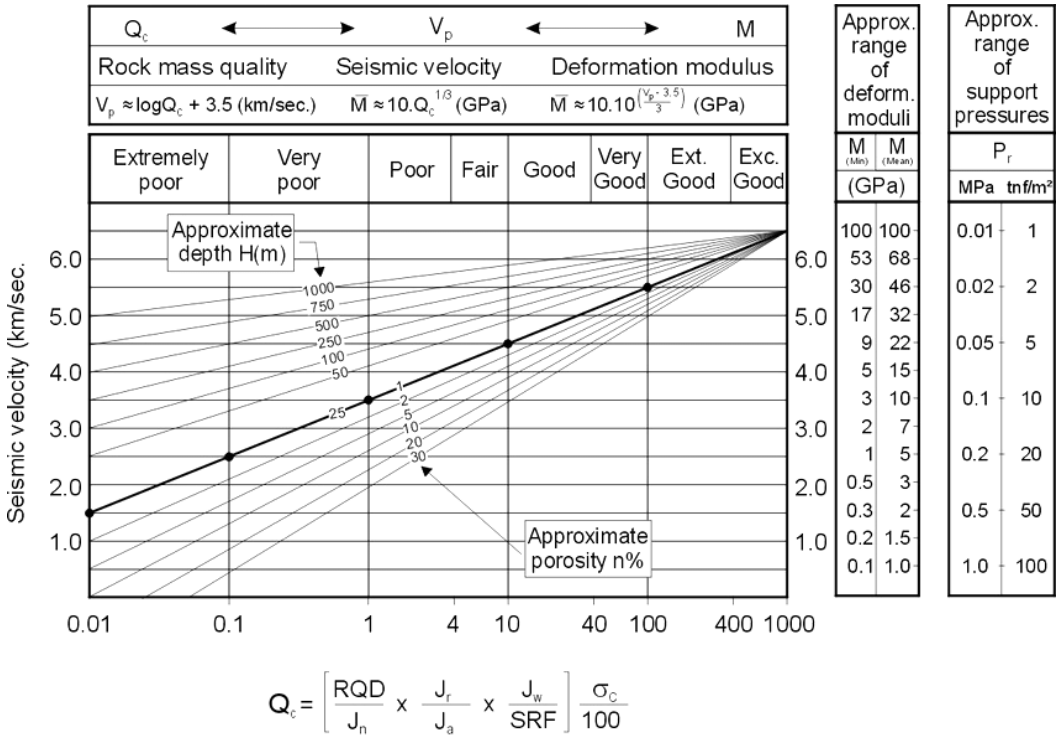


Figure 2.8. The correlations among rock mass quality, seismic velocity, and modulus of deformation (Barton, 1995)

Initially, the maximum value of SRF was 20 for competent rocks under a rock-stress condition (Barton et al., 1974). However, significant changes were made in the characterization of SRF for hard, massive rock in a high-stress environment, resulting in an increase in the SRF rating from 20 to 400 (Grimstad & Barton, 1993). These changes were based on the relationship between RQD/Jn and SRF in hard rock under stress. Low values of $RQD/J_n$ did not experience any real stress problems. The $RQD/J_n$ ratio refers to the relative block size suitable for

differentiating between massive rock that is prone to rock-bursts. The $RQD/J_n$ ratio for rock-burst-prone rock typically ranges from 25 to 200, while a typical jointed rock mass has a ratio of 10 (Barton, 2002).

The Q system has been utilized in the Hoek-Brown failure criterion (Brown & Hoek, 1980), which is a technique used to assess the strength of a rock mass. One of the key benefits of the Q system is that it can detect even small variations in rock properties. Additionally, the Q system's support recommendations consider the span and objective of the excavation, with varying support measures suggested for the excavation's roof, walls, and temporary excavations. The Q system's use in designing support has progressed over time, and the updated version incorporates a support chart with fiber-reinforced shotcrete (NGI, 2015).

### 2.3.3 Limitations of the RMR and Q Systems

The main advantage of using the RMR classification system is its simplicity in application. However, it may not be very effective in detecting small variations in the rock mass quality. Therefore, when designing tunnels, it is important to take into account the behavior of the ground and select appropriate support measures with a clear understanding of the situation (Stille & Palmström, 2008). The RMR system has been utilized in numerous tunnel projects to determine the support or excavation classes. Nonetheless, relying solely on RMR as an indicator may not be adequate, particularly when dealing with in-situ stresses or time-dependent rock properties that are significant factors in rock engineering (Stille & Palmström, 2003). With the progress in classification systems, older forms of rock-mass classification systems may not always align well with new design approaches. In conclusion, the RMR method is often criticized for its lack of sensitivity to small changes in rock quality, and its support recommendations are considered overly cautious and not updated to incorporate new reinforcement techniques (Milne et al., 1998).

The RMR method does not include specific guidelines for selecting support quantities for underground openings with dimensions different from a 10 m span and vertical stress rather than 25 MPa. Thus, users may need to check other empirical guidelines or apply numerical methods to determine the appropriate rock bolt lengths and spacing for tunnel diameters other than 10 m. Numerical or finite element analysis can account for these factors, but it requires more detailed input data and can be computationally intensive.

One major advantage of the Q system is that it was originally developed based on extensively documented case records. However, when compared to the RMR system, it is not as comprehensive in its scope of application. As a result, the support chart provided by the Q system only offers a general recommendation for the support to be used, and this should be adjusted based on practical engineering judgment (Palmström & Broch, 2006). The Q-system support chart relies on both Q value and equivalent dimension ($D_e$) to decide on the necessary level of support. $D_e$ is derived from the tunnel's span and ESR. It is important to consider the safety criteria of the region when determining the ESR value to ensure the safety, as each country has its own standards. The Q system is commonly used in jointed rock formations that are not excessively strained and is most effective for tunnels with $D_e$ measurements between 2.5 and 30 with Q values ranging from 0.1 to 40 (Palmström & Broch, 2006). The Q system does not explicitly account for the actual nature of the rock mass, which is essential in predicting the necessary support measures for dealing with phenomena like popping ground, squeezing, or swelling (Stille & Palmström, 2003).

Using classification systems can facilitate communication and establish correlations in certain geological contexts. However, they should not be the main means of designing primary support. Q index does not provide factual information about the engineering geology of a rock formation. Firstly, the Q index requires a considerable amount of interpretation. Secondly, they are specific to a particular structure at a particular depth (P. J. N. Pells & Bertuzzi, 2007).

Numerical analyses have been increasingly used to enhance the Q-tunneling index system and to provide more accurate support recommendations. The use of numerical simulations can help to evaluate the effects of different rock mass properties such as strength, deformation modulus, and joint spacing, on tunnel stability and support requirements. It can also incorporate a strain criterion to identify the ultimate failure. The Q-tunneling index system does not embrace a strain criterion for determination of the support system. However, numerical analyses allows for the deformation analysis to improve the accuracy of support recommendations in the Q-tunneling index system. In summary, while the Q tunneling index is a useful tool for assessing the stability of the rock mass, it has several weaknesses that require improved.

### 2.3.4 Correlations between RMR and Q systems

The widely used RMR and Q tunneling index have many similarities; however, their unique structure makes them unavailable for direct conversion. Some of the input parameters overlap between the parameters used in the two classification systems, but their range, values and weighting on the overall score varies.

There have been several studies in the past with attempts to develop empirical correlations between the RMR and Q systems. These correlations are often based on statistical analysis of large data from real case studies. Generally, researchers have combined the expert view with the field experience.

Bieniawski (1976) presents the initial association between the RMR and Q systems in terms of linear regression on 111 data identified both in terms of RMR and Q systems for the same rock masses. Equation 2.7 was derived from the case studies in Australia, Europe, North America, South Africa, and Scandinavia as shown in Figure 2.9.

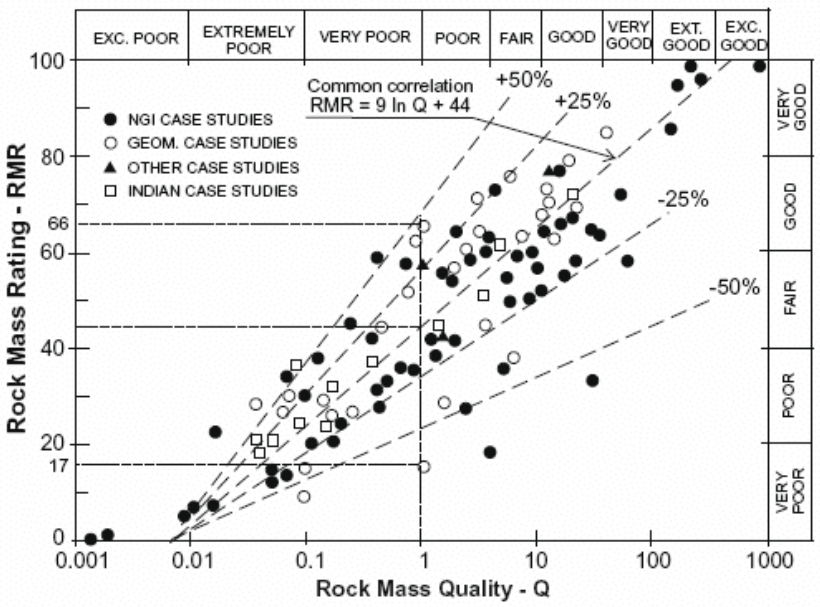


Figure 2.9. Correlation between the RMR and Q scores (Bieniawski, 1989)

$$RMR = 9 \ln Q + 44 \qquad \text{Equation 2.7}$$

Table 2.6 shows other associations between RMR and Q classification systems.

Table 2.6 Empirical correlations between the RMR and Q scores

| Empirical Correlation | Author | Origin of the Study |
|---|---|---|
| $RMR = 9lnQ + 44$ | Bieniawski (1976) | Australia, Europe, North America, South Africa Scandinavia |
| $RMR = 5.9 \ln Q + 43$ $= 13.5 \log Q + 43$ | Rutledge & Preston (1979) | New Zealand |
| $RMR = 5 \ln Q + 60.8$ | Cameron-Clarke & Budavari (1981) | South Africa |

Table 2.6 (continued)

| | | |
|---|---|---|
| $RMR = 5.4 \ln Q + 55.2$<br>$= 12.5 \log Q + 55.2$ | Tallon (1982) | Spain |
| $RMR = 10.5 \ln Q + 41.8$ | Abad et al. (1983) | Spain |
| $RMR = 7.5\ lnQ\ + 42$ | Baczynski (1982) | Australia |
| $RMR = 5.3lnQ\ + 50.81$<br>$= 12.11logQ\ + 50.81$ | Udd & Wang (1985) | Canada |
| $RMR\ = 6.3lnQ\ + 41.61$ | Kaiser et al. (1986) | Canada |
| $RMR = 43.89 - 9.19 \ln Q$ | Tamanes (1984) | Spain |
| $RMR = 10lnQ\ + 39$ | Choquet & Charette (1988) | Canada |
| $RMR = 7lnQ\ + 36$ | Tuğrul (1998) | Türkiye |
| $RMR = 5{,}97lnQ\ + 49.5$ | Sunwoo & Hwang (2001) | South Korea |
| $RMR = 3.7lnQ\ + 53.1$ | Sari & Pasamehmetoglu (2004) | Türkiye |
| $RMR = 6{,}63lnQ\ + 35.53$ | Castro-Fresno et al. (2010) | Spain |
| $RMR = 6{,}7lnQ\ + 45{,}4$ | Lertxundi et al. (2014) | Spain |
| $RMR = 5.614lnQ\ + 49.395$ | Soufi et al. (2018) | Morocco |
| $RMR = 7.5lnQ\ + 41.8$ | Russo & Hormazabal (2019) | Chile |
| $RMR = 6.7InQ + 46.762$ | Bilal et al. (2021) | Pakistan |
| $RMR = 6.63lnQ\ + 32.76$ | Hassanpour et al. (2022) | Iran |

### 2.3.5 Geological Strength Index (GSI)

The Geological Strength Index (GSI), as described by Hoek & Brown (1997) is based on visual observation of rock formations. Following a series of investigations by Hoek et al. (1998), Hoek & Marinos (2000), and Marinos & Hoek (2001) this index was adjusted to be applicable to weak rock masses and to give a more quantitative numerical analysis of the GSI categorization system Sonmez & Ulusay (1999).

Hoek et al., (1995) developed the Geological Strength Index (GSI) to determine variations in rock mass strength under different geological conditions and was included as a parameter in the empirical Hoek & Brown failure criterion for rock mass failure to replace the RMR.

In 1998, Hoek revised the GSI classification system by adding foliated-laminated-sheared and massive/intact rock mass groups. In their studies, Sönmez and Ulusay (1999) proposed the inclusion of two parameters, the 'Structural Rating (SR)' and the 'Surface Condition Rating (SCR)'.

Marinos and Hoek (2001) proposed a new chart for determining GSI scores for heterogeneous rock masses such as flysch. According to this chart, the GSI score is obtained depending on the proportion of shale and siltstone in sandstones. Figure 2.10 indicates the basic chart for GSI in jointed rock masses (Hoek & Marinos, 2000).

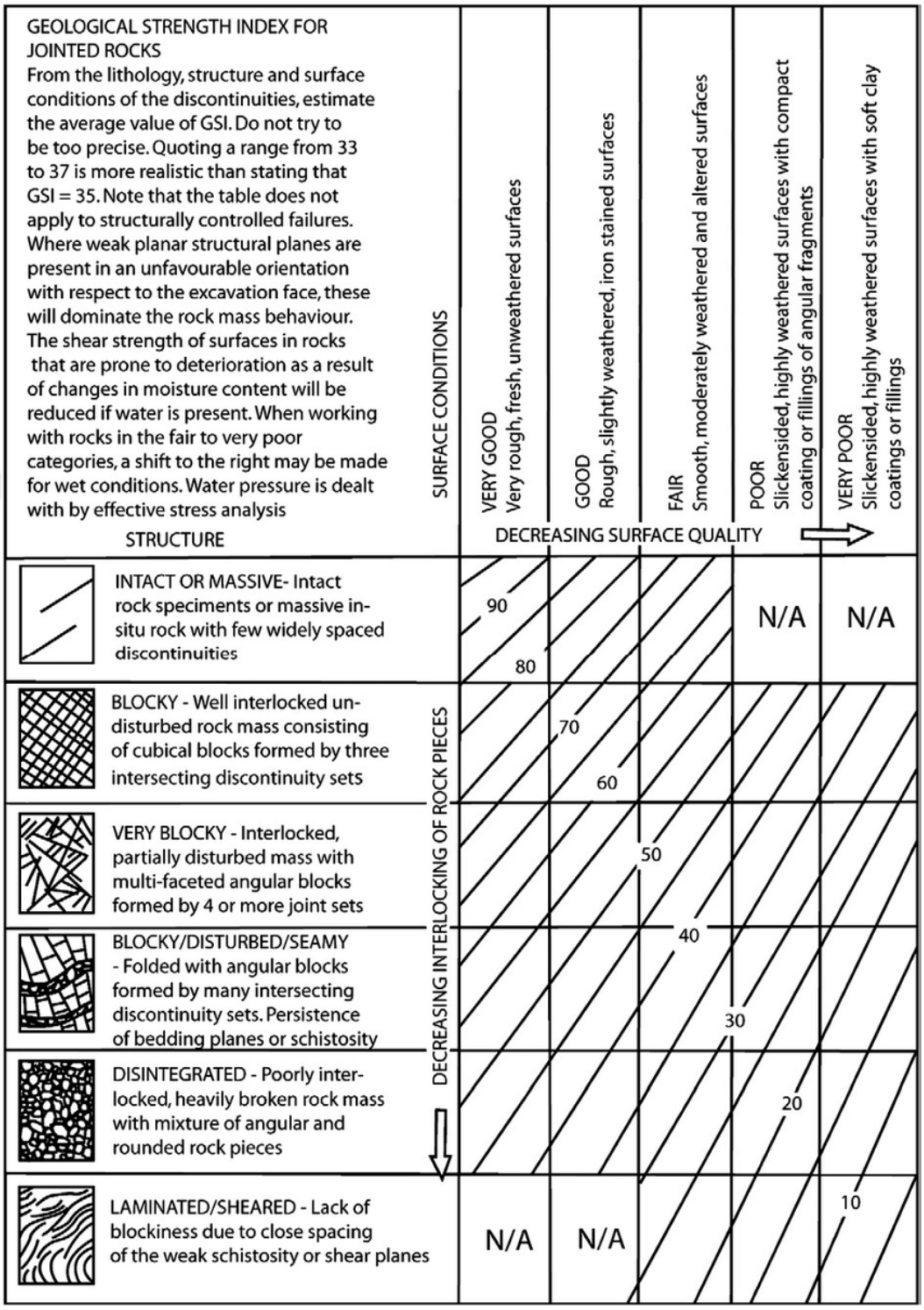


Figure 2.10. Geological Strength Index (GSI) chart (Hoek & Marinos, 2000)

The RMR system can also be used to determine the GSI score. In this situation, the rock mass is assumed to be completely dry, and the orientation of the discontinuities is assumed to be "very favorable." Therefore, when determining the basic RMR score, no correction is made based on the position of the discontinuity planes. The groundwater rating is assumed to be 10 for the $RMR_{76}$ version and 15 for the $RMR_{89}$ version. If the 1976 version of the RMR system is used for GSI calculation, the lowest possible score that can be obtained from the rock mass classification is 18. Thus, if $RMR_{76} > 18$, then GSI can be assumed to be equal to $RMR_{76}$. If the 1989 version of the RMR system is used to determine the GSI value, the lowest possible score that can be obtained from the rock classification is 23. This value is slightly higher than the minimum value in the 1976 version. In this context, if $RMR_{89} > 23$, then Equation 2.8 can be taken

$$GSI = RMR_{89} - 5 \qquad \text{Equation 2.8}$$

Somodi et al., (2021) investigated the conversion equations for determining GSI, which are summarized in Table 2.7. It should be noted that the data used in these expressions mainly applies to rock masses with GSI scores ranging from 30 to 80, and thus the formulas should be used with caution when dealing with low quality rock masses. Specifically, for rock masses with RMR values below 30, Osgoui & Ünal (2005) propose an exponential relationship that is given in Equation 2.9.

$$GSI = 6e^{0.05RMR} \qquad \text{Equation 2.9}$$

where:

RMR= RMR in dry conditions and without correction for fracture orientation,

GSI=Geological Strength Index.

Table 2.7 Formulas that describe the relationships between $RMR_{89}$ and GSI (from (Somodi et al., 2021)

| Rock Mass Type | Equation | Author(s) |
|---|---|---|
| Various | $GSI = RMR - 5$ | Hoek et al. (1995) |
| Sandstones | $GSI = 0.739\,RMR + 12.097$ | Irvani et al. (2015) |
| Metamorphic | $GSI = 0.7393\,RMR - 4.3349$ | J. L. Singh & Tamrakar (2013) |
| Gabbro, ultrabasic | $GSI = 0.9932\,RMR - 4.913$ | Ali et al. (2014) |
| Various | $GSI = 1.2092\,RMR - 18.6143$ | Zhang et al. (2019) |
| Various | $GSI = 1.265\,RMR - 21.49$ | Siddique & Khan (2019) |

## 2.4 Estimation of Geomechanical Properties of Rock Mass

The geomechanical properties of the rock mass are critical in geotechnical engineering as they provide a basis for the stability analyses. Laboratory studies, in-situ measurements, and empirical correlations based on the field and lab data are all used for determination of the rock properties. Laboratory tests such as uniaxial compressive strength, triaxial compression, and direct shear testing aid in determining the strength and stiffness of rocks. When direct testing is not practical or cost-effective, empirical correlations based on geological and geotechnical data are frequently used to estimate the geomechanical parameters. Although mechanical testing proposes the best accuracy, the cost factor and labor intensive practices may drive rock engineers through predictive methods. The common practice is to estimate the compressive strength, tensile strength and elastic modulus,

### 2.4.1 Estimation of the Uniaxial Compressive Strength

The ‘Uniaxial Compressive Strength’ (UCS) depicts the ultimate load capacity of the rock and is extensively used in rock engineering. To determine the UCS in the laboratory, cylindrical specimens undergo uniaxial compression tests following standardized procedures. For irregularly shaped rock specimens indirect index tests may provide an approximate value. Several researchers have established relationships between the UCS and measurable parameters such as the indentation of a geological hammer or point load strength index (Is) (Vračević et al., 2019).

Physical and index tests typically require very brief or even no sample preparation, which makes them feasible to develop empirical equations to correlate their results with the UCS. There exist several empirical equations in the literature that estimate UCS using inputs such as the Is, Schmidt Hammer Rebound index (SRH), Block Punch Index (BPI), Effective Porosity (n), and Density (d) (Aladejare, 2020).

Dinc et al. (2011) indicated the difficulty of preparing laboratory specimens that accurately represent the rock mass due to the inherent discontinuity patterns present in the rock mass. Therefore, researchers have turned their attention to developing empirical equations that estimate the stress-strain behavior of the rock mass. Various empirical equations have been proposed in the literature to estimate the UCS of a rock mass relying on RMR, GSI, and Q scores. Table 2.8 presents a compilation of empirical relationships proposed by different researchers to estimate the UCS based on indirect experimental data.

Table 2.8 Empirical relations to estimate the Uniaxial Compressive Strength (UCS)

| **Input Data** | **Empirical Regression Equation** | **Reference Authors** |
|---|---|---|
| Point Load Test Index Is (50)<br><br>UCS: for intact rocks | $UCS = 23.7 \times Is\,(50)$ | Broch & Franklin (1972) |
| | $UCS = 23 \times Is\,(50)$ | Bieniawski (1975) |
| | $UCS = 16.5 \times Is\,(50) + 51$ | Gunsallus & Kulhawy (1984) |
| | $UCS = 16 \times Is\,(50)$ | Ghosh & Srivastava (1991) |
| | $UCS = 23.7 \times Is\,(50)$ | Singh & Singh (1993) |
| | $UCS = 19 \times Is\,(50) + 12.7$ | Ulusay et al. (1994) |
| | $UCS = 12.5 \times Is\,(50)$ | Chau & Wong (1996) |
| | $UCS = 14.3 \times Is\,(50)$ | Smith (1997) |
| | $UCS = 15.25 \times Is\,(50)$ | Tuğrul & Zarif (1999) |
| | $UCS = (14.5 \div 27) \times Is\,(50)$ | Romana (1999) |
| | $UCS = 8.41 \times Is\,(50) + 9.51$ | Kahraman (2001) |
| | $UCS = 15.31 \times Is\,(50)$ | Ulusay et al. (2001) |
| | $UCS = 23 \times Is\,(50)$<br>$UCS = 7.3 \times Is\,(50)^{1.71}$ | Tsiambaos & Sabatakakis (2004) |
| | $UCS = 9.08 \times Is\,(50) + 39.32$ | Fener et al. (2005) |
| | $UCS = 10.22 \times Is\,(50) + 24.31$ | Kahraman et al. (2005) |
| Schmidt Rebound Hammer (SRH) UCS: for intact rocks | $UCS = 13.4 \times Is\,(50)$ | Agustawijaya (2007) |
| | $UCS = 8.2 \times Is\,(50) + 36.43$<br>$UCS = 18.45 \times Is\,(50) - 13.63$<br>$UCS = 29.77 \times Is\,(50) - 51.49$<br>$UCS = 10.92 \times Is\,(50) + 24.24$ | Kahraman & Gunaydin (2009) |
| | $UCS = 11.103 \times Is\,(50) + 37.659$ | Basu & Kamran (2010) |
| | $UCS = 21.69 \times Is\,(50)$ | Tahir et al. (2011) |

Table 2.8 (continued)

| | | |
|---|---|---|
| | $UCS = 14.63 \times Is\,(50)$ | Mishra & Basu (2012) |
| | $UCS = 17.6 \times Is\,(50) + 13.5$ | Aliyu et al. (2019) |
| | $UCS = 0.99 \times SRH - 0.38$ | Haramy & DeMarco (1985) |
| | $UCS = 4.85 \times SRH - 76.18$ | O'Rourke (1989) |
| | $UCS = 4.29 \times SRH - 67.52$ | Sachpazis (1990) |
| | $UCS = 18.17 \times e^{(0.02\rho SRH)}$ | Cargill & Shakoor (1990) |
| | $UCS = 0.0001 \times SRH^{3.2658}$ | Gokceoglu 1996) |
| | $UCS = 8.36 \times SRH - 416$ | Tuğrul & Zarif (1999) |
| | $\ln UCS = 0.067 \times SRH \pm 0.231$ | Katz et al. (2000) |
| | $UCS = \exp(0.818 + 0.059 \times SRH)$ | Yılmaz & Sendir (2002) |
| | $UCS = 1.45 \times e^{0.07SRH}$ | Aydin & Basu (2005) |
| | $UCS = 0.0137 \times SRH^{2.27210}$ | Kılıç & Teymen (2008) |
| | $UCS = 0.64 \times SRH + 37.5$ | Gupta (2009) |
| | $UCS = 0.0682 \times SRH + 57.973$ | Yurdakul et al. (2011) |
| | $UCS = 12.83 \times e^{0.0487SRH}$ | Nazir et al. (2013) |
| $UCS_i$, RMR, $N_k$, $J_p$, GSI, Q<br>$UCS_i$: for intact rock<br>$UCS_{RM}$: for rock mass | $UCS_{RM} = UCS_i \sqrt{s}$ (s=$e^{\frac{RMR-100}{9}}$) | Hoek & Brown (1980) |
| | $UCS_{RM} = UCS_i \exp(7.65\frac{RMR-100}{100})$ | Yudhbir et al. (1983) |
| | $UCS_{RM} = UCS_i \exp(\frac{RMR-100}{18.5})$ | Ramamurthy (1986) |
| | $UCS_{RM} = UCS_i \exp(\frac{RMR-100}{24})$ | Kalamaras & Bieniawski (1995) |
| | $UCS_{RM} = UCS_i \times Jp$ | Palmström (1995) |
| | $UCS_{RM} = UCS_i \exp(\frac{RMR-100}{20})$ | Sheorey (1997) |
| | $UCS_{RM} = 0.0016 \times RMR^{2.5}$ | Aydan et al. (1997) |

Table 2.8 (continued)

| | | |
|---|---|---|
| | $UCS_{RM} = UCS_i \left(\frac{RMR}{RMR + \beta(100 - RMR)}\right) \beta$ $= 6$ | Aydan & Dalgic (1998) |
| | $UCS_{RM} = UCS_i \left[\exp\left(\frac{GSI100}{9}\right)\right]^a$ | Hoek et al. (2002) |
| | $UCS_{RM} = UCS_i\, e^{\frac{GSI-100}{9-3D}\left[\frac{1}{2}+\frac{1}{6\left(e^{-\frac{GSI}{15}}-e^{-\frac{20}{3}}\right)}\right]}$ | Hoek et al. (2002) |
| | $UCS_{RM} = 5\rho\left(Q\frac{UCS_i}{100}\right)^{\frac{1}{3}}$ | Barton (2002) |
| | $UCS_{RM} = UCS_i\ \alpha(\frac{1+\log(N_k)^{\frac{i}{f}}}{1+\log(N_k)^i})$ | Vardar (2005) |

α: ratio of reducing strength of rock according to anisotropic loading condition ($0.2 \leq \alpha \leq 1$), $UCS_{RM}$ and $UCS_i$: uniaxial compressive strength of rock mass and intact rock material, respectively, RMR: Rock Mass Rating, GSI: Geological Strength Index, a: curvature constant of Hoek and Brown criterion i:number of inhomogenity, f: number of Strength Reducing value ($3 \leq f \leq 40$), Nk: number of rock pieces affected in the construction area(rock element number), JP: joint parameter, Q:rock mass quality, ρ:density, s:rock mass constant.

### 2.4.2 Estimation of the Tensile Strength

The tensile strength is another feature of the rock mass that determines the excavation support systems and the stability of the surrounding rocks. Direct testing of the rock mass tensile strength is difficult due to the complexity of the required test set up. Alternatively, there are various methods in the lab scale to determine the tensile strength and project the values to the rock mass scale.

The tensile strength is an indicator of the roof stability in an underground opening. Direct tensile test, indirect (Brazilian) tensile test, and bending tests can be used to assess the tensile strength of intact rocks. Considering the influence of inherent fractures such as microcracks and mineralogical composition of the rock mass in the tensile strength can be an essential part of the interpretation. Performing several tests using different techniques can be posed as a strategy to minimize the risk of uncertainty.

Considering the size effect in lab scale tests and difficulty of field scale experiments, predictive methods come up as a plausible alternative that relies on statistical analysis of data obtained from laboratory tests or in situ measurement. Table 2.9 shows some common empirical approaches for determining the tensile strength.

Table 2.9 Prediction of the rock tensile strength

| **Input Data** | **Empirical Equation** | **Reference Authors** |
|---|---|---|
| UCS (Rock mass compressive strength) | $\sigma_{tm} = \frac{UCS_{rm}}{8}$ | Griffith (1921) |
| P, D, t;<br>P (The maximum load),<br>D (Diameter of the rock specimen)<br>t (thickness of the rock specimen) | $\sigma_t = \frac{0.636P}{Dt}$ | Fairhurst (1964) |

Table 2.9 (continued)

| | | |
|---|---|---|
| s, $\sigma_{ci}$, $m_b$<br>$\sigma_{ci}$ is the uniaxial compressive strength (UCS) of the intact rock sample, s and $m_b$ rock mass constants | $\sigma_{tm} = 0.5\sigma_{ci}\left[m_b - (m_b{}^2 + 4s^{\frac{1}{2}})\right]$ | Hoek & Brown (1980) |
| s, $\sigma_{ci}$, $m_b$<br>$\sigma_{ci}$ (Uniaxial compressive strength of the intact rock sample),<br>s and $m_b$ are rock mass constants | $\sigma_{tm} = \frac{s\sigma_{ci}}{m_b}$ | Hoek et al. (2002) |
| UCS (Rock mass compressive strength) | $\sigma_{tm} = \frac{UCS_{rm}}{13}$ | Exadaktylos (2005) |
| $\sigma_t$, RMR<br>$\sigma_t$ (Tensile strength of intact rock<br>RMR (Rock mass rating) | $\sigma_{tm} = \sigma_t(\frac{RMR}{RMR + 6(100 - RMR)}$ | Tokashiki & Aydan (2010) |
| $P_a$, Is50, N, $\gamma$, $\gamma_w$<br>Is50 (Point load index),<br>N (Schmidt rebound number),<br>$\gamma$ (Unit weight),<br>$P_a$ (Air pressure),<br>$\gamma_w$ (Unit weight of water, kN/m$^3$) | $\sigma_t = P_a\left(\frac{1.58\,Is50}{P_a} - 0.443N + 26.22\frac{\gamma}{\gamma w} - 78.12\right)$ | Gurocak et al. (2012) |
| UCS (Uniaxial compressive strength of intact rock, MPa) | $BTS = \frac{UCS - 24.30}{4.87}$ | Karaman et al. (2015) |
| BTS (Brazilian Tensile Strength, MPa) | $BTS = \frac{UCS}{14.035}$ | Ribeiro et al. (2016) |
| C (cohesion, MPa) | $\sigma_t = \frac{c - 10.44}{2.438}$ | Shen & Jimenez (2018) |

### 2.4.3 Estimation of Elastic Modulus

Elastic modulus, also known as Young's modulus, is an important parameter in mechanics that defines the elastic behavior of the material under load. The elastic modulus is typically measured experimentally in the lab through static and dynamic deformability tests. Alternatively, field scale testing may provide more accurate results.

In case there is no specimen suitable for testing in the lab and in-situ tests are not viable, empirical correlations are commonly used to predict the parameter based on the material's density and strength properties. These correlations are often developed from a large database of experimental data and can provide reasonably accurate estimates of the deformation modulus for a wide range of materials. Another approach is to use theoretical models based on the microstructure of the material. For example, the deformation modulus of a composite material can be estimated using models based on the properties of the constituent materials and their arrangement within the composite.

It is important to note that the accuracy of any estimation method will depend on the specific properties of the material being considered and the quality of the available data. Therefore, it is always recommended to validate any estimated values of the deformation modulus through additional laboratory testing.

Moreover, the rock mass elastic modulus is an important parameter in stability analyses. Determining this parameter in the field is quite difficult. Therefore, a series of studies have been carried out to develop a method for estimating this value depending on the rock classification systems. Bieniawski (1978), who analyzed various problems encountered in excavations, proposed the following correlation for estimating the rock mass deformation modulus in GPa for intact rock mass with RMR>50 (equation 2.10).

$$E_{rm} = 2RMR_{76} - 100 \qquad \text{Equation 2.10}$$

where; $E_{rm}$ is the rock mass modulus, RMR is the rock mass rating.

Based on the analysis of sample excavations including the deformation modulus of dam foundations, which are evaluated through the back analysis method, Serafim and Pereira (1983) suggested the equation 2.11 as a relationship between $E_{rm}$ and RMR. Figure 2.11 depicts the correlation between the elastic modulus of rock mass and RMR score based on the Serafim, Pereira and Bieniawski's theories.

$$E_{rm} = 10^{\frac{(RMR-10)}{40}} \qquad \text{Equation 2.11}$$

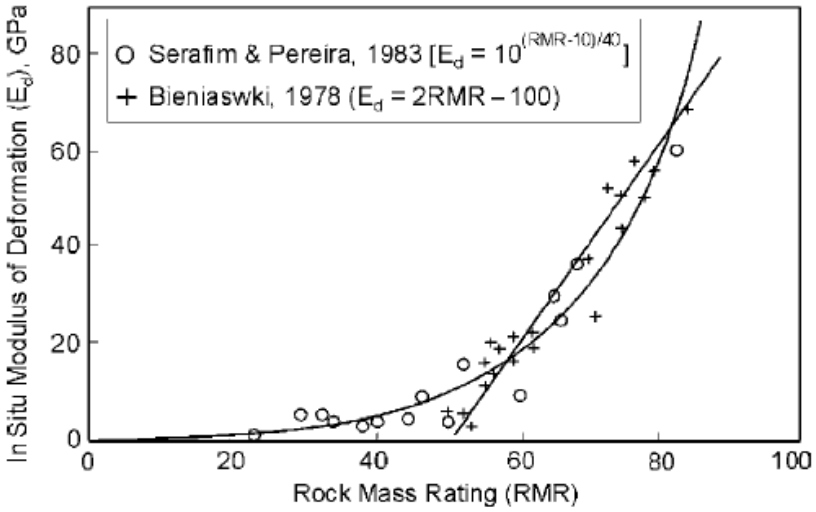


Figure 2.11. Correlation between the elastic modulus of rock mass and RMR score (Bieniawski, 1984)

Table 2.10 shows the suggested correlations between the elastic modulus of the rock mass and the common rock mass classification systems apart from the above-mentioned equations.

Table 2.10 Empirical relations between the rock mass quality and the elastic modulus of rock mass

| **Equation** | **Author** |
|---|---|
| $E_{rm} = c\ logQ$ (GPa) for Q>1 | Barton et al. (1981) |
| $E_{rm} = 25\ logQ$ (GPa) | Grimstad & Barton (1993) |
| $E_{rm} = 10Q^{\frac{1}{3}}$ (GPa) | Barton (1995) |
| $E_{rm} = 0.1\left(\frac{RMR}{10}\right)^3$ (GPa) | Mitri (1995) |
| $E_{rm} = 5.6RMi^{0.3}$ (GPa) (for RMi>0.1) | Palmström (1996) |
| $E_{rm} = e^{(4.407+0.081\times RMR)}$ (GPa) | Jašarević & Kovačević (1996) |
| $E_{rm} = 0097RMR^{3.54}$ (MPa) | Aydan et al. (1997) |
| $E_{rm} = 10^{(\frac{GSI-10}{40}}\sqrt{\frac{\sigma_{ci}}{100}}$ (GPa) | Hoek & Brown (1997) |
| $E_{rm} = 7(\pm(3)\sqrt{10^{\frac{RMR-44}{21}}}$ (GPa) | Diederichs & Kaiser, (1999) |
| $E_{rm} = \left(1-\frac{D}{2}\right)\sqrt{\frac{\sigma_{ci}}{100}10^{\left(\frac{GSI-10}{40}\right)}}$ (GPa) (for $\sigma_{ci}$ <100 MPa) | Hoek et al. (2002) |
| $E_{rm} = 10\left(Q\frac{\sigma_{ci}}{100}\right)^{\frac{1}{3}}$ (GPa) | Barton (2002) |
| $E_{rm} = 10^{\frac{15logQ+40}{40}} + 40$ (GPa) for Q<1 RMR<50 | Barton (2002) |
| $E_{rm} = 0.135\ \left[E_i\ 1 + \frac{1}{WD}\frac{RQD}{100}\right]^{1.1811}$ (GPa) | Kayabasi et al. (2003) |
| $E_{rm} = 0.0876RMR + 1.056(RMR-50) +$ $(0.015(RMR-50)^2$ (GPa) for RMR≤50<br><br>$E_{rm} = 0.0876RMR$ (GPa) (for RMR>50) | Galera et al. (2005) |
| $E_{rm} = 100\ \frac{(1-0.5D)}{1+e^{\left(\frac{75+25D-GSI}{11}\right)}}$ (GPa) | Hoek & Diederichs (2006) |
| $E_{rm} = 0.058e^{0.0785\ RMR}$ (GPa) | Alemdag et al. (2015) |

## 2.5 Rock Support Design

A universally accepted method for determining rock support design does not exist due to the fact that each design is tailored to the particular circumstances of the rock mass and adheres to national regulations and expertise. The intricate configuration resulting from the material and underground openings makes this process highly complex (Hoek, 1991). Prediction and evaluation of the suitable support for underground openings mostly rely on the perceptions, proficiency and subjective opinions of individuals engaged in tunnel construction, as stated by Brekke and Howard (1972). This section presents the underground openings support types and briefly presents the support design criteria.

### 2.5.1 Common Support Types used in Underground Mining Openings

In the past, timber was the frequently used material for support due to its viability, strength and capacity to handle deformation under stress. Typically, timber has been broadly used to provide support in coal mines, including those that are shallow, since the rocks associated with coal measures are weak and require roof support. In the context of hard rock mines, this has not consistently been the situation, as the more robust rock types typically allow for safe, self-supporting openings, especially in shallow depths. However, wood's load-deformation traits make it a suitable material for supporting mines, as it can still bear loads even when strained to high levels and even after failing. The herringbone system was an initial application of wood for tunnel support and led to the creation of steel arch support. Timber support requires substantial skill sand considerable time and effort to complete the support operations (Reid et al., 1952).

When working in densely fractured ground conditions, significant quantity of wood was necessary, and even then, such support was typically unsatisfactory due to the significant voids that were inevitably left. However, the implementation of rolled steel joists played a significant role in decreasing the amount of time, effort, and

skill required to build mine roadway supports. The switch from timber to steel supports in mine openings and roadways led to a substantial increase in safety (Whittaker, 1986).

In most modern mines of developed countries, wood is seldomly utilized as the primary form of tunnel support. Instead, steel sets and rockbolts are the most widely implemented forms of support in mine excavations. Besides, concrete and/or shotcrete supported openings are typically reserved for specific situations rather than serving as a general technique for tunnel lining. Table 2.11 shows the different sorts of mine excavation supports, which are generally used and illustrates briefly the application of different support types with remarks on the operational aspects and geological situations.

Table 2.11 Overview of primary support methods utilized in mining excavations (Hoek, 2007; Jovičić et al., 2009; Whittaker, 1986)

| **Support type** | **Field of Application** | **Characteristics** |
|---|---|---|
| 1- The inherent support provided by rock formations | 1- Constrained to stable rock formations under low in situ stress conditions. | 1- Mesh may be put in place in certain hard rock mines with the help of rock bolts to prevent the detachment and spalling of blocks and slabs. However, in such conditions, the bolts are not necessarily acknowledged as a support system. |
| | 2- Often utilized in various mining conditions related to metallic and evaporite deposits. | |

Table 2.11 (continued)

| | | |
|---|---|---|
| 2-Rock Reinforcement / Rock Bolting | 1- Hard rock mining conditions where mechanical anchor bolts are utilized | 1- A vast array of bolt types has been created to address various mining issues and geological situations, such as Swellex bolts, split sets, cable bolting, and so on |
| | 2- To enhance stability in weaker rock conditions, bonded bolts encompassing the entire column are utilized. | |
| | 3- Appropriate for systematically pillar mined rectangular roadways and chambers. | 2- Meshing and/or shotcrete are frequently used in combination with it to reinforce unstable roof conditions. |
| | 4- It is employed as an additional support in combination with steel sets. | 3- A widely used method for supporting mine tunnels on a global scale. |
| | 5- Truss bolting is suitable for stable rock formations. | 4- Bolts that are not bonded to columns may be susceptible to issues with corrosion, installation, and performance. |
| | 6- It is appropriate for roadway and face development in longwall retreat mining. | |

Table 2.11 (continued)

| | | |
|---|---|---|
| 3- Steel Sets | 1- They have gained popularity globally in coal mines due to their ability to operate without depth limitations and in areas with significant yield zones. | 1- Steel exhibits advantageous behavior after yielding, in that the steel section usually does not fail entirely under high loads but forms a plastic hinge, which reduces the support's strength but does not typically lead to complete failure under normal mining deformations. |
| | 2- Ideal for longwall mining operations where the use of rock bolts is impractical. | |
| | 3- Steel sets have proven to be effective in a variety of conditions and are suitable for long-term use in large-scale arrangements tailored to specific strata conditions. | 2- The behavior of a support system is influenced by its auxiliary components, such as connecting plates, struts, and the deformation of stilts. |
| | 4- Successfully utilized versions of both rigid and yielding types are available. | 3- Can be used for various types of tunnel shapes and sizes. |

Table 2.11 (continued)

| | | |
|---|---|---|
| 4-Concrete/Shotcrete Supports | 1- The mining industry has utilized segmental, monolithic, and shotcrete support methods. | 1- The weight and size of segmental concrete supports pose handling and transportation challenges, particularly in confined mine tunnel spaces, which makes them relatively difficult to manage and transport. |
| | 2- The use of monolithic concrete is prevalent in the mining industry for constructing the bottom areas of shafts where they are far away from stresses induced by mining activities. | 2- The proper functioning of this support system is heavily reliant on the quality of backfilling, which can be challenging to achieve in fractured rock formations. |
| | 3- Advantages gained from the stability provided by the shaft pillar. | 3- Monolithic concrete is easier to transport but has limited applications as it does not provide much yield once constructed |
| | 4- Can be readily adjusted to suit larger cross-sectional areas. | 4- Concrete supports can pose challenges for repair work if they fail because of their considerable physical size and weight. |

Table 2.11 (continued)

| | | |
|---|---|---|
| 5-Fibre reinforced shotcrete/concrete | 1- Steel fiber reinforced concrete has become widely accepted around the world as a viable alternative to conventional wire mesh reinforced plain shotcrete. | 1 Spraying steel fiber reinforced concrete can be a more challenging task as the fibers have a tendency to clog the pressure lines. |
| | 2- the use of fibre-concrete lining resulted in a faster reduction of initial deformations. | |
| | 3- The fiber-concrete lining remained capable of bearing load even after experiencing significant deformations, because of its high ductility and relatively high post-crack strength. | 2- A high chance of localized failures occurring before the sprayed concrete reaches its full strength. |

### 2.5.2 Shotcrete/Concrete Support Systems

Concrete and/or shotcrete is the most common material used for underground excavations in rock; yet there have been situations where it has been successfully used to generate tunnels through altered cohesionless, and loose soils. Common underground shotcrete applications include diverting water flows, designing temporary support and permanent linings, and enhancing or replacing traditional support materials like lagging and steel sets (US Army Corps of Engineers, 1996).

Tunnel support is often achieved by Spraying shotcrete on the rock surface. Shotcrete has been used for a long time as a support measure and is becoming more and more popular due to its advantages, including its high tensile capacity and adaptability (Palmström & Nilsen, 2000).

The main benefits of applying shotcrete to support rocks are (Palmström & Nilsen, 2000):

- Ready to use quickly (batching plant on site);
- Applicable in rough excavation profile
- Easy to integrate with various support systems;
- Flexible deformation qualities.

The principal drawbacks are:

- It can collapse when used on rock types that swell (can be enhanced by combining fibers or reinforced with casting steel);
- It has low tensile strength (which can be increased by combining fibers or reinforced with steel casting);
- It is difficult to apply to sedimentary rock types with little cohesiveness.

Shotcrete can support rocks in a variety of ways.

1. Regular shotcrete, sprayed in layers as thick as 60 to 100 mm.
2. Shotcrete reinforced with mesh. This is created by spraying a layer of concrete first, then installing a mesh made of steel bars with a typical diameter of 5 to 6 mm. The mesh is then completely covered by a second layer, and occasionally much more.
3. Shotcrete with fiber reinforcement. The wet concrete is blended with steel or plastic fibers.
4. When used with steel beams, lattice girders, or ribs. All the aforementioned techniques are frequently combined with rock bolts to secure loose blocks, wire mesh, or steel sets (Palmström & Nilsen, 2000).

In the context of support, structural components are included to reduce excessive displacements near the excavation's boundary, such as steel arches or concrete rings. Support systems modify the boundary conditions of the underground opening but does not directly increase the rock mass's inherent strength as shown in Figure 2.12 (Hudson & Harrison, 1997). The maximum support that shotcrete can maintain and stiffness depends on the unconfined compressive strength (MPa), Young’s modulus (MPa), Poisson’s ratio, and thickness of the shotcrete (m).

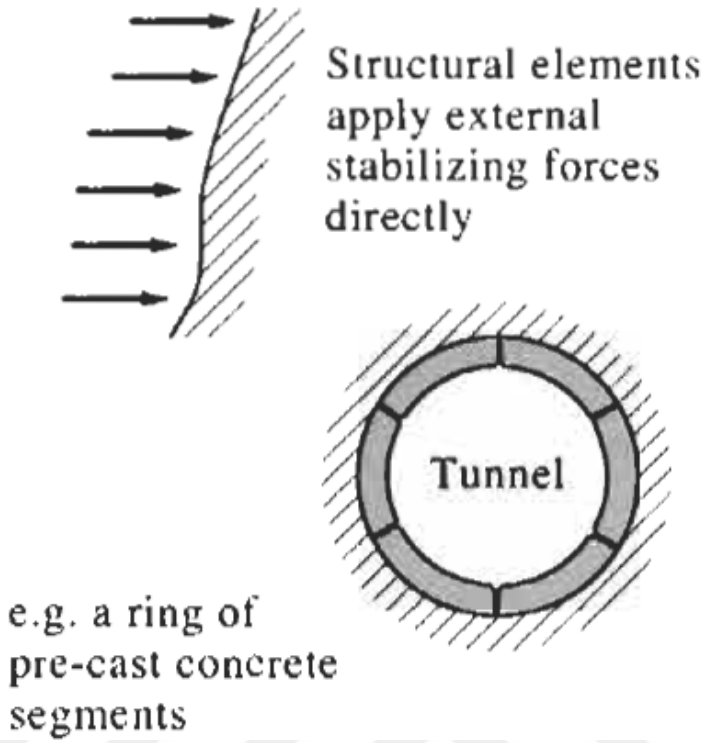


Figure 2.12. Principles of rock support (Hudson & Harrison, 1997)

### 2.5.3 Rock Reinforcement Systems/ Rock Bolts

Rock bolt systems are commonly used in underground mining to provide support for excavations and other underground structures. The system typically consists of a steel bolt that is inserted into a hole drilled into the rock, along with a steel plate or other hardware that is used to secure the bolt in place. The sketch in Figure 2.13 represents the mechanically anchored bolts installed in the rock mass surrounding a circular tunnel of radius R.

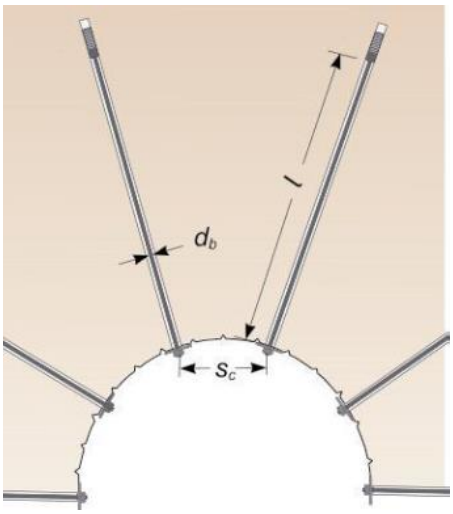


Figure 2.13. A sample ungrouted mechanical-anchored bolt (Hoek, 2008) where $d_b$ is the diameter and $s_c$ is the spacing between the bolts or cables installed in the cross-section.

The maximum support pressure and the stiffness of a rock bolt (its ability to resist deformation under load) provided by rock bolt systems depend on the ultimate strength, length, diameter and spacing of rock bolts, elastic modulus of rock bolt and load deformation characteristics. To explain the process of determining the constants for the ultimate strength ($T_{bf}$) and load deformation characteristics (Q) through bolt testing, the diagram presented in Figure 2.14 can be considered. This diagram depicts the outcomes of a pull-out test conducted by Stillborg (1994). The test involved a mechanically anchored bolt with a diameter of 16 mm and a length of 3 m, which was installed in a concrete block with a compressive strength of $\sigma_{cc}$ = 60 MPa. In the diagram, the line labeled OE represents the elastic deformation measured at the wall of the concrete block. This measurement encompasses the combined deformation of various components, including the shank, plate, anchor, nut and washer.

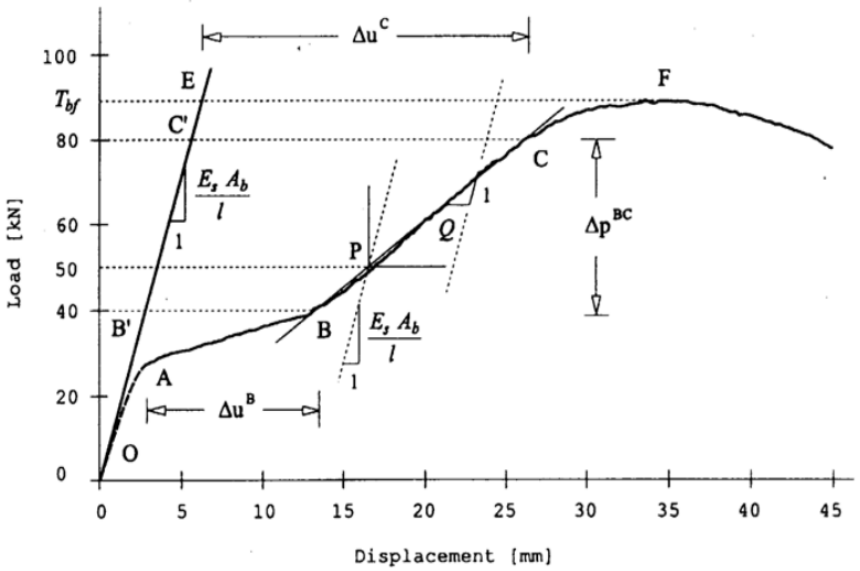


Figure 2.14. Results of a pull-out test performed on a mechanically anchored bolt (Stillborg, 1994).

The rapid displacement observed in the AB segment of the curve is linked to the initial flexibility of the plate, nut and washer assembly. The steeper BC section corresponds to the deformation of the bolt shank and the anchor. When reaching point C on the curve, the bolt begins to exhibit yielding, and at point F, it eventually fails. Point F in Figure 2.14 establishes the fixed value for the ultimate strength of the rock bolt, denoted as $T_{bf}$. In practical applications, the bolt is typically pre-tensioned during installation to prevent the initial flat segment AB, which corresponds to the compliance of the plate and its associated components.

Ideally, the determination of $T_{bf}$ and Q is based on pull-out tests conducted directly on bolts installed in their actual rock environment. The obtained values vary depending on the specific rock type and the mechanical properties of the tested bolt. Reference values for $T_{bf}$ and Q, obtained from tests performed on various rock types, are listed by Brown and Hoek (1980). Table 2.12 provides a selection of these values.

Table 2.12 Ultimate strength and load deformation characteristics of typical rockbolts (modified from Brown & Hoek, 1980)

| Bolt Diameter (mm) | Bolt Length (m) | Anchor Type | Rock Type | $T_{bf}$ (MN) | Q (m/MN) |
|---|---|---|---|---|---|
| 16.0 | 1.2 | Expansion Shell | Good Rock | 0.049 | 0.160 |
| 16.0 | 1.8 | Expansion Shell | Shale | 0.058 | 0.241 |
| 16.0 | 1.2 | Expansion Shell | Unknown | 0.04 | 0.053 |
| 16.0 | 1.2 | Expansion Shell and Resin | Unknown | 0.062 | 0.030 |
| 19.0 | 1.2 | Expansion Shell | Good Rock | 0.051 | 0.126 |
| 19.0 | 1.8 | Expansion Shell | Unknown | 0.089 | 0.024 |
| 19.0 | 1.8 | Expansion Shell and Resin | Unknown | 0.098 | 0.029 |
| 19.0 | 3.0 | Slotted Bolt and wedge | Unknown | 0.098 | 0.074 |
| 22.0 | 3.0 | Expansion Shell | Gneiss | 0.214 | 0.032 |
| 22.0 | 3.0 | Expansion Shell | Sandstone | 0.196 | 0.042 |
| 22.0 | 3.0 | Expansion Shell | Sandy Shale | 0.122 | 0.069 |
| 22.0 | 3.0 | Expansion Shell | Shale | 0.058 | 0.126 |
| 25.4 | 6.0 | Expansion Shell | Massive Gneiss | 0.323 | 0.051 |
| 25.4 | 1.8 | Expansion Shell | Granite | 0.254 | 0.143 |
| 25.4 | 1.9 | Resin Anchor | Granite | 0.285 | 0.018 |
| 25.4 | 1.2 | Slotted Bolt and wedge | Good Rock | 0.089 | 0.064 |
| 25.4 | 1.8 | Resin Anchor | Shale | 0.160 | 0.020 |

Stillborg (1994) also conducted a series of experiments on rockbolts and dowels installed across a simulated joint, employing two blocks of reinforced concrete with high strength. This testing method provides a more accurate representation of the conditions encountered in underground settings compared to a standard pull-out test. The rockbolts and dowels were installed in holes drilled by percussion techniques, replicating the installation methods used in typical underground mining operations. The installed support systems were subjected to a test where the two concrete blocks were pulled apart at a fixed rate, and the displacement across the

simulated joint was measured. The outcomes of Stillborg's tests are summarized in Figure 2.15, presenting load deformation curves for all the tested bolts and dowels (Hoek, 2007).

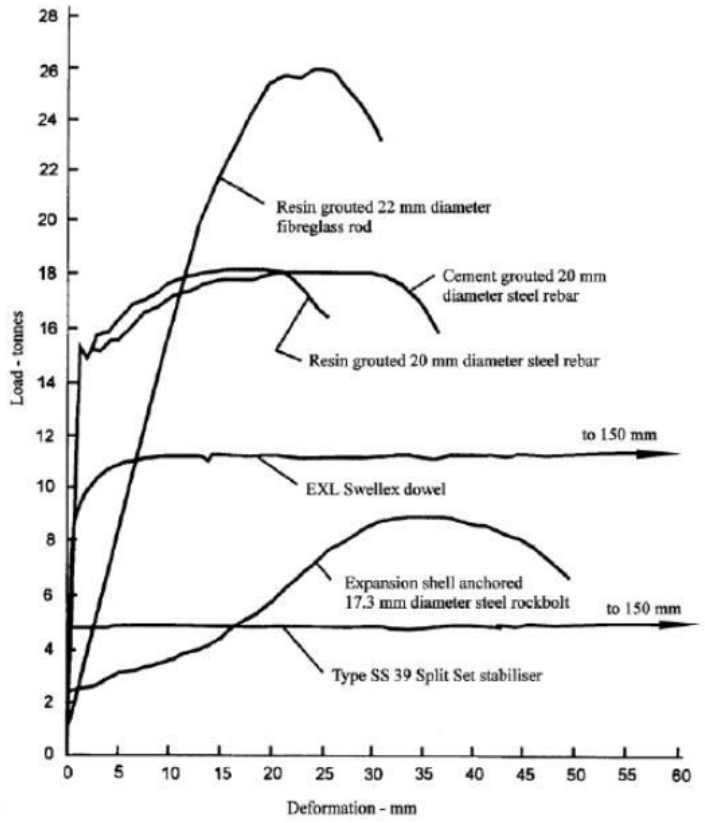


Figure 2.15. The experiments involved using high strength reinforced concrete blocks with a uniaxial compressive strength of 60 MPa. To simulate real rock conditions, the holes were drilled using a percussion rig. (Stillborg, 1994)

Moreover, Chen (1994) stated that the spacing of rock bolts should be designed such that the active zone of individual bolts can intersects otherwise arc building can be impossible. As the bolt spacing decreases, bolt systems yield a higher strength.

### 2.5.4 Steel Sets/Ribs Support System

Considering steel sets spaced a unit length apart in three directions of the tunnel axis, the maximum pressure provided from the steel ribs and the stiffness of a closed circular steel depend basically on the yield strength of the steel (MPa), the cross-sectional area of the section ($m^2$), spacing along the tunnel axis and Young's modulus of the rock block (MPa) (Hoek, 1980).

Generally, when constructing steel arches, two or more beam sections are joined together and supported in the excavation area with the aid of connecting plates. In situations where there is a need to withstand lateral pressure and uplift from the ground, a closed ring of steel sets may be used instead of an arched shape. To create a closed ring, steel ribs can be connected to form a circular shape or a curved concrete or shotcrete can be used at the base. An illustration of different steel rib configurations is shown in Figure 2.16.

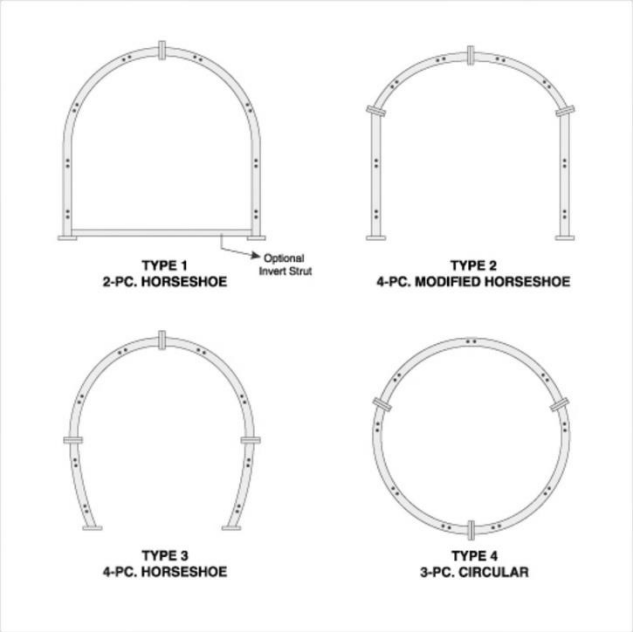


Figure 2.16. Example of steel rib support configurations (dsi underground, 2023)

In modern tunneling projects, especially those using TBM boring techniques, the steel supports are often positioned directly with the rock or shotcrete used to fill in overbreak areas as shown in Figure 2.17.

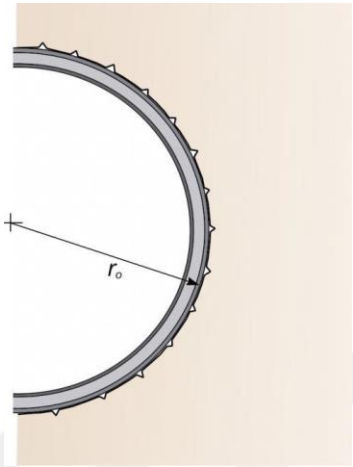


Figure 2.17. Steel reinforced support in direct contact with the rock (Hoek et al., 2008)

## 2.6 Underground Mining Transport, Haulage and Materials Handling Systems

A typical underground mine layout commonly relies on an adit, a decline - ramp system, or a shaft to provide access to the production zones and to transport the ore to the surface processing plant. The best decision for underground mine access is usually determined regarding the depth of the orebody.

A decline - ramp system is a spiral path that follows the deposit. To construct the portal, a box-cut is created to serve as an entry. It's important to consider the opening is excavated inside the overburden or bedrock. The overburden refers to the rock mass above the orebody. In essence, a decline – ramp system refers to a network of dipping drives with a straight or spiral path that connects the production levels. Designing a decline – ramp system is subject to several crucial physical limitations arising from the mobile equipment limitations. One of these is ensuring

that the decline is positioned at a safe distance from the orebody. Additionally, it is vital to ensure that the decline geometrically conforms to the trucks and other mining equipment in terms of the gradient and curvature (Brazil et al., 2008).

A shaft refers to a permanent opening that is either vertical or inclined. It provides access to various levels of the mine while also serving material transportation and emergency. Shaft design is tailored to the specific requirements and demands of the mine. The shaft profile must be suitable to host all the requirements of the mine. The size of the shaft is mainly relies on the minimum size necessary to accommodate the production target and required air intake (Vergne, 2008).

On a hillside or a mountainous terrain, adits may serve as a better access road for the underground mine. Adits are horizontal openings that are used by miners to reach the production zones.

Figure 2.18 presents a schematic of an underground mine, which includes the permanent and temporary openings. Regardless of the extraction method, the development excavations have similar functions and require an equivalent geomechanical performance (Brady and Brown, 2006).

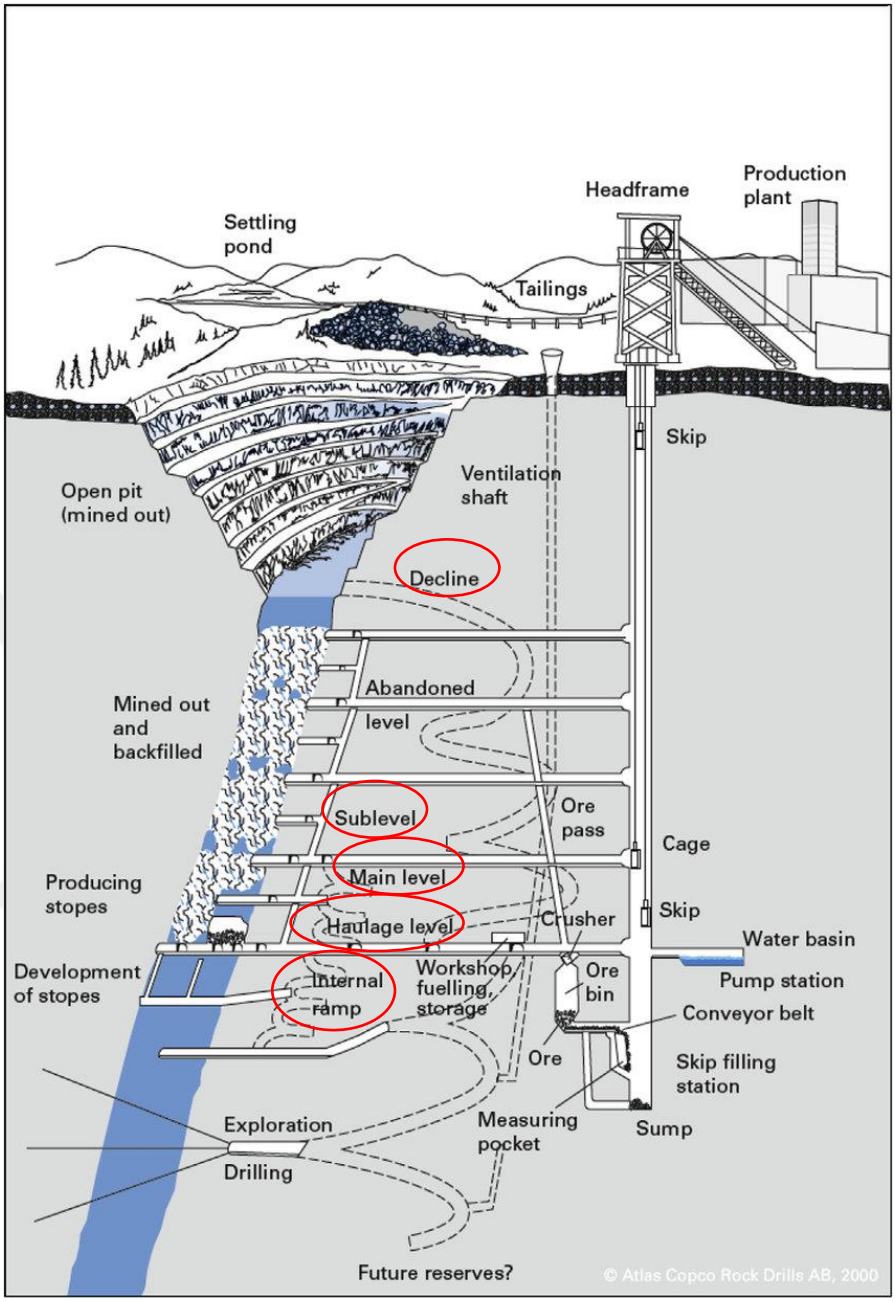


Figure 2.18. The layout of an underground mine showing different haul road types (Atlas Copco, 2007)

The permanent openings in an underground mine must match the strict performance standards for long durations as explained by Brady & Brown (2006). For instance, haul roads should enable the safe and efficient operation of various

vehicles, including loaders, trucks, conveyors, and transport for personnel. The primary goal is to ensure that the permanent openings can perform according to their design throughout the mine's operational life. From a rock mechanics standpoint, the placement of openings should be strategically chosen in regions where displacements, strains, and tilts within the rock mass remain within acceptable limits. The extent of mining-related disturbances in the rock mass around and above an ore deposit is influenced by the size and nature of the displacements caused by mining activities in the ore body's immediate surroundings. These disturbances can be assessed using analytical or computational techniques.

The process of accessing a mine via a ramp entail driving a downward-sloping path with horizontal turns that allows a mobile rubber-tired equipment haul from the surface to the orebody. This method is especially useful for shallow ore deposits, when a decline can be placed around an existing open pit. Ramps can be built with grades ranging up to 20% if operated by LHDs (Tatiya, 2013). The ramp angle is determined by the ability of vehicles to handle declines, with 15% being a typical grade, usually applied in the metalliferous underground mining operation in Türkiye, 11-12% for curves, and 9-10% for level intersections. Table 2.13 illustrates a comparison of key parameters for driving underground mine openings using different methods, including conventional drilling and blasting, road headers, and tunneling machines.

Although for underground mining operations, there is no regulated standards for haul width in Türkiye, in underground mining operations the mine haul roads can be designed by considering at least 1.5 meters of lateral space between the widest point of the largest mobile equipment and both sides of the ramp or any obstacles that the equipment may encounter. Additionally, other services, such as service pipes, ventilation ducts and clearance to sidewalls, allowance is required for underground mine haul roads as shown in Figure 2.19.

Table 2.13 Comparison of key parameters for driving tunnels and underground mine openings in terms of configuration (Tatiya, 2013)

| **Parameters** | **Drilling & Blasting** | **TBM** | **Road headers** |
|---|---|---|---|
| Layout and Design | | | |
| **Size** | Any | 1.75–11 m dia. in civil, 1.75–8 m dia. in mining | Determined by the boom height |
| **Shape** | Any | Any | Arch and rectangular |
| **Length** | ≤ 3 km | ≥ 3 km | ≤ 3 km; may be longer |
| **Gradient** | ≤ 18° | ≤ 6° | ≤ 6° |
| **Turning Radius** | Any | 30–60 m | 30–60 m |

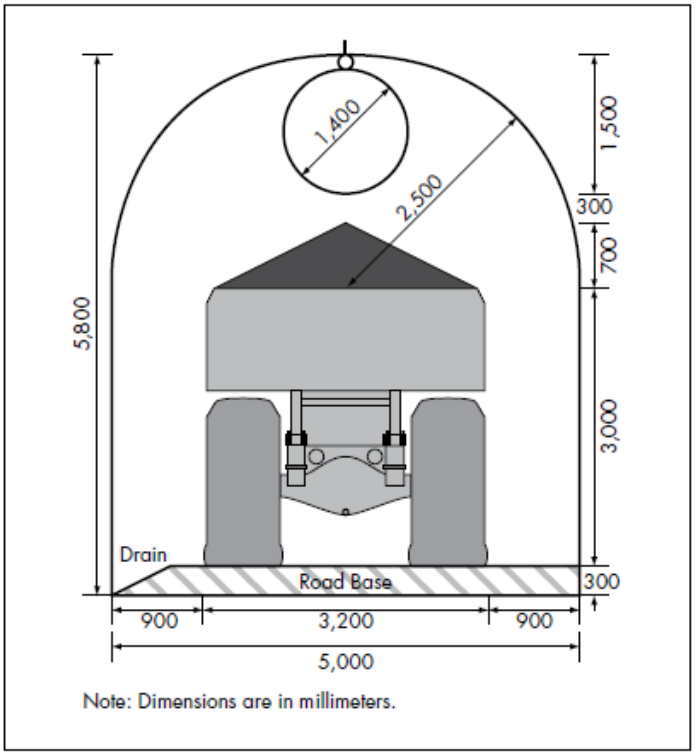


Figure 2.19. A sample haul road profile in an underground mine (Atkinson, 1992)

## 2.7 Numerical Modelling Methods Used in Support Analyses of Underground Openings

Numerical modeling relies on mathematical models and computational procedures to obtain the stress-strain behavior of materials under load. Variation in the material type can be presented by dividing the rock or soil mass into individual regions associated with different geomechanical properties. The results of numerical models can be used as an auxiliary tool to compare with the empirical methods. The geomechanical parameters define the stress-strain relations of a simulated body under load. Commonly, the Young's Modulus, Poisson's ratio, cohesion, internal friction angle and tensile strength are used to simulate the elastoplastic behavior of the rock mass. Numerical analyses offer cost-effective and

accurate solutions where analytical methods do not exist and field trials are not practical.

Numerical analyses are also widely used for designing mine access roads. It provides comprehensive knowledge on stress, deformations, fracture propagation, failure, and groundwater flow. The finite element method (FEM) is the most common method for stress and deformation analysis in geomechanics. The discrete element method (DEM) is another method that can simulate the fracture propagation and rockfall by particles. The numerical techniques that are most frequently used in the design of underground excavations in rock engineering at present are indicated in Table 2.14.

Table 2.14 Frequently used numerical techniques in Rock Engineering (Barla, 2016)

| **Continuum** | **Discontinuum** | **Hybrid Methods** |
|---|---|---|
| Boundary Element Method, BEM | Particle Flow Method, PFC | Hybrid FEM/DEM and |
| Finite Element Method, FEM | Discontinuous Deformation Analysis, DDA | Hybrid DEM/BEM |
| Finite Difference Method, FDM | Discrete Element Method, DEM | Hybrid FEM/BEM |

Regarding the material features, various material models can be implemented in numerical simulations, such as Mohr-Coulomb, Drucker-Prager, Hoek-Brown, and visco-plastic models. Additionally, different reinforcement/support applications like rock bolts, anchors and dowels can be simulated. Similarly, shotcrete, steel sets, or concrete liners can be introduced using the components such as beams and liner plate elements (Barla, 2016).

Numerical modeling is frequently used to analyze sophisticated underground excavations that might not be amenable to resolution by means of conventional methods. This research makes use of RS2 (Rocscience, Inc., 2022) software, which is a plane-strain based continuum code. RS2 conducts 2D finite element analysis on geotechnical structures that are used in civil and mining applications. It can be used for analysis of both rock and soil excavations. It is capable of implementing the support design, underground and surface excavations, embankments, foundations, consolidation, dynamic analysis and groundwater seepage (Rocscience, 2022).

Continuum methods provide computational advantages for the analysis of rock mass deformation analysis in massive, unweathered, weak, soil-like or highly fragile rocks. Continuum modeling assumes that the material is free of discontinuities throughout the entire mass. Computational costs arise from the model dimensions, the mesh density, and complexity of the material model. Figure 2.20 shows a sample view from the continuum modeling of a twin tunnel (discretized and meshed) in RS2 with reinforcement within various discrete geological structures.

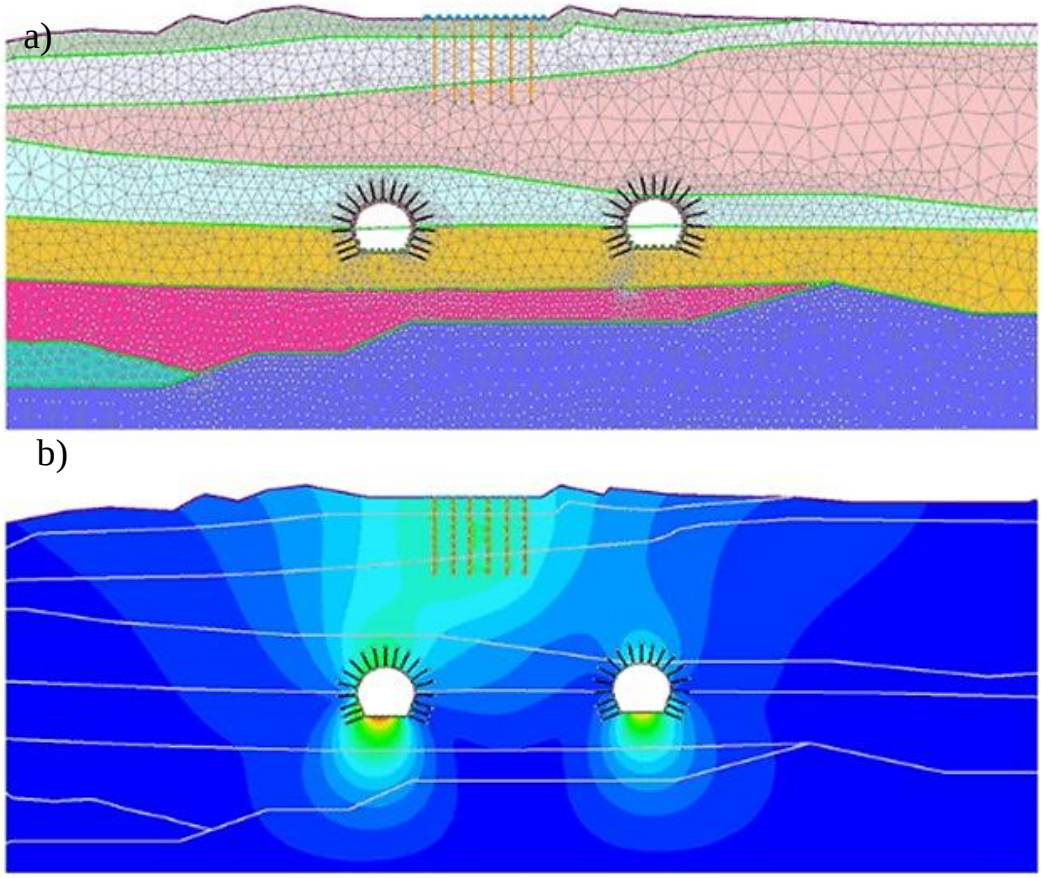


Figure 2.20. A sample continuum models of twin tunnels in RS2, a) model generated, b) after computing the model, interpretation tab view (Rocscience, 2023)

### 2.7.1 Numerical Modelling/Finite Element Method (FEM)

The Finite Element Method (FEM) is a numerical solution for mechanical problems. The first use of FEM took place in the field of Civil Engineering around the 1950s. The method is based on the Ritz Technique (1909). Its effective use became possible with the advances of computer technology. It is applied to problems in almost every branch of mathematical physics and engineering (e.g., stress-strain analysis, fluid mechanics, heat conduction, wave propagation, static and dynamic elasticity problems, etc.). Currently, the application area of numerical

modeling methods is increasing, and they are particularly helpful in determining potential yielding or failure zone in underground mining operations, as well as the suitable support and layout of underground excavations.

Pande et al., (1990) identified the Finite Element Method (FEM), Finite Difference Method (FDM), and Boundary Element Method (BEM) as the primary continuum methods employed in rock mechanics. These methods involve discretizing either the medium and its boundaries (FEM and FDM) or only the boundaries (BEM). The FEM is the most commonly used numerical method in rock mechanics. It divides the continuum body into small, regularly shaped elements that intersect at nodes, as shown in Figure 2.21. By using interpolation functions, the FEM assumes that displacements at any point within the element can be accurately obtained from the displacements at the nodes (Bobet et al., 2009).

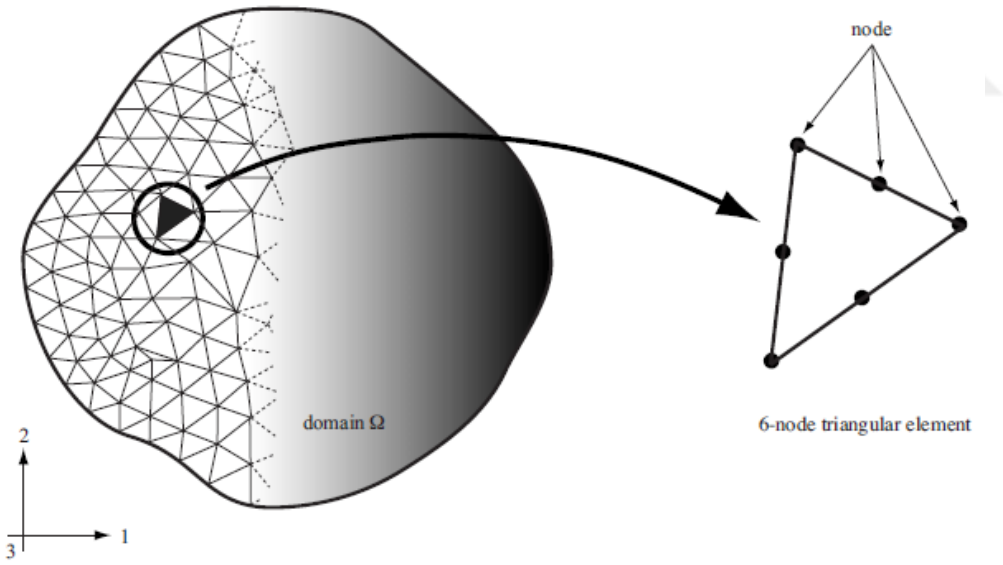


Figure 2.21. A continuum model and finite-element discretization (Bobet et al., 2009)

With the advances in computational technologies, recent years have driven the geomechanics through machine learning techniques. The following section presents one of the widely used machine learning technique in geomechanics.

## 2.8 Artificial Neural Networks (ANN)

ANN is an advanced statistical approach that simulates the workflow of a simple biological nervous system. They are made up of fictitious neurons connected to each other to create a network. These networks have the capacity to learn, store information, and reveal relationships between data. In other words, ANN can solve problems that typically require a human's natural ability of thinking and observation. The human ability to generate solutions for problems requiring sophisticated interpretation relies on the learning ability of the human brain by experimentation.

Neural network algorithms can now be useful in estimating the behavior of rocks and rock formations in a variety of applications, such as mining and geotechnical engineering. One common method for using neural networks in rock mechanics is to train the network on a dataset of rock properties and related behavior before using it to predict the behavior of new rock samples. Moreover, the behavior of rock formations under various situations, such as changes in pressure by tectonic activities or external loading etc., or stress, can be modeled using neural networks algorithm. This can be helpful in estimating how rock formations will behave during drilling or excavation as well as knowing how rock formations will behave over the long term throughout geological time scales.

The initial studies on artificial neural networks (ANN), also known as perceptron networks, were done by McCulloch and Pitts (1943; 1947) as well as (Hebb, 1950). These networks were initially developed as models of biological neurons. The original ANNs, however, had issues and were limited in their ability to handle linearly correlated data. Nevertheless, these drawbacks prompted researchers to

upgrade the original single-layer perceptron architecture to multilayer networks (Smits et al., 1994; Zupan & Gasteiger, 1991). Hopfield (1982) developed an innovative method in 1982 by adding nonlinearity between the input and output data. The performance of ANNs significantly improved as a result of this new perceptron architecture. Werbos & John (1974) developed the back-propagation learning algorithm, which aids in the popularization of ANN in addition to the Holpfield study.

ANN approaches, in general, refer to a class of mathematical models based on how the human brain operates. In its construction, all ANN structures have neurons, also known as hidden units. Each neuron is the biological equivalent of a synapse, and each hidden unit is made up of activation functions that regulate signal transmission to the next layer. The hidden unit is made up of a regression equation that analyses the input data and produces a non-linear output. Non-linear relationships can be managed by combining numerous neurons to produce an ANN (Suzuki, 2013). Figure 2.22 depicts the similarities between a human neuron and an ANN neuron.

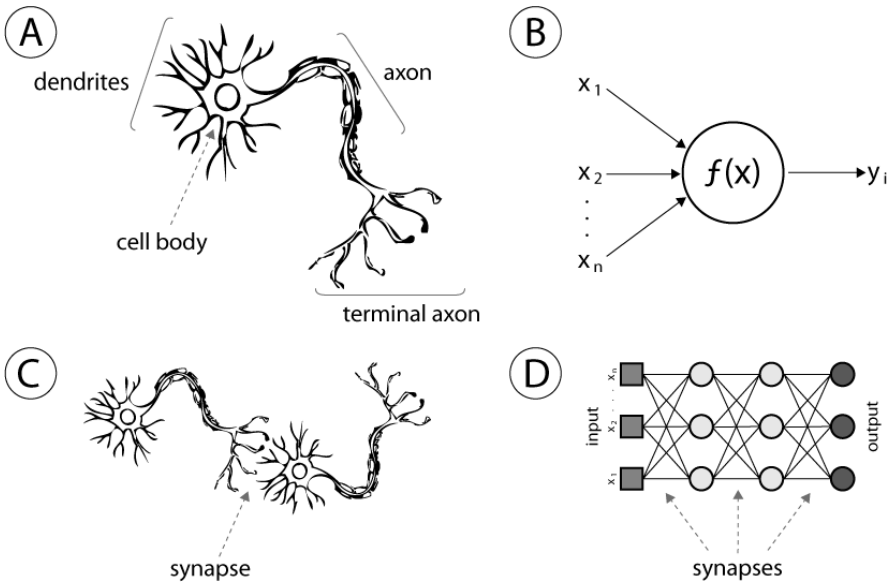


Figure 2.22. (A) Human neuron; (B) artificial neuron or hidden unity; (C) biological synapse; (D) ANN synapses (Suzuki, 2013)

Generally, it is believed that each unit contributes to the input of the connected unit in an additive manner. The combined input of unit *k* is obtained by adding the weighted outputs from each connected unit, along with a bias or offset term $\theta_k$ as depicted in Equation 2.1 (Alavala, 2007).

$$s_k(t) = \sum_j w_{jk}(t) y_j(t) + \theta_k(t) \qquad \text{Equation 2.11}$$

When $w_{jk}$ is positive, it is considered as an excitation, and when $w_{jk}$ is negative, it is considered as an inhibition. In certain cases, more intricate regulations for combining inputs are utilized, where a differentiation is made between excitatory and inhibitory inputs. This is referred to as a propagation rule (Equation 2.12 for sigma units (Alavala, 2007).

$$s_k(t) = \sum_j w_{jk}(t) \prod_m y_{jm}(t) + \theta_k(t) \qquad \text{Equation 2.12}$$

The $y_{jm}$ values undergo weighting before multiplication. Although such units are not commonly utilized, they hold significance in the gating of input and implementation of lookup tables (Alavala, 2007).

It is also necessary to have a regulation that determines how the total input affects the unit's activation. The required function $F_k$ takes into account the total input $s_k(t)$ and the current activation $y_k(t)$, and generates a new value, presented in Equation 2.13, for the unit's activation, *k* (Alavala, 2007).

$$y_k(t+1) = F_k(y_k(t), (s_k(t)) \qquad \text{Equation 2.13}$$

Frequently, the activation function increases in value as the total input of the unit increases in accordance with Equation 2.14.

$$y_k(t+1) = F_k\big(s_k(t)\big) = F_k\left(\sum_j w_{jk}(t)\, y_j(t) + \theta_k(t)\right) \text{Equation 2.14}$$

Although activation functions are not limited to non-decreasing functions, they typically employ a threshold function, such as a hard limiting threshold function (a sgn function), a linear or semi-linear function, or a smoothly limiting threshold (as shown in Figure 2.23). A sigmoid (S-shaped) function, in line with Equation 2.15, is frequently employed for the smoothly limiting function. In certain applications, a hyperbolic tangent is utilized, which yields output values ranging from -1 to +1 (Alavala, 2007).

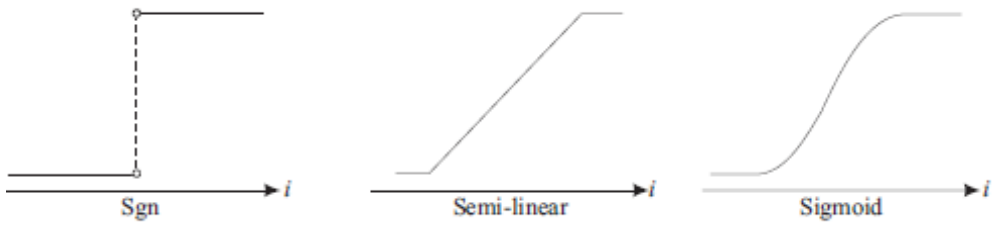


Figure 2.23. Different activation functions for a unit.

$$y_k = F(s_k) = \frac{1}{1+e^{-s_k}}$$ Equation 2.15

In order to predict tunnel support stability in a railway tunnel in Taiwan, Leu et. al. (2001) used data mining with artificial neural networks. According to the study, neural networks perform better than previous approaches at predicting support stability. The significance of information management is emphasized, as being the capability of data mining to derive insightful information from huge quantities of data. Based on rock mechanical properties and construction-related parameters, the study illustrates how data mining may be used to identify tunnel support stability. In addition, Elbaz et al. (2023) suggested using a deep reinforcement learning (DRL) model to enhance performance of tunnel boring machines. The model combines the extreme learning machine (ELM)-based deep-Q learning algorithm (DQL) and particle swarm optimization (PSO). The study also examines the difficulties in obtaining accurate geological conditions and the significance of optimizing the shield settings for maximum tunneling performance.

# CHAPTER 3

# PARAMETRIC ANALYSIS OF STABILITY IN A TYPICAL UNDERGROUND MINE HAUL ROAD

This section presents a parametric study to investigate the effects of various support systems on a typical underground mine haul road excavated in different rock mass qualities. Although in-situ measurements provide the best insight about the support performance, representation of various rock mass conditions requires costly and exhaustive field works. Alternatively, geomechanical simulations can generate a virtual model of any underground opening to test the behavior of the surrounding rock and support systems. This approach also allows for testing different support configurations to determine the best fitting one. Considering the validity of empirical methods are restricted to specific cases, the proposed workflow offers potential to cover a larger solution space and provide more accurate recommendations for the intermediate conditions. The following section presents the numerical modeling scheme developed in this study to investigate the performance of different support systems in underground mine haul roads.

## 3.1 Determination of the Representative Geomechanical Properties for Different Rock Mass Quality Classes

Simulation of field scale models is always tricky as the numerical outputs hugely depend on material properties. Considering direct measurement of these parameters are both costly and labor intensive, this study relies on empirical approaches in determining the elastic and plastic properties for some significant rock mass quality classes. The final support decision should always rely on the geomechanical assessments specifically designed for the case. However, the current study aims to

provide a useful understanding for the preliminary support assessments where empirical methods are dominantly used.

Conforming to the common approach of rock mass classification systems, the current study defines the mechanical properties for five distinct quality classes named by the prefix 'MP'. The number of MP increases as the material properties refer to weaker conditions. These milestones were intended to shed light on the intermediate cases to imply an approximate solution. In accordance with the other empirical approaches, the elastoplastic material properties in Table 3.1 were used to numerically analyse the support performance for various considerations.

Table 3.1 Rock mass properties used in the numerical models

| | | **Geomechanical Property Classes** | | | | |
|---|---|---|---|---|---|---|
| | | **$MP_1$** | **$MP_2$** | **$MP_3$** | **$MP_4$** | **$MP_5$** |
| **GSI** | | 90 | 70 | 50 | 30 | 20 |
| **Rock Mass Quality based on RMR** | | Very Good | Good | Fair | Poor | Very Poor |
| **Modulus of Elasticity (MPa)** [(a)] | | 8363 | 3212 | 3072 | 1949 | 795 |
| **Poisson's Ratio** | | 0.25 | 0.25 | 0.25 | 0.25 | 0.25 |
| **Uniaxial Compressive Strength (MPa)** [(b)] | | 57.0 | 13.3 | 10.0 | 5.2 | 1.3 |
| **Peak** | **Cohesion (MPa)** | 11.8 | 3.1 | 2.6 | 1.5 | 0.5 |
| | **Internal Friction Angle (°)** [(c)] | 45 | 40 | 35 | 30 | 15 |
| | **Tensile Strength (MPa)** [(d)] | 2.1 | 1.7 | 1.3 | 0.7 | 0.2 |
| **Residual** | **Cohesion (MPa)** [(e)] | 7.8 | 2.1 | 1.7 | 1.0 | 0.3 |
| | **Internal Friction Angle (°)** [(f)] | 30 | 27 | 23 | 20 | 10 |
| | **Tensile Strength (MPa)** [(g)] | 1.4 | 1.1 | 0.8 | 0.4 | 0.1 |
| **Dilation Angle (°)** [(h)] | | 5 | 4 | 4 | 3 | 2 |

The material properties in Table 3.1 were majorly determined by interpreting Bieniawski's association of the rock mass mechanical parameters to RMR scores (1989), the Generalised Hoek and Brown criterion (Hoek et al., 2002) and Hoek and Diedrichs (Hoek & Diederichs, 2006) recommendations. Considering each method has drawbacks under specific conditions some adjustments and assumptions were made to make a better prediction representing the mechanical parameters. The following section describes the assumptions and adjustments in detail for the parameters marked by upper letter indices in the table :

(a) = The rock mass elastic modulus estimation for $MP_1$, $MP_2$ and $MP_3$ calculated from the Generalised Hoek & Diedrichs method. The other values were extracted from Carranza-Torres and Corkum (2008) to adjust the values assigned to the fair to very poor rock qualities. For example; Equation 3.1 was used as the $\sigma_{ci}$<100 MPa for $MP_4$;

$$E_{rm}(GPa) = \left(1 - \frac{D}{2}\right) \times \sqrt{\frac{\sigma_{ci}}{100}}\, 10^{((GSI-10)/40)} \qquad \text{Equation 3.1}$$

where; $E_{rm}$=Rock Mass Modulus, D=Disturbance factor was taken as 0, $\sigma_{ci}$ =38 MPa was assumed and GSI was taken as 30 to be equivalent to poor rock quality. So, the rock mass modulus is equal to 1949 MPa according to Equation 3.1.

(b) = calculated from the Mohr - Coulumb Failure Criterion as in Equation 3.2;

$$\sigma_1 = \sigma_3 tan^2\left(45 + \frac{\emptyset}{2}\right) + 2ctan\left(45 + \frac{\emptyset}{2}\right) \qquad \text{Equation 3.2}$$

Where, $c$ is cohesion, $\emptyset$ is the internal friction angle, $\sigma_3$ is the minor principal stress.

(c) = $MP_1$, $MP_2$, and $MP_3$ were taken from $RMR_{89}$ table coresponding to very good, good and fair rock masses, others calculated from the Generalised Hoek and

Diedrichs Theory as to fit to the geomechanically equivalent to Mohr-Coulmb Parameters.

Intack rock strength was taken from the $RMR_{89}$ table and the related GSI values calculated basen on Equation 3.3

$$GSI = RMR_{89} - 5 \qquad \text{Equation 3.3}$$

(d) = $MP_1$ was calculated from Generalised Hoek and Diedrichs Theory to be consistent with the overall rock mass properties, others were calculated from UCS value based on the Griffith's Theory (1921).

Griffith (1921) states that if a dry material satisfies the following Equation 3.4, 3.5 and 3.6, it leads to the Griffith failure.

If $\sigma_1 + 3\sigma_3 \geq 0$

$$(\sigma_1 - \sigma_3)^2 = 8T_o(\sigma_1 + \sigma_3) \qquad \text{Equation 3.4}$$

If $\sigma_1 + 3\sigma_3 \leq 0$

$$\sigma_3 = -8T_o \qquad \text{Equation 3.5}$$

When $\sigma_3 = 0$ it means uniaxial compression, so that the UCS estimated by Equation 3.6. ($\sigma_1 = UCS$)

$$UCS = 8T_o \qquad \text{Equation 3.6}$$

where $T_0$ is the uniaxial tensile strength.

(e), (f), (g) = the residual values were assmued as the 2/3 of the peak cohesion, internal friction angle and tensile strength values.

(h) = Dilation Angle was obtained by dividing the internal friction angle into 10.

To validate the conformity of geomechanical parameters with the implied rock mass quality a literature survey was carried out. For instance, Hoek (2001) determined the compressive strength for very good quality rock mass as 64.8 MPa while it was only 1.7 MPa for very poor quality rock mass. Checking Table 3.1 for

the values proposed in this study 57.0 MPa and 1.3 MPa are close to these values and can be considered to be valid. In comparing the plastic parameters, Hoek (2001) proposed the cohesion for the average and very poor rock quality rock masses as 3.5 MPa and 0.55 MPa. Similarly, this study recommends 2.1 MPa and 0.3 MPa. For the elastic parameters, Hoek (2001) claims that the modulus of elasticity for very poor rock mass varies between 398 - 870 MPa. This study proposes an elastic modulus of 795 MPa for the same rock mass quality. In summary, the rock mass properties proposed in Table 3.1 for the five quality classes namely $MP_1$ to $MP_5$ conform with the common sense and previous studies. Thus, they are suitable for use in the numerical models.

Because RS2 code makes use of small deformation theory, weak quality rock mass parameters like $MP_4$ and $MP_5$ frequently turned out a converge error, which is a results of the large deformations. Despite the unsupported cases could not be simulated to see the full deformations, supported models fixed the converge issues by clearly showing the contribution of supports on the overall stability.

## 3.2 Determination of the Representative Support System Properties for Numerical Modeling

In this study rock bolts and concrete liners are used in the numerical assessment of stability improvement achieved by support systems. The parameters used to define the support elements in FEM models are presented in Table 3.2. Briefly, Dextra GEOTEC Solid Bar 25 rock bolt was used as a basis to define a typical rock bolts in underground mine haul roads.

The concrete liner is another widely used support element in the mining industry. The concrete specifications were taken from the regulations and descriptions explained in ACI committee 318 (2011) and Turkish Standards Institute TS 500 (2000).

Table 3.2 Rock bolt and liner parameters used in FEM analyses

| **Concrete Liner Properties** | |
|---|---|
| Thickness (cm) | [6, 12] |
| Young's Modulus (GPa) | 30 |
| Poisson Ratio | 0.15 |
| Compressive Strength (MPa) | 17 |
| Tensile Strength (MPa) | 1.5 |
| **Rock Bolt Properties** | |
| Bolt Length (m) | [1.0, 1.5, 2.0, 2.5] |
| Bolt Spacing (m) | 1.0, 1.5 |
| Bolt Type | Fully Bonded |
| Bolt Diameter (mm) | 25 |
| Bolt Modulus, E (GPa) | 50 |
| Selected Common Type | Dextra GEOTEC Solid Bar 25 |
| Tensile Capacity (MN) | 0.35 |
| Residual Tensile Capacity (MN) | 0 |

Although the typical support characteristics were introduced to the RS2 software in practice, it should be noted that different rock bolt and concrete types with other means of support elements (like steel sets) may be used alone or in combination. The performance of the support elements may vary depending on the characteristics of each particular case.

## 3.3 Numerical Models: Geometry, Boundary Conditions and Parametric Study

In the first part of the hypothetical case study, 819 elasto-plastic mechanical models were created with a horseshoe-shape of 5 m roof span. The rock mass quality considered to be ranging from very poor to very good. The models were designed to involve the combinations of the specified support parameters in Table 3.2. In accordance with Table 3.3, a total of 819 different models were created with the RS2 code for each of the five rock mass quality classes (ranging from $MP_1$ to $MP_5$), at three depths (200, 400, and 600 m), and three different k-ratios (0.5, 1.0,

and 1.5). Furthermore, for support parameters, four different rock bolt lengths (1.0, 1.5, 2.0, and 2.5 m), two rock bolt spacings (1 and 1.5 m), and two liner thicknesses (6 cm and 12 cm) were modeled. The meaningful combinations of the aforementioned parameters were tested numerically with FEM solutions.

Table 3.3 The range of parameters used in FEM models

| **Inputs Parameters** | **Range of Input Parameters** |
|---|---|
| Geomechanical Quality of Rock Mass | [$MP_1$, $MP_2$, $MP_3$, $MP_4$, $MP_5$] |
| Depth (m) | [200, 400, 600] |
| In-situ Stress Ratio (k) | [0.5, 1.0, 1.5] |
| Rock Bolt Length (m) | [1.0, 1.5, 2.0, 2.5] |
| Rock Bolt Spacing (m) | [1.0, 1.5] |
| Liner Thickness (cm) | [6, 12] |

Figures 3.1 and 3.2 shows the sample models for unsupported and supported (bolt and liner) conditons at 400 m depth and hydrostatic loading conditions.

The models were implemented with an isotropic material for the significant stages of excavation. As can be seen in Figure 3.1 and 3.2, in order to have the best accuracy for stress and deformation analyses around the periphery of the opening, the mesh element density was increased.

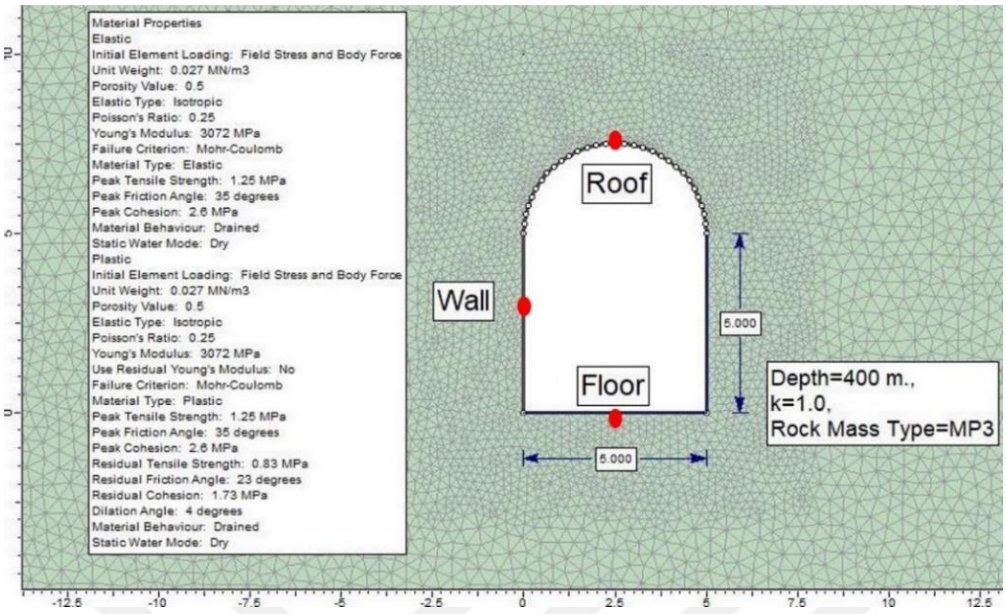


Figure 3.1. A sample FEM model of a typical underground mine haul road with no support, 400m. depth, hydrostatic loading conditions, excavated in $MP_3$ type rock mass

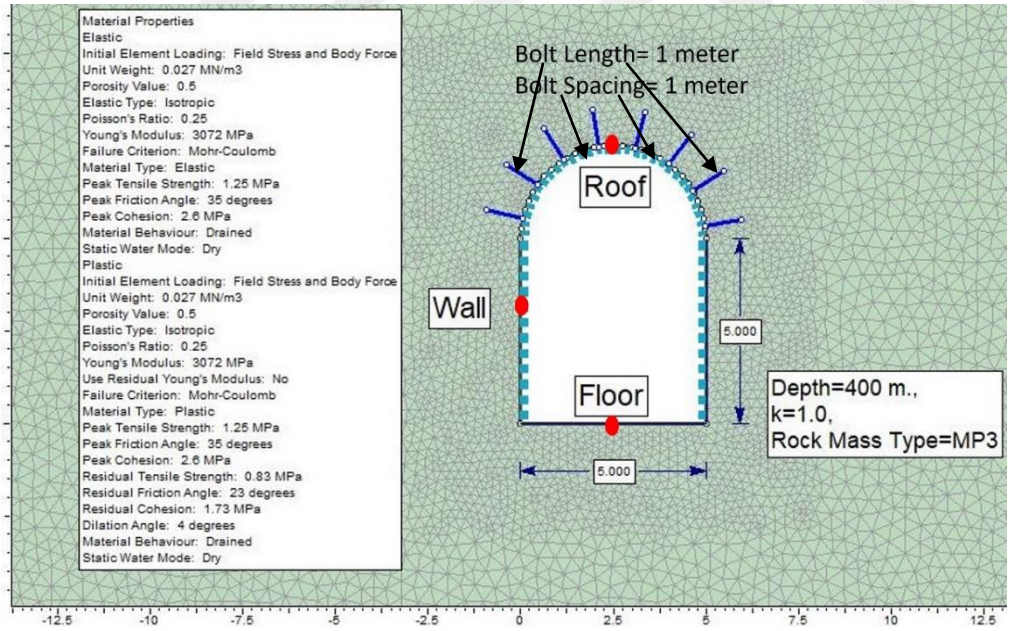


Figure 3.2. A sample FEM model of a typical underground mine haul road with liner and pattern bolts, 400 m depth, hydrostatic loading conditions and excavated in $MP_3$ type rock mass

## 3.4 Interpretations of the Numerical Modelling

In total 22131 mechanical readings were recorded from 819 models from the supported and unsupported models. In the initial stage of the data interpretation, the conventional statistical modeling was used to interpret the database and to compare the consistency and accuracy of the empirical support reccomendations offered by RMR and Q systems. The data extracted from three different points of the excavation (roof, wall, and floor) were tabulated in terms of the vertical displacement, horizontal displacement, maximum principal stress, minimum principal stress, major and minor principal strains, and the span of yielded elements around the opening. In supported models the axial forces was also recorded from the rock bolts and liner. Table 3.4 shows the mechanical parameters recorded around the underground opening and the exact locations for the readings. In each model 19 different data were recorded for unsupported models. In supported models 11 readings add up to check the performance of the applied support configuration.

Table 3.4 Mechanical readings and their locations on the FEM models of a typical underground mine haul road opening

| | **Locations of the Mechanical Readings** | | |
|---|---|---|---|
| **Mechanical Parameters** | **Roof** | **Wall** | **Floor** |
| Vertical displacement (m) | ✓ | | ✓ |
| Horizonal displacement (m) | | ✓ | ✓ |
| Major principal stress (MPa) | ✓ | ✓ | ✓ |
| Minor principal stress (MPa) | ✓ | ✓ | ✓ |
| Major principal strain (ε, %) | ✓ | ✓ | ✓ |
| Minor principal strain (ε, %) | ✓ | ✓ | ✓ |
| Span of the yielded elements (m) | ✓ | ✓ | ✓ |
| Rock bolt axial force (MN) | ✓ | | |
| Liner axial force (MN) | ✓ | ✓ | |

Figure 3.3 shows a solved model for one of the unsupported cases whose geomechanical properties were identified as $MP_3$ (fair rock), the depth is 400 meter

and under hydrostatic loading. On the other hand, Figure 3.4 shows the supported mode with 1 m bolt length, 1 m bolt spacing and 12 cm liner thickness. As shown in Figure 3.3 and Figure 3.4, the mechanical readings were obtained from the roof, wall and floor individually by taking querry records. The figures prove that the major principal strain value was measured as 1.3% when the model was unsupported. However, the deformations reduced down to 0.4% with the mentioned support configuration. Additionally, the span of the yielded elements on the roof and sidewalls were 2.1 m and 3.3 m, respectively, in the unsupported model. However, the support configuration reduced this span down to 0 m and 3.0 m, respectively. Other mechanical readings such as the vertical and horizontal displacements, the major and minor principal stresses are given in Appendix G together with the rest of the database covering other combinations.

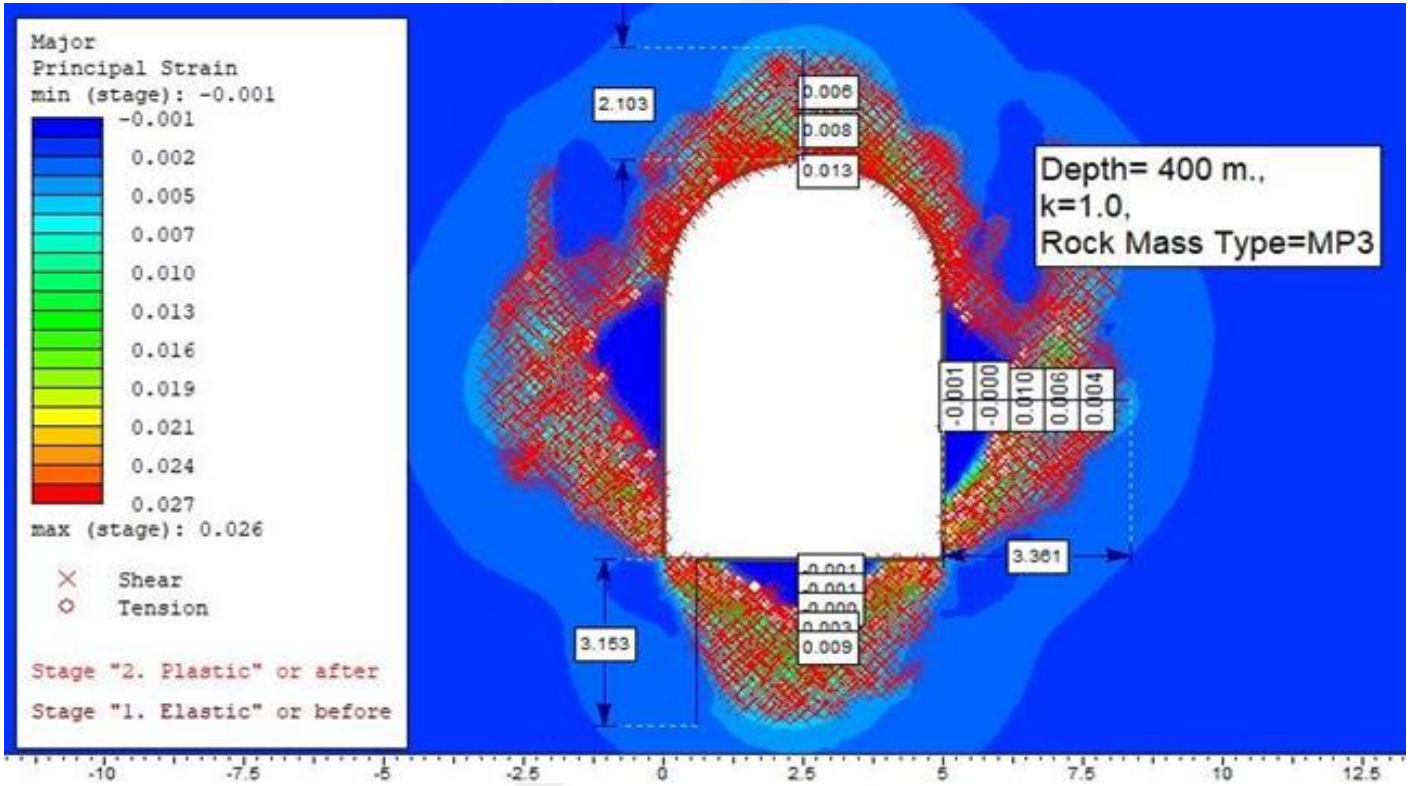


Figure 3.3. The major principal strain and the span of yielded elements for the unsupported case where the excavation is 400 m deep in MP3 and under hydrostatic loading

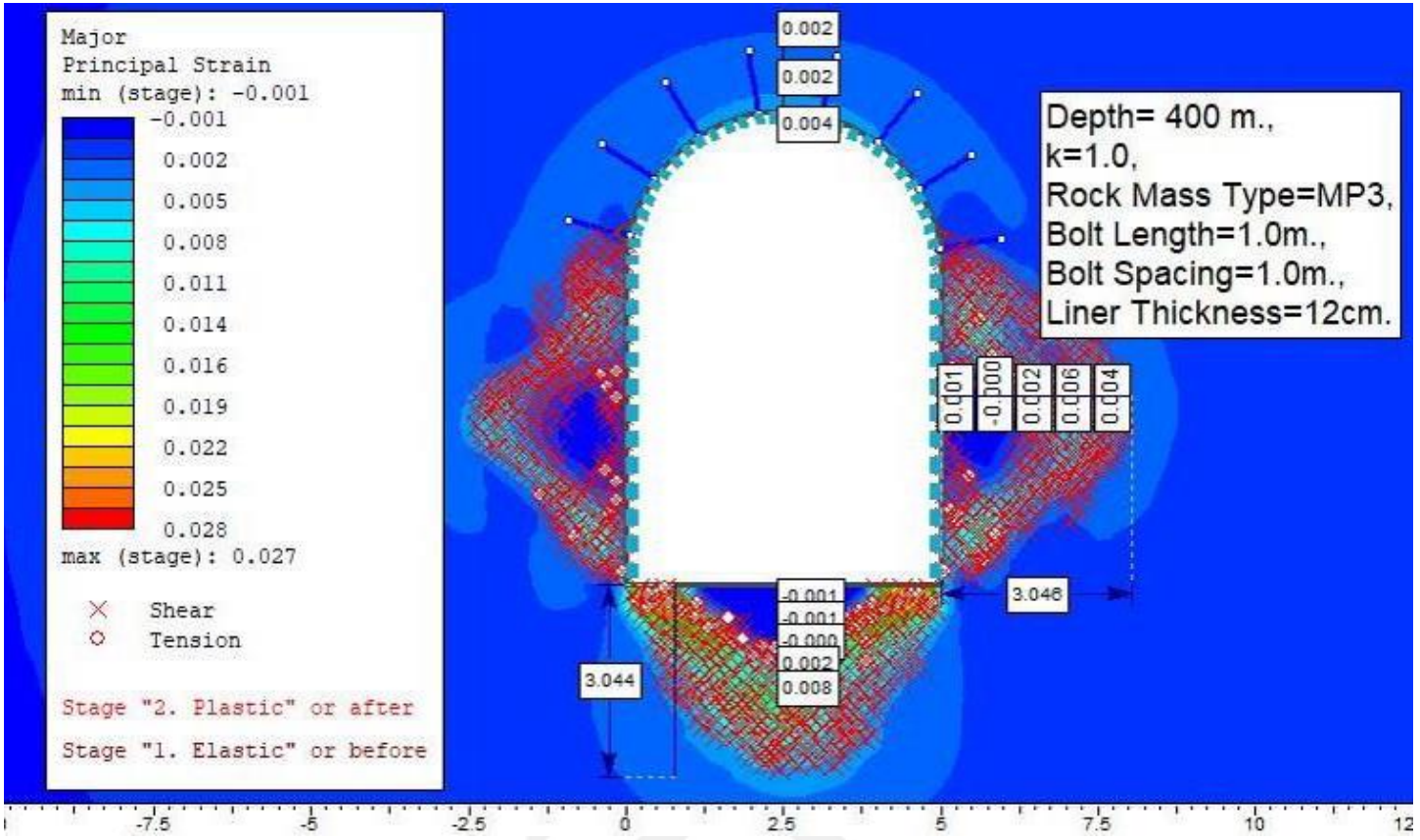


Figure 3.4. The major principal strain and the span of yielded elements for the supported case where the excavation is 400 m deep in $MP_3$ and under hydrostatic loading

## 3.5 A Proposed System Based on Machine Learning for Support Decision

The mechanical outputs obtained from modeling a typical underground mine haul road under various conditions were initially interpreted using conventional scatter plots. A sample plot is presented in Figure 3.5 for the vertical displacement at the opening roof under different depths and rock mass quality conditions for unsupported and supported excavations. In the legend, the abbreviations UNS, BS, BL, SH, and MP correspond to the different support types and rock mass qualities. Specifically, UNS represents an unsupported model, BS refers to a rock bolted model with a specific bolt spacing, BL represents a model with a specific bolt length, SH symbolizes models with liner, and MP denotes different rock mass quality classes. As the figure implies, it is extremely difficult to clearly show and read large number of input data using conventional statistical presentations. Two dimensional scatter plots can present only the major variables on the vertical and horizontal axes but the rest needs to be indicated by numerous data series. For the common parameters valid for the whole the data, the plot needs to be repeated showing the new data series under that condition. For instance, the plot in Figure 3.5 shows the vertical displacements at the excavation roof when k=0.5. The other in-situ stress ratio values need to be represented with different plots. Alternatively three dimensional graphs may be used. However, their drawback is the difficulty of presenting and reading the surface or volumes on the two dimensional space of hard copies. Therefore, machine learning algorithms may be used to train non-linear statistical models to predict the mechanical indicators of the support performance under various conditions with a reasonable accuracy.

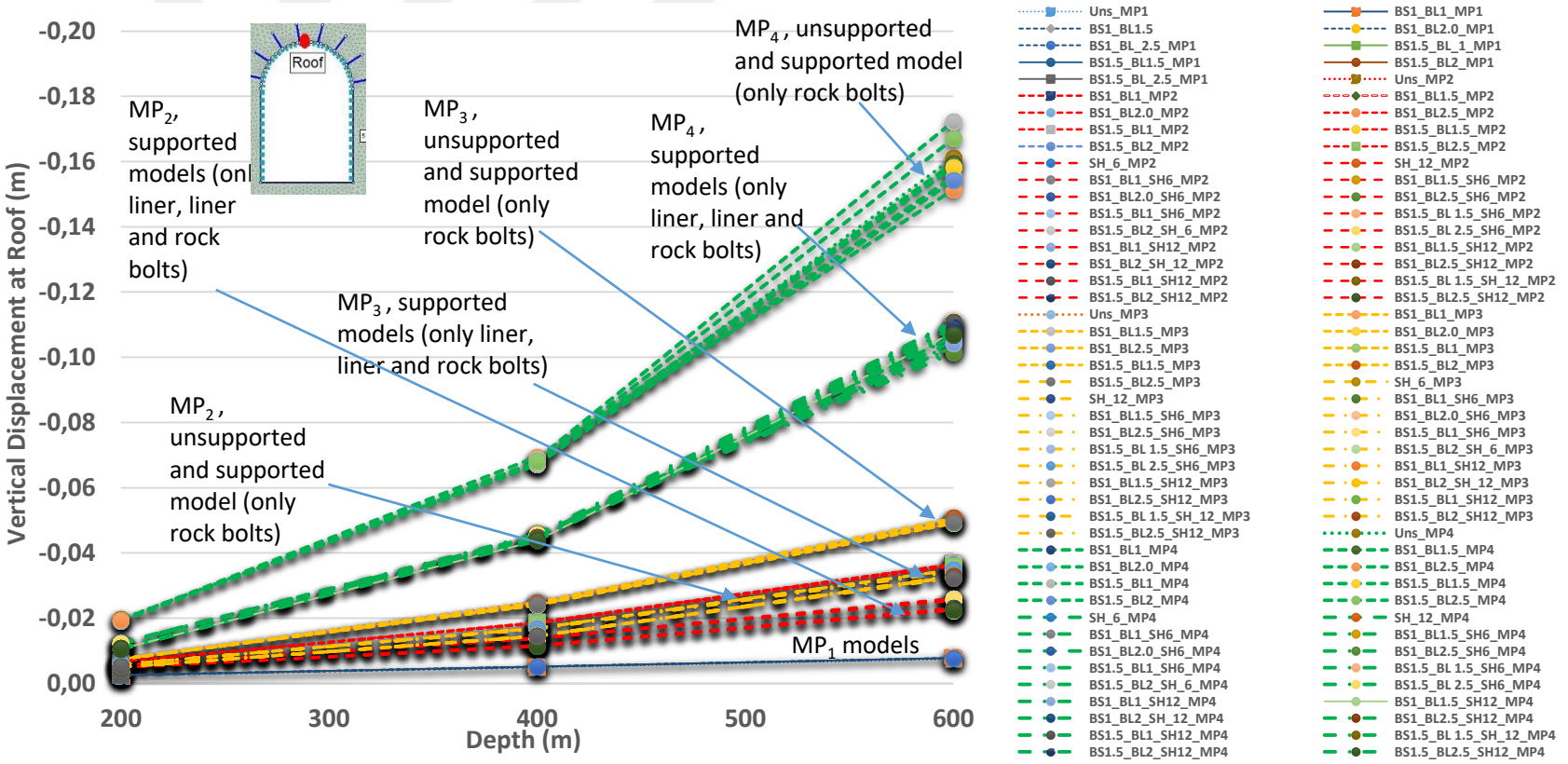


Figure 3.5. A sample plot showing the vertical displacements (m) at the roof of haul road opening excavated in various rock mass quality conditions vs. depth (m) when k=0.5

This study proposes the use of numerical simulation results representing only the significant cases to predict the intermediate conditions based on artificial neural networks. Mainly, the mechanical indicator of failure and support performance was considered to be the span of the yielded region around the excavation. The ANN model relies on :

- geomechanical properties (MP#),
- depth (m),
- in-situ stress ratio (k) ,
- rock bolt length (m)
- rock bolt spacing (m),
- liner thickness (cm),
- vertical displacement (m),
- horizontal displacement (m),
- the maximum and minimum principal stresses (MPa),
- the major principal strain (ε),
- axial force on bolts and the liner (MN)

to predict the yielded length. The ANN structure given in Figure 3.6 presents the model used for predicting the yielded span. The proposed method aims to replace the complex plots given in Figure 3.5.

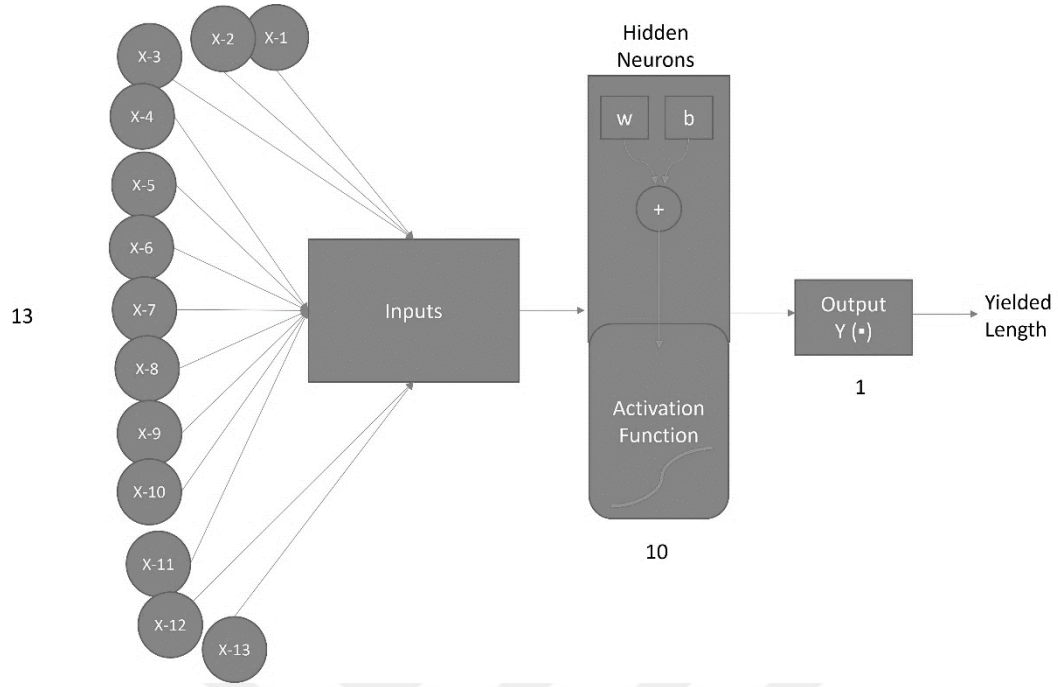


Figure 3.6. Schematic of the feedforward artificial neural network model

The ANN model was validated by comparing the predictions with the values obtained from numerical simulations and they turned out acceptable results. Chapter 4 presents the details of the validation and test procedures.

The default transfer functions built in the MATLAB ANN toolbox were used, which were a sigmoid transfer function in the hidden layer and a linear transfer function in the output layer (The MathWorks, Inc., 2018b). The network was trained using the Levenberg-Marquardt backpropagation technique. This method was selected because it excels at lowering the error between predictions and actual outputs during network training, leading to a more reliable and accurate model. The layout of the feedforward neural network model is given in Figure 3.7.

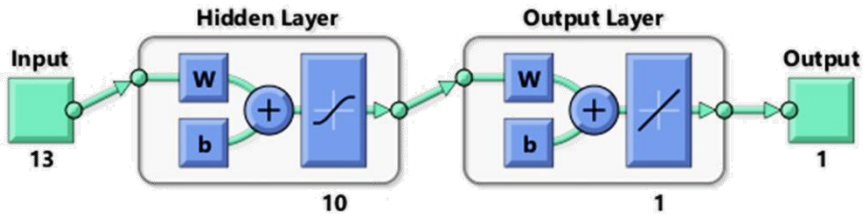


Figure 3.7. The block diagram of the artificial neural network created in the Matlab neural net fitting toolbox

In order to prepare the data for these parameters, 819 models were generated and then subjected to numerical analysis. 7453 of data is used for training the dataset from 573 individual numerical models and 1597 of the data were used for test from the 123 numerical models. A feed-forward backpropagation network type was selected for artificial neural network training, with the Levenberg-Marquardt (LM) algorithm for backpropagation, hyperbolic tangent sigmoid transfer function (tansig) as the activation function, and regression as the performance metric. Levenberg-Marquardt backpropagation techniques are used by the artificial neural network to modify its weighting parameters, enabling it to adapt to new input data and predict output values. Finding the ideal compromise between making large enough steps to quickly converg at a satisfactory solution while making small enough steps to prevent overshooting or oscillating around the minimum is the aim of changing the weighting factors. Thus, in order to improve the convergence and predictability of the learining process, an adjustment can be performed automatically by the training algorithm itself. For data training, a hidden layer with 10 neurons was utilized due to reaching a compromise between adapting to moderate complexity in the data while reducing the risk of overfitting. It allows the network to be trained effectively, generalize well to new data, and ensures a relatively quicker training process.

# CHAPTER 4

## RESULTS AND DISCUSSION

This section compares and discusses the results of the conventional and the proposed support design methods. Initially, the performance of support recommendations offered by the conventional empirical methods were tested based on numerical simulations. Through parametric analyses, various mechanical, geological and structural conditions are investigated thoroughly. Subsequently, in the following part, the proposed ANN method was tested with reference to the benchmark cases. Finally, it should be noted that in the assessment of numerical models the plastic analyses were interpreted by considering a critical strain to identify a potential failure.

The graphical representation of the major principal strain and corresponding displacement values solved in FEM models for the opening roof at 200, 400, and 600 m depth for different rock material properties with k=1 value is presented between Figure 4.1 to Figure 4.6 displaying the variations in strain and displacement characteristics at different depths and rock properties. The graphs provide valuable insights into the structural response of the opening's roof under varying geological conditions, aiding in understanding the behavior and stability of the opening in different scenarios. In the legend, the abbreviations UNS, BS, BL, SH, and MP correspond to the different support types and rock mass qualities. The numbers next to these abbreviations indicate the values of bolt spacing and bolt length used in meters for the respective models. Additionally, the number next to SH represents the concrete thickness in centimeters. For example, the model labeled as BS1_BL_2_SH_6 would represent a model with a bolt spacing of 1 meter, a bolt length of 2 meters, and a concrete liner thickness of 6 centimeters. The other graphs including the horizontal displacement at wall, major principal

strain at wall, major and minor principal stress at roof and wall are given Appendix A, B, C, D, E and F.

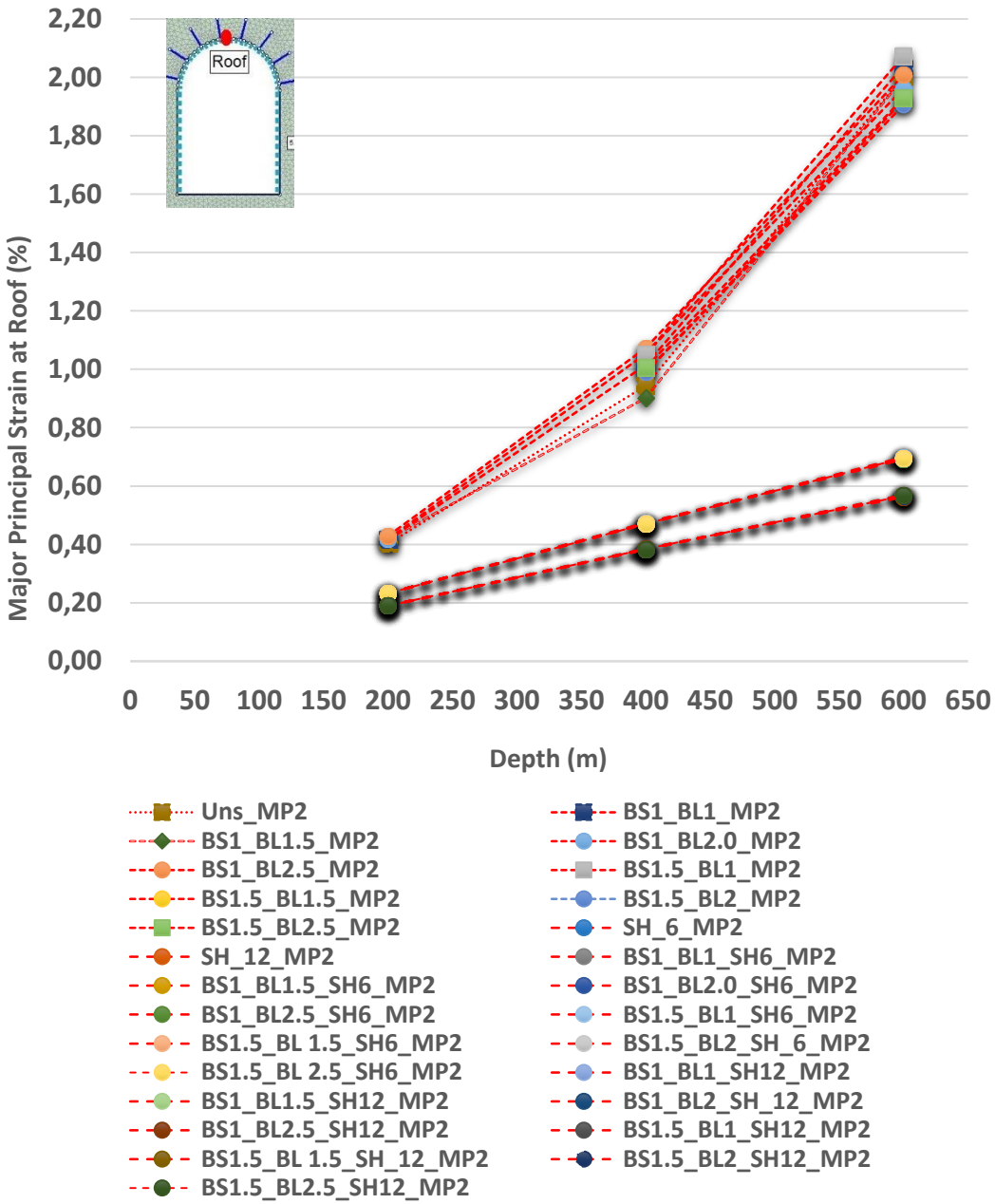


Figure 4.1. Simulated major principal strain at roof (%) vs. depth (m) for k=1.0 for $MP_2$

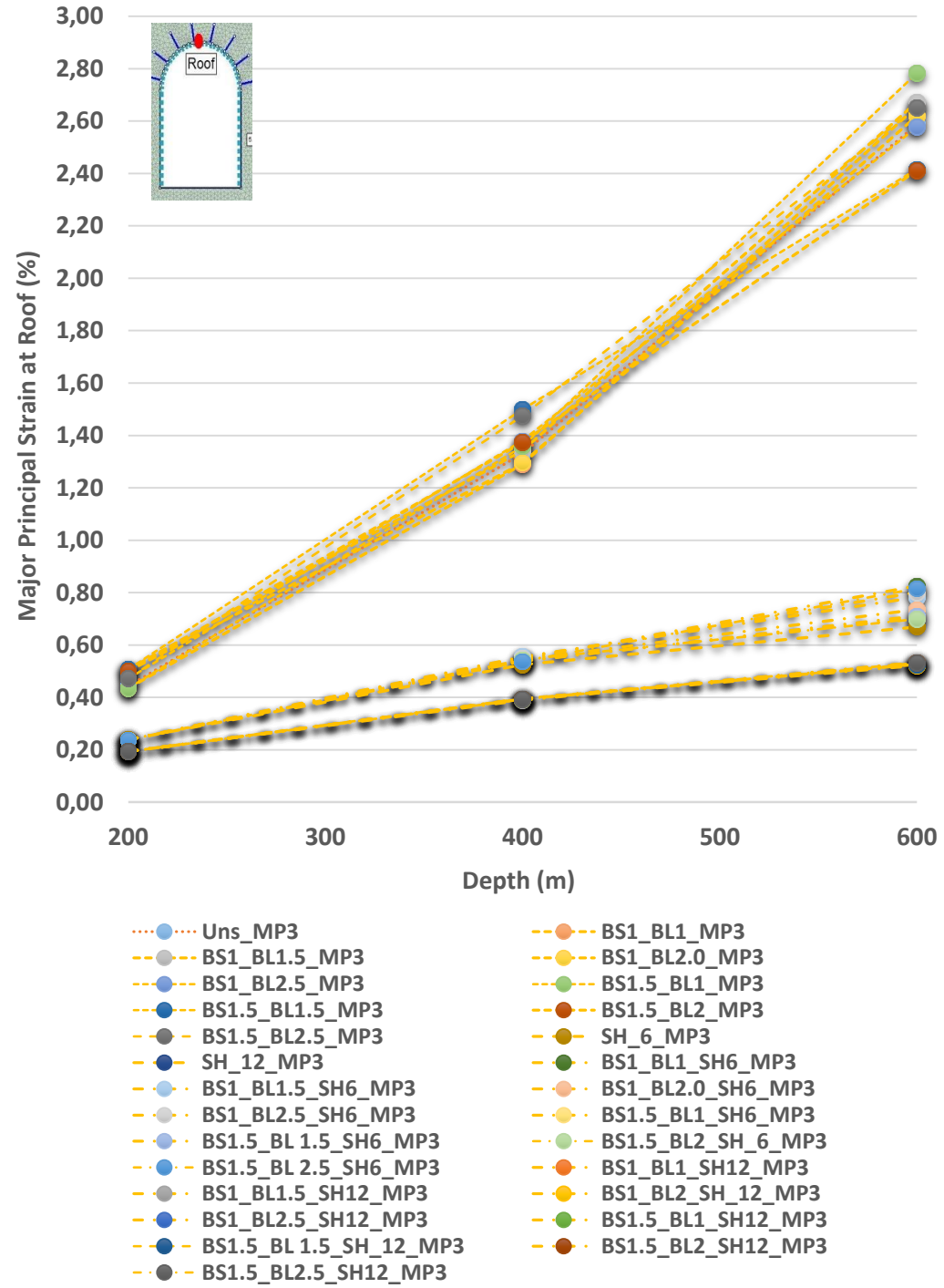


Figure 4.2. Simulated major principal strain at roof (%) vs. depth (m) for k=1.0 for $MP_3$

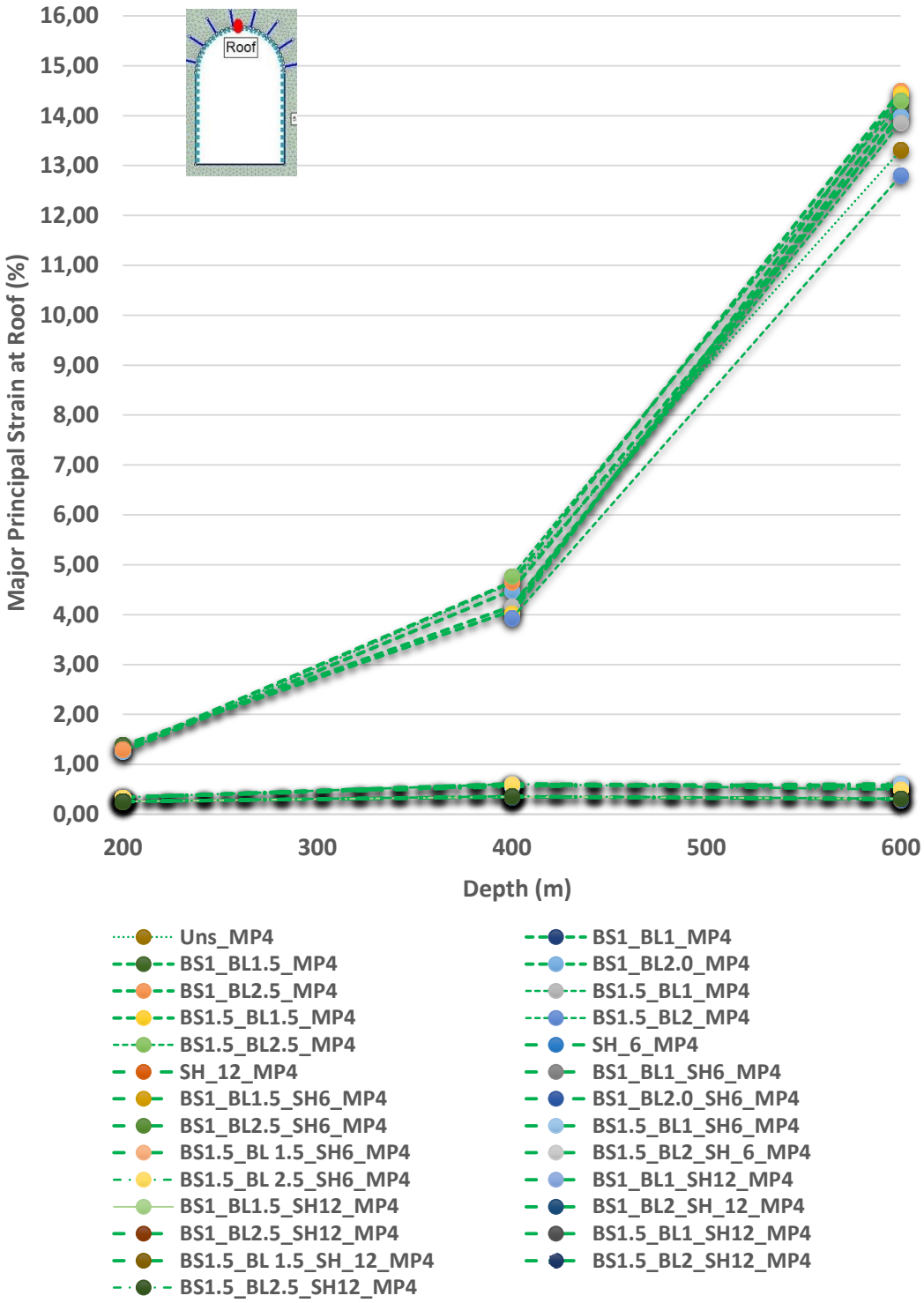


Figure 4.3. Simulated major principal strain at roof (%) vs. depth (m) for k=1.0 for $MP_4$

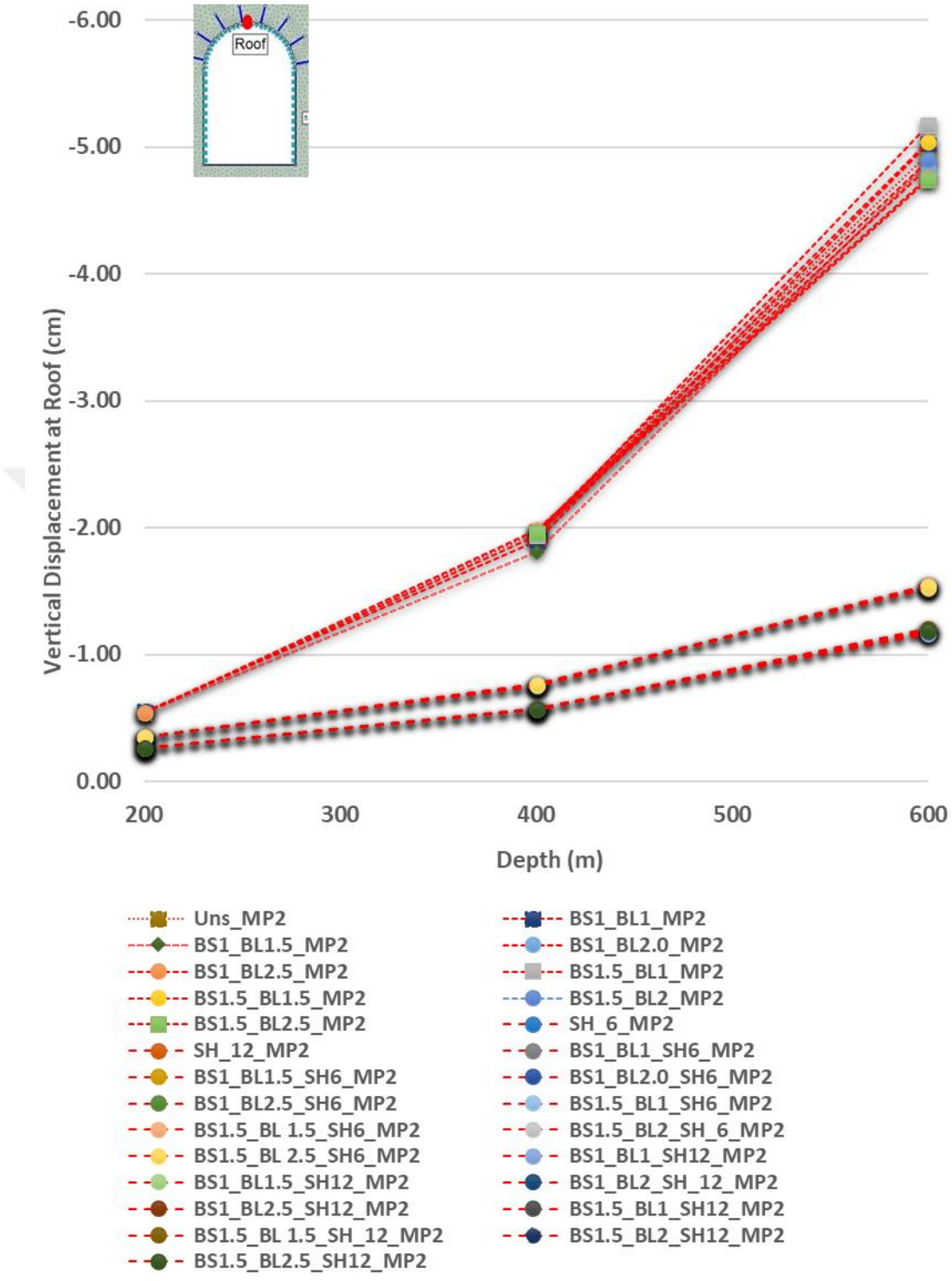


Figure 4.4. Simulated vertical displacement at roof (m) vs. depth (m) for k=1.0 for $MP_2$

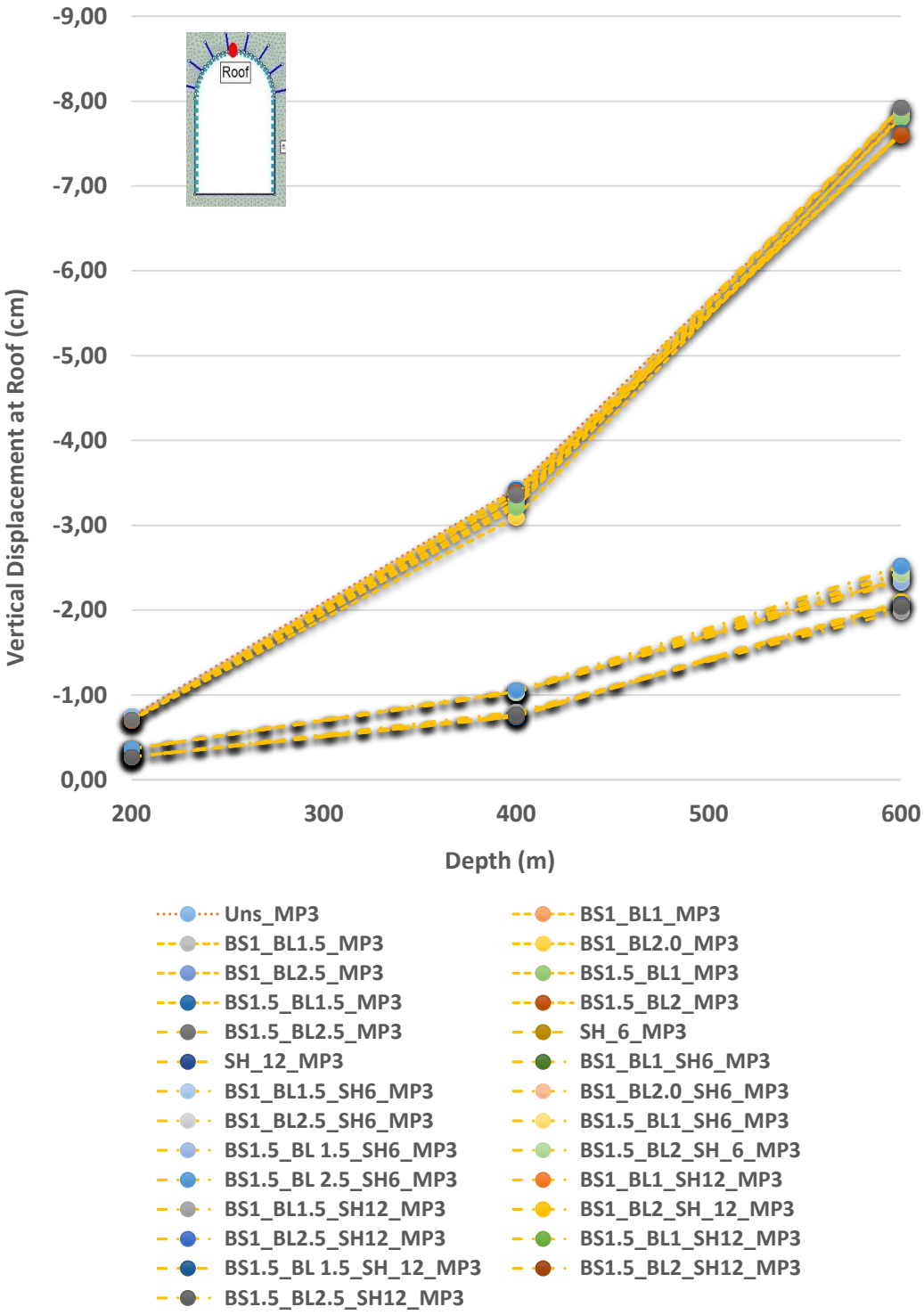


Figure 4.5. Simulated vertical displacement at roof (m) vs. depth (m) for k=1.0 for $MP_3$

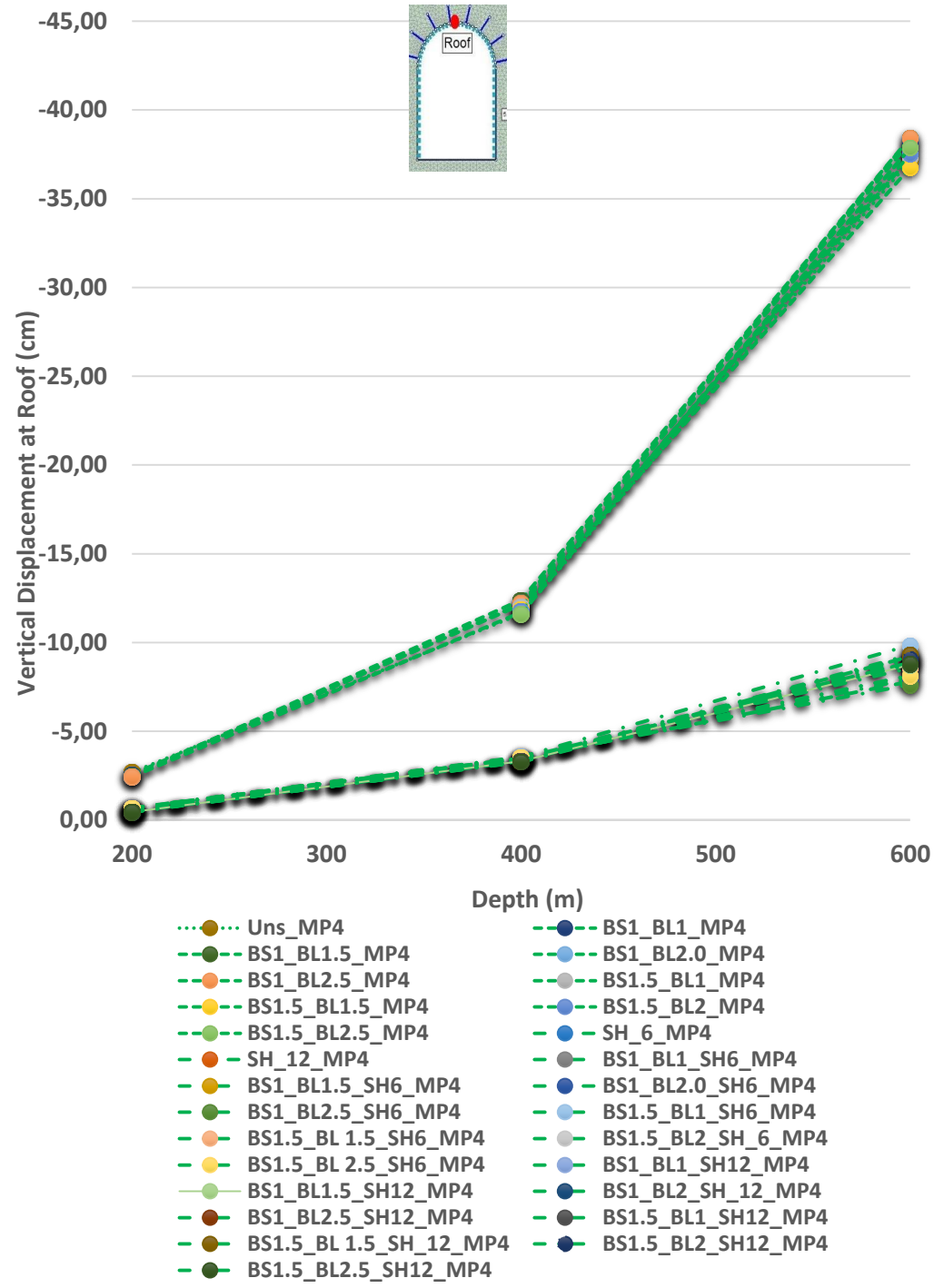


Figure 4.6. Simulated vertical displacement at roof (m) vs. depth (m) for k=1.0 for $MP_4$

Six hypothetical benchmark cases were generated and the support reccomendations of RMR and Q-tunneling index systems were compared. As it is not practical to observe the performance of each support system under the related condition on the field, the geomechanical simulations were regarded as the benchmark. Figure 4.7 shows six of the hypothetical case generated from the Q index interpretation table.

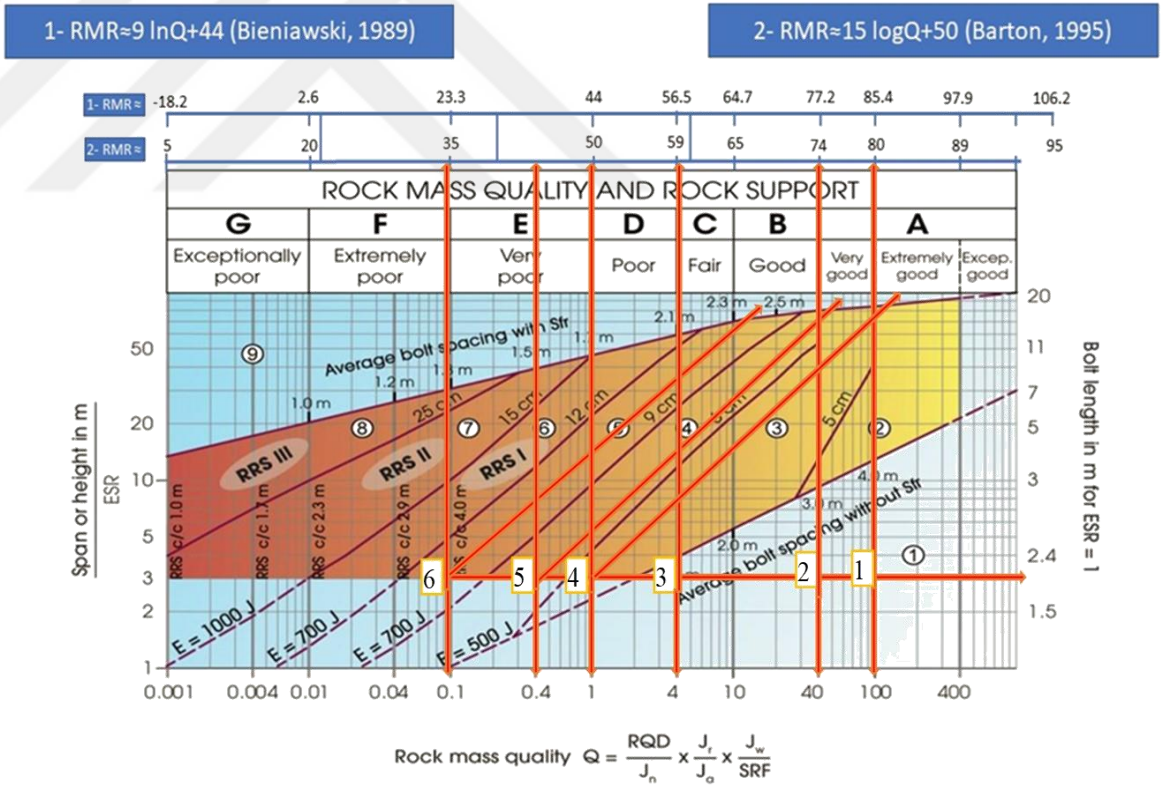


Figure 4.7. Six randomly generated hypothetical cases to compare the performance of support recommendations of empirical systems with the numerical benchmarks

The typical underground mine haul road was determined to have 5 m roof span. The ESR (Equivalent Support Ratio) value of 1.60 was assumed for the study as it is valid for permanent underground openings like inclines, ramps, and shafts that are intended to be used for the entire operational life of the mine. The equivalent dimension ($D_e$) was calculated as 3.12, which was used for determining the support recommendation from the Q index. For the comparative study, Table 4.1 demonsrates the equivalent rock mass quality scores in terms of the other systems. In the benchmark analysis, certain specific values of the Q index were used as references, and accordingly, the other rock mass quality scores were modified to align with the given Q index values. This adjustment allowed for a consistent and coherent comparison of rock mass qualities across the benchmark analysis.

It is important to highlight that although the GSI and RMR scores were adjusted to fit the Q index, the differences in the GSI and RMR scores still fall within or close the range of corresponding rock mass classes.

Table 4.1 Equivalent rock mass quality scores of the hypothetical cases

| **CASE NO** | **RMR Score** | **Q-Tunneling Index** | **GSI Score** | **Rock Mass Geomechanical Properties** |
|---|---|---|---|---|
| 1 | 85 | 100 | 80 | MP1 |
| 2 | 77 | 40 | 72 | MP2 |
| 3 | 56 | 4 | 51 | MP3 |
| 4 | 44 | 1 | 39 | MP4 |
| 5 | 35 | 0.4 | 30 | MP4 |
| 6 | 23 | 0.1 | 18 | MP5 |

*For conversions $RMR_{89}=9\ln Q+44$; and $GSI=RMR_{89}-5$ were used.

Figure 4.8 shows the relationship between stand-up time and RMR scores for the unsupported span of the hyphothetical cases. The stand-up time is given for the

unsupported span of the excavation. Five of the six cases marked on the figure are between the curves, which stands for they are in the transition zone between the immediate collapse and no support required regions. Only the sixth case falls inside the immediate collapse region as the rock mass quality is very poor.

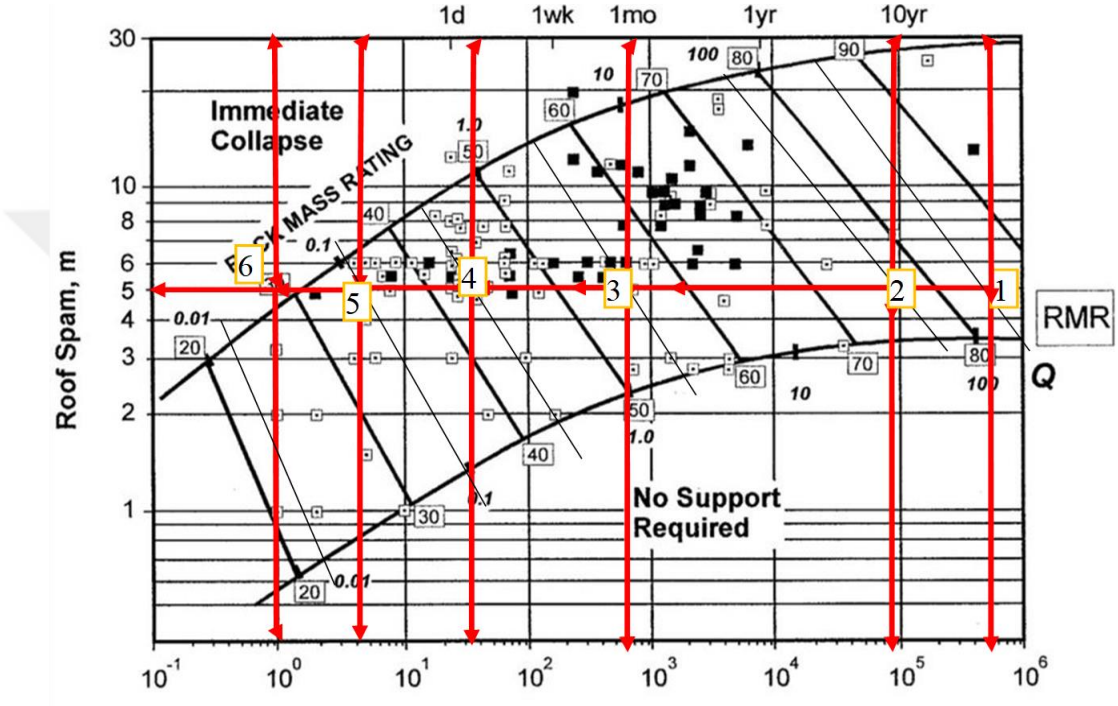


Figure 4.8. Unsupported stand-up time for the six hypothetical cases

As stated in Table 4.2, for very high quality rock mass, the Q and RMR systems state that there is no need for rock support, and spot bolting alone is sufficient, as also confirmed by numerical analysis. For good quality rock mass, the Q system similarly suggests no need for support, while the RMR system recommends occasional wire mesh and 50 mm shotcrete in crown when required. However, the numerical analysis points out that there is no need for support at 200 meters and a minimum of 6 cm liner and spot bolting will be needed at 400 m and 600 m.

For average quality rock mass, the Q system indicates no need for support or spot bolting with 1.5 m spacing without fiber reinforced sprayed concrete, while the RMR system recommends 4 m long rock bolts with 1.5-2 m spacing both in crown and walls with wire mesh and 50-100 mm shotcrete in crown, and 30 mm in side walls. Numerical analysis confirms that there is no need for support at 200 m but single layer and spot bolting may be necessary through the life of mine, systematic bolting with varying lengths of 1.0, 1.5, 2, 2.5 meters with 1 m spacing between roof bolts at 400 m, and a minimum of 6 cm liner reinforcement and systematic bolting at 600 m are required for the stability.

For poor or very poor quality rock mass, the Q system suggests liner reinforced with fibers and systematic bolting, with a thickness of approximately 5 cm. The length of the rock bolts is around 1.7 m, while the spacing between the roof bolts in areas where concrete used is around 4 m. The RMR score in this case does not fall below 44, so the reinforcement recommendation remains the same as in the previous case. Furthermore, the numerical analysis shows that for poor or very poor rocks, models do not converge, indicating large deformations where heavy support configuration will be useful.

Table 4.2 Recommended rock support systems for the hypothetic cases

| **Hypothetical Cases** | | | **Comparison of the Support Recommendations** | | |
|---|---|---|---|---|---|
| **Rock Mass Quality Class** | | | **Q-Tunneling index** | **$RMR_{89}$** | **Numerical Analysis (FEM)** |
| **CASE 1** | | | $1^{st}$ support category.<br>Unsupported or spot bolting.<br>Bolt length=1.7 m. (same for all cases) | no support, spot bolting may be used<br>~20 years stand up time | When k=1<br>spot bolting |
| Q (100) | RMR (85) | FEM ($MP_1$) | | | |
| **CASE 2** | | | $1^{st}$ support category.<br>Unsupported or spot bolting.<br>Bolt length=1.7 m. | Local bolts in crown, 3 m long, spaced 2.5 m with occasional wire mesh, 50 mm shotcrete in crown where required'<br>~10 years stand up time | When k=1<br>for depth = 200 m<br>spot bolting<br>for depth = 400 m<br>liner (single layer), spot bolting<br>for depth = 600 m<br>liner (single layer), spot bolting |
| Q (40) | RMR (77) | FEM ($MP_2$) | | | |

Table 4.2 (continued)

| | | | | | |
|---|---|---|---|---|---|
| **CASE 3** | | | 1st support category.<br>Unsupported or spot bolting with 1.5 m spacing without fibre reinforced sprayed concrete<br>Bolt length=1.7 m. | Systematic bolts 4 m long, spaced 1.5-2 m in crown and walls with wire mesh in crown<br>Shotcrete- 50-100 mm in crown, and 30 mm in sides<br>~1 month Stand Up Time | when k=1<br><u>for depth = 200 m</u><br>liner (single layer), spot bolting<br><u>for depth = 400 m</u><br>systematic bolting with 1 m spacing and 1.5 m length and occasional steels sets<br><u>for depth = 600 m</u><br>liner (single layer), systematic bolting and occasional steel sets |
| Q (4) | RMR (56) | FEM ($MP_3$) | | | |
| **CASE 4** | | | 3rd support category.<br>Concrete reinforced with fibers, thickness 5 cm<br>Systematic bolting, bolt length of 1.7 m, bolt spacing 4 m. | Systematic bolts 4 m long, spaced 1.5-2 m in crown and walls with wire mesh in crown, 50-100 mm shotcrete in crown, and 30 mm in sides,<br>~3 days stand up time | When k=1<br><u>for depth = 200 m</u><br>liner (single layer), spot bolting<br><u>for depth = 400 m</u><br>liner (single layer), systematic bolting with 1 m spacing and 2 m length and systematic steels sets<br><u>for depth = 600 m</u><br>liner (single layer), systematic bolting with 1 m spacing and 2 m length and systematic steels sets |
| Q (1) | RMR (44) | FEM ($MP_4$) | | | |

Table 4.2 (continued)

| | | | | | |
|---|---|---|---|---|---|
| **CASE 5** | | | $4^{th}$ support category. liner reinforced with fibers and bolting, thickness = 6 cm. bolt length 1.7 m, bolt spacing 3 m. | Systematic bolts 4-5 m long, spaced 1-1.5 m in crown and walls with wire mesh, liner 100-150 mm in crown and 100 mm in side walls<br>Steel Sets - Light ribs spaced 1.5 m where required.<br>~4 hours Stand up Time | When k=1<br><u>for depth = 200 m</u><br>liner (single layer), spot bolting<br><u>for depth = 400 m</u><br>liner (double layers), systematic bolting with 1 m spacing and 2 m length and systematic steels sets<br><u>for depth = 600 m</u><br>liner (double layers), systematic bolting with 1 m spacing and 2 m length and systematic steels sets |
| Q (0.4) | RMR (35) | FEM ($MP_4$) | | | |
| **CASE 6** | | | $5^{th}$ support category. concrete reinforced with fibers and bolting, thickness = 9 cm. Bolt length = 1.7 m, bolt spacing = 2.4 m. | Systematic bolts 4-5 m long, spaced 1-1.5 m in crown and walls with wire mesh.<br>Liner 100-150 mm in crown and 100 mm in sides<br>Steel Sets - Light ribs spaced 1.5 m<br>Stand Up Time < 1 hour | Models do not convergence because of the large deformations. Indicates a heavy support configuration is needed. Cast concrete and steel sets can be considered |
| Q (0.1) | RMR (23) | FEM ($MP_5$) | | | |

Based on the numerical modeling study of support systems' performance, several conclusions can be drawn. Firstly, the rock bolt as a primary support alone may not be sufficient for mine access roads during the service life of a mine for the depth of 400 and 600 m. However, for 200 m depth, rock bolts may provide the required stability for the excavation. However, when an enhanced support system is installed, meaning the rock bolt applications together with liners, the total support system can sustain mining-induced loads to the end of the planned mining sequence for $MP_2$, $MP_3$, $MP_4$ type rock masses corresponding the good to poor rock mass qualities. In addition to that, thicker concrete liner appeared to be effective.

Based on the numerical study, some comparison can be made with the RMR and Q index in terms of support recommendations and other geomechanical matters. While these systems are important tools, there are certain potential flaws to be aware of:

1- The Q and $RMR_{89}$ systems rely primarily on geologists' and engineers' subjective opinion. This can lead to inconsistencies in judgments since various experts may have different perspectives on the same rock mass.
2- The RMR system takes into account only a few parameters, such as rock quality, joint spacing, and groundwater conditions. Other essential elements, such as in situ stresses and depths, are disregarded.
3- The dynamic behavior of the rock mass, such as the effects of blasting or seismic activity, is not taken into account by RMR and the Q system.
4- The RMR system is mostly applicable to hard rock masses, and may not be as effective for assessing the stability of weak or fractured rock masses.
5- In-situ stress conditions have a large influence on the behavior of the rock mass. The stress in the rock mass increases with depth, making the rock mass more prone to deformation and failure. Rock masses can be highly anisotropic, and this anisotropy can significantly affect their behavior

during excavation. The Q index, however, does not account for this stress-dependent behavior, therefore the projected rock mass attributes may not precisely reflect the rock mass's actual behavior.

6- The Q index was originally developed for shallow excavations and may not be adequate for deep openings, where the rock mass is subjected to higher stresses and may exhibit different behavior.

The numerical assessment of support recommended by the Q system provided significant insights into the existing state of knowledge. In other words, this study highlighted the limitations of the Q index system in providing clear guidelines for support proposals. The Q index system primarily relies on the engineer's experience and judgement and does not explicitly consider mechanical criteria for failure. This limitation can result in inaccurate support recommendations. Besides, numerical simulations can evaluate the effects of different rock mass parameters on excavation stability and support requirements and can also incorporate mechanical criteria for failure. This approach can provide more accurate and reliable support recommendations. The study also provided practical guidance for engineers on the use of the Q index system and numerical simulations for support design in underground openings. Engineers should carefully evaluate the rock mass parameters and consider strain criteria for failure when designing support systems. They should also use numerical simulations to enhance the accuracy and reliability of support recommendations.

Finally, the study emphasized the shortcomings of the empirical classification approach as well as the potential benefits of applying numerical simulations for support recommendations. The findings of this study can help to establish a more dependable and effective support design technique for tunneling projects because the quality and dependability of support system designs for underground excavations can be considerably increased with the use of numerical modeling.

Neural networks can be a valuable tool in rock mechanics for predicting the behavior of rocks and rock formations under various conditions, and for estimating the rock mass quality scores to determine the required support systems. It might enable to estimate the necessary support systems based on the geological, structural and mechanical parameters by training a neural network.

In addition to modeling and analyzing complicated behaviors of rocks and rock masses, neural networks have also been applied in the field of rock mechanics. These applications include prediction and classification tasks. The safety and effectiveness of mining operations could be greatly enhanced by using neural networks, specifically for support recommendations.

In this study, prior to employing the ANN, critical factors that influence the stability of mine access roads were identified for staged numerical modeling. These parameters were the in-situ stress ratio, depth of the excavation, excavation span and rock mass quality. These may be crucial aspects for mine planers to examine carefully before constructing the mine access roads. This study leads to the development of an alternative methodology for designing mine access roads. The study relies on:

1- Determination of geomechanical data for the rock mass where the access roads will be located.
2- Verification of the ANN with numerical simulations.
3- Recommendation of a support system by considering yielded span around the excavation.

This section presents the interpretation of numerical solutions using artificial neural networks. The model outputs were used to train and test an ANN model to compare its performance with the benchmark cases. With an overall correlation coefficient of 99%, the ANN predictions agreed well with the simulated models. This implies that the ANN model can account for any bias in the yielded span observed in numerical modeling. Correlation plots for training, validation, and overall model performance are given in Figures 4.9 and 4.10. The outliers on the correlation plots

are mainly due to the non-converging models. As explained before, RS2 is a numerical code based on a small deformation theory. Therefore, the models turn out computational errors when excessive deformations are observed. Overall, the correlation coefficients close to 1 proves that the ANN method provides reliable predictions. Considering that the trained model can be easily implemented in a graphical user interface using computer programming tools, the conventional 2D or 3D plots can be replaced with the proposed method to benefit the user-friendly and precise modeling scheme.

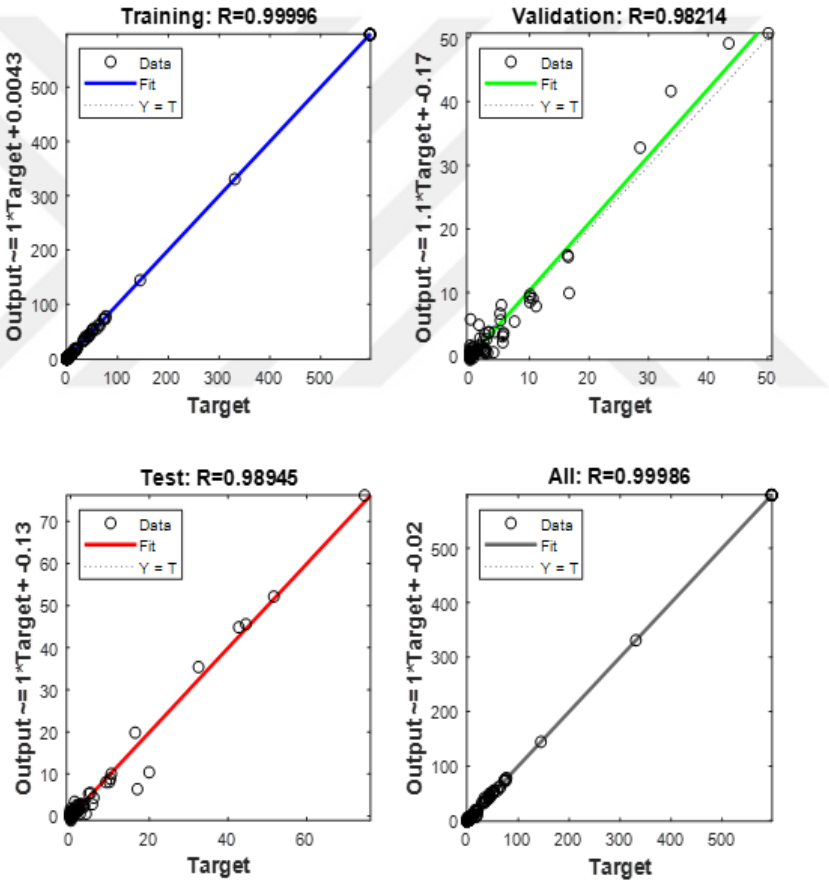


Figure 4.9. Correlation of the numerical simulation outputs with the training, validation, and test data of the ANN model predicting the yielded span in the roof

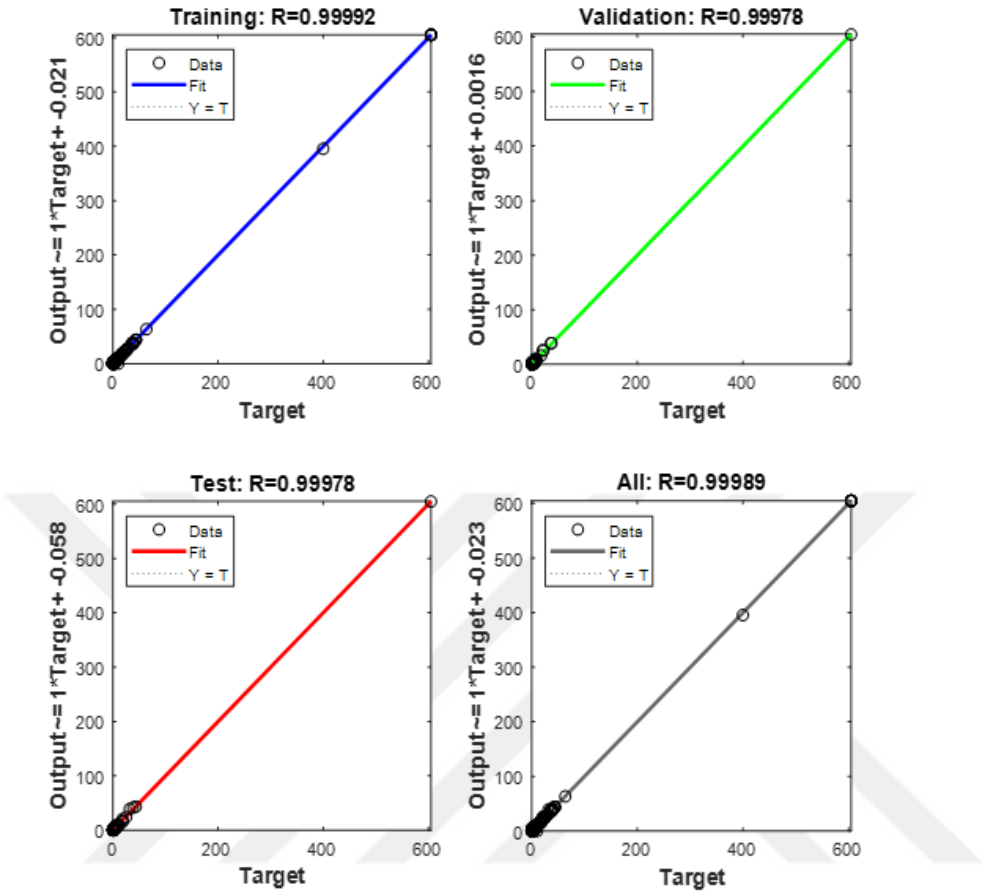


Figure 4.10. Correlation of the numerical simulation outputs with the training, validation, and test data of the ANN model predicting the yielded span in the wall

The graphs comparing the yielded span on the roof and wall of the excavation based on the numerical analysis and the ANN estimates are given in Figure 4.11 and 4.12. It is observed that the simulated and predicted values are significantly close to each other.

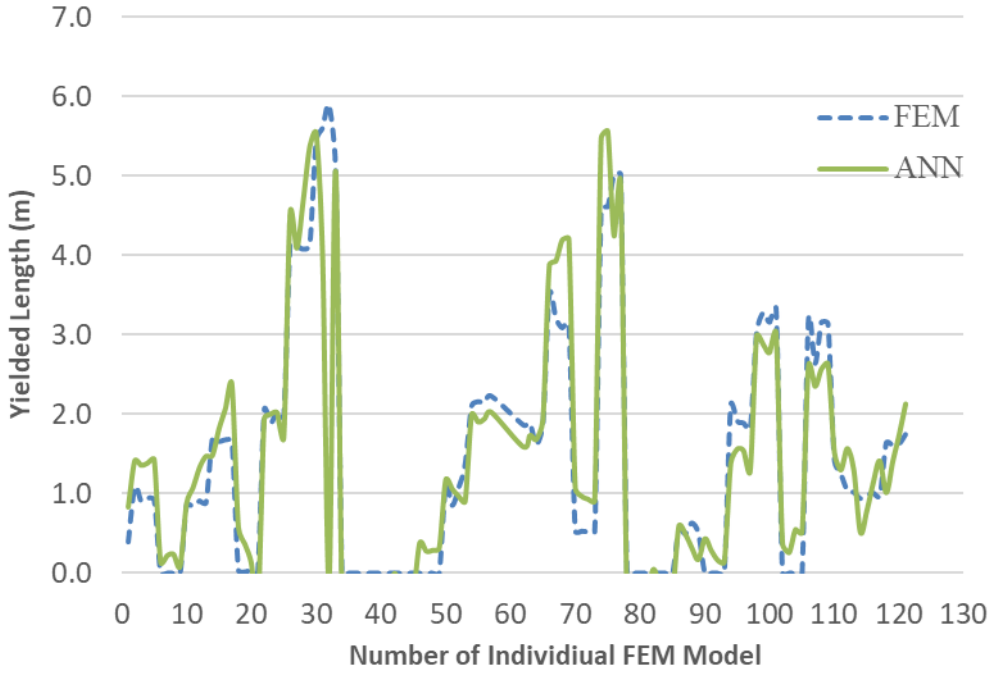


Figure 4.11. Comparison of the yielded span on the roof obtained from the numerical analysis and the ANN model

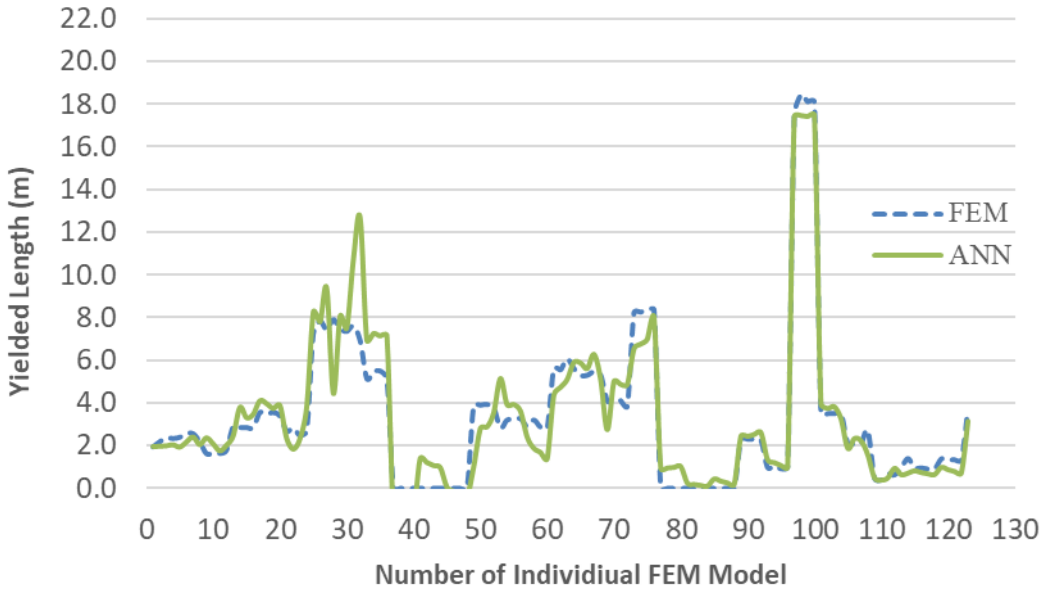


Figure 4.12. Comparison of the yielded span on the wall obtained from the numerical analysis and the ANN model

The yielded span range was narrowed down on the y-axis of the graphs to allow for better observation and closer approximation to realistic values. In this scatter plots, each point represents a data sample from 123 the test dataset divided randomly by the Matlab code. The x-axis shows the actual values from the test dataset and the corresponding predicted values from neural network analysis, y-axis shows the yielded span as meters. Deviations from these line may indicate the model's errors or inaccuracies. These graphs can be used to measure the performance of the model created and visually assess how well the model predictions match the real values of the test data.

Table 4.3 and 4.4 compares the yielded span around the excavation obtained from the numerical analysis and the ANN predictions for six of the randomly selected model settings. The inputs of RS2 and the error in terms of meters and percentage are shown. As the tables show, the highest error percentage is around 5% and majority of the models have around 1% error. This analysis approves that ANN model is successful.

Table 4.3 Comparison of the yielded span on the roof from the numerical analysis and the ANN model

**INPUTS**

| Model No | GSI | Depth (m) | In-situ stress ratio | Bolt Length (m) | Bolt Spacing (m) | Liner Thickness (cm) |
|---|---|---|---|---|---|---|
| 104 | 20 | 200 | 1.5 | 2.0 | 1.0 | - |
| 122 | 70 | 400 | 1.0 | 1.0 | 1.0 | - |
| 243 | 50 | 200 | 1.0 | 1.5 | 1.5 | - |
| 434 | 70 | 400 | 1.5 | 2.0 | 1.0 | 6 |
| 601 | 30 | 600 | 1.5 | 1.5 | 1.5 | 6 |
| 819 | 30 | 600 | 1.5 | 2.5 | 1.5 | 12 |

**OUTPUTS**

| Model No | $\sigma_3$ Roof (MPa) | $u_y$ Roof (m) | $\varepsilon_1$ Roof (%) | Bolt No:1 $F_{ax}$ (MN) | Bolt No:4 $F_{ax}$ (MN) | Liner $F_{ax}$ Wall (MN) | Liner $F_{ax}$ Roof (MN) |
|---|---|---|---|---|---|---|---|
| 104 | -7.3 | -1.853 | 0.62 | 0.0 | 0.0 | 0.0 | 0.0 |
| 122 | -10.3 | -0.019 | 0.01 | 0.1 | 0.3 | 0.0 | 0.0 |
| 243 | -5.2 | -0.007 | 0.01 | 0.1 | 0.1 | 0.0 | 0.0 |
| 434 | -4.1 | -0.004 | 0.01 | 0.2 | 0.1 | 1.0 | 15.6 |
| 601 | -10.1 | -0.059 | 0.01 | 0.3 | 0.3 | 6.6 | 15.4 |
| 819 | -8.6 | -0.098 | 0.01 | 0.3 | 0.3 | 6.7 | 15.2 |

**Yielded Span at the Roof (m)**

| Model No | FEM | ANN | Error (m) | Error (%) |
|---|---|---|---|---|
| 104 | 50.1 | 50.7 | -0.63 | 1.3 |
| 122 | 1.1 | 1.1 | 0.02 | 2.3 |
| 243 | 0.9 | 0.9 | 0.04 | 4.6 |
| 434 | 0.3 | 0.3 | -0.01 | 4.0 |
| 601 | 2.5 | 2.5 | -0.03 | 1.5 |
| 819 | 1.5 | 1.5 | -0.06 | 4.3 |

**$\sigma_3$** = Minimum Principal Stress,
**$\varepsilon_1$** = Major Principal Strain,
**$u_y$** = Vertical displacement
**Bolt No:# $F_{ax}$** = Axial force on the #$^{th}$ bolt at roof from left side,
**Liner $F_{ax}$ Wall/Roof** = Liner axial force at the middle of the wall/roof

Table 4.4 Comparison of the yielded length on the wall from the numerical analysis and the ANN model

**INPUTS**

| Model No | GSI | Depth (m) | In-situ stress ratio | Bolt Length (m) | Bolt Spacing (m) | Liner Thickness (cm) |
|---|---|---|---|---|---|---|
| 40 | 30 | 600 | 0.5 | - | - | - |
| 118 | 70 | 400 | 0.5 | 1.0 | 1.0 | - |
| 239 | 50 | 200 | 0.5 | 1.5 | 1.5 | - |
| 315 | 50 | 600 | 1 | 1.5 | 1.5 | - |
| 436 | 50 | 400 | 0.5 | 1.0 | 1.0 | 6 |
| 552 | 50 | 400 | 1.5 | 1.0 | 1.5 | 6 |

**OUTPUTS**

| Model No | $\sigma_1$ Wall (MPa) | $u_x$ Wall (m) | $\varepsilon_1$ Wall (%) | Bolt No:1 $F_{ax}$ (MN) | Bolt No:4 $F_{ax}$ (MN) | Liner $F_{ax}$ Wall (MN) | Liner $F_{ax}$ Roof (MN) |
|---|---|---|---|---|---|---|---|
| 40 | -8.0 | -0.389 | 0.00 | 0.0 | 0 | 0 | 0 |
| 118 | -2.5 | -0.018 | 0.00 | 0.2 | 0.1 | 0 | 0 |
| 239 | 0.3 | -0.006 | 0.00 | 0.0 | 0.0 | 0 | 0 |
| 315 | -11.7 | -0.100 | 0.00 | 0.2 | 0.3 | 0 | 0 |
| 436 | -5.2 | -0.024 | 0.00 | 0.1 | 0.1 | 5.7 | 3.6 |
| 552 | -6.6 | -0.052 | 0.00 | 0.2 | 0.2 | 3.2 | 15.5 |

| Yielded Span at the Wall (m) | | | | |
|---|---|---|---|---|
| **Model No** | **FEM** | **ANN** | **Error (m)** | **Error (%)** |
| 40 | 10.7 | 10.8 | -0.13 | 1.2 |
| 118 | 2.8 | 2.7 | 0.08 | 2.9 |
| 239 | 2.3 | 2.3 | 0.04 | 1.5 |
| 315 | 5.5 | 5.5 | 0.02 | 0.3 |
| 436 | 3.5 | 3.7 | -0.18 | 5.2 |
| 552 | 2.4 | 2.4 | 0.03 | 1.3 |

**$\sigma_1$ =** Maximum principal stress,
**$\varepsilon_1$ =** Major principal strain,
**$u_x$ =** Horizontal displacement
**Bolt No:# $F_{ax}$ =** Axial force on the #$^{th}$ bolt at roof from left side,
**Liner $F_{ax}$ Wall/Roof =** Liner axial force at the middle of the wall/roof

# CHAPTER 5

## CONCLUSIONS AND RECOMMENDATIONS

This study investigated the support recommendations of empirical systems using more advance numerical modeling. For numerical modeling, the geomechanical properties of the rock masses have been thoroughly examined, along with various approaches. Numerical simulations were used to assess the stability of a typical underground mine main haul road within specific rock masses with certain support types, and the results of numerical analysis were compared with the widely accepted RMR and Q systems. In doing so, 819 different FEM models were generated, resulting in a total of 22,131 individual data points, taking into account the factors affecting the stability of rock mass. The simulation results were used to train an ANN model for easier interpretation. The accuracy of the model was tested and the proposed model was validated. The results showed that the ANN model provided reasonable outcomes, indicating that the intermediate conditions no more need to be simulated numerically. In another aspect, by combining numerical analysis and artificial neural networks, many other unknown conditions that are not included in traditional rock mass classification methods can be revealed.

The empirical systems are capable of making recommendations based on scant information. Besides, they might not always be able to offer reasonable proposals for specific circumstances such as changes in depth or particular differences in the characteristics of rock masses. Numerical models, on the contrary, may allow for the evaluation of results via two-dimensional graphs by assigning two variables to the x and y axes, or by the composition of additional variables with data series. Nevertheless, as the number of data series expands, displaying data becomes more difficult, and also three-dimensional graphs may be impractical for these situations. As a consequence, instead of forming standard scatter plots, an alternative method

may be beneficial. In this particular instance, it would be appropriate to research the utilization of Artificial Neural Networks by directly training a machine to produce a more practical systematic. In doing so, a data series was generated through numerical analysis and output values were selected based on the geomechanical properties of specific rock masses. These data were examined using the Artificial Neural Networks approach, and the results indicated a correlation value of around 99% with an error margins of less than mostly 5%. The following recommendations and conclusions can be derived from the research of the review of support proposals in the empirical systems based on numerical analyses:

- Engineers and/or researchers should continue to evaluate the accuracy and reliability of numerical simulations for support recommendations in underground opening projects and develop practical guidelines for their use in support design.

- The RMR and Q index systems have limitations in providing clear guidelines for support recommendations, and its reliance on the engineer's experience and judgement can result in inaccurate support recommendations.

- The integration of numerical simulations into the empirical methods for support recommendations requires further research but has the potential to provide more accurate and reliable support recommendations.

Furthermore, within the context of the mathematical algorithms, neural networks can make recommendations for support design and arrangement that are specific to the requirements of the mine access roads of a mining site by assessing a huge quantity of input data, including rock mass qualities, geotechnical factors, and support system features. There can be various areas of future work that should be

investigated to better develop the usage of neural net fitting networks for support recommendations in rock mechanics. Further research should focus on evaluating the effects of different rock mass parameters, such as strength, deformation modulus, joint spacing, and different opening dimensions on underground opening stability and support requirements, and incorporating mechanical criteria for failure in support design and may concentrate on gathering, generating and preparing high quality and reliable data from a variety of mining sites to construct effective and accurate deep learning models. The architecture and training of the neural network models play a critical role in their accuracy and effectiveness. Future work should also explore different architectures and training algorithms to identify the most effective approaches for support recommendation in rock mechanics. As a result, future research should most importantly concentrate on enhancing model validation and uncertainty analysis methods that may be utilized in the context of rock mechanics.

In order to provide a more comprehensive understanding of rock mass behavior and support system performance, neural network models should be combined with other modeling methodologies such as numerical modeling and physical experiments. Moreover, to provide more exact and reliable estimates, hybrid models capable of combining these features of many modeling approaches can be required.

## REFERENCES


Abad, J., Celada, B., Chacon, E., Gutierrez, V., & Hidalgo, E. (1983). Application of geomechanical classification to predict the convergence of coal mine galleries and to design their supports. *5th ISRM Congress 1983*. https://doi.org/10.1016/0148-9062(84)92847-x

ACI committee 318. (2011). Building Code Requirements for Structural Concrete and Commentary (ACI 318M-11). In *American Concrete Institute, Farmington Hills, MI*.

Aladejare, A. E. (2020). Evaluation of empirical estimation of uniaxial compressive strength of rock using measurements from index and physical tests. *Journal of Rock Mechanics and Geotechnical Engineering*, *12*(2), 256–268. https://doi.org/10.1016/J.JRMGE.2019.08.001

Alavala, C. R. (2007). *Fuzzy Logic and Neural Networks: Basic Concepts and Application*. New Age International (P) Limited, Publishers. https://books.google.com.tr/books?id=jABjAQAACAAJ

Alemdag, S., Gurocak, Z., & Gokceoglu, C. (2015). A simple regression based approach to estimate deformation modulus of rock masses. *Journal of African Earth Sciences*, *110*. https://doi.org/10.1016/j.jafrearsci.2015.06.011

Ali, W., Mohammad, N., & Tahir, M. (2014). *Rock Mass Characterization for Diversion Tunnels at Diamer Basha Dam, Pakistan-a design perspective*.

Aliyu, M. M., Shang, J., Murphy, W., Lawrence, J. A., Collier, R., Kong, F., & Zhao, Z. (2019). Assessing the uniaxial compressive strength of extremely hard cryptocrystalline flint. *International Journal of Rock Mechanics and Mining Sciences*, *113*, 310–321. https://doi.org/10.1016/J.IJRMMS.2018.12.002

Atkinson, T. (1992). Selection and sizing of excavating equipment. *SME Mining Engineering Handbook*, *2*, 1311–1333.

Aydan, O., & Dalgic, S. (1998). Prediction of deformation behavior of 3-lanes Bolu tunnels through squeezing rocks of North Anatolian fault zone (NAFZ). *Proc. Reg. Symp. on Sedimentary Rock Engng*, 228–233.

Aydan, O., Ulusay, R., & Kawamoto, T. (1997). Assessment of rock mass strength for underground excavations. *International Journal of Rock Mechanics and Mining Sciences & Geomechanics Abstracts*, *34*(3–4). https://doi.org/10.1016/S1365-1609(97)00273-6

Aydin, A., & Basu, A. (2005). The Schmidt hammer in rock material characterization. *Engineering Geology*, *81*(1), 1–14. https://doi.org/10.1016/J.ENGGEO.2005.06.006

Baczynski, N. R. P. (1982). Application of various rock mass classifications to unsupported openings at Mount Isa, Queensland: A case study : Baczynski, N R P Proc 3rd Australia-New Zealand Conference on Geomechanics, Wellington, 12–16 May 1980, V2, P137–143. Publ Wellington: New Zealand Institution of Engineers, 1980. *International Journal of Rock Mechanics and Mining Sciences & Geomechanics Abstracts*, *19*(6), 140. https://doi.org/10.1016/0148-9062(82)91513-3

Barla, G. (2016). Applications of numerical methods in tunnelling and underground excavations: Recent trends. *ISRM International Symposium - EUROCK 2016*.

Barton, N. (1995). The influence of joint properties in modelling jointed rock masses. *8th ISRM Congress*.

Barton, N. (2002). Some new Q-value correlations to assist in site characterisation and tunnel design. *International Journal of Rock Mechanics and Mining Sciences*, *39*(2). https://doi.org/10.1016/S1365-1609(02)00011-4

Barton, N., Lien, R., & Lunde, J. (1974). Engineering classification of rock masses for the design of tunnel support. *Rock Mechanics Felsmechanik Mécanique Des Roches*, *6*(4). https://doi.org/10.1007/BF01239496

Barton, N., Løset, F., Lien, R., & Lunde, J. (1981). Application Of Q-System In Design Decisions Concerning Dimensions And Appropriate Support For Underground Installations. In *Subsurface Space: Environmental Protection Low Cost Storage Energy Savings* (Vol. 2). https://doi.org/10.1016/B978-1-4832-8421-7.50080-6

Basu, A., & Kamran, M. (2010). Point load test on schistose rocks and its applicability in predicting uniaxial compressive strength. *International Journal of Rock Mechanics and Mining Sciences*, *47*(5), 823–828. https://doi.org/10.1016/J.IJRMMS.2010.04.006

Bieniawski, Z. T. (1975). The point-load test in geotechnical practice. *Engineering Geology*, *9*(1), 1–11. https://doi.org/10.1016/0013-7952(75)90024-1

Bieniawski, Z. T. (1978). Determining rock mass deformability: experience from case histories. *International Journal of Rock Mechanics and Mining Sciences And*, *15*(5). https://doi.org/10.1016/0148-9062(78)90956-7

Bieniawski, Z. T. (2011). Misconceptions in the applications of rock mass classifications and their corrections. *ADIF Seminar on Advanced Geotechnical Characterization for Tunnel Design*.

Bobet, A., Fakhimi, A., Johnson, S., Morris, J., Tonon, F., & Yeung, M. R. (2009). Numerical Models in Discontinuous Media: Review of Advances for Rock Mechanics Applications. *Journal of Geotechnical and Geoenvironmental Engineering*, *135*(11). https://doi.org/10.1061/(asce)gt.1943-5606.0000133

Brady, B. H. G., & Brown, E. T. (2006). Rock Mechanics for underground mining: Third edition. In *Rock Mechanics for underground mining: Third edition*. https://doi.org/10.1007/978-1-4020-2116-9

Brazil, M., Grossman, P. A., Lee, D. H., Rubinstein, J. H., Thomas, D. A., & Wormald, N. C. (2008). Decline design in underground mines using constrained path optimisation. *Transactions of the Institutions of Mining and*

*Metallurgy, Section A: Mining Technology*, *117*(2). https://doi.org/10.1179/174328608X362668

Broch, E., & Franklin, J. A. (1972). The point-load strength test. *International Journal of Rock Mechanics and Mining Sciences & Geomechanics Abstracts*, *9*(6), 669–676. https://doi.org/10.1016/0148-9062(72)90030-7

Brown, E. T., & Hoek, E. (1980). Underground Excavations in Rock. In *Underground Excavations in Rock*. https://doi.org/10.1201/9781482288926

Cameron-Clarke, I. S., & Budavari, S. (1981). Correlation of rock mass classification parameters obtained from borecore and In-situ observations. *Engineering Geology*, *17*(1–2), 19–53. https://doi.org/10.1016/0013-7952(81)90019-3

Cargill, J. S., & Shakoor, A. (1990). Evaluation of empirical methods for measuring the uniaxial compressive strength of rock. *International Journal of Rock Mechanics and Mining Sciences And*, *27*(6). https://doi.org/10.1016/0148-9062(90)91001-N

Celada, B., Tardáguila, I., Varona, P., Rodríguez, A., & Bieniawski, Z. T. (2014). Innovating Tunnel Design by an Improved Experience-based RMR System. *Proceedings of the World Tunnel Congress 2014 – Tunnels for a Better Life*, *3*.

Celada Tamanes, B. (1984). *Fourteen Years Of Experience On Rock Bolting In Spain*. https://doi.org/10.1201/9780203740507-28

Chau, K. T., & Wong, R. H. C. (1996). Uniaxial compressive strength and point load strength of rocks. *International Journal of Rock Mechanics and Mining Sciences & Geomechanics Abstracts*, *33*(2), 183–188. https://doi.org/10.1016/0148-9062(95)00056-9

Chen, D. (1994). *Design of rock bolting systems for underground excavations*.

Chen, W., Wan, W., & Peng, W. (2022). Prediction of rock mass rating using neural network with an improved rider optimization algorithm. *Evolutionary Intelligence*, *15*(4), 2567–2579. https://doi.org/10.1007/s12065-021-00606-w

Copco, A. (2007). Mining methods in underground mining. *Atlas Copco: Nacka, Sweden.*

D. S. Agustawijaya. (2007). The Uniaxial Compressive Strength of Soft Rock. *Civil Engineering Dimension*, *9*(1).

*DSI Underground* (n.d.). DSI Underground Retrieved March 20, 2023, from https://www.dsiunderground.com.au/

da Silva Ribeiro, P. C. P., Oliveira, M. M., & Nelson, P. (2016). Correlation between uniaxial compressive strength and Brazilian tensile strength using different rock types. *ISRM VII Brazilian Symposium on Rock Mechanics, SBMR 2016*. https://doi.org/10.20906/cps/gj-13-0005

Diederichs, M. S., & Kaiser, P. K. (1999). Tensile strength and abutment relaxation as failure control mechanisms in underground excavations. *International Journal of Rock Mechanics and Mining Sciences*, *36*(1). https://doi.org/10.1016/S0148-9062(98)00179-X

Dinc, O. S., Sonmez, H., Tunusluoglu, C., & Kasapoglu, K. E. (2011). A new general empirical approach for the prediction of rock mass strengths of soft to hard rock masses. *International Journal of Rock Mechanics and Mining Sciences*, *48*(4). https://doi.org/10.1016/j.ijrmms.2011.03.001

Elbaz K., Zhou A., Shen S., Deep reinforcement learning approach to optimize the driving performance of shield tunnelling machines, Tunnelling and Underground Space Technology, Volume 136, 2023,. https://doi.org/10.1016/j.tust.2023.105104.

Exadaktylos, G. E. (2005). *Mechanical properties of intact sedimentary and metamorphic rocks, Final Report of DIAS, Project No. DIAS-EVK4-CT2002-00080*.

Fairhurst, C. (1964). On the validity of the "Brazilian" test for brittle materials. *International Journal of Rock Mechanics and Mining Sciences And*, *1*(4). https://doi.org/10.1016/0148-9062(64)90060-9

Fener, M., Kahraman, S., Bilgil, A., & Gunaydin, O. (2005). A comparative evaluation of indirect methods to estimate the compressive strength of rocks. *Rock Mechanics and Rock Engineering*, *38*(4). https://doi.org/10.1007/s00603-005-0061-8

Galera, J. M., Álvarez, M., & Bieniawski, Z. T. (2005). Evaluation of the Deformation Modulus of Rock Masses: Comparison of Pressuremeter and Dilatometer Tests with RMR Prediction. *Proceedings of the ISP5-PRESSIO 2005*.

Gholami, R., Rasouli, V., & Alimoradi, A. (2013). Improved RMR rock mass classification using artificial intelligence algorithms. *Rock Mechanics and Rock Engineering*, *46*(5), 1199–1209. https://doi.org/10.1007/s00603-012-0338-7

Ghosh D.K and Srivastava M. (1991). Point load strength: an index for classification of rock material : Ghosh, D K; Srivastava, M Int Assoc Engng Geol BullN44, Oct 1991, P27–33. *International Journal of Rock Mechanics and Mining Sciences & Geomechanics Abstracts*, *29*(5), 279. https://doi.org/10.1016/0148-9062(92)92688-9

Gokceoglu, C. (1996). Schmidt sertlik çekici kullanılarak tahmin edilen tek eksenli basınç dayanımı verilerinin güvenilirliği üzerine bir değerlendirme. *Jeoloji Mühendisliği*, *48*, 78–81.

Griffith, A. A. (1921). VI. The phenomena of rupture and flow in solids. *Philosophical Transactions of the Royal Society of London. Series A,*

*Containing Papers of a Mathematical or Physical Character*, *221*(582–593), 163–198.

Grimstad, E., & Barton, N. (1993). Updating the Q-system for NMT. In *Proc. int. symp. on sprayed concrete-modern use of wet mix sprayed concrete for underground support*.

Gunsallus, K. L., & Kulhawy, F. H. (1984). A comparative evaluation of rock strength measures. *International Journal of Rock Mechanics and Mining Sciences & Geomechanics Abstracts*, *21*(5), 233–248. https://doi.org/10.1016/0148-9062(84)92680-9

Gupta, V. (2009). Non-destructive testing of some Higher Himalayan Rocks in the Satluj Valley. *Bulletin of Engineering Geology and the Environment*, *68*(3). https://doi.org/10.1007/s10064-009-0211-4

Gurocak, Z., Solanki, P., Alemdag, S., & Zaman, M. M. (2012). New considerations for empirical estimation of tensile strength of rocks. *Engineering Geology*, *144–145*. https://doi.org/10.1016/j.enggeo.2012.06.005

Haramy, K. Y., & DeMarco, M. J. (1985). Use Of The Schmidt Hammer For Rock And Coal Testing. *Proceedings - Symposium on Rock Mechanics*, *1*. https://doi.org/10.1016/0148-9062(86)90704-7

Hebb D. O. (1950). Hebb, D. O. The organization of behavior: A neuropsychological theory. New York: John Wiley and Sons, Inc., 1949. 335 p. $4.00. *Science Education*, *34*(5). https://doi.org/10.1002/sce.37303405110

Hoek, E. (1991). When is a design in rock engineering acceptable? *7th ISRM Congress*. https://doi.org/10.1016/0148-9062(94)92605-0

Hoek, E. (2007). Model to demonstrate how rockbolts work. In *Practical Rock Engineering*.

Hoek, E., & Brown, E. T. (1980). Empirical strength criterion for rock masses. *Journal of the Geotechnical Engineering Division, ASCE*, *106*(GT9, Proc. Paper, 15715). https://doi.org/10.1061/ajgeb6.0001029

Hoek, E., & Brown, E. T. (1997). Practical estimates of rock mass strength. *International Journal of Rock Mechanics and Mining Sciences*, *34*(8). https://doi.org/10.1016/S1365-1609(97)80069-X

Hoek, E., Carranza, C., & Corkum, B. (2002). Hoek-brown failure criterion – 2002 edition. *Narms-Tac*.

Hoek, E., & Diederichs, M. S. (2006). Empirical estimation of rock mass modulus. *International Journal of Rock Mechanics and Mining Sciences*, *43*(2). https://doi.org/10.1016/j.ijrmms.2005.06.005

Hoek, E., Kaiser, P. K., & Bawden, W. F. (1995). Support of underground excavations in hard rock. In *Support of Underground Excavations in Hard Rock*. https://doi.org/10.2113/gseegeosci.ii.4.610

Hoek, E., & Marinos, P. (2000). Predicting tunnel squeezing problems in weak heterogeneous rock masses. *Tunnels and Tunnelling International Part*, *1*(December).

Hoek, E., Marinos, P., & Benissi, M. (1998). Applicability of the geological strength index (GSI) classification for very weak and sheared rock masses. The case of the Athens Schist Formation. *Bulletin of Engineering Geology and the Environment*, *57*(2). https://doi.org/10.1007/s100640050031

Hopfield, J. J. (1982). Neural networks and physical systems with emergent collective computational abilities. *Proceedings of the National Academy of Sciences of the United States of America*, *79*(8). https://doi.org/10.1073/pnas.79.8.2554

Hudson, J. A., & Harrison, J. P. (1997). In situ stress. In *Engineering Rock Mechanics*. https://doi.org/10.1016/b978-008043864-1/50005-7

Hustrulid, W. A. (1982). *Underground mining methods handbook*.

Irvani, I., Wilopo, W., & Karnawati, D. (2015). Determination Of Nuclear Power Plant Site In West Bangka Based On Rock Mass Rating And Geological Strength Index. *Journal of Applied Geology*, *5*(2). https://doi.org/10.22146/jag.7210

Jalalifar, H., Mojedifar, S., Sahebi, A. A., & Nezamabadi-pour, H. (2011). Application of the adaptive neuro-fuzzy inference system for prediction of a rock engineering classification system. *Computers and Geotechnics*, *38*(6), 783–790. https://doi.org/10.1016/J.COMPGEO.2011.04.005

Jašarević, I., & Kovačević, M. S. (1996). Analyzing applicability of existing classification for hard carbonate rock in mediterranean area. *ISRM International Symposium - EUROCK 1996*.

Kahraman, S. (2001). Evaluation of simple methods for assessing the uniaxial compressive strength of rock. *International Journal of Rock Mechanics and Mining Sciences*, *38*(7), 981–994. https://doi.org/10.1016/S1365-1609(01)00039-9

Kahraman, S., & Gunaydin, O. (2009). The effect of rock classes on the relation between uniaxial compressive strength and point load index. *Bulletin of Engineering Geology and the Environment*, *68*(3). https://doi.org/10.1007/s10064-009-0195-0

Kahraman, S., Gunaydin, O., & Fener, M. (2005). The effect of porosity on the relation between uniaxial compressive strength and point load index. *International Journal of Rock Mechanics and Mining Sciences*, *42*(4), 584–589. https://doi.org/10.1016/J.IJRMMS.2005.02.004

Kaiser, P. K., MacKay, C., & Gale, A. D. (1986). Evaluation of rock classifications at B. C. Rail tumbler ridge tunnels. *Rock Mechanics and Rock Engineering*, *19*(4). https://doi.org/10.1007/BF01039996

Kalamaras, G. S., & Bieniawski, Z. T. (1995). A rock mass strength concept for coal seams incorporating the effect of time. *8th ISRM Congress*.

Karaman, K., Cihangir, F., Ercikdi, B., Kesimal, A., & Demirel, S. (2015). Utilization of the Brazilian test for estimating the Uniaxial compressive strength and shear strength parameters. *Journal- South African Institute of Mining and Metallurgy*, *115*, 185–192. https://doi.org/10.17159/2411-9717/2015/v115n3a3

Katz, O., Reches, Z., & Roegiers, J. C. (2000). Evaluation of mechanical rock properties using a Schmidt Hammer. *International Journal of Rock Mechanics and Mining Sciences*, *37*(4), 723–728. https://doi.org/10.1016/S1365-1609(00)00004-6

Kayabasi, A., Gokceoglu, C., & Ercanoglu, M. (2003). Estimating the deformation modulus of rock masses: A comparative study. *International Journal of Rock Mechanics and Mining Sciences*, *40*(1). https://doi.org/10.1016/S1365-1609(02)00112-0

Kılıç, A., & Teymen, A. (2008). Determination of mechanical properties of rocks using simple methods. *Bulletin of Engineering Geology and the Environment*, *67*(2). https://doi.org/10.1007/s10064-008-0128-3

Kirsch, G. (1898). Die Theorie der Elastizit¨at und die Bed¨urfnisse der Festigkeitslehre. Zeitschrift des Vereines deutscher Ingenieure 42, 797–807.

Kohno, M., & Maeda, H. (2012). Relationship between point load strength index and uniaxial compressive strength of hydrothermally altered soft rocks. *International Journal of Rock Mechanics and Mining Sciences*, *50*, 147–157. https://doi.org/10.1016/J.IJRMMS.2012.01.011

Koutsoftas, D. C. (2018). Discussion of “Rock quality designation (RQD): Time to rest in peace.” In *Canadian Geotechnical Journal* (Vol. 55, Issue 4). https://doi.org/10.1139/cgj-2017-0497

Laginha Serafim, J., & Paulino Pereira, J. (1983). *Considerations On The Geomechanical Classification Of Bieniawski. 1*. https://doi.org/10.1016/0148-9062(84)90053-6

Leu, S.S.; Chen, C.N.; Chang, S.L. Data Mining for Tunnel Support Stability: Neural Network Approach. Autom. Constr. 2001,10, 429–44

Marinos, P., & Hoek, E. (2001). Estimating the geotechnical properties of heterogeneous rock masses such as flysch. *Bulletin of Engineering Geology and the Environment*, *60*(2). https://doi.org/10.1007/s100640000090

Martins, F. F., & Miranda, T. F. S. (2012). Estimation of the Rock Deformation Modulus and RMR Based on Data Mining Techniques. *Geotechnical and Geological Engineering*, *30*(4), 787–801. https://doi.org/10.1007/s10706-012-9498-1

Mishra, D. A., & Basu, A. (2012). Use of the block punch test to predict the compressive and tensile strengths of rocks. *International Journal of Rock Mechanics and Mining Sciences*, *51*, 119–127. https://doi.org/10.1016/J.IJRMMS.2012.01.016

Mitri, H. S. , E. R. , & H. J. G. (1995). *Finite-element modeling of cable-bolted stopes in hard-rock underground mines. Transactions-Society for Mining Metallurgy and Exploration Incorporated, 298*.

Nazir, R., Momeni, E., Armaghani, D. J., & Amin, M. F. M. (2013). Prediction of unconfined compressive strength of limestone rock samples using l-type schmidt hammer. *Electronic Journal of Geotechnical Engineering*, *18 I*.

NGI. (2015). Using the Q-system: rock mass classification and support design. *Norwegian Geotechnical Institute*.

Nilsen B, P. A. (2000). *Engineering geology and rock engineering. Hand book no. 2. Norwegian Group for Rock Mechanics (NBG) in co-operation with Norwegian Tunneling Society (NFF)*.

O'Rourke, J. E. (1989). Rock index properties for geoengineering in underground development. *Mining Engineering*, *41*(2). https://doi.org/10.1016/0148-9062(89)92513-8

Osgoui, R., & Ünal, E. (2005). Rock reinforcement design for unstable tunnels originally excavated in very poor rock mass. *Underground Space Use: Analysis of the Past and Lessons for the Future - Proceedings of the 31st ITA-AITES World Tunnel Congress*, *1*. https://doi.org/10.1201/noe0415374521.ch44

Palmström, A. (1995). RMi – a rock mass characterization system for rock engineering purposes. *Sciences-New York.*

Palmström, A. (1996). RMi - a system for characterizing rock mass strength for use in rock engineering. *Journal of Rock Mechanics and Tunnelling Technology*, *1*(2).

Palmstrom, A., & Broch, E. (2006). Use and misuse of rock mass classification systems with particular reference to the Q-system. *Tunnelling and Underground Space Technology*, *21*(6), 575–593. https://doi.org/10.1016/J.TUST.2005.10.005

Pande, G. N., Beer, G., & Williams, J. (1990). *Numerical methods in rock mechanics*.

Pells, P. J., Bieniawski, Z. T., Hencher, S. R., & Pells, S. E. (2017). Rock quality designation (RQD): Time to rest in peace. *Canadian Geotechnical Journal*, *54*(6), 825–834. https://doi.org/10.1139/cgj-2016-0012

Pells, P. J. N., & Bertuzzi, R. (2007). Limitations of rock mass classification systems. *Tunnels and Tunnelling International, APR.*

Pells, P. J., & Pells, S. E. (2018). Reply to the discussion by koutsoftas on "Rock quality designation (Rqd): Time to rest in peace." In *Canadian Geotechnical Journal* (Vol. 55, Issue 4). https://doi.org/10.1139/cgj-2017-0550

Ramamurthy, T. (1986). STABILITY OF ROCK MASS. *Indian Geotechnical Journal*, *16*(1). https://doi.org/10.1016/0148-9062(86)92357-0

Rehman, H., Ali, W., Naji, A. M., Kim, J. J., Abdullah, R. A., & Yoo, H. K. (2018). Review of rock-mass rating and tunneling quality index systems for tunnel design: Development, refinement, application and limitation. In *Applied Sciences (Switzerland)* (Vol. 8, Issue 8). MDPI AG. https://doi.org/10.3390/app8081250

Reid, W., Hollingsworth, B. C., & Wilson, H. H. (1952). The use of timber in mining. *Forestry*, *25*(2). https://doi.org/10.1093/oxfordjournals.forestry.a063064

Romana, M. (1999). Correlation between uniaxial compressive and point-load (Franklin test) strengths for different rock classes. *9th ISRM Congress*.

Russo, A., & Hormazabal, E. (2019). Correlations Between Various Rock Mass Classification Systems, Including Laubscher (MRMR), Bieniawski (RMR), Barton (Q) and Hoek and Marinos (GSI) Systems. *Geotechnical Engineering in the XXI Century: Lessons Learned and Future Challenges*.

Rutledge, J. C., & Preston, R. L. (1979). New Zealand Experience With Engineering Classifications Of Rock For The Prediction Of Tunnel Support. *Electric Power Research Institute (Report) EPRI EL*. https://doi.org/10.1016/0148-9062(80)90352-6

Sachpazis, C. I. (1990). Correlating schmidt hardness with compressive strength and young's modulus of carbonate rocks. *Bulletin of the International Association of Engineering Geology*, *42*(1). https://doi.org/10.1007/BF02592622

Shen, J., & Jimenez, R. (2018). Predicting the shear strength parameters of sandstone using genetic programming. *Bulletin of Engineering Geology and the Environment*, *77*(4), 1647–1662. https://doi.org/10.1007/s10064-017-1023-6

Sheorey, P. R. (1997). Empirical rock failure criteria. In *Empirical rock failure criteria*.

Siddique, T., & Khan, E. A. (2019). Stability appraisal of road cut slopes along a strategic transportation route in the Himalayas, Uttarakhand, India. *SN Applied Sciences*, *1*(5). https://doi.org/10.1007/s42452-019-0433-4

Singh, J. L., & Tamrakar, N. K. (2013). Rock Mass Rating and Geological Strength Index of rock masses of Thopal-Malekhu River areas, Central Nepal Lesser Himalaya. *Bulletin of the Department of Geology*, *16*(0), 29–42. https://doi.org/10.3126/bdg.v16i0.8882

Singh, V. K., & Singh, D. P. (1993). Correlation between point load index and compressive strength for quartzite rocks. *Geotechnical and Geological Engineering*, *11*(4). https://doi.org/10.1007/BF00466369

Smith, H. J. (1997). The point load test for weak rock in dredging applications. *International Journal of Rock Mechanics and Mining Sciences*, *34*(3–4), 295.e1-295.e13. https://doi.org/10.1016/S1365-1609(97)00063-4

Smits, J. R. M., Melssen, W. J., Buydens, L. M. C., & Kateman, G. (1994). Using artificial neural networks for solving chemical problems. Part I. Multi-layer feed-forward networks. In *Chemometrics and Intelligent Laboratory Systems* (Vol. 22, Issue 2). https://doi.org/10.1016/0169-7439(93)E0035-3

Somodi, G., Bar, N., Kovács, L., Arrieta, M., Török, Á., & Vásárhelyi, B. (2021). Article study of rock mass rating (RMR) and geological strength index (GSI) correlations in granite, siltstone, sandstone and quartzite rock masses. *Applied Sciences (Switzerland)*, *11*(8). https://doi.org/10.3390/app11083351

Sonmez, H., & Ulusay, R. (1999). Modifications to the geological strength index (GSI) and their applicability to stability of slopes. *International Journal of Rock Mechanics and Mining Sciences*, *36*(6). https://doi.org/10.1016/S0148-9062(99)00043-1

Standard practice for shotcrete. (1995). *Standard Practice for Shotcrete*. https://doi.org/10.1016/0148-9062(96)91726-x

Stillborg, B. (1994). Professional users handbook for rock bolting, 2nd edn. ClausthalZellerfeld: Trans Tech Publications. In *Stillborg, B.*

Stille, H., & Palmström, A. (2003). Classification as a tool in rock engineering. *Tunnelling and Underground Space Technology*, *18*(4), 331–345. https://doi.org/10.1016/S0886-7798(02)00106-2

Suzuki, K. (2013). *Artificial neural networks: Architectures and applications*. BoD–Books on Demand.

Tahir, M., Mohammad, N., & Din, F. (2011). Strength parameters and their inter-relationship for limestone of Cherat and Kohat areas of Khyber Pakhtunkhwa. In *Journal of Himalayan Earth Sciences* (Vol. 44, Issue 2).

Tatiya, R. R. (2013). Surface and Underground Excavations. In *Surface and Underground Excavations*. https://doi.org/10.1201/b14818

Tokashiki, N., & Aydan, Ö. (2010). The Stability Assessment Of Overhanging Ryukyu Limestone Cliffs With An Emphasis On The Evaluation Of Tensile Strength Of Rock Mass. *Doboku Gakkai Ronbunshuu C*, *66*(2), 397–406. https://doi.org/10.2208/jscejc.66.397

Tsiambaos, G., & Sabatakakis, N. (2004). Considerations on strength of intact sedimentary rocks. *Engineering Geology*, *72*(3–4), 261–273. https://doi.org/10.1016/J.ENGGEO.2003.10.001

Tuğrul, A. (1998). The application of rock mass classification systems to underground excavation in weak limestone, Ataturk Dam, Turkey. *Engineering Geology*, *50*(3–4). https://doi.org/10.1016/S0013-7952(98)00034-9

Tuğrul, A., & Zarif, I. H. (1999a). Correlation of mineralogical and textural characteristics with engineering properties of selected granitic rocks from

Turkey. *Engineering Geology*, *51*(4), 303–317. https://doi.org/10.1016/S0013-7952(98)00071-4

Tuğrul, A., & Zarif, I. H. (1999b). Correlation of mineralogical and textural characteristics with engineering properties of selected granitic rocks from Turkey. *Engineering Geology*, *51*(4), 303–317. https://doi.org/10.1016/S0013-7952(98)00071-4

Udd, J. E., & Wang, H. (1985). Comparison Of Some Approaches To The Classification Of Rock Masses For Geotechnical Purposes. *Proceedings - Symposium on Rock Mechanics*, *1*. https://doi.org/10.1016/0148-9062(86)90760-6

Ulusay, R., Gokceoglu, C., & Sulukcu, S. (2001). Draft ISRM suggested method for determining block punch strength index (BPI). *International Journal of Rock Mechanics and Mining Sciences*, *38*(8), 1113–1119. https://doi.org/10.1016/S1365-1609(01)00078-8

Ulusay, R., Türeli, K., & Ider, M. H. (1994). Prediction of engineering properties of a selected litharenite sandstone from its petrographic characteristics using correlation and multivariate statistical techniques. *Engineering Geology*, *38*(1–2), 135–157. https://doi.org/10.1016/0013-7952(94)90029-9

Vardar, M. (2005). Time dependent stability problems in tunnels and time-dependent behavior of the rock mass. *ITA/AITES Training Course Tunnel Engineering, Istanbul,*.

Vergne, D. La. (2008). Hard Rock Miners Handbook. In *Hard Copy Edition CD and Web Edition* (Vol. 4, Issue 4).

Vračević, D., Dugonjić Jovančević, S., Peranić, J., & Hodanić, M. (2019). Determination of Uniaxial Compressive Strength of Limestone. *Zbornik Radova*, *22*(1). https://doi.org/10.32762/zr.22.1.8

Werbos, P., & John, P. (1974). *Beyond regression : new tools for prediction and analysis in the behavioral sciences /*.

Whittaker, B. N. (1986). Supports in Mining and Design of Support Systems, | by C. Bir/Sn and E. Arloglu. Birsen Kitabevi, Istanbul. 360 pages of text, equations, illustrations, graphs and tables of data.(Published in Turkish). *Mining Science and Technology*, *3*(4), 311. https://doi.org/10.1016/S0167-9031(86)90684-5

Ylmaz, I., & Sendr, H. (2002). Correlation of Schmidt hardness with unconfined compressive strength and Young's modulus in gypsum from Sivas (Turkey). *Engineering Geology*, *66*(3–4), 211–219. https://doi.org/10.1016/S0013-7952(02)00041-8

Yudhbir, Lemanza, W., & Prinzl, F. (1983). An empirical failure criterion for rock masses. *Proc. 5th Congress International Society for Rock Mechanics, Melbourne, 1983. Vol.1*.

Yurdakul, M., Ceylan, H., & Akdas, H. (2011). A predictive model for uniaxial compressive strength of carbonate rocks from Schmidt hardness. *45th US Rock Mechanics / Geomechanics Symposium*.

Zhang, Q., Huang, X., Zhu, H., & Li, J. (2019). Quantitative assessments of the correlations between rock mass rating (RMR) and geological strength index (GSI). *Tunnelling and Underground Space Technology*, *83*, 73–81. https://doi.org/10.1016/j.tust.2018.09.015

Zupan, J., & Gasteiger, J. (1991). Neural networks: A new method for solving chemical problems or just a passing phase? In *Analytica Chimica Acta* (Vol. 248, Issue 1). https://doi.org/10.1016/S0003-2670(00)80865-X

# APPENDICES

## A. Vertical Displacements at Roof for K Values 0.5, 1.0, 1.5 and Different Rock Mass Properties at 200, 400, 600 Meters Depths

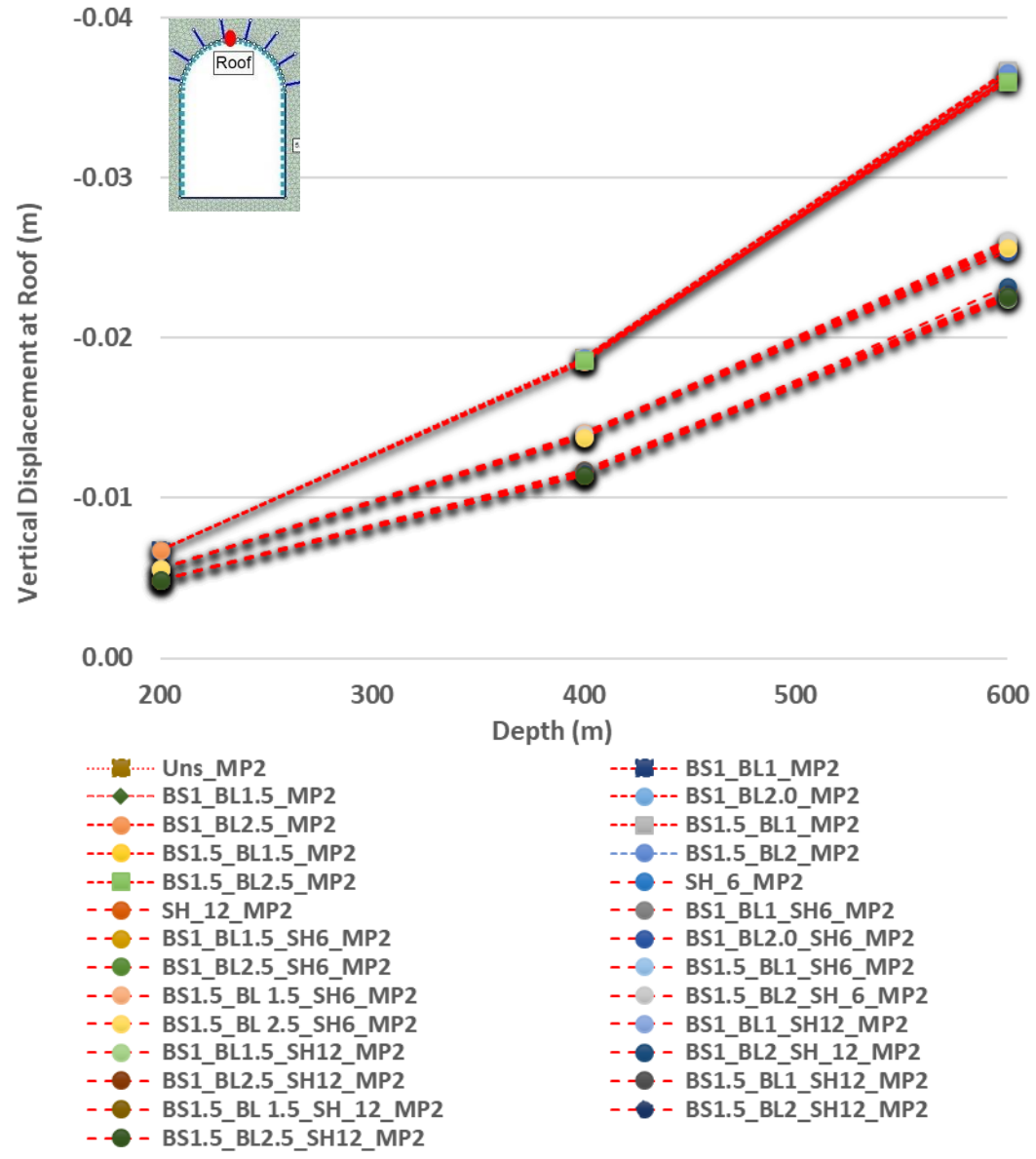


Figure A.1 Vertical displacement at roof (m) vs. depth (m) for k=0.5 for $MP_2$

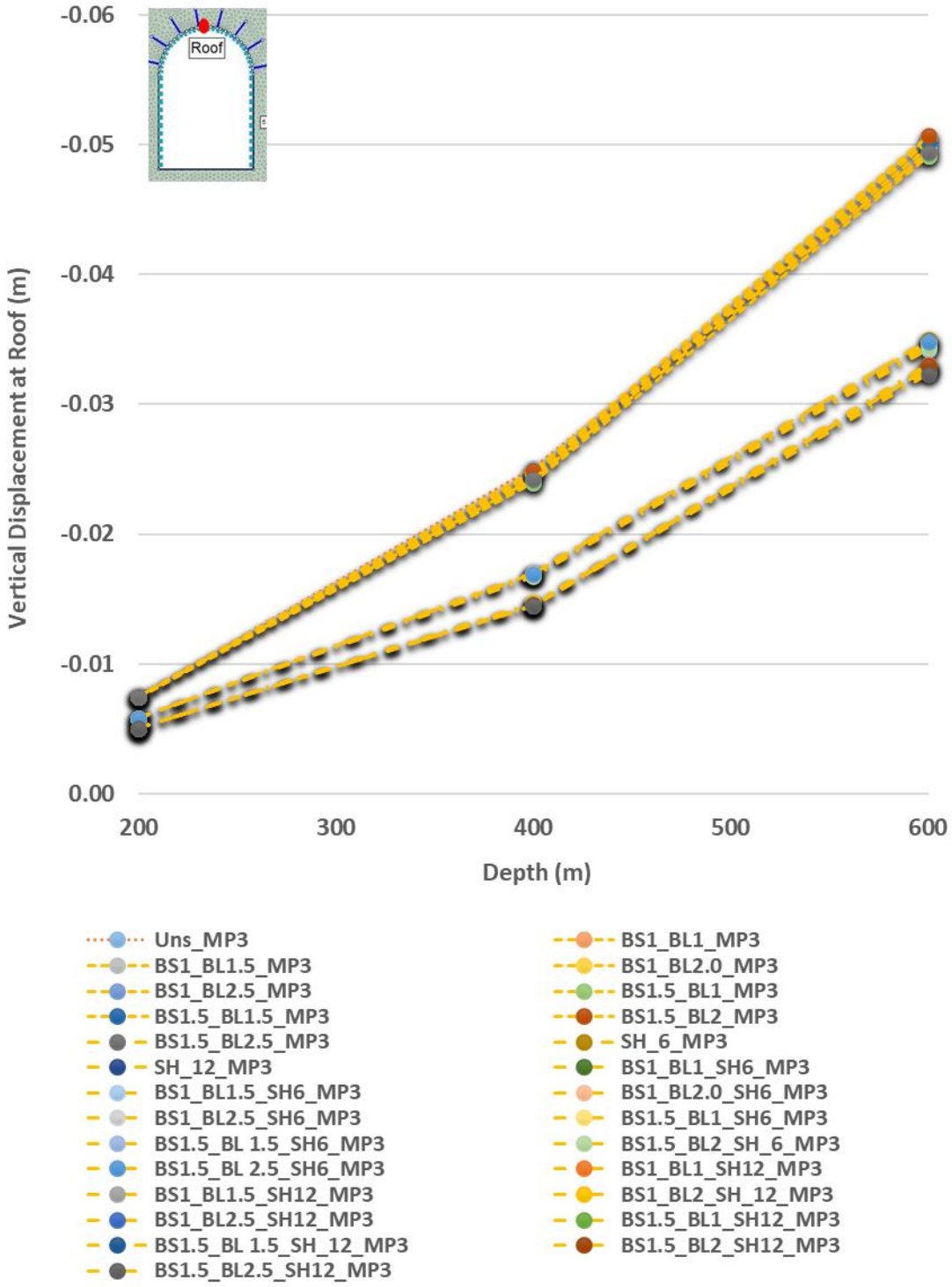


Figure A.2 Vertical displacement at roof (m) vs. depth (m) for k=0.5 for $MP_3$

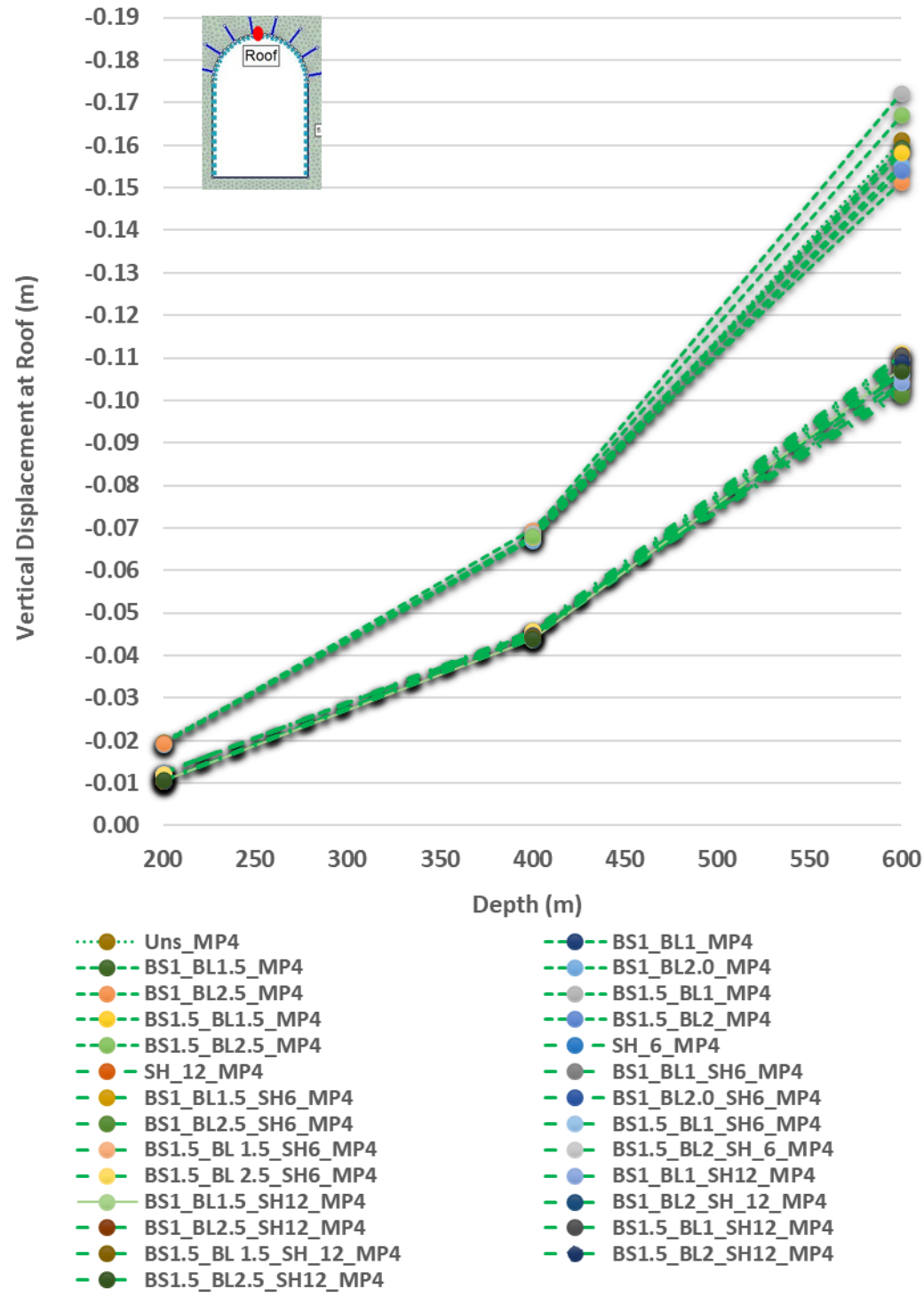


Figure A.3 Vertical displacement at roof (m) vs. depth (m) for k=0.5 for $MP_4$

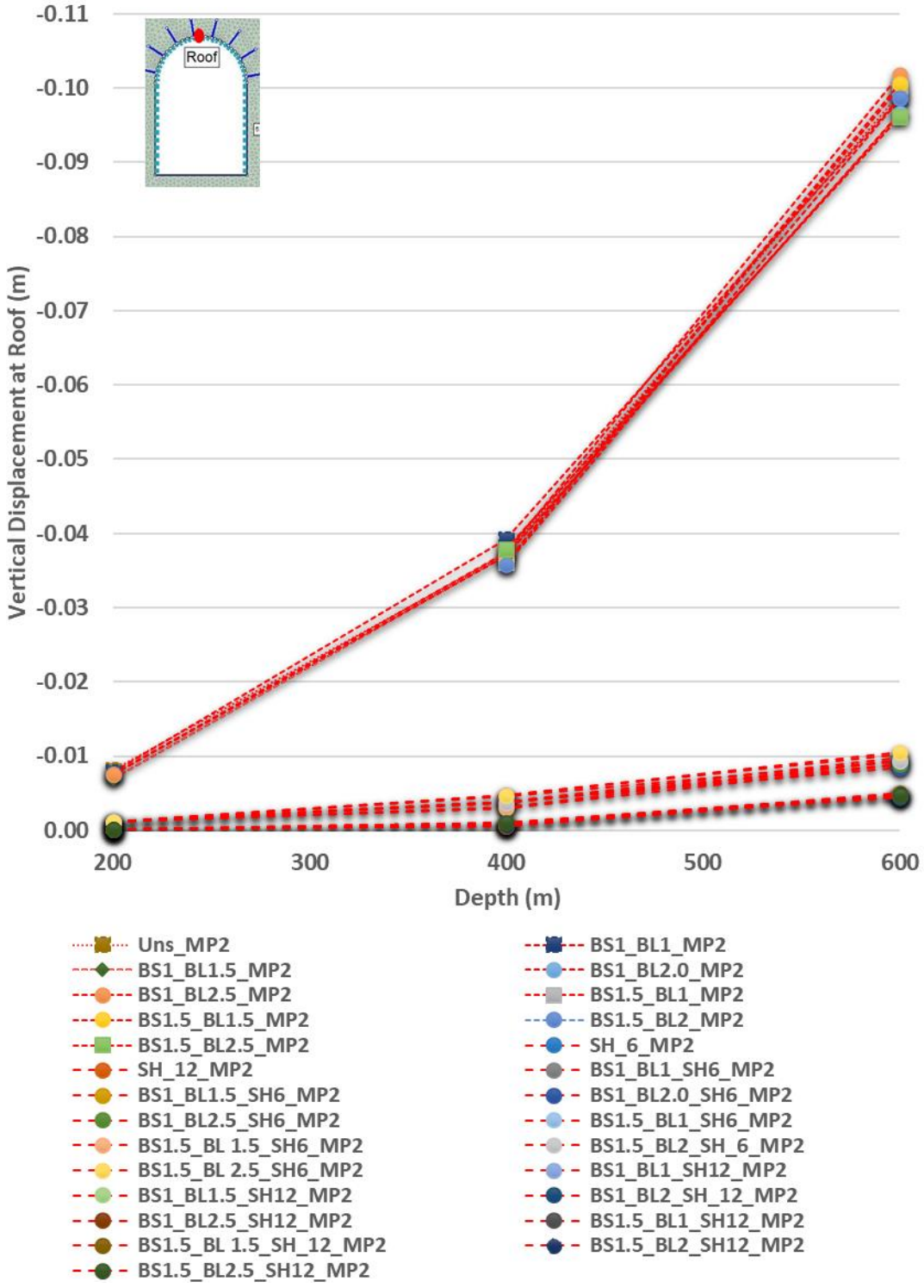


Figure A.4 Vertical displacement at roof (m) vs. depth (m) for k=1.5 for $MP_2$

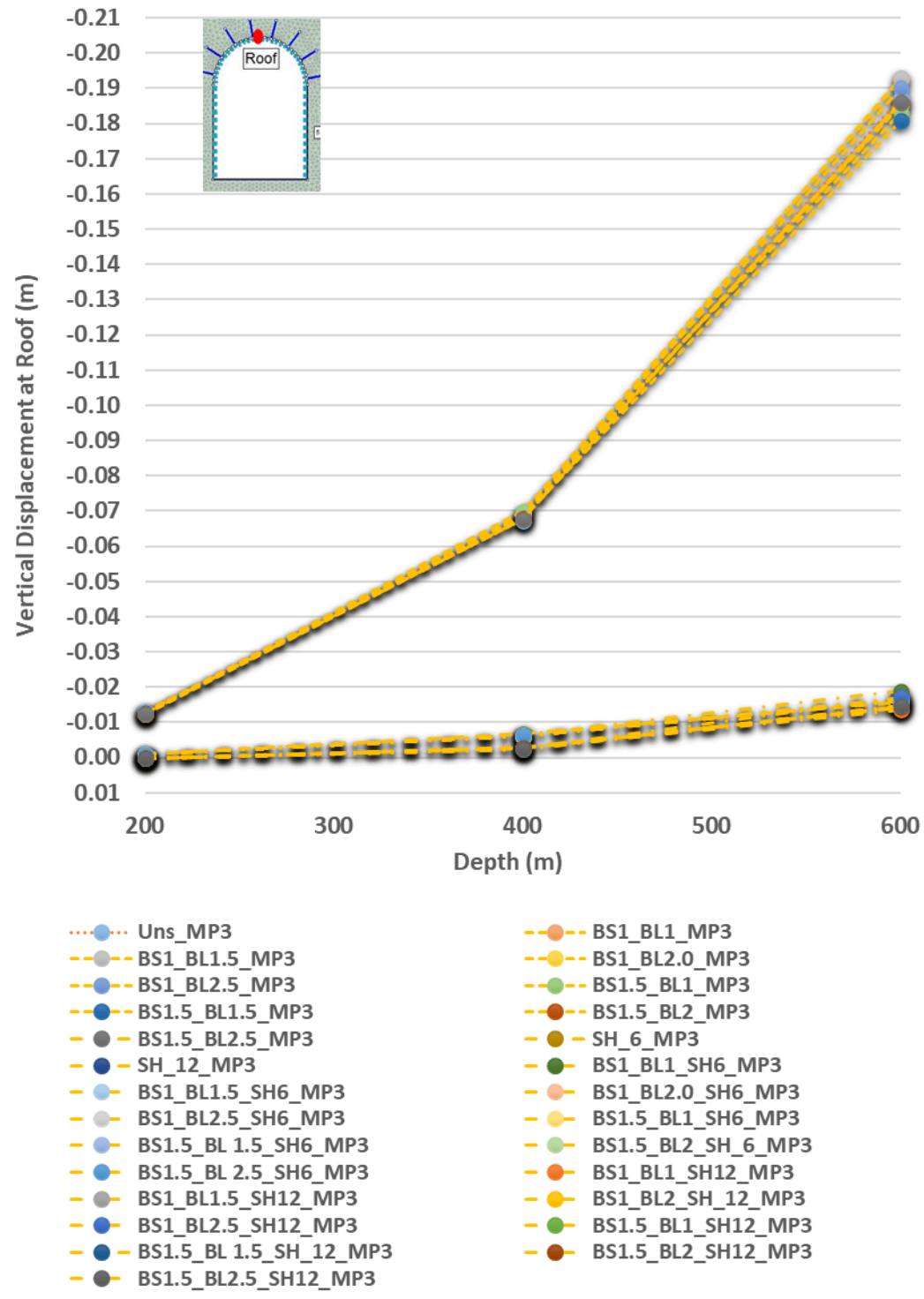


Figure A.5 Vertical displacement at roof (m) vs. depth (m) for k=1.5 for $MP_3$

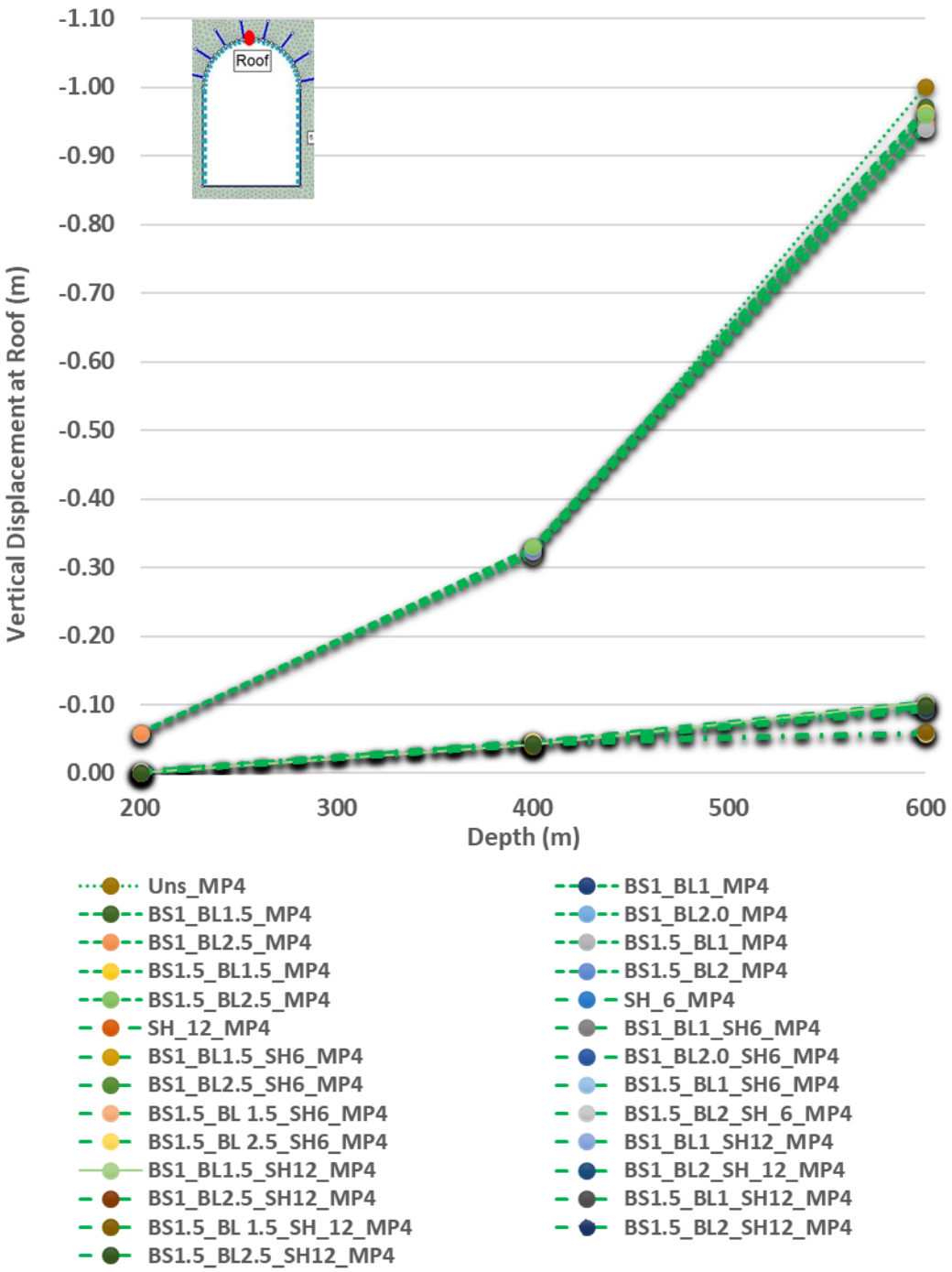


Figure A.6 Vertical displacement at roof (m) vs. depth (m) for k=1.5 for $MP_4$

**B. Roof Major Principal Strain for K Values 0.5, 1.0, 1.5 and Different Rock Mass Properties at 200, 400, 600 Meters Depths**

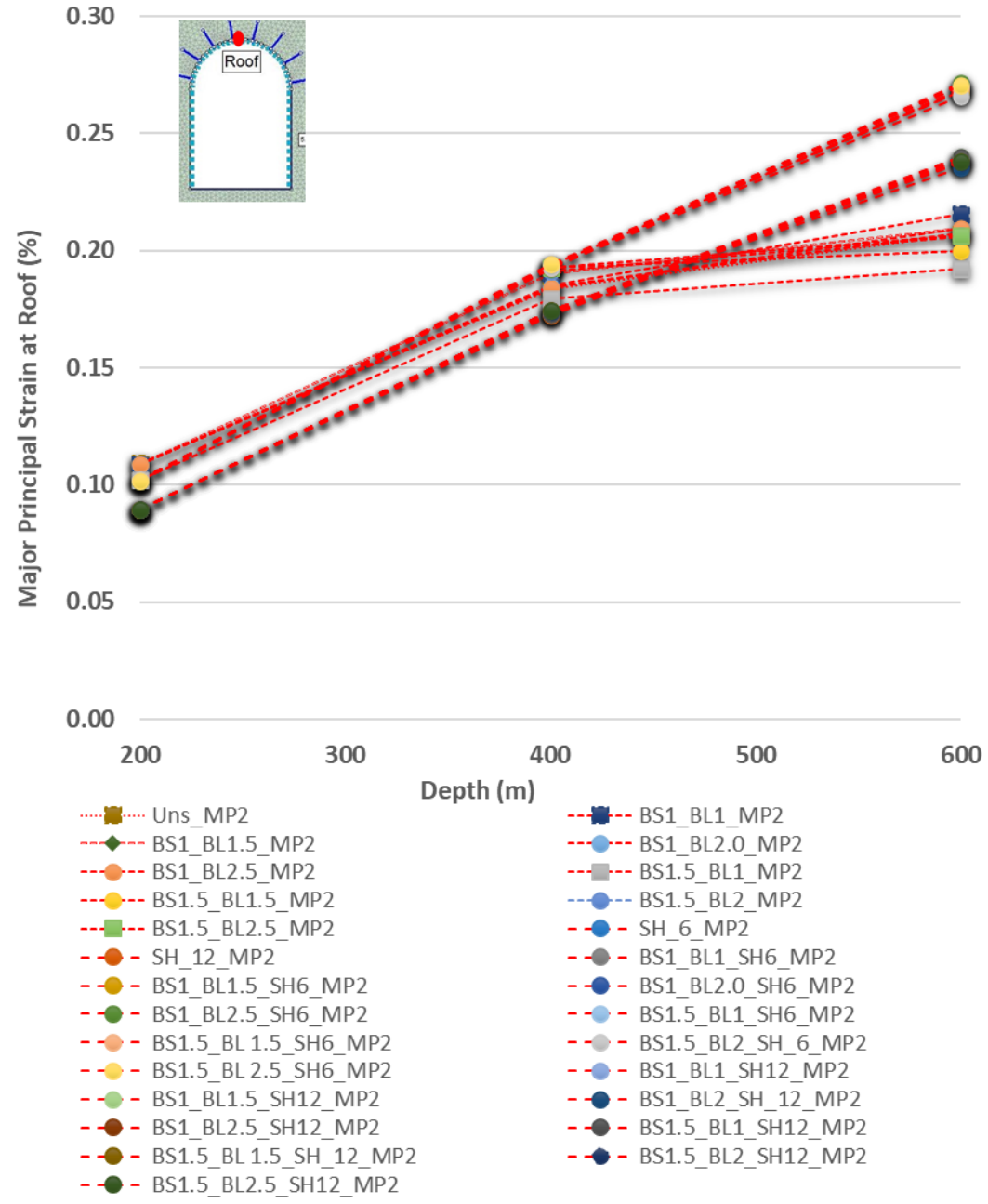


Figure B.1 Major principal strain at roof (%) vs. depth (m) for k=0.5 for $MP_2$

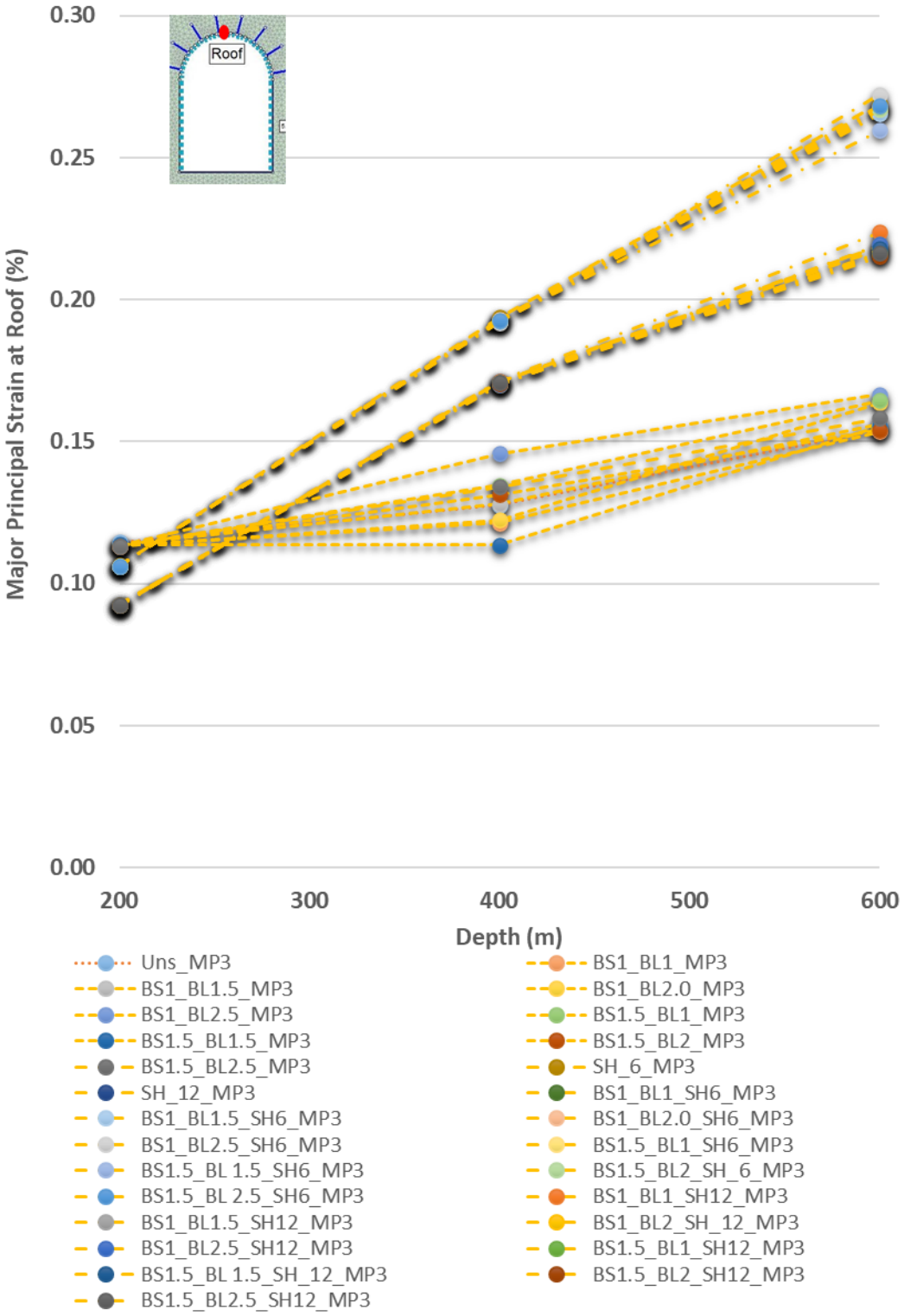


Figure B.2 Major principal strain at roof (%) vs. depth (m) for k=0.5 for $MP_3$

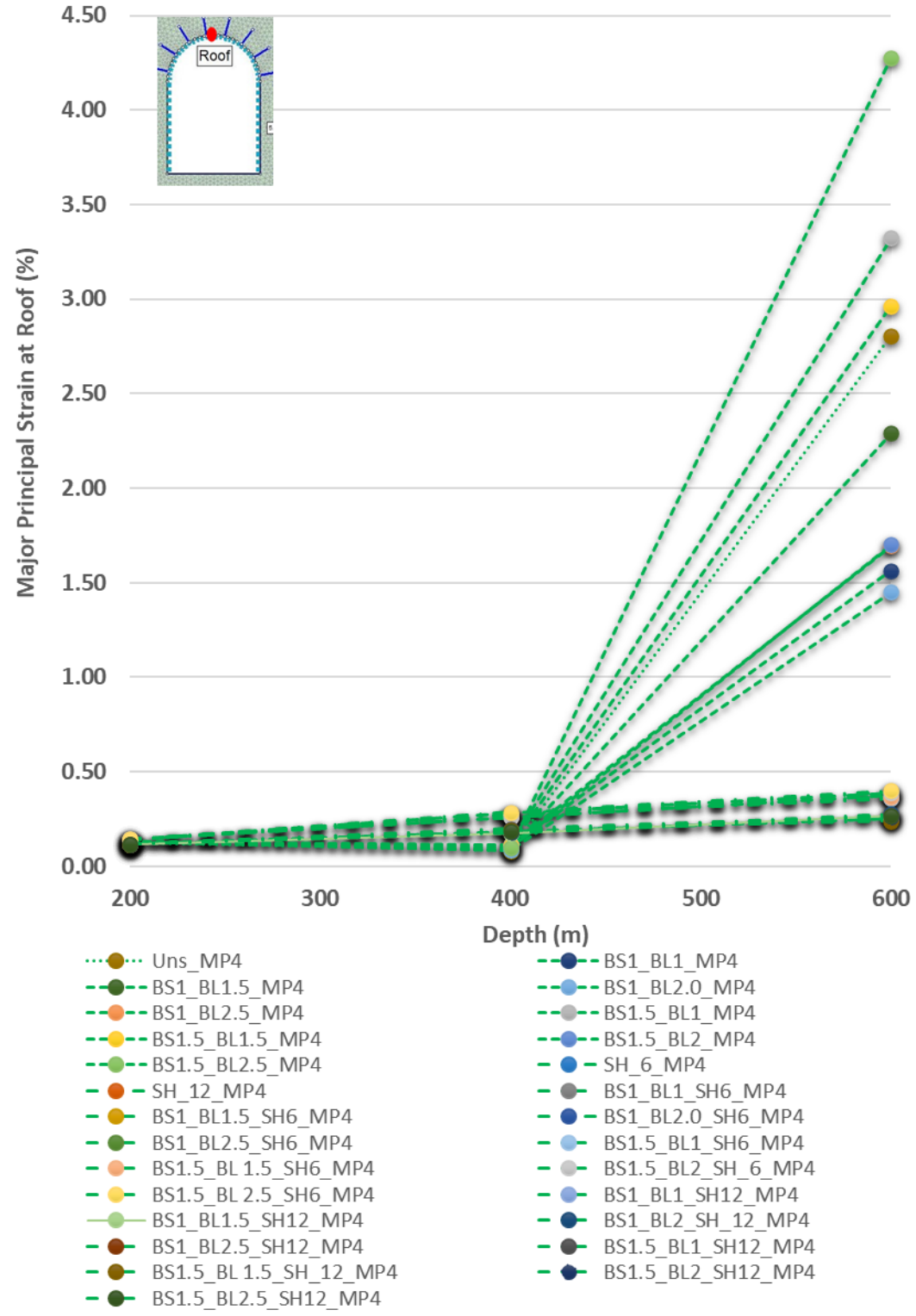


Figure B.3 Major principal strain at roof (%) vs. depth (m) for k=0.5 for $MP_4$

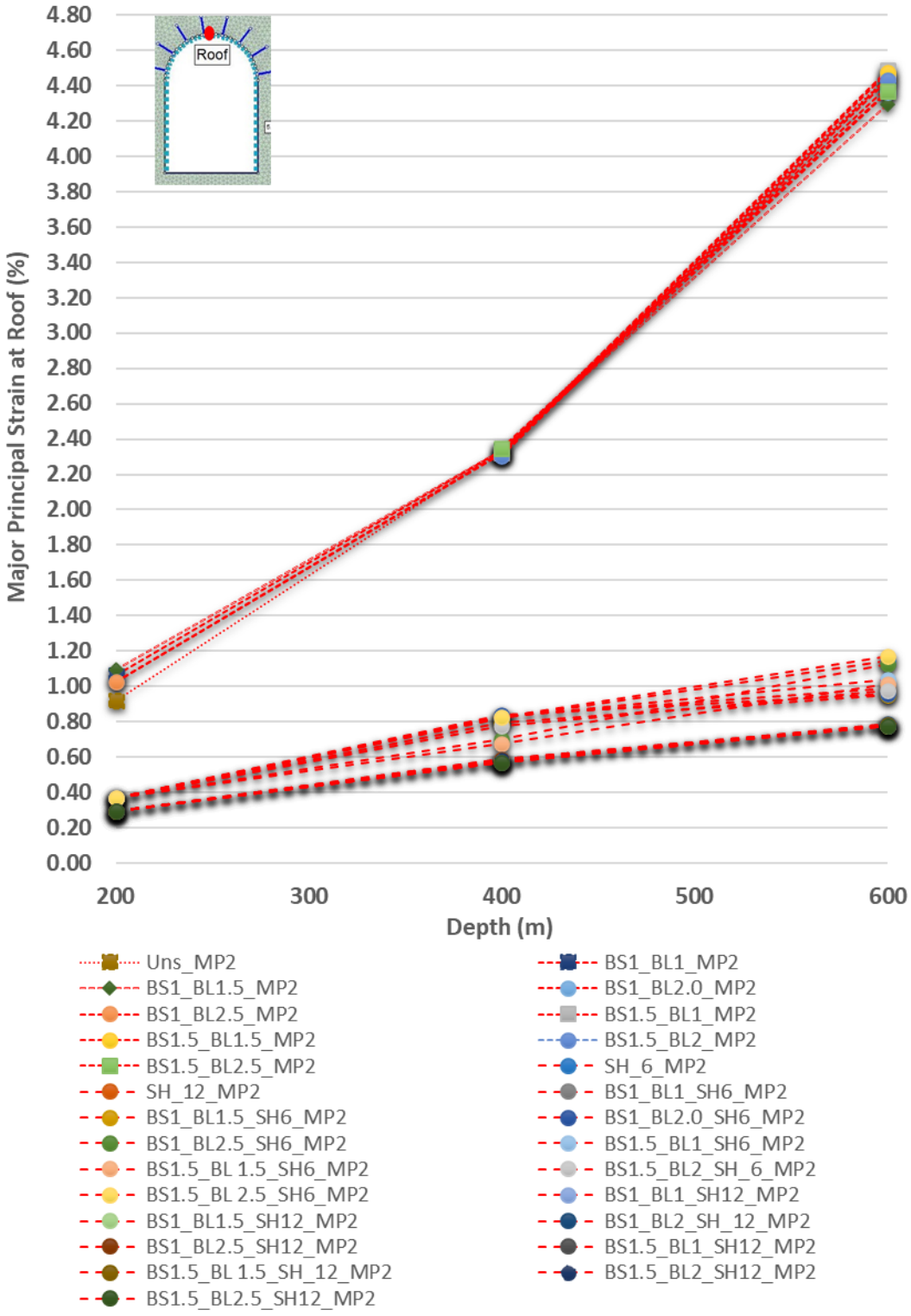


Figure B.4 Major principal strain at roof (%) vs. depth (m) for k=1.5 for $MP_2$

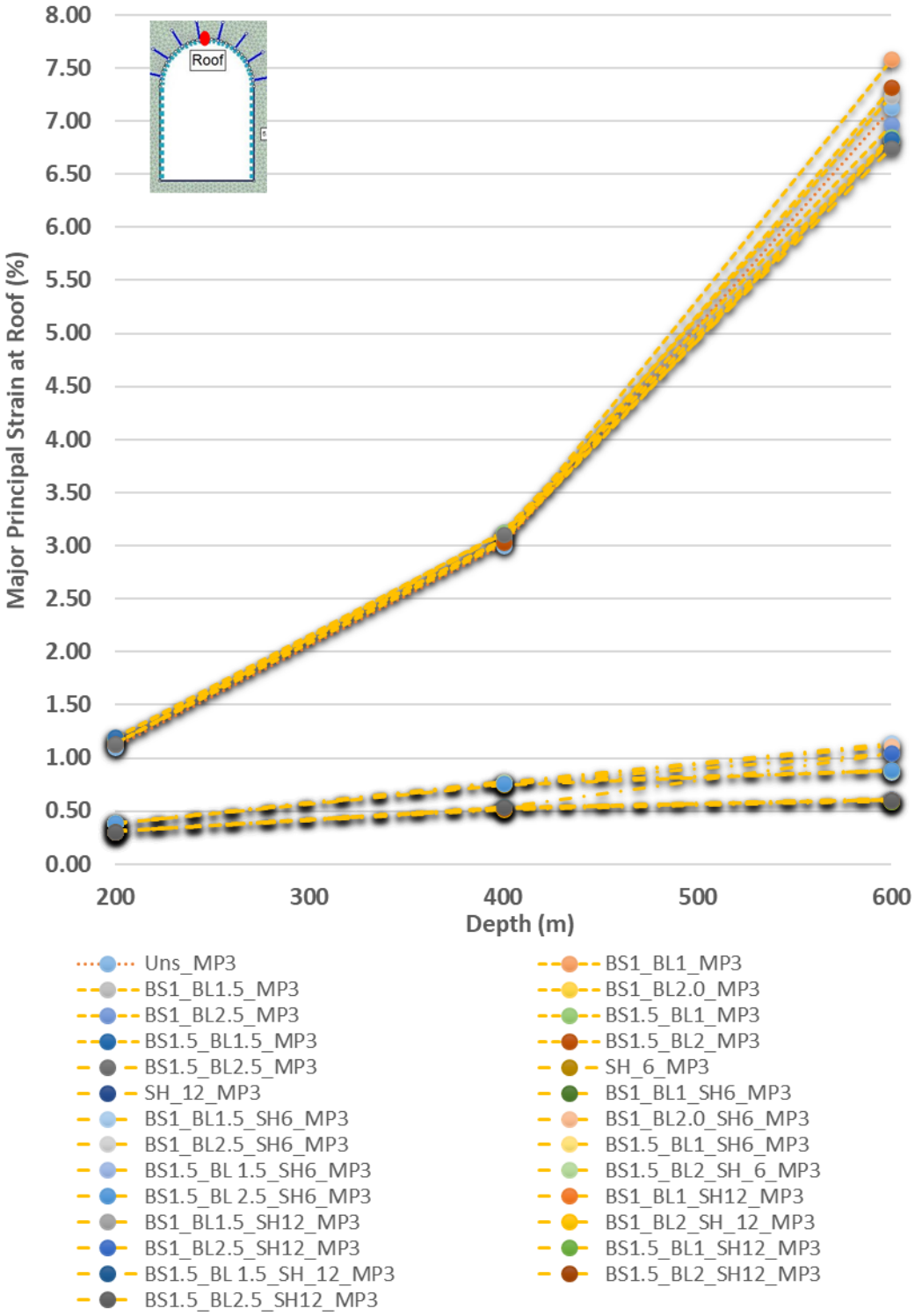


Figure B.5 Major principal strain at roof (%) vs. depth (m) for k=1.5 for MP3

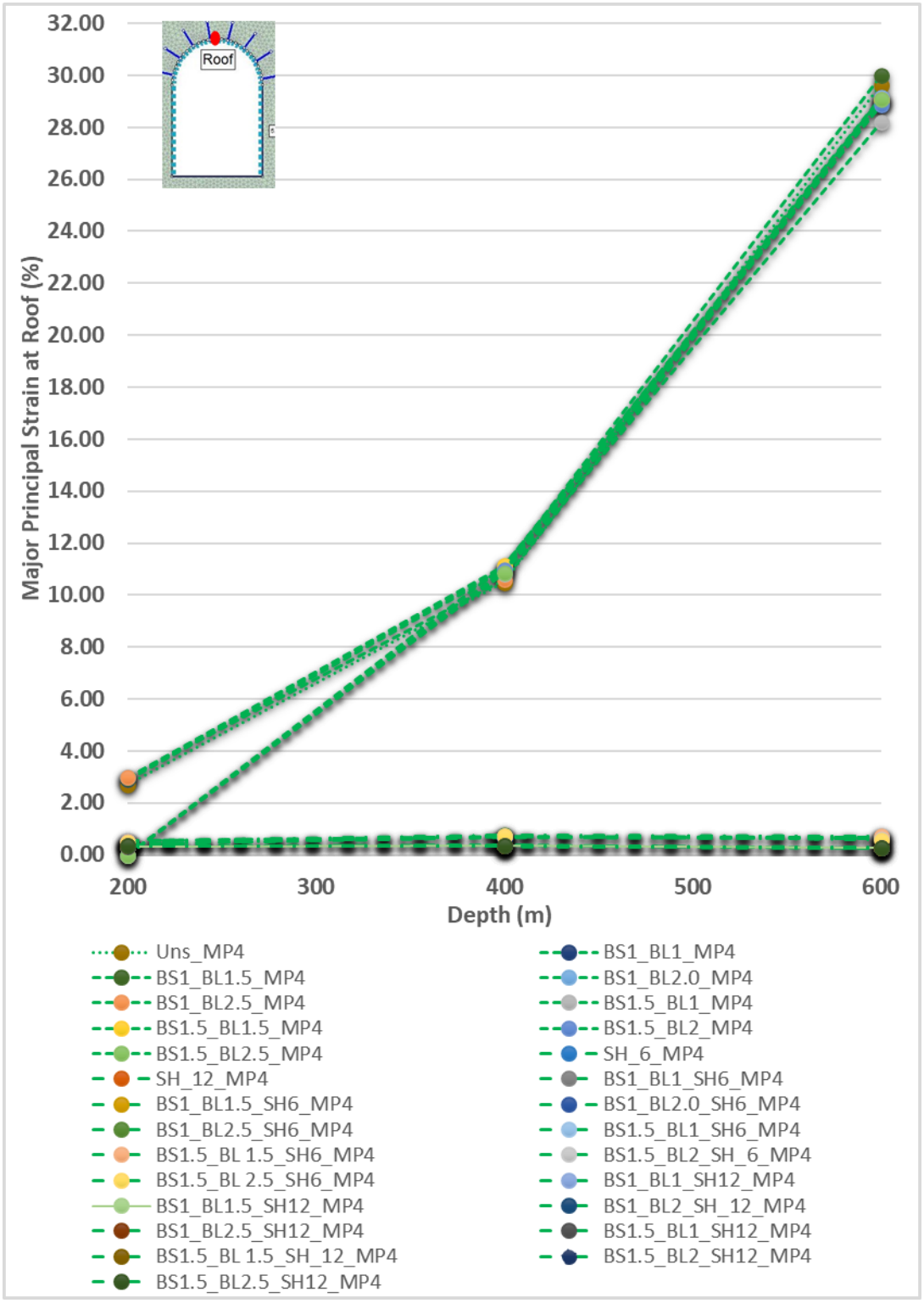


Figure B.6 Major principal strain at roof (%) vs. depth (m) for k=1.5 for $MP_4$

## C. Roof Minimum Principal Stresses for K Values 0.5, 1.0, 1.5 and Different Rock Mass Properties at 200, 400, 600 Meters Depths

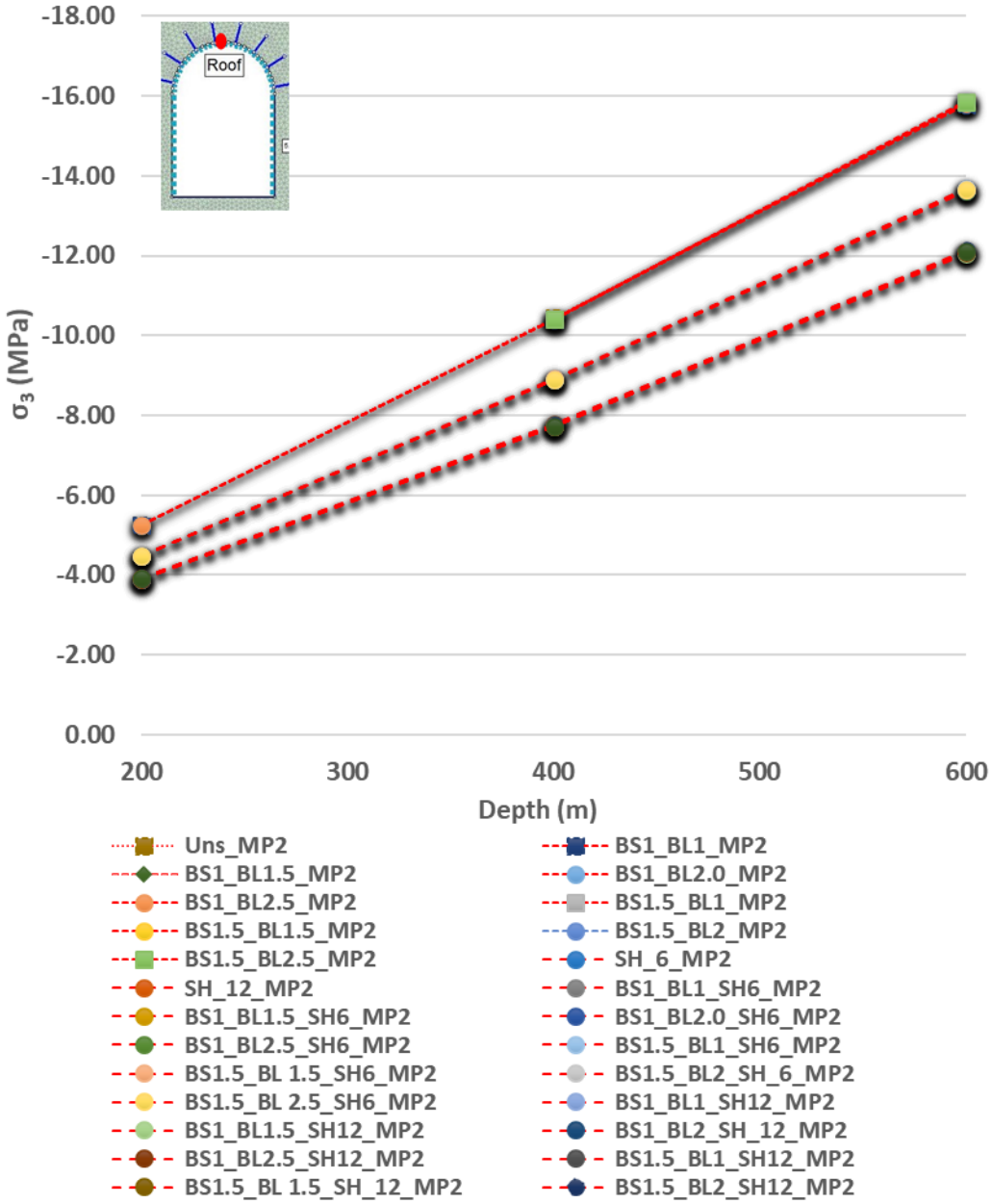


Figure C.1 Minimum principal stress at roof (MPa) vs. depth (m) for k=0.5 for $MP_2$

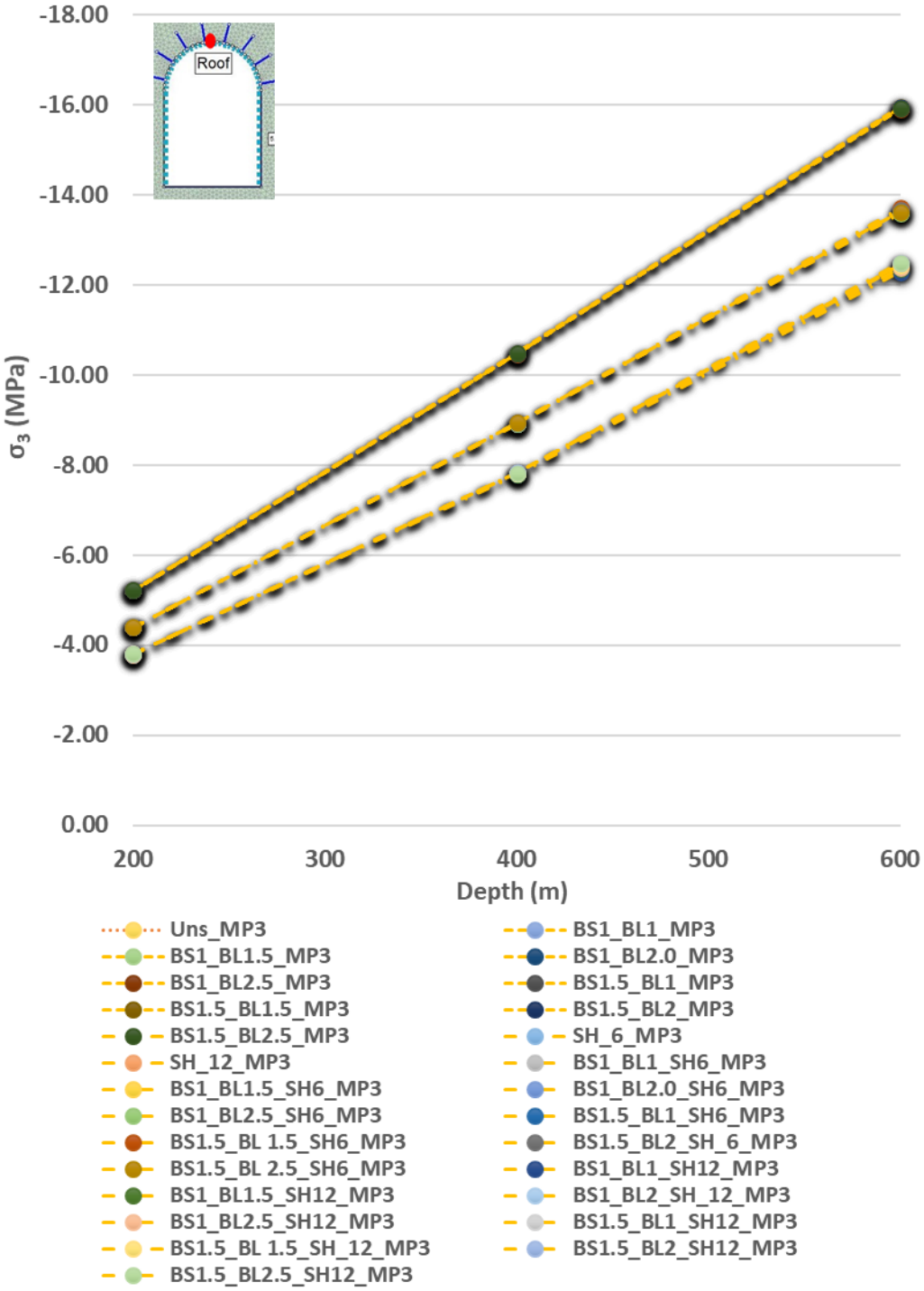


Figure C.2 Minimum principal stress at roof (MPa) vs. depth (m) for k=0.5 for $MP_3$

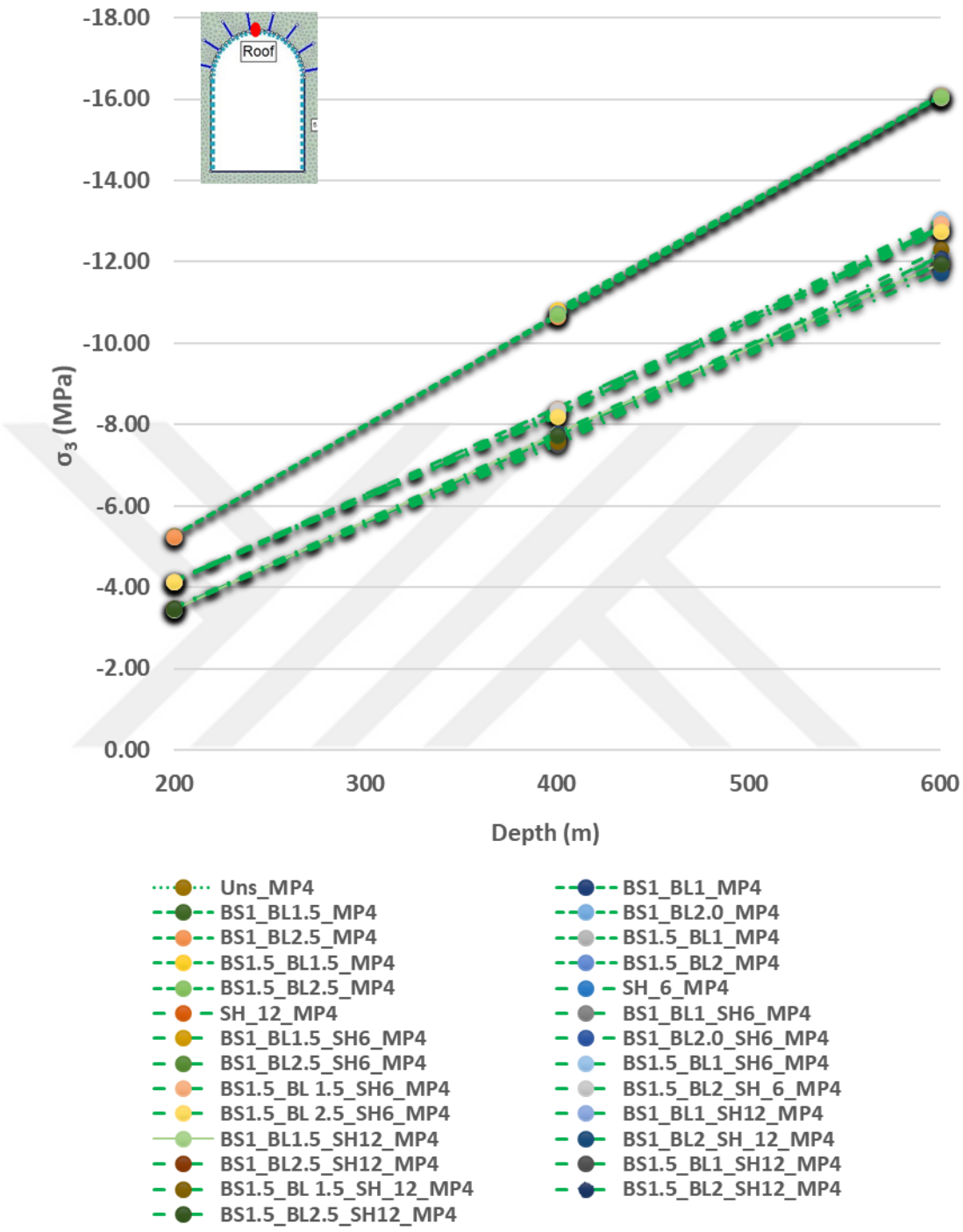


Figure C.3 Minimum principal stress at roof (MPa) vs. depth (m) for k=0.5 for $MP_4$

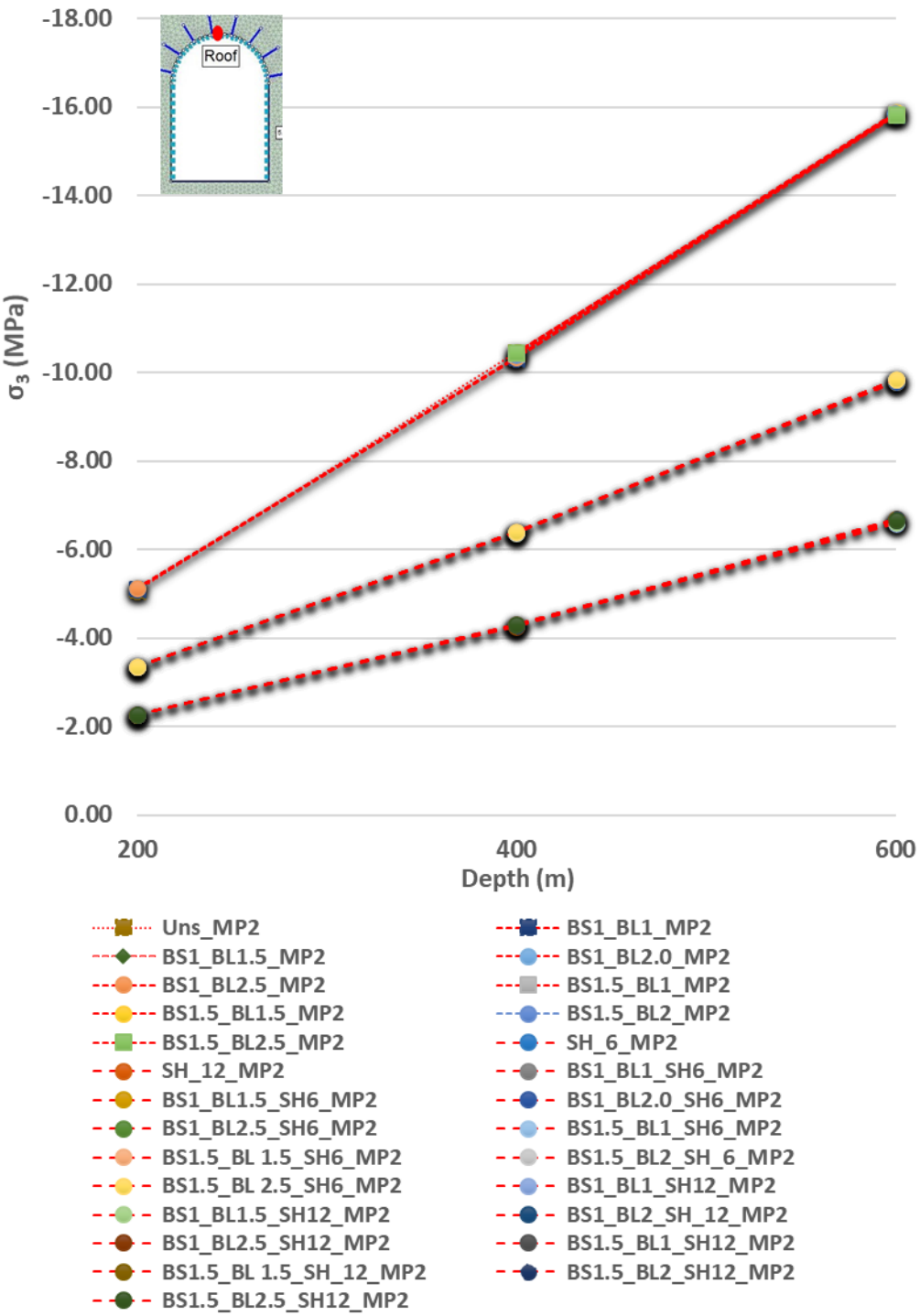


Figure C.4 Minimum principal stress at roof (MPa) vs. depth (m) for k=1.0 for $MP_2$

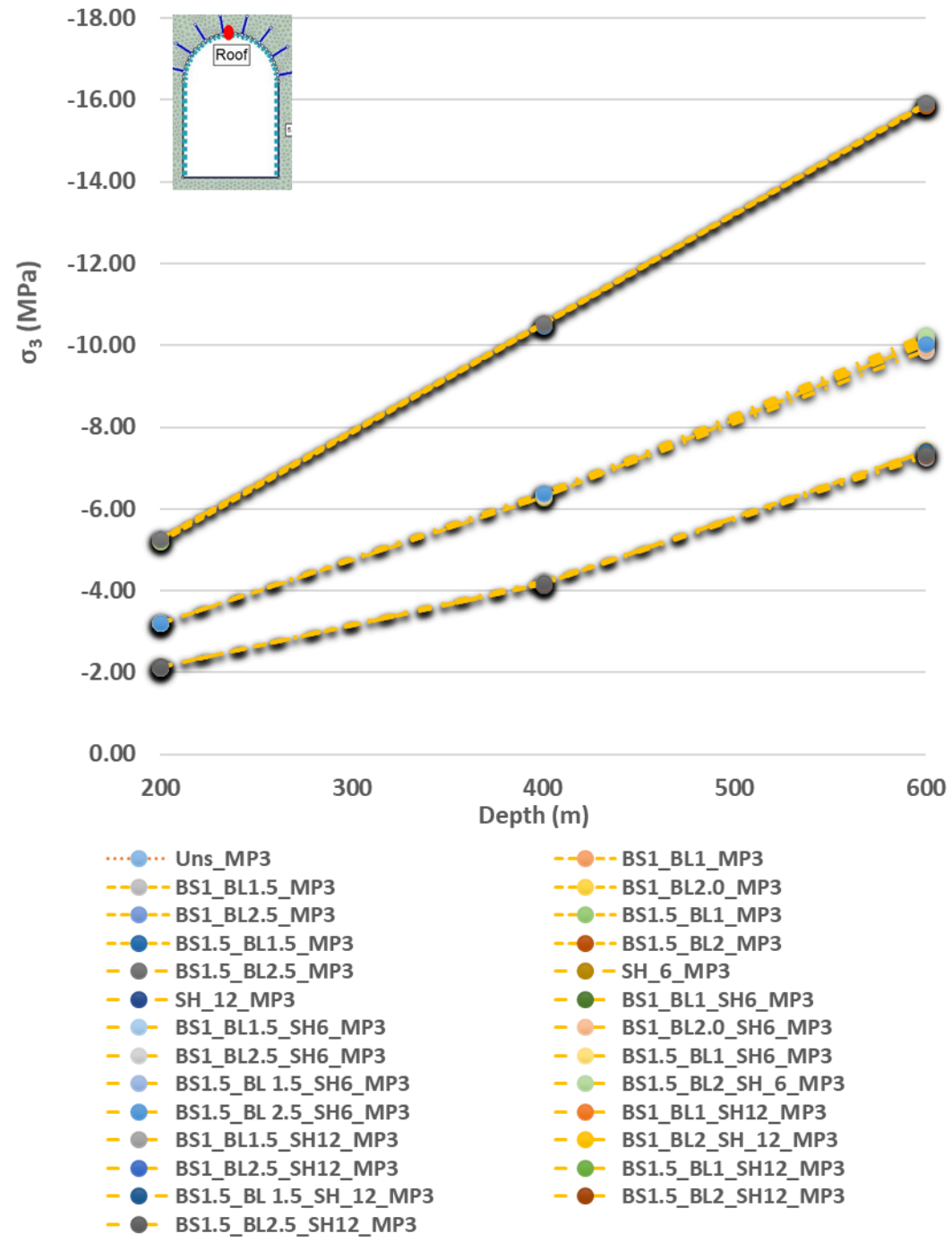


Figure C.5 Minimum principal stress at roof (MPa) vs. depth (m) for k=1.0 for $MP_3$

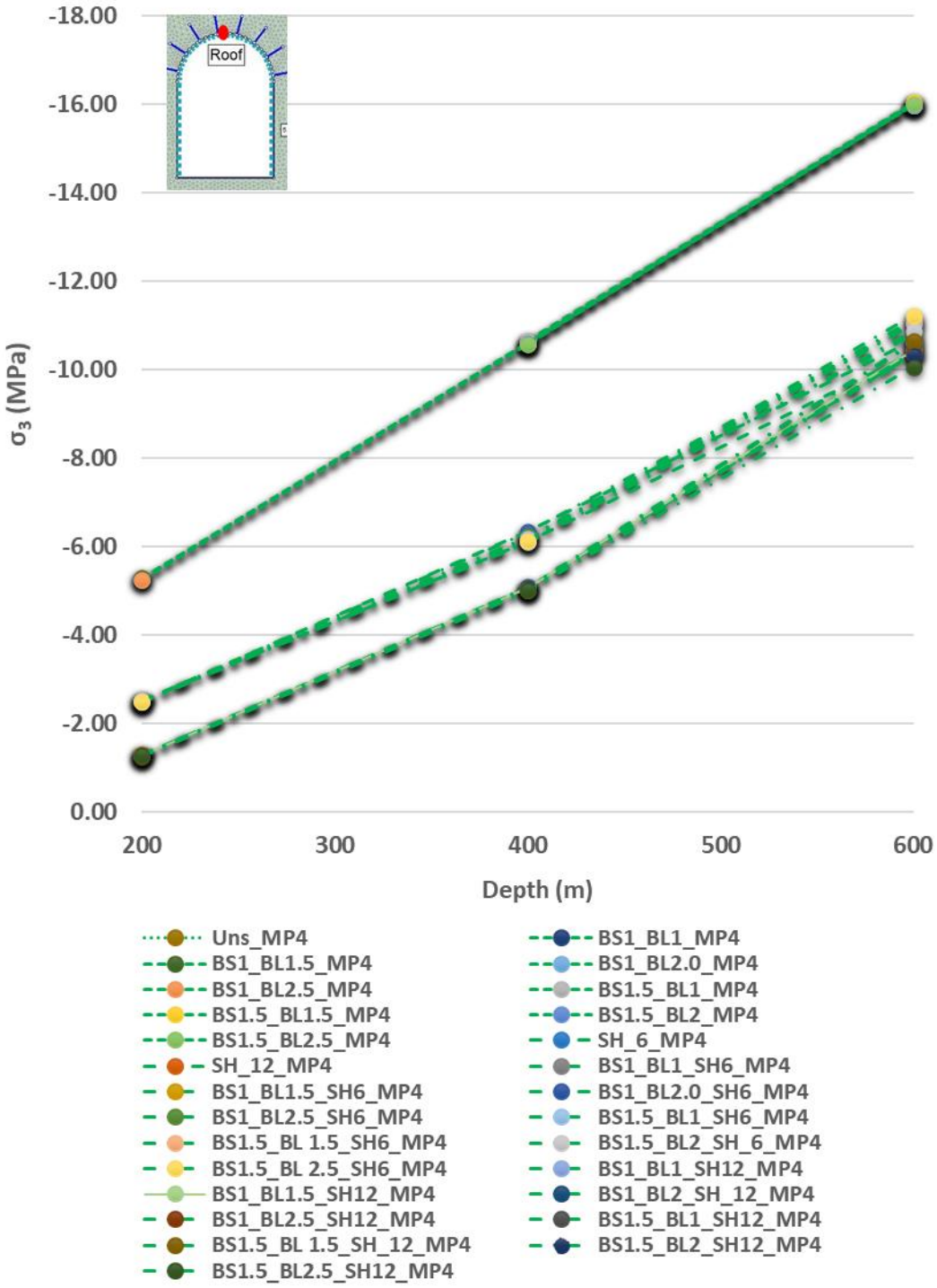


Figure C.6 Minimum principal stress at roof (MPa) vs. depth (m) for k=1.0 for $MP_4$

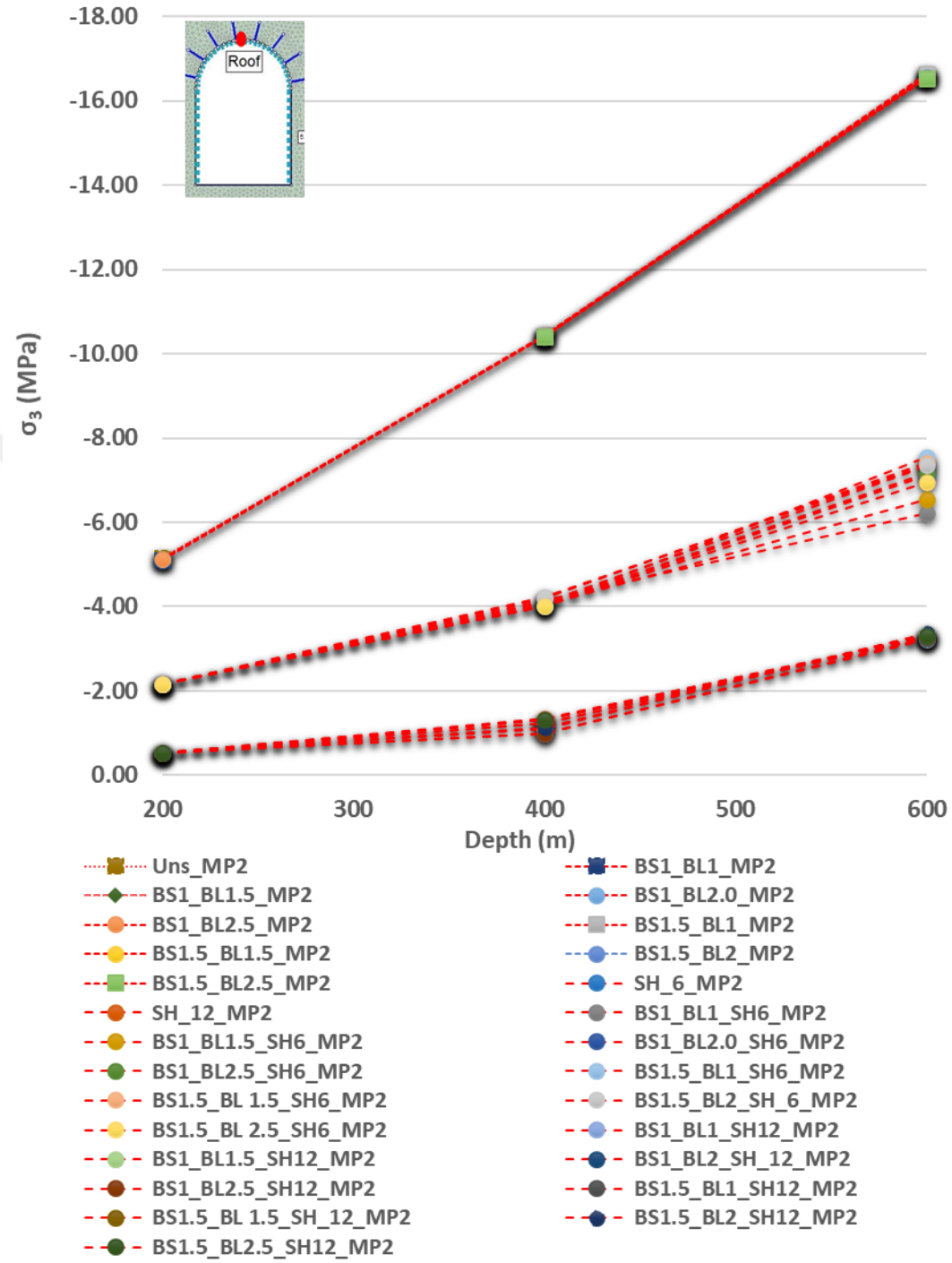


Figure C.7 Minimum principal stress at roof (MPa) vs. depth (m) for k=1.5 for $MP_2$

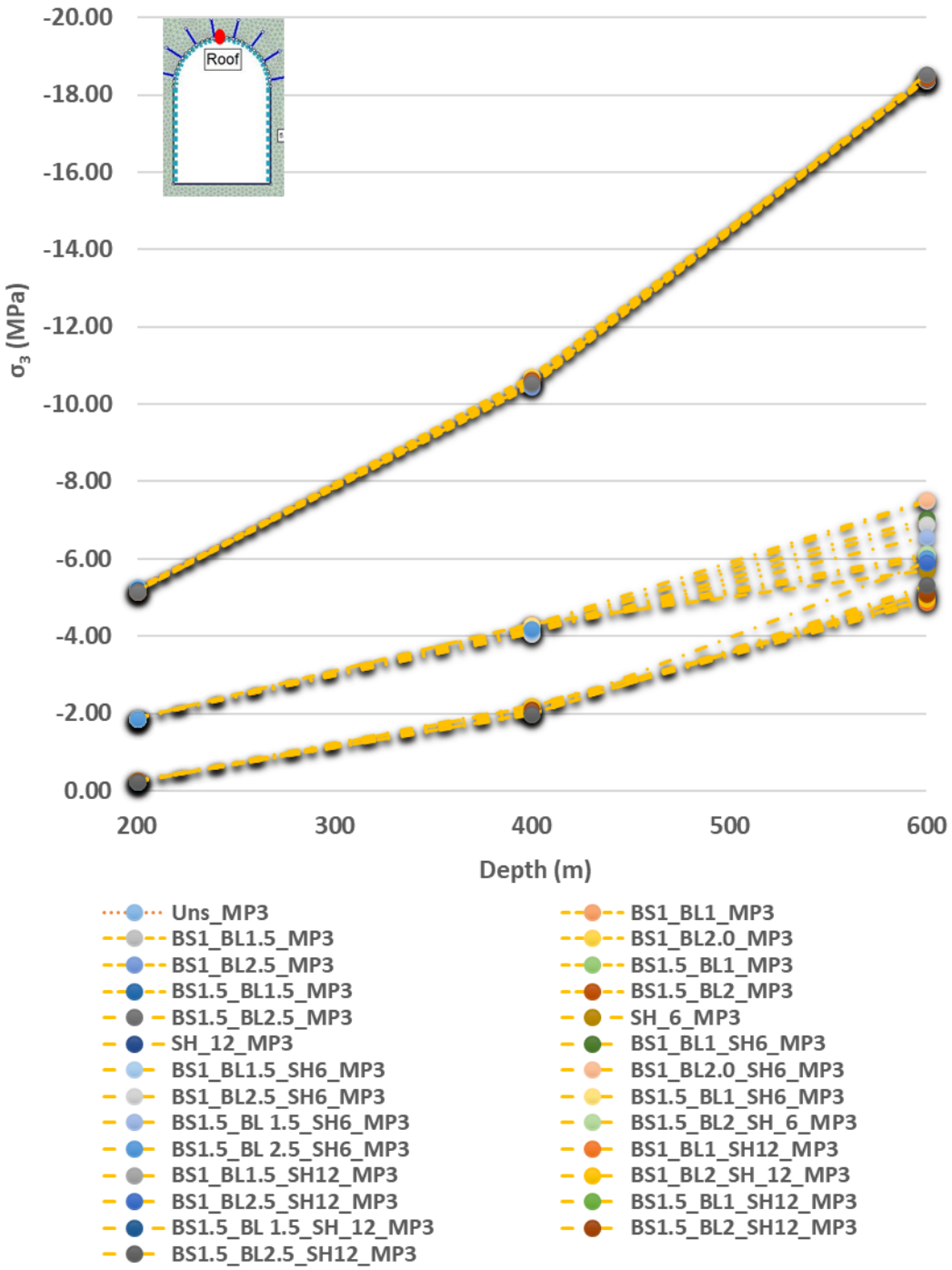


Figure C.8 Minimum principal stress at roof (MPa) vs. depth (m) for k=1.5 for $MP_3$

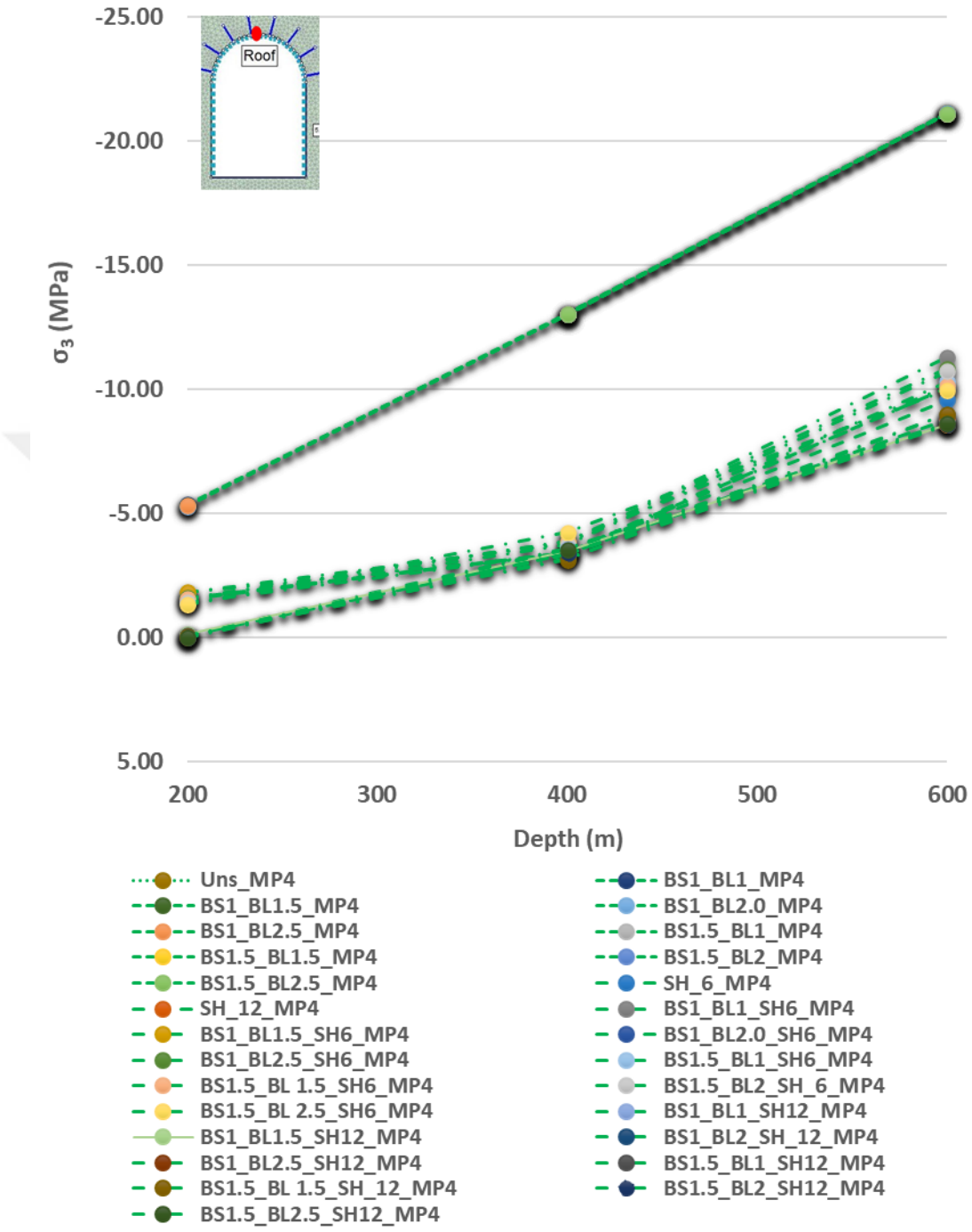


Figure C.9 Minimum principal stress at roof (MPa) vs. depth (m) for k=1.5 for $MP_4$

## D. Horizontal Displacements at Wall for K Values 0.5, 1.0, 1.5 and Different Rock Mass Properties at 200, 400, 600 Meters Depth

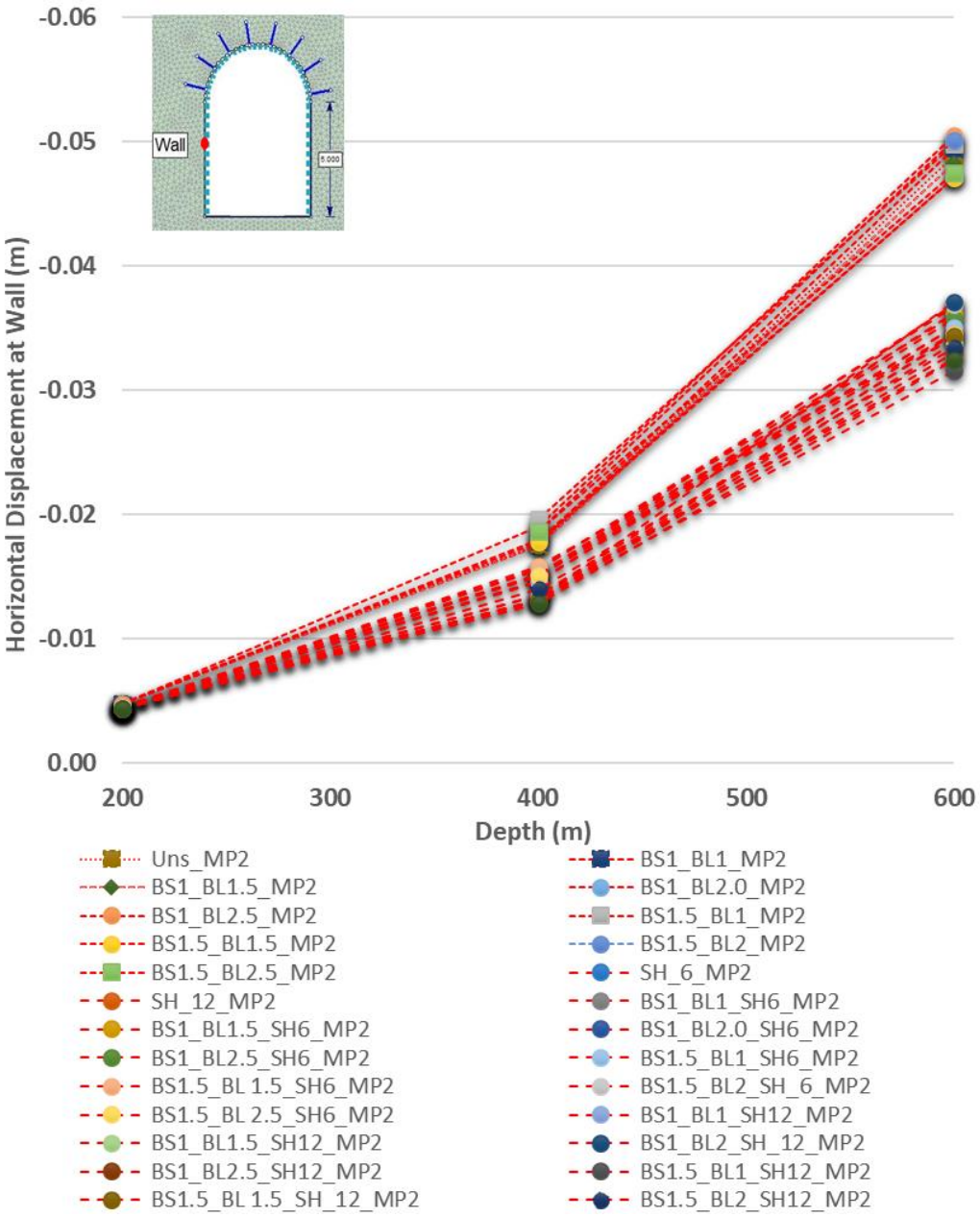


Figure D.1 Horizontal displacement at wall (m) vs. depth (m) for k=0.5 for $MP_2$

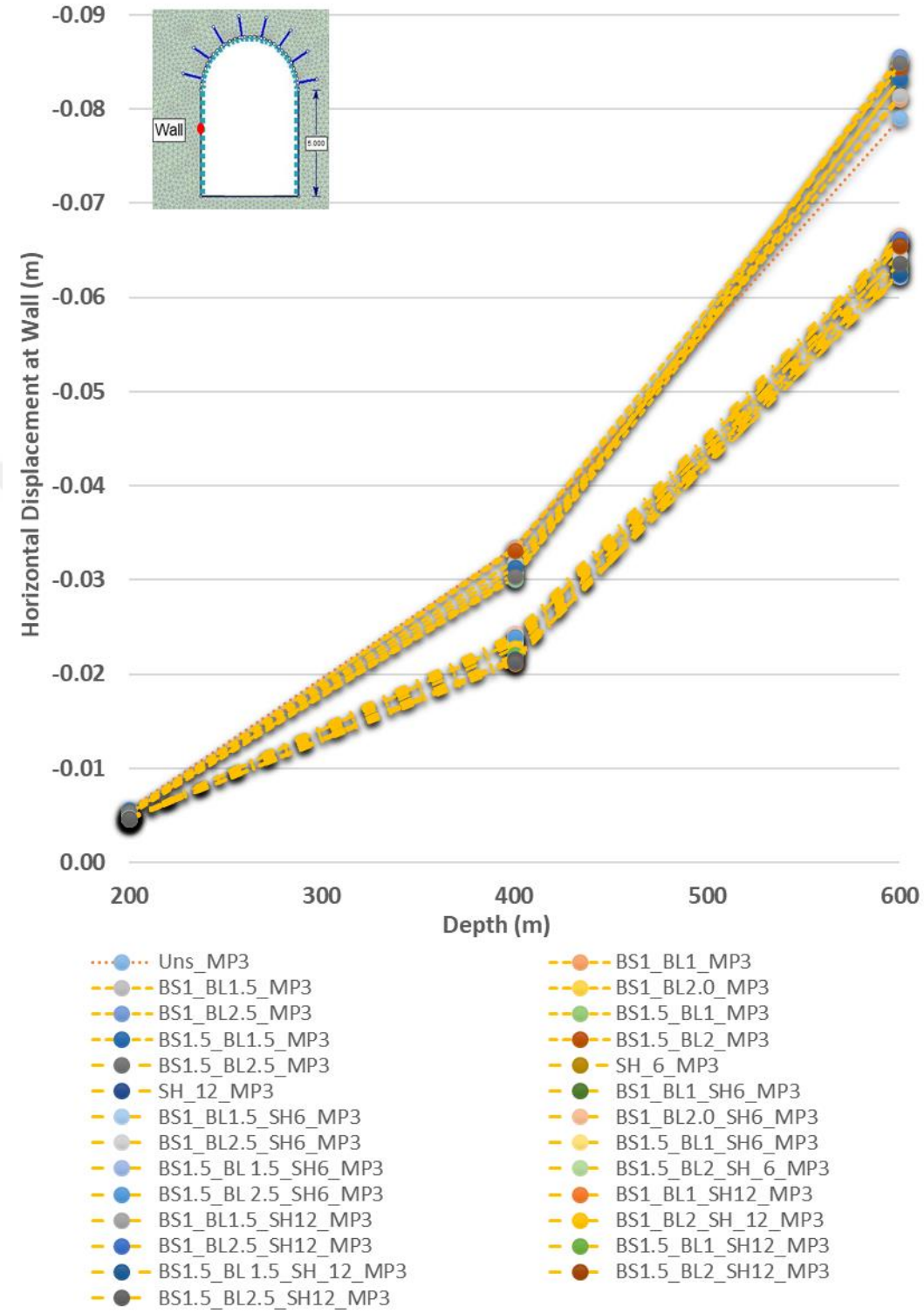


Figure D.2 Horizontal displacement at wall (m) vs. depth (m) for k=0.5 for $MP_3$

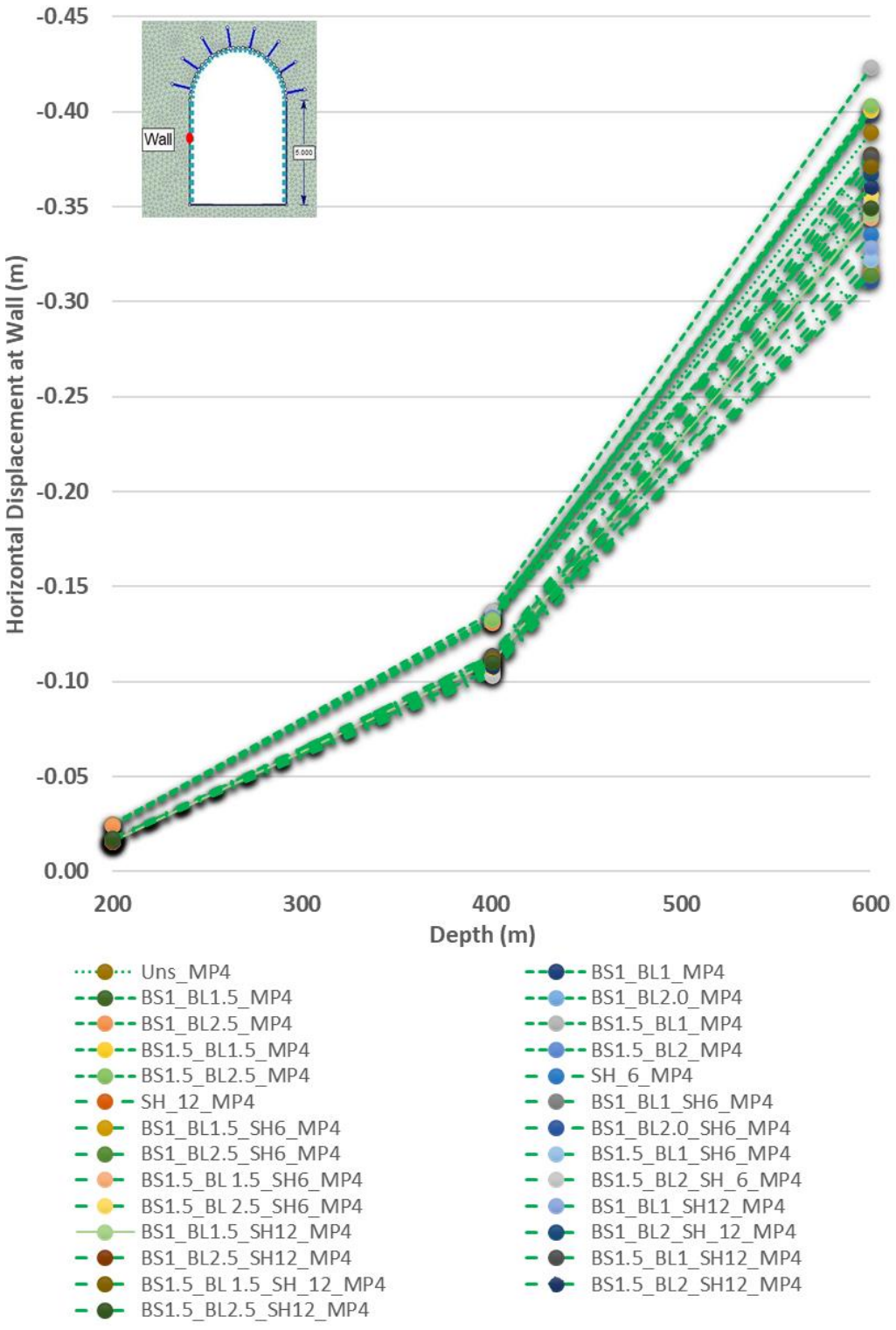


Figure D.3 Horizontal displacement at wall (m) vs. depth (m) for k=0.5 for $MP_4$

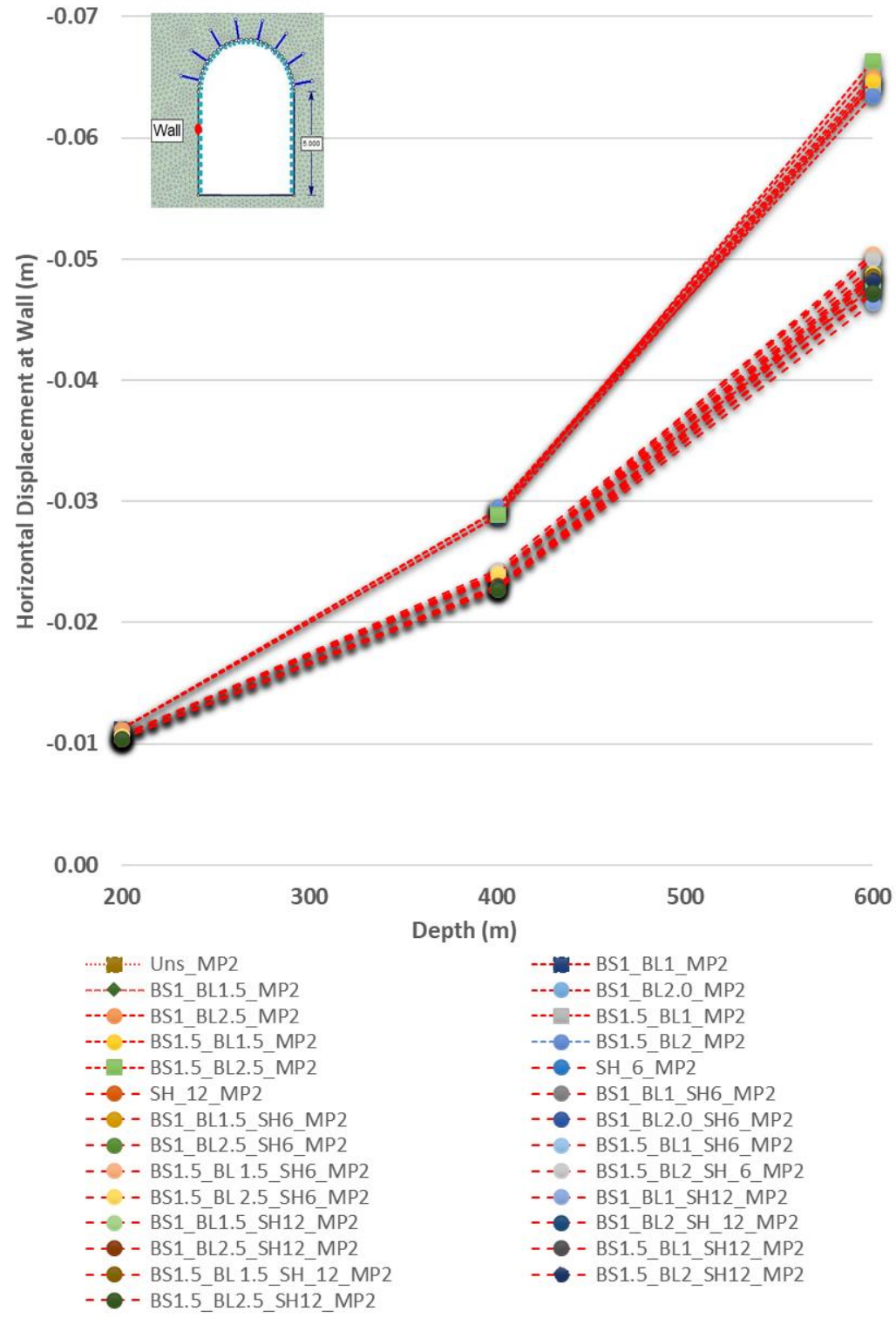


Figure D.4 Horizontal displacement at wall (m) vs. depth (m) for k=1.0 for $MP_2$

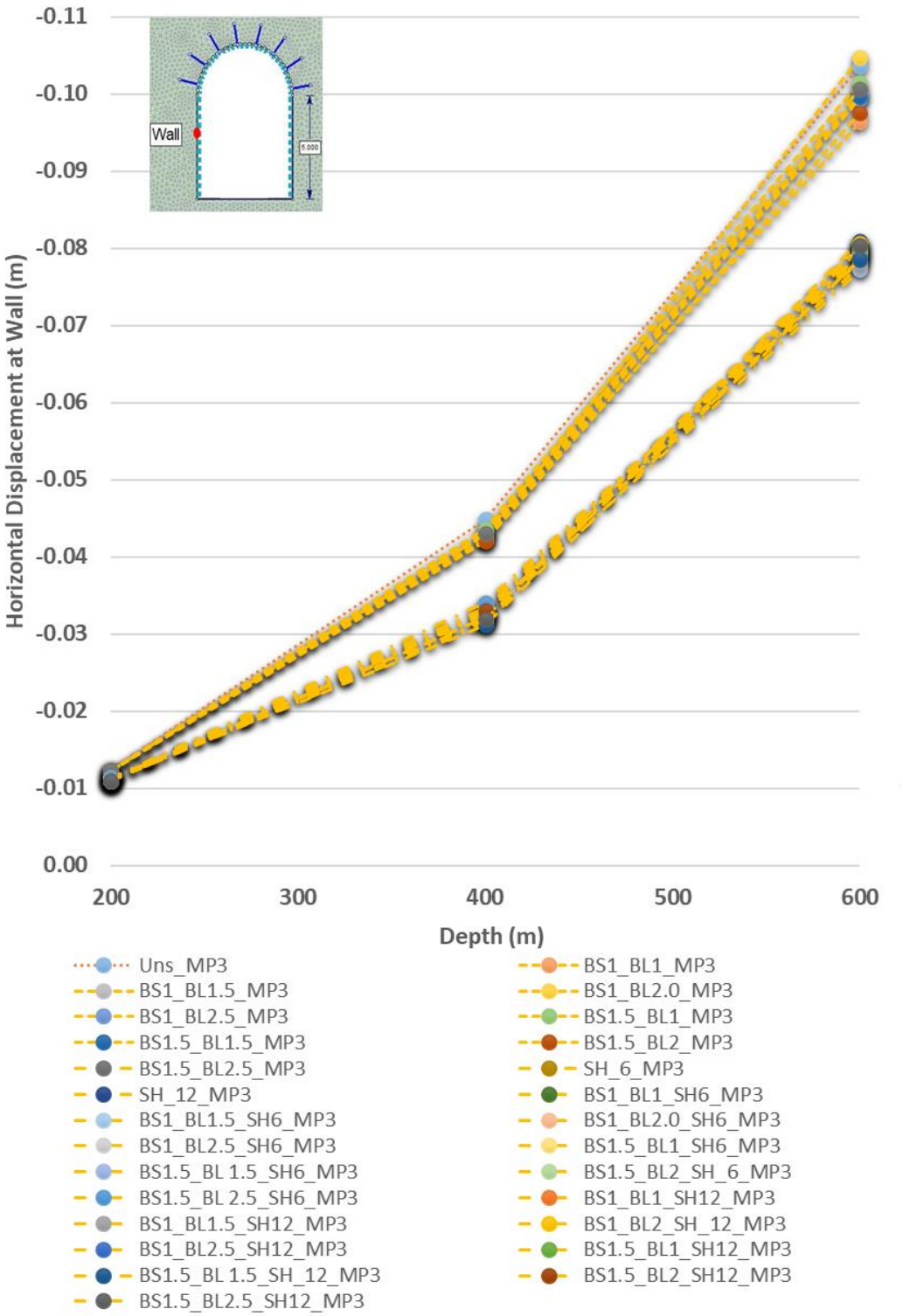


Figure D.5 Horizontal displacement at wall (m) vs. depth (m) for k=1.0 for $MP_3$

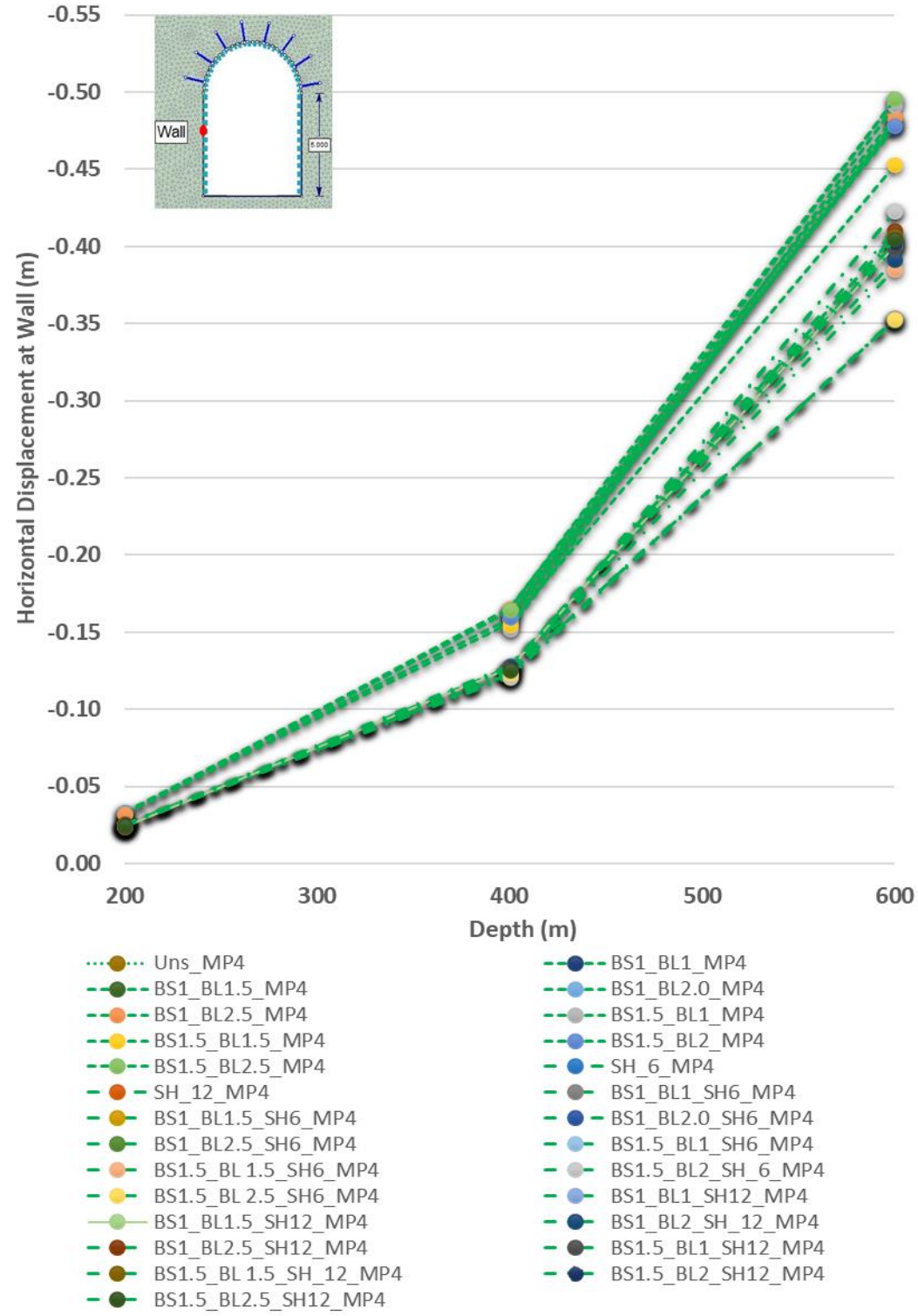


Figure D.6 Horizontal displacement at wall (m) vs. depth (m) for k=1.0 for $MP_4$

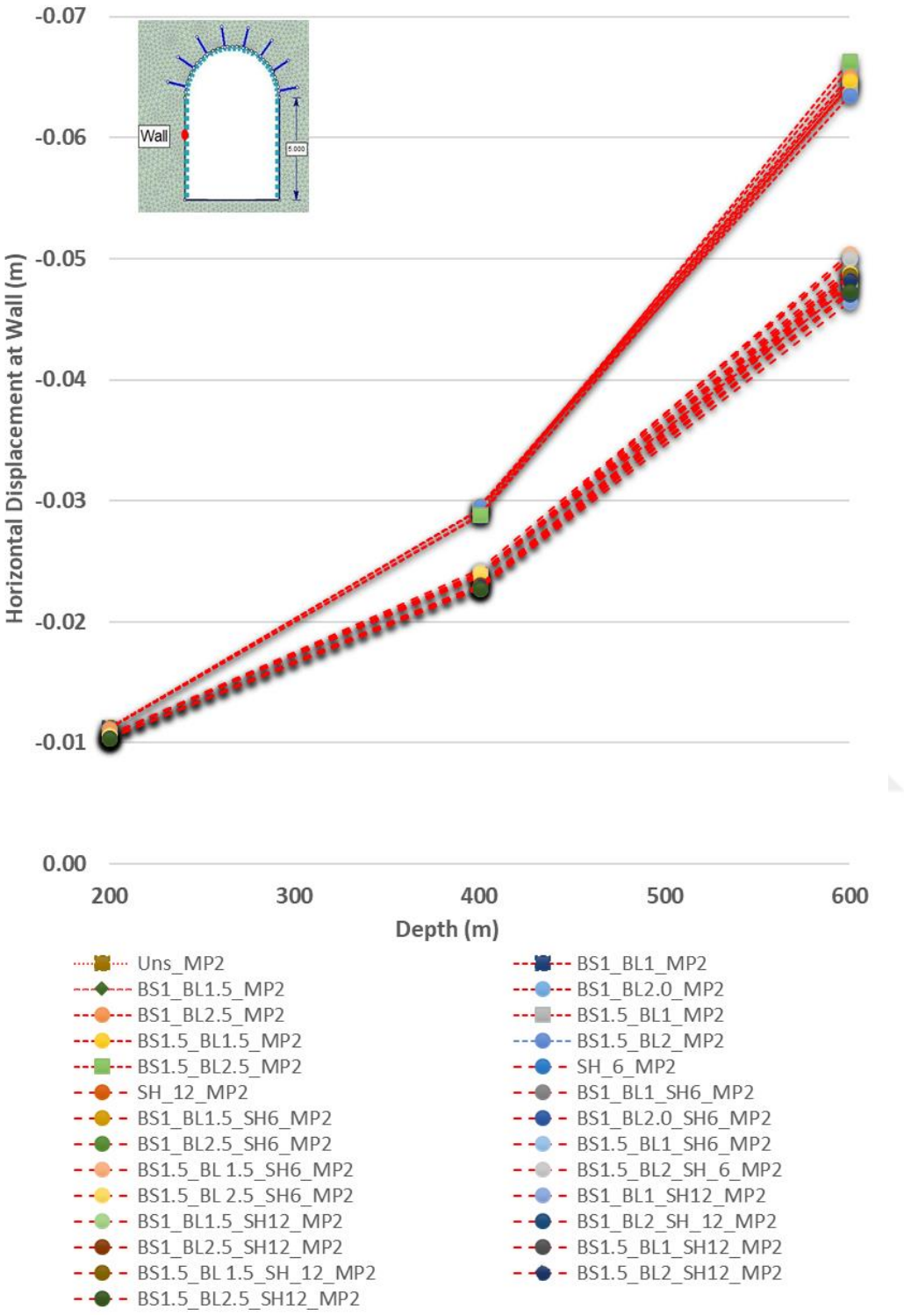


Figure D.7 Horizontal displacement at wall (m) vs. depth (m) for k=1.5 for $MP_2$

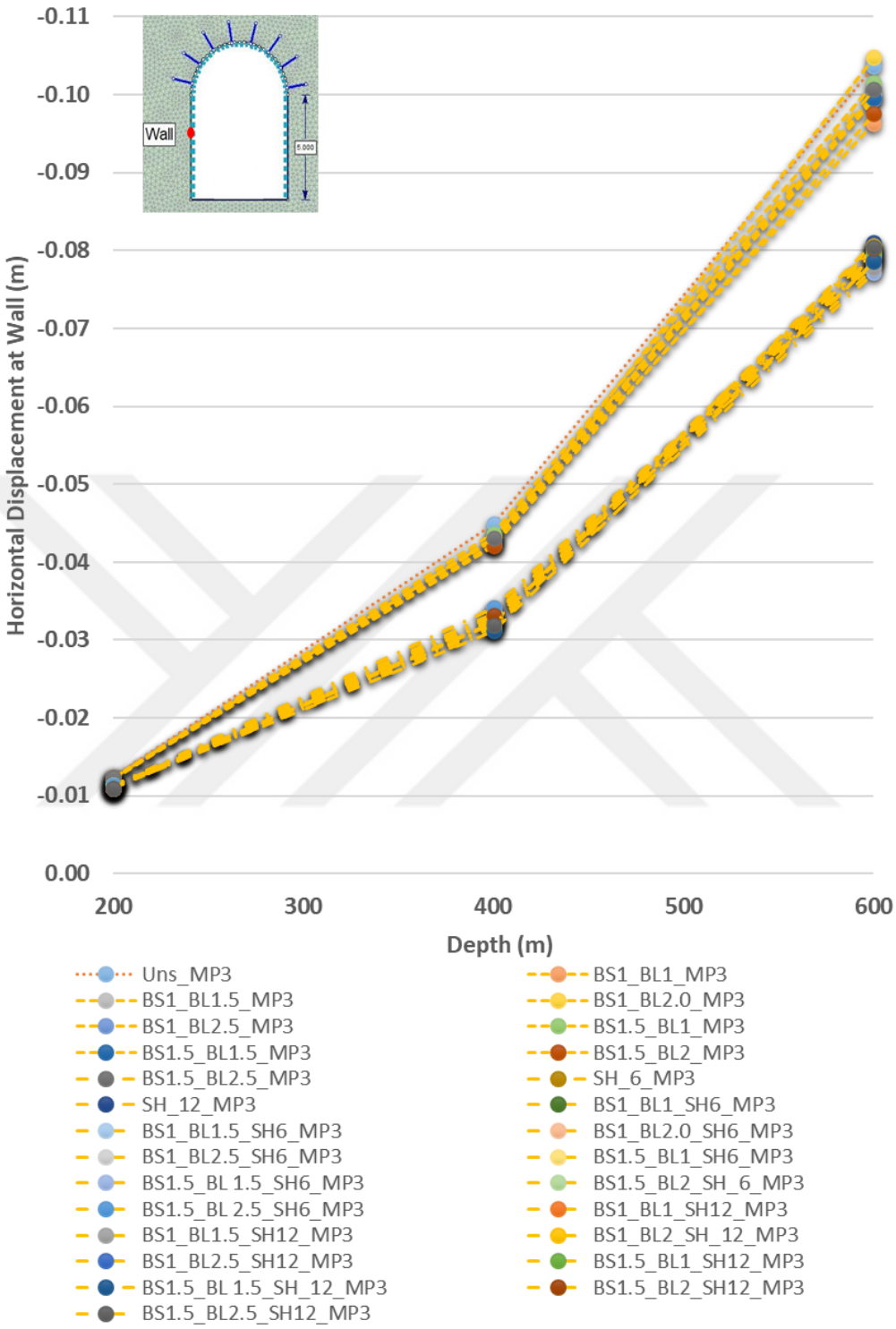


Figure D.8 Horizontal displacement at wall (m) vs. depth (m) for k=1.5 for $MP_3$

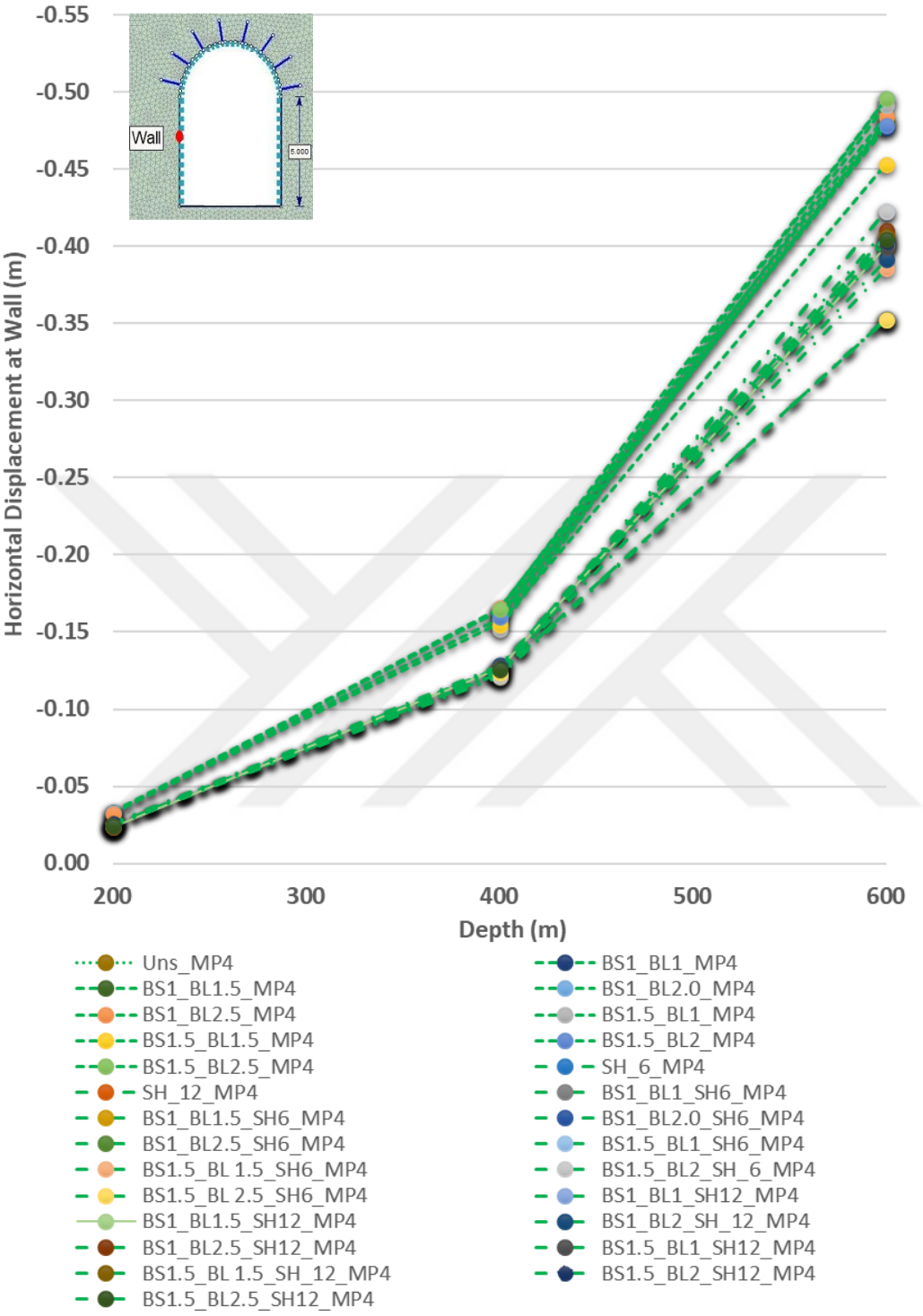


Figure D.9 Horizontal displacement at wall (m) vs. depth (m) for k=1.5 for $MP_4$

## E. Wall Major Principal Strain for K Values 0.5, 1.0, 1.5 and Different Rock Mass Properties at 200, 400, 600 Meters Depths

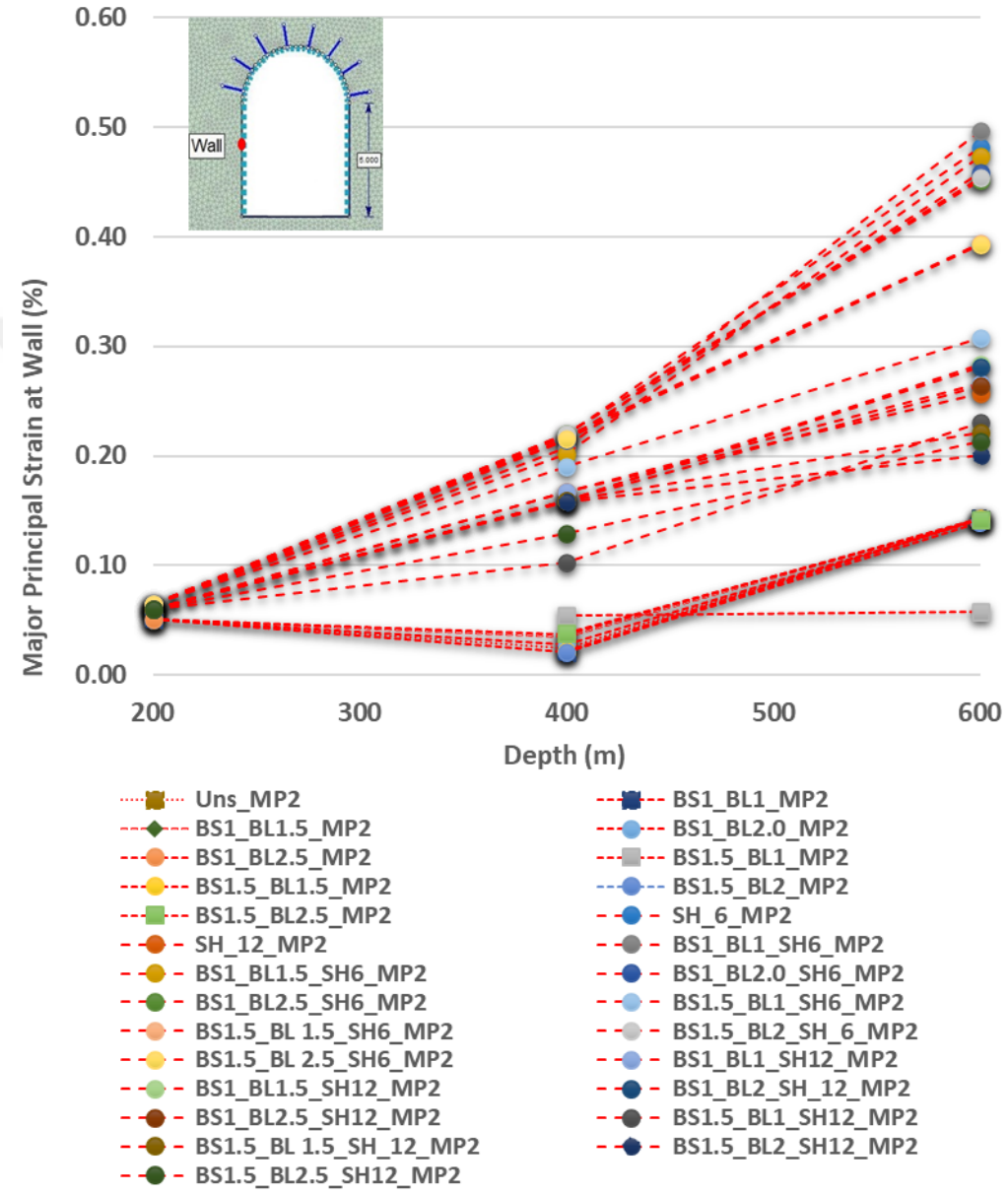


Figure E.1 Major principal strain (%) at wall (m) vs. depth (m) for k=0.5 for $MP_2$

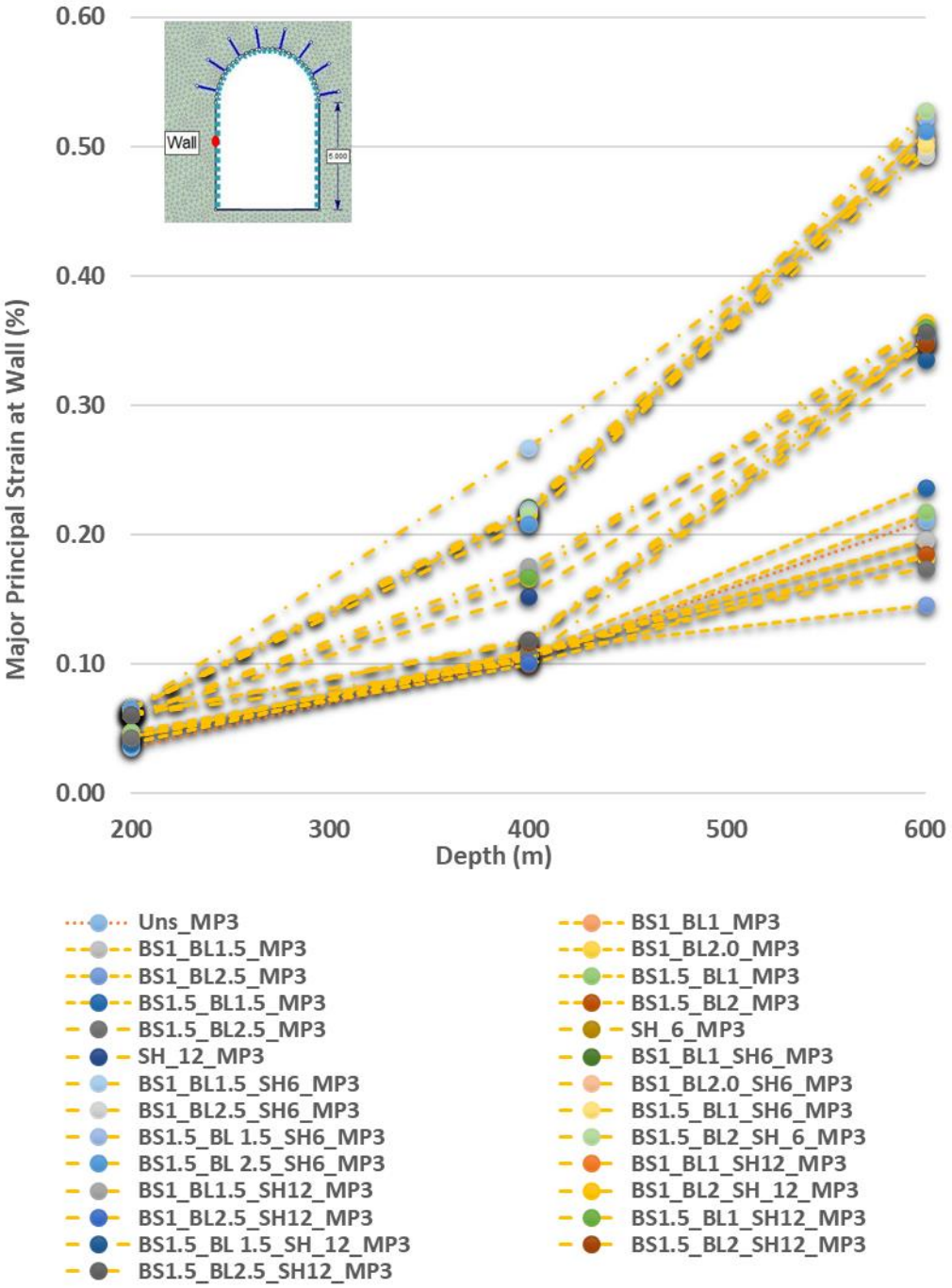


Figure E.2 Major principal strain (%) at wall (m) vs. depth (m) for k=0.5 for $MP_3$

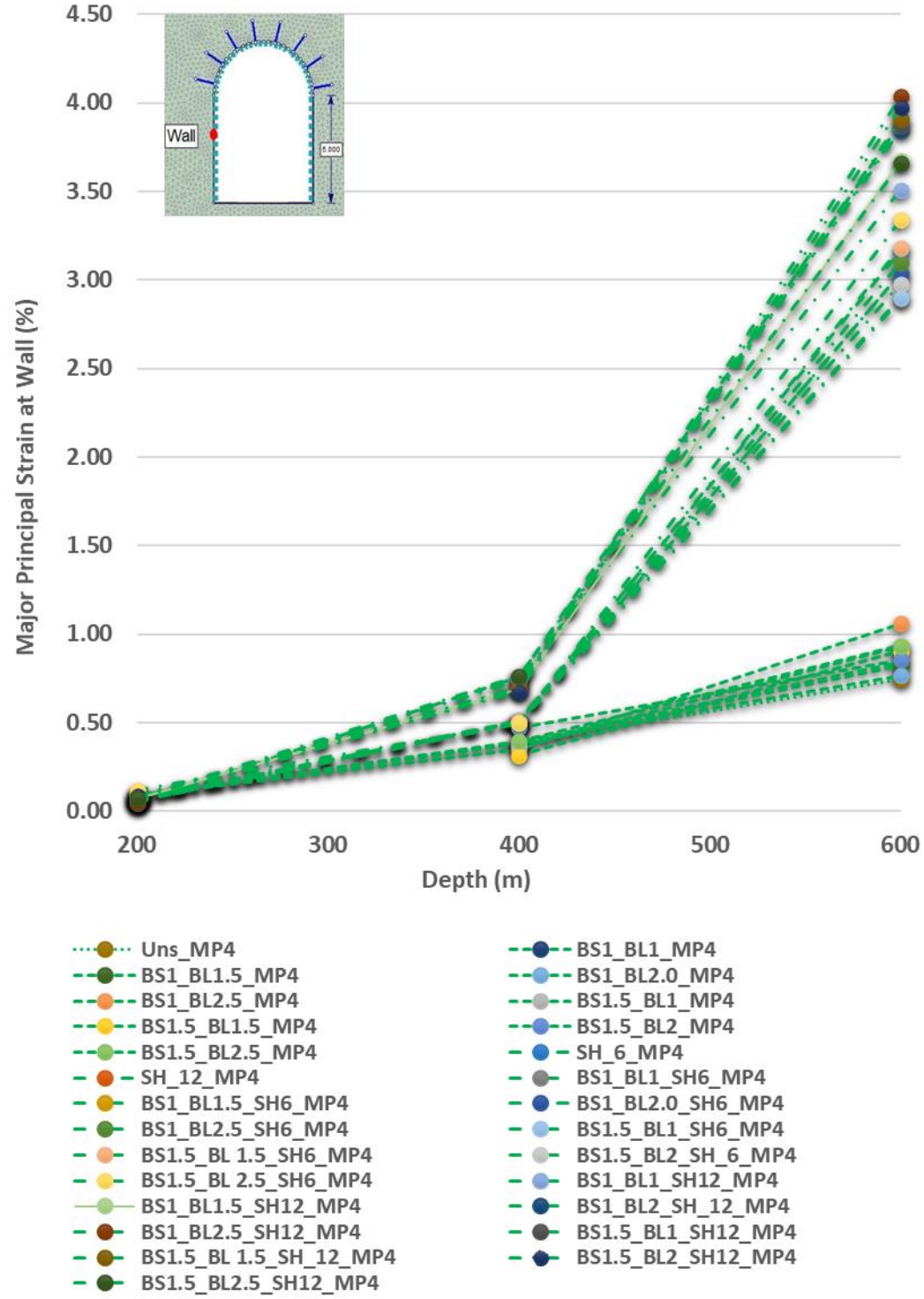


Figure E.3 Major principal strain (%) at wall (m) vs. depth (m) for k=0.5 for $MP_4$

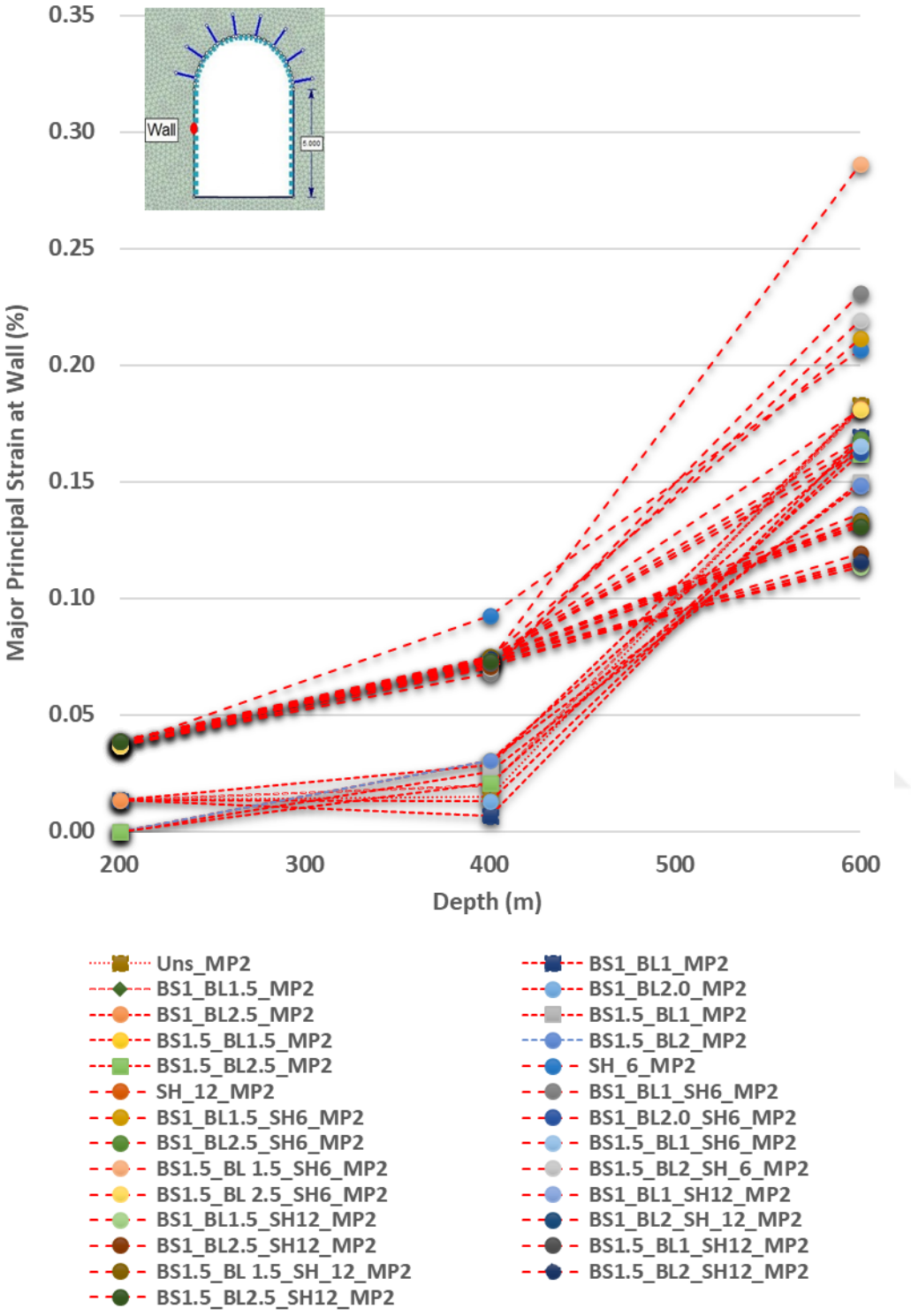


Figure E.4 Major principal strain (%) at wall (m) vs. depth (m) for k=1.0 for $MP_2$

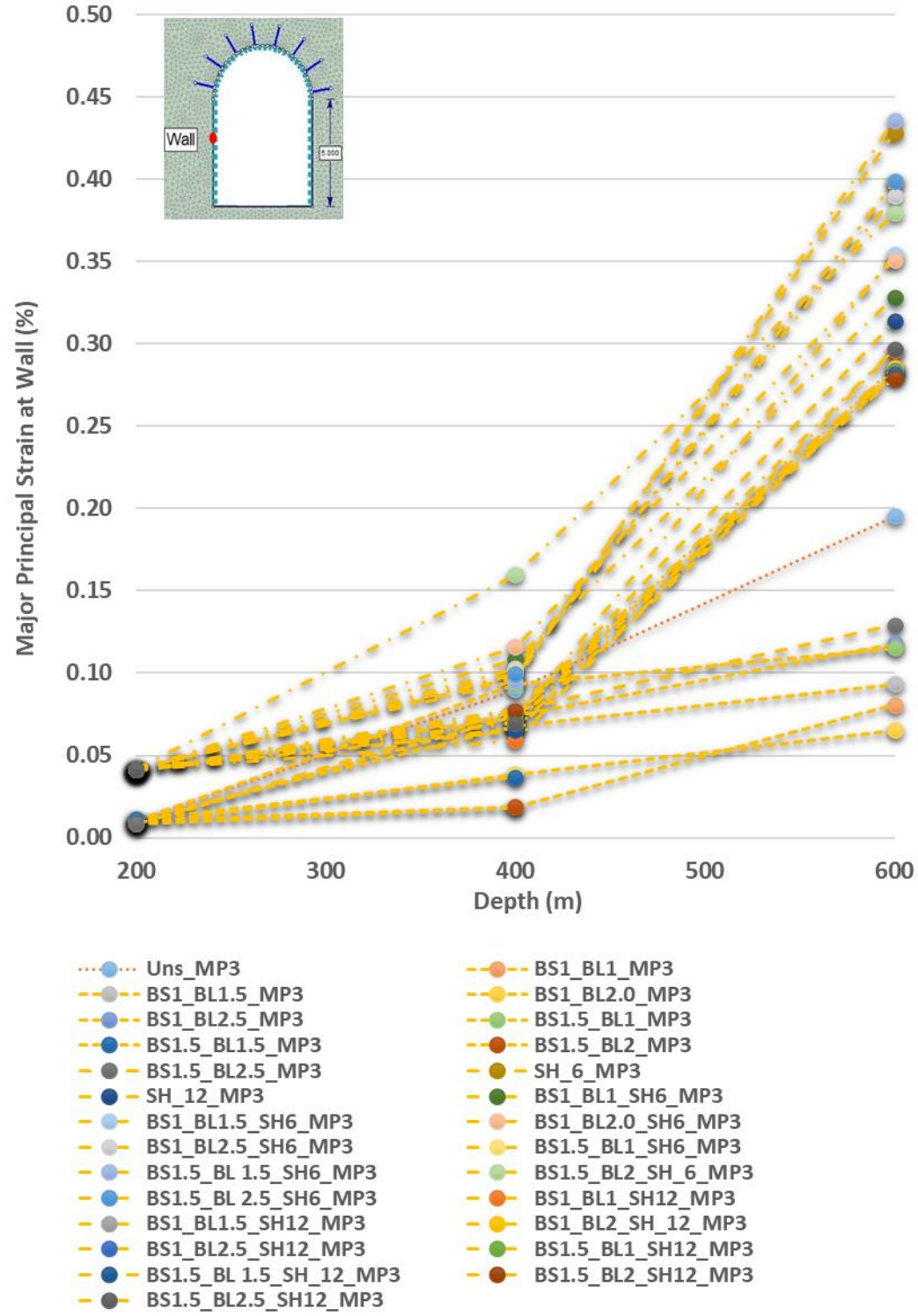


Figure E.5 Major principal strain (%) at wall (m) vs. depth (m) for k=1.0 for $MP_3$

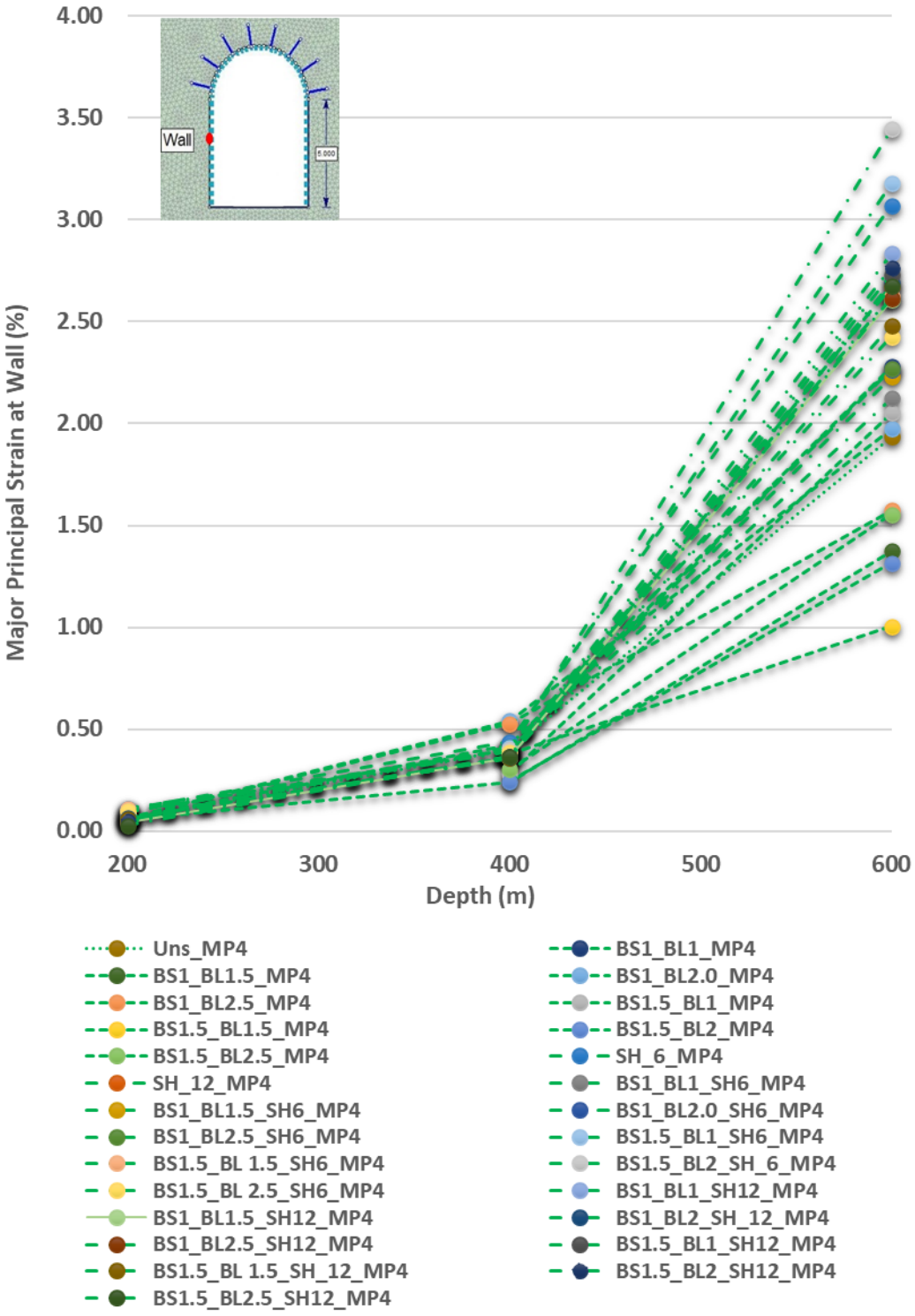


Figure E.6 Major principal strain (%) at wall (m) vs. depth (m) for k=1.0 for $MP_4$

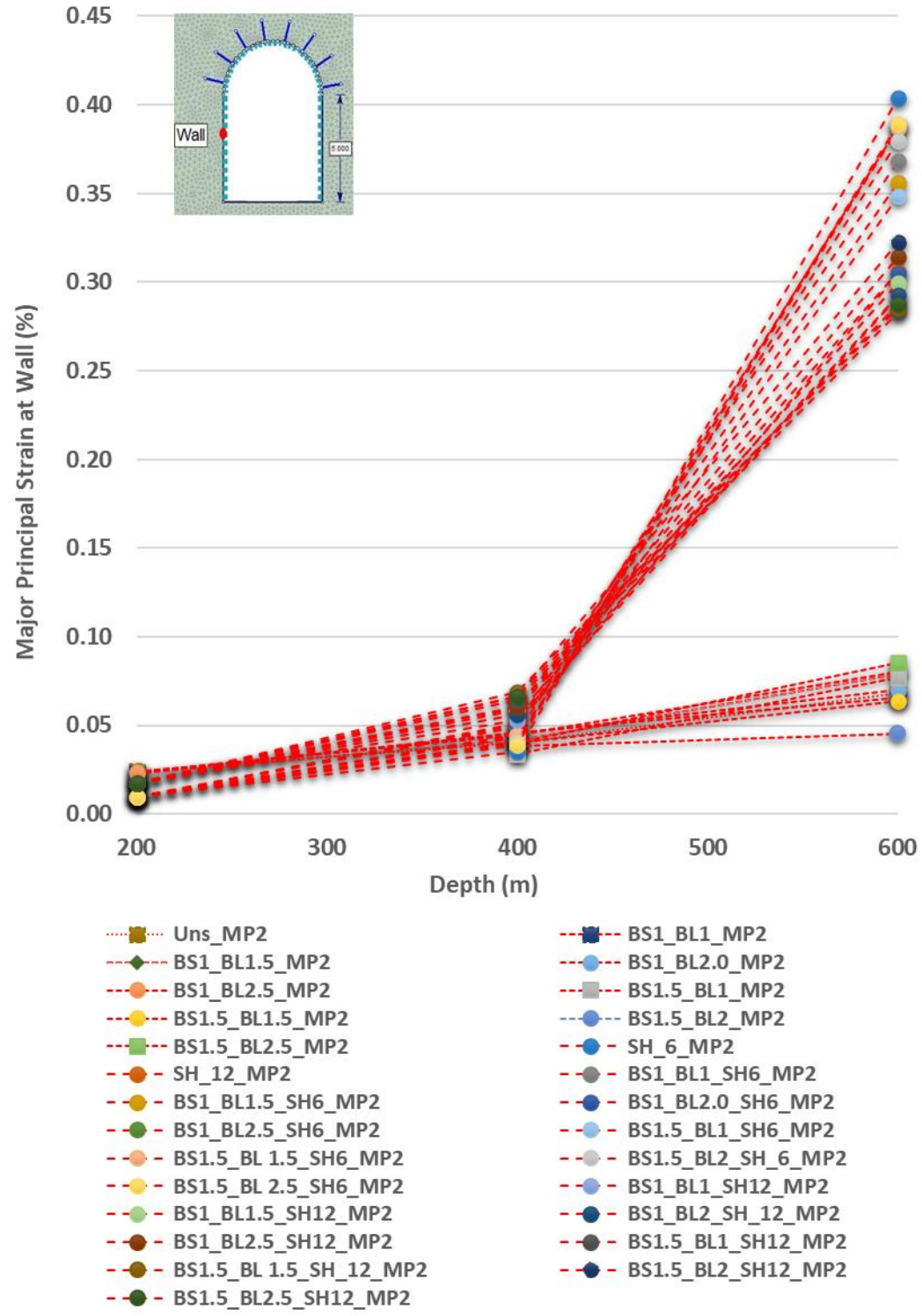


Figure E.7 Major principal strain (%) at wall (m) vs. depth (m) for k=1.5 for $MP_2$

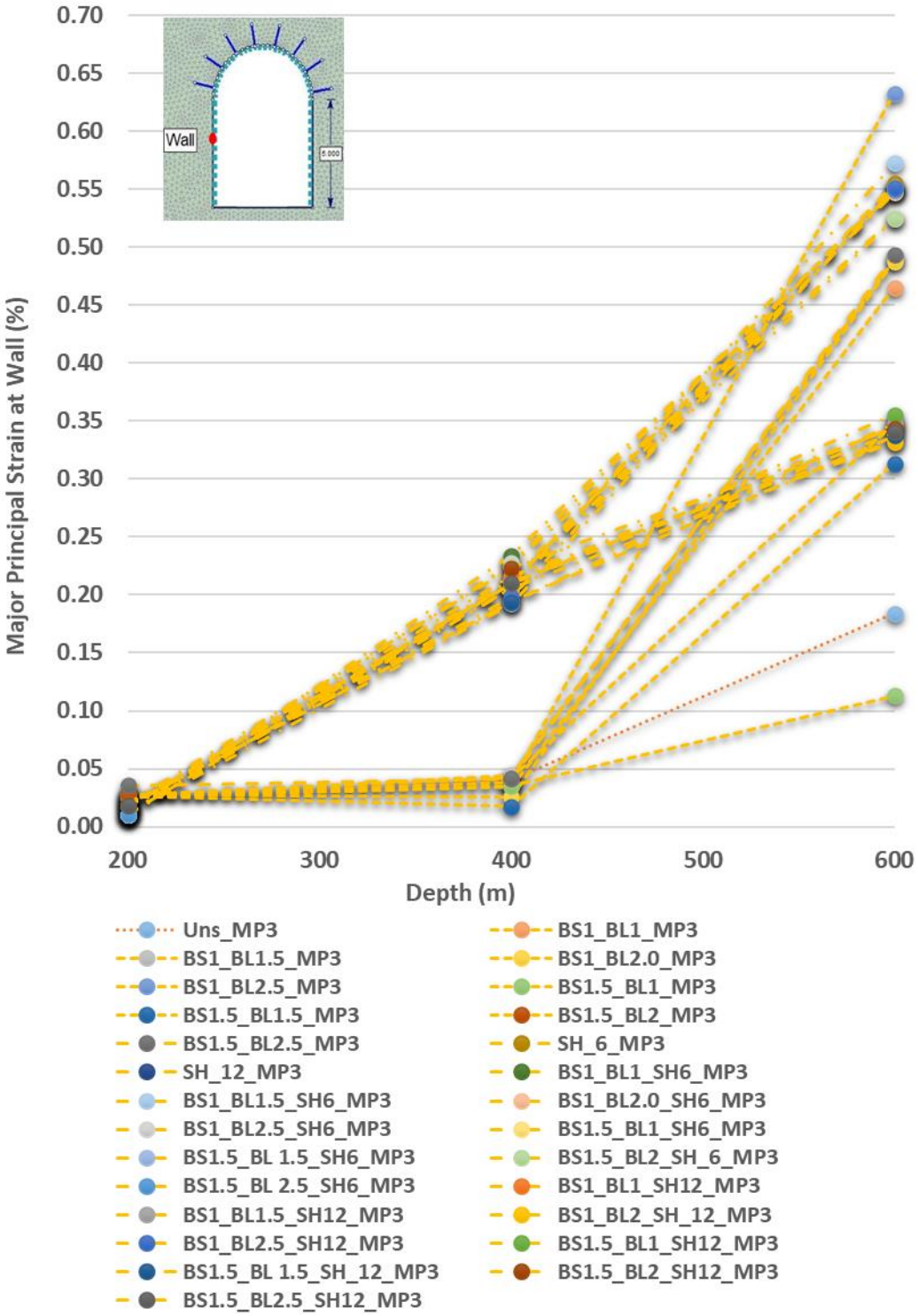


Figure E.8 Major principal strain (%) at wall (m) vs. depth (m) for k=1.5 for $MP_3$

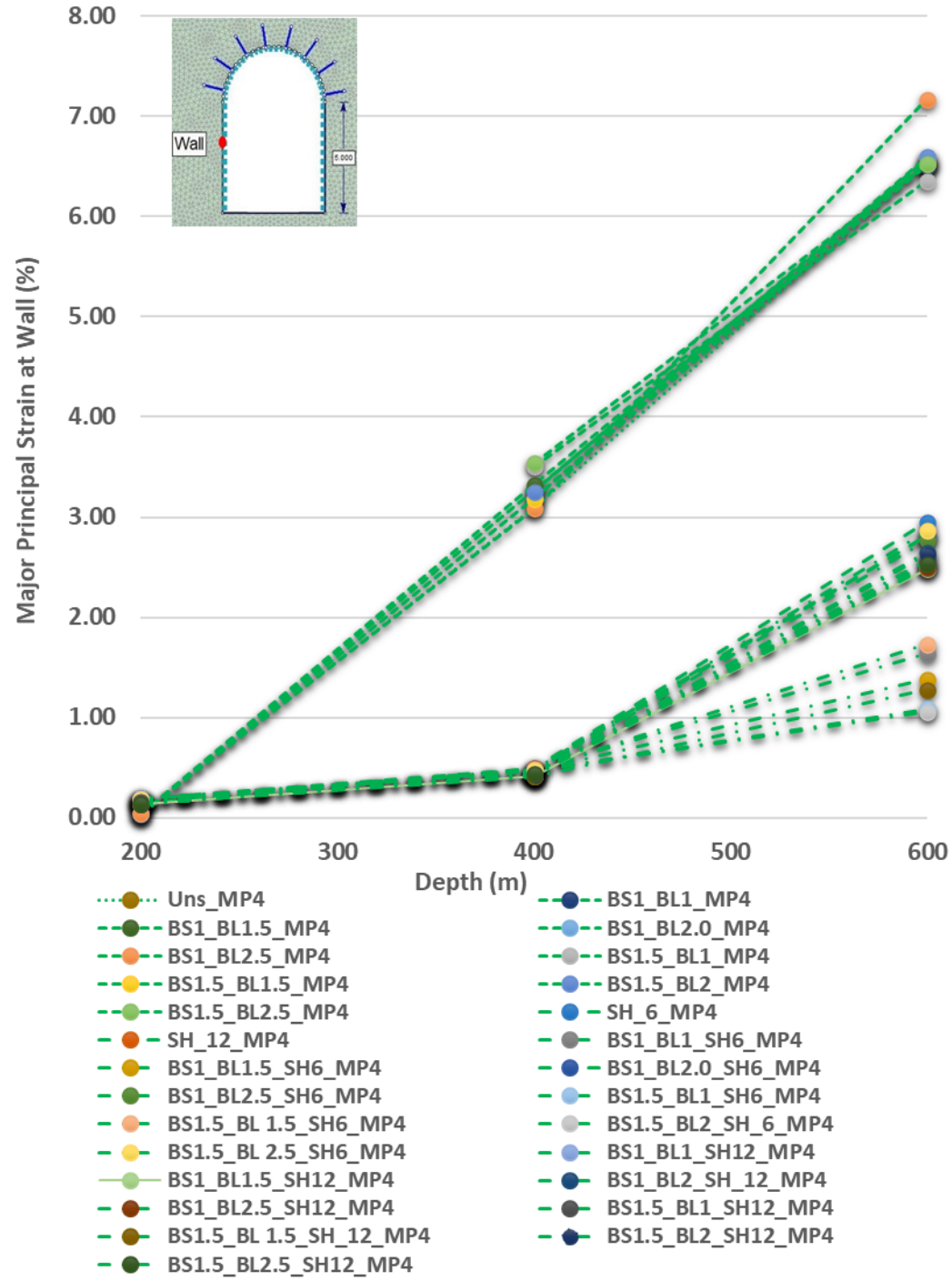


Figure E.9 Major principal strain (%) at wall (m) vs. depth (m) for k=1.5 for $MP_4$

## F. Wall Maximum Principal Stresses for K Values 0.5, 1.0, 1.5 and Different Rock Mass Properties at 200, 400, 600 Meters Depths

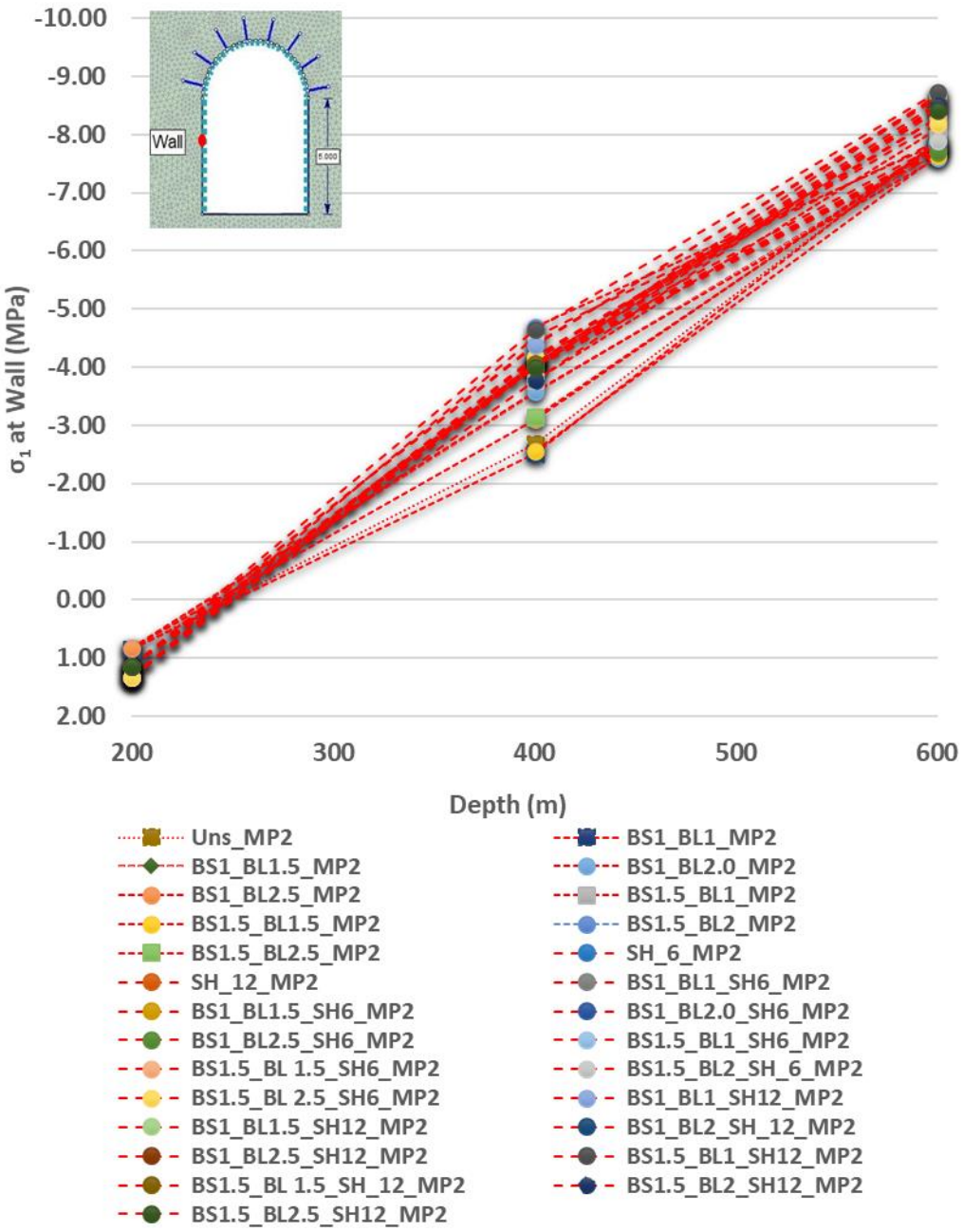


Figure F.1 Maximum principal stress (MPa) at wall (m) vs. depth (m) for k=0.5 for $MP_2$

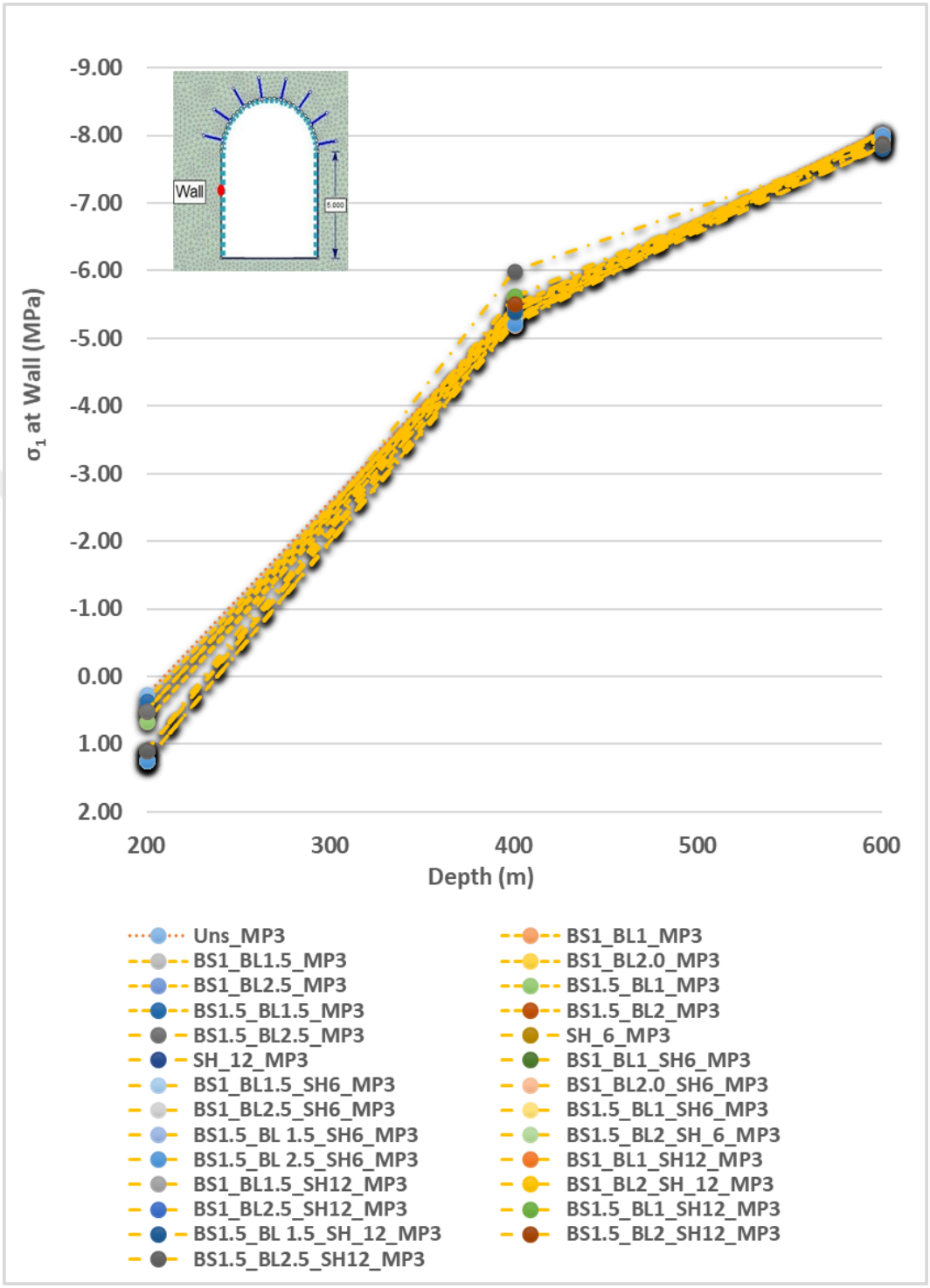


Figure F.2 Maximum principal stress (MPa) at wall (m) vs. depth (m) for k=0.5 for $MP_3$

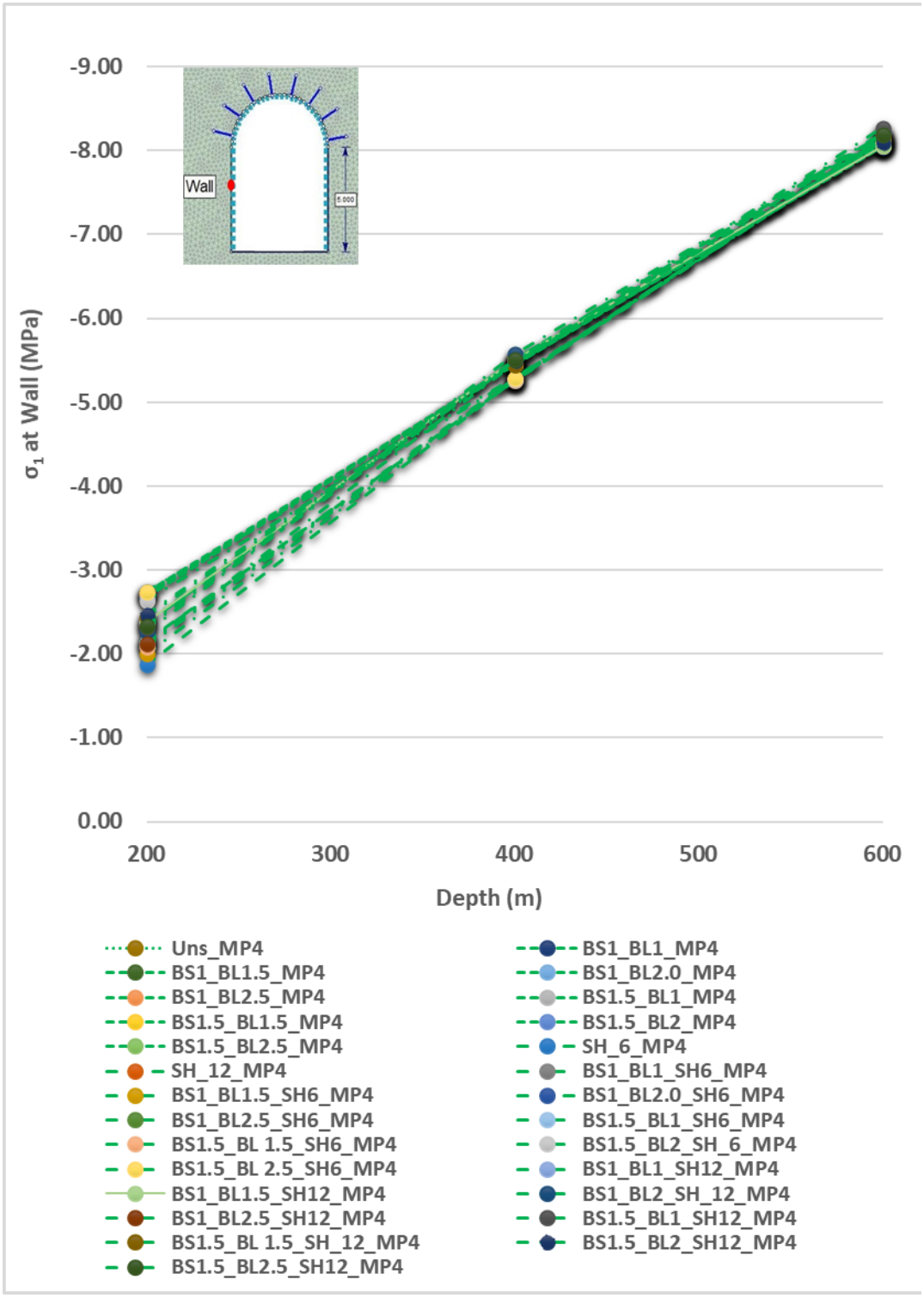


Figure F.3 Maximum principal stress (MPa) at wall (m) vs. depth (m) for k=0.5 for $MP_4$

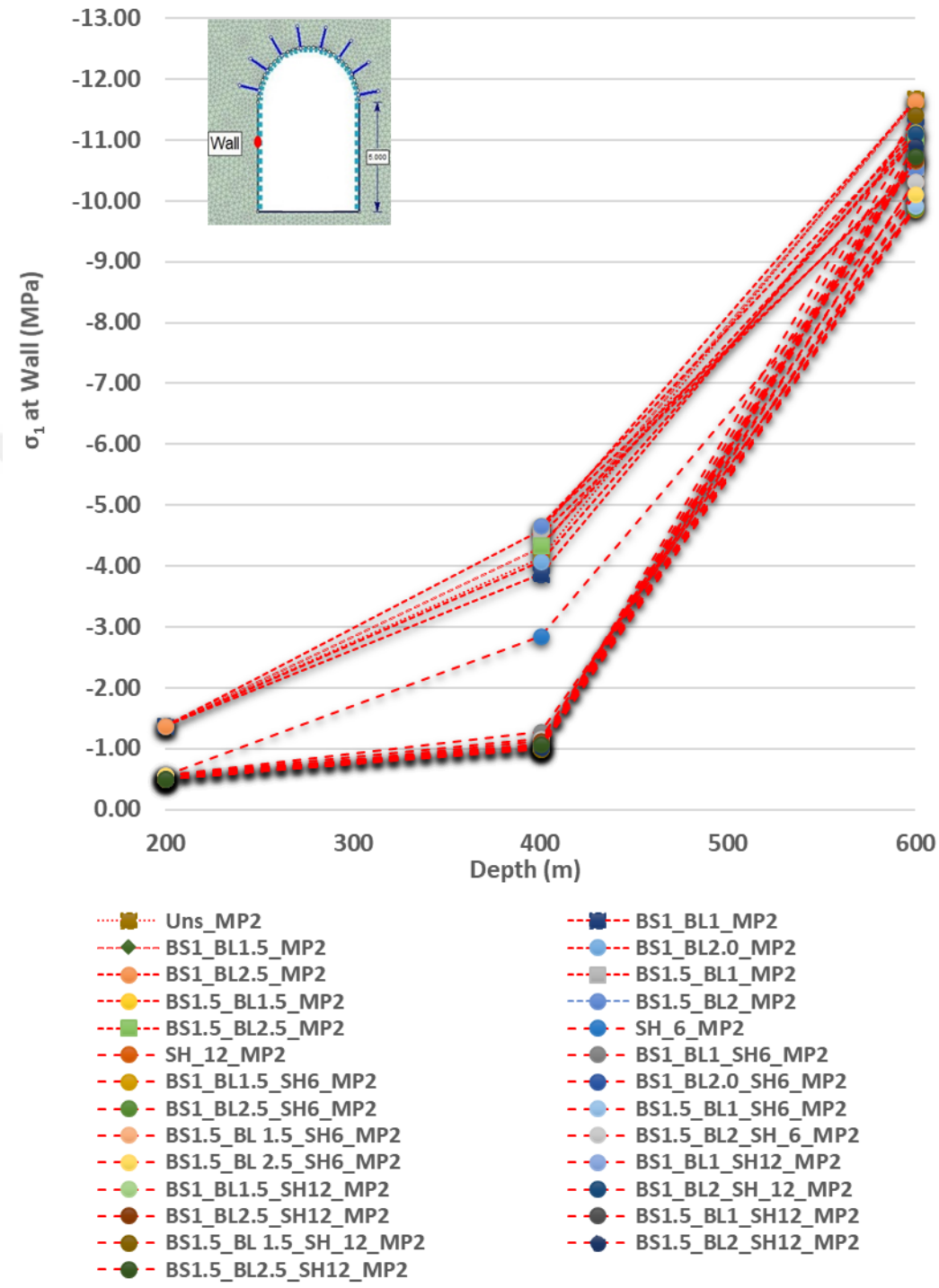


Figure F.4 Maximum principal stress (MPa) at wall (m) vs. depth (m) for k=1.0 for $MP_2$

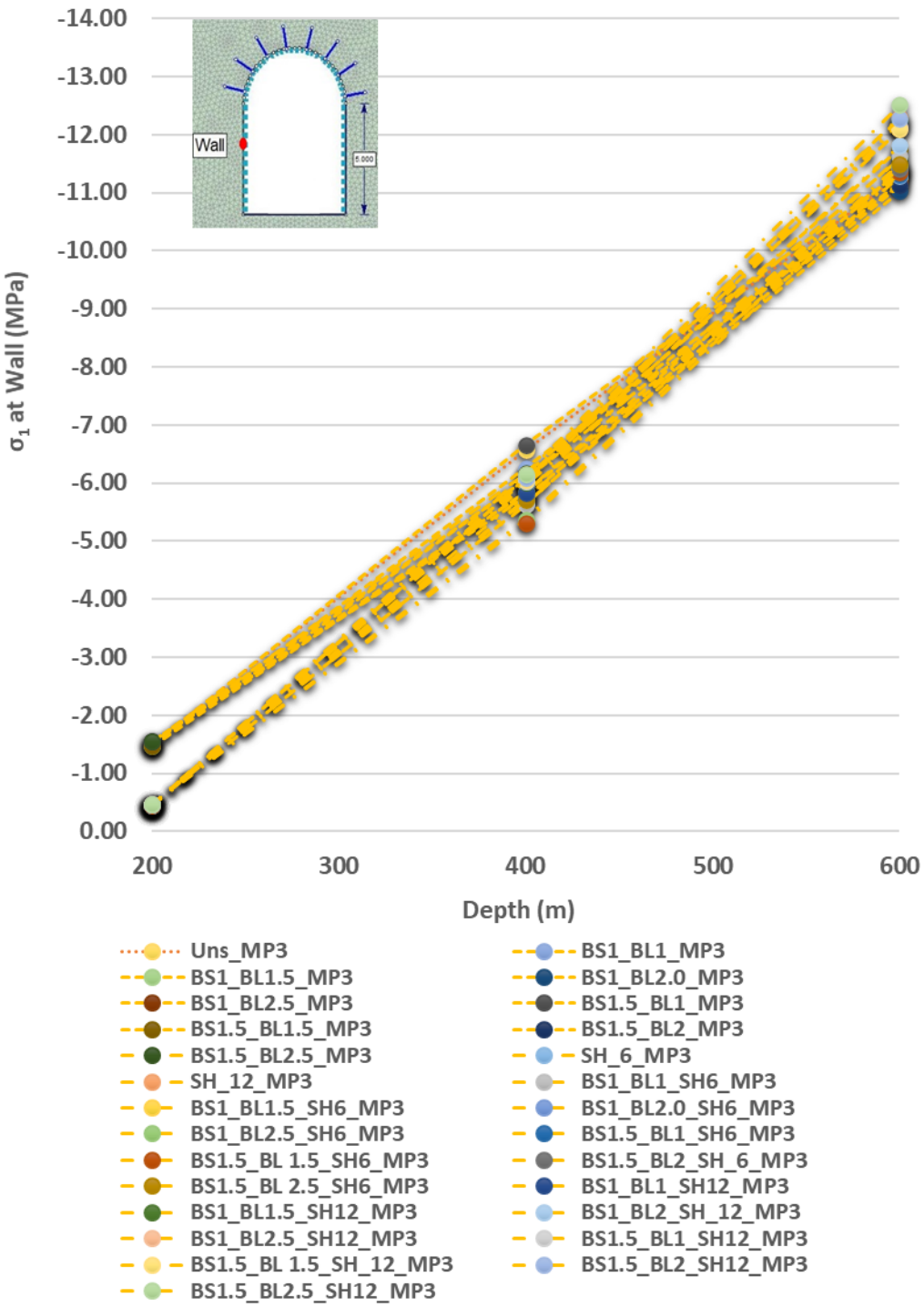


Figure F.5 Maximum principal stress (MPa) at wall (m) vs. depth (m) for k=1.0 for $MP_3$

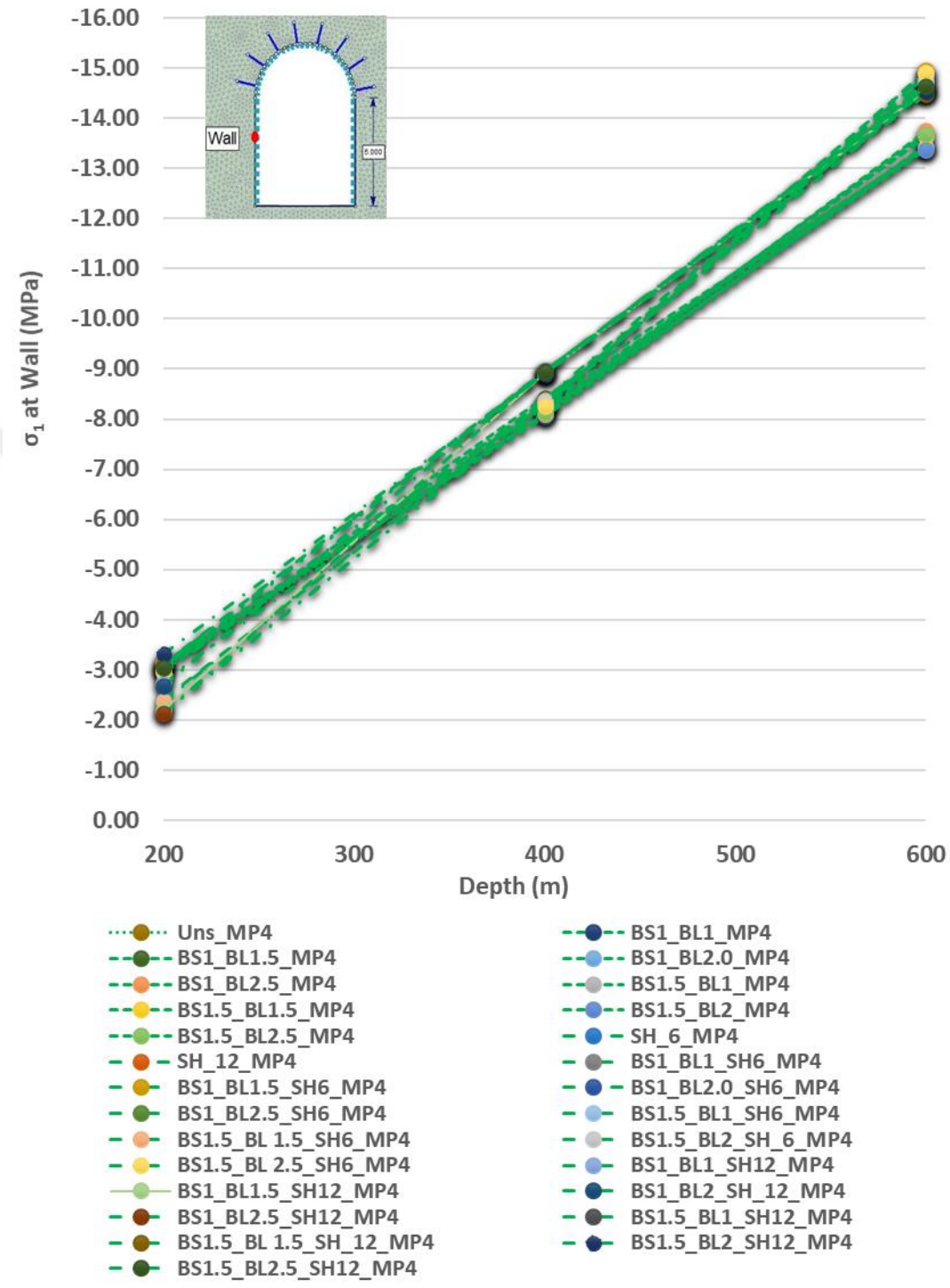


Figure F.6 Maximum principal stress (MPa) at wall (m) vs. depth (m) for k=1.0 for $MP_4$

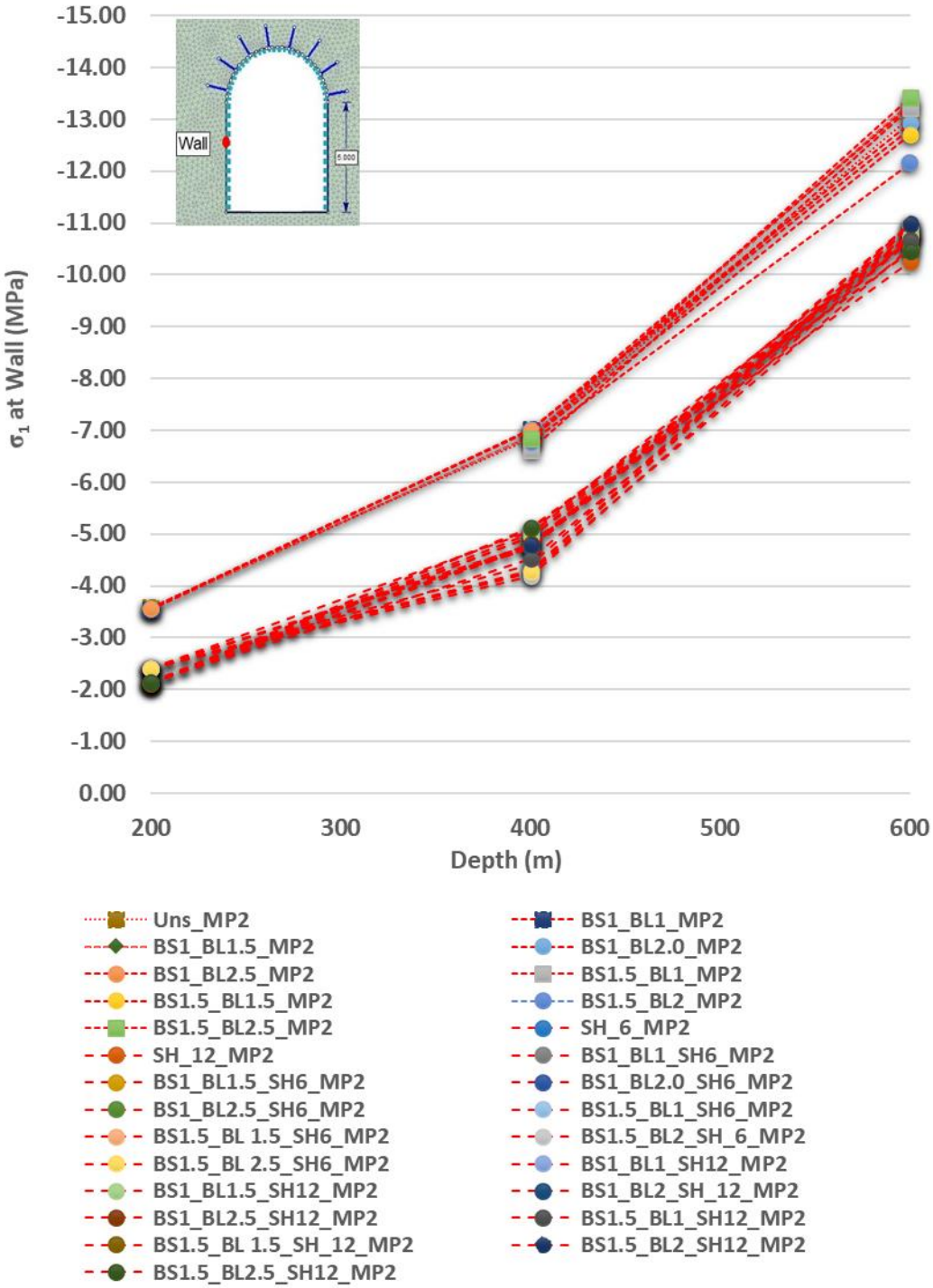


Figure F.7 Maximum principal stress (MPa) at wall (m) vs. depth (m) for k=1.5 for $MP_2$

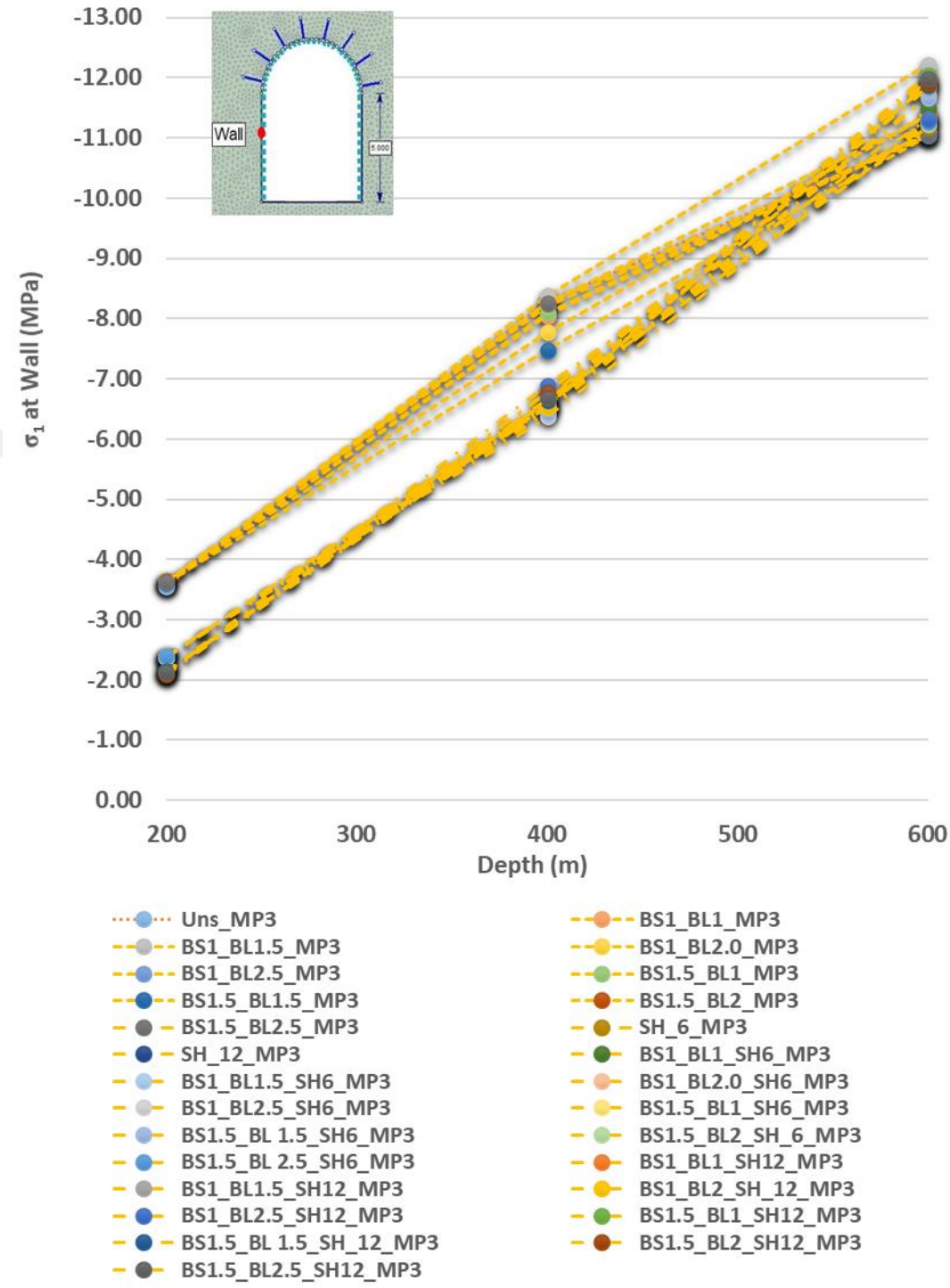


Figure F.8 Maximum principal stress (MPa) at wall (m) vs. depth (m) for k=1.5 for $MP_3$

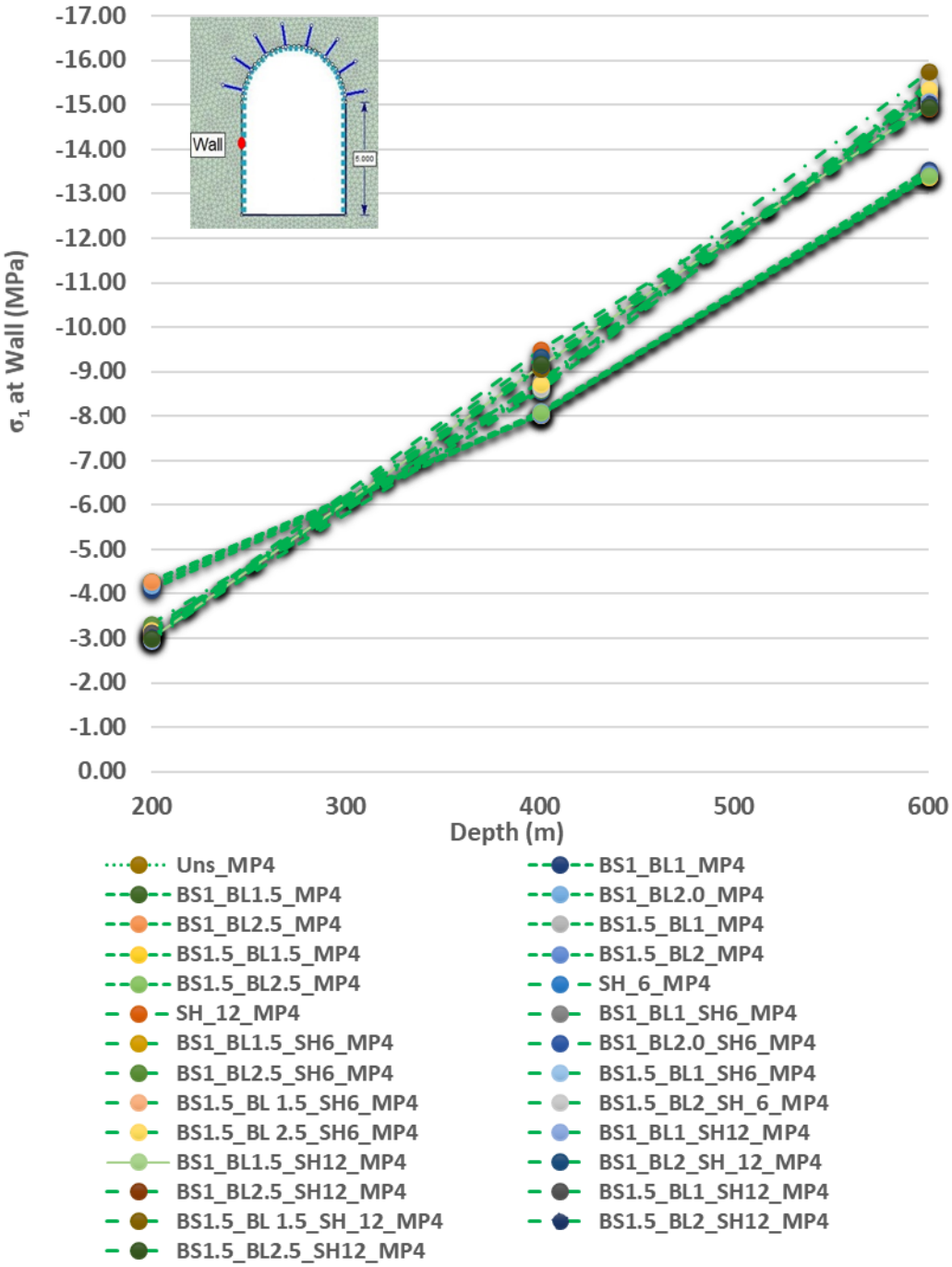


Figure F.9 Maximum principal stress (MPa) at wall (m) vs. depth (m) for k=1.5 for $MP_4$

## G. Results After Computation and Interpretation of The Supported Model in Terms of Vertical and Horizontal Displacements, Maximum and Minimum Stresses

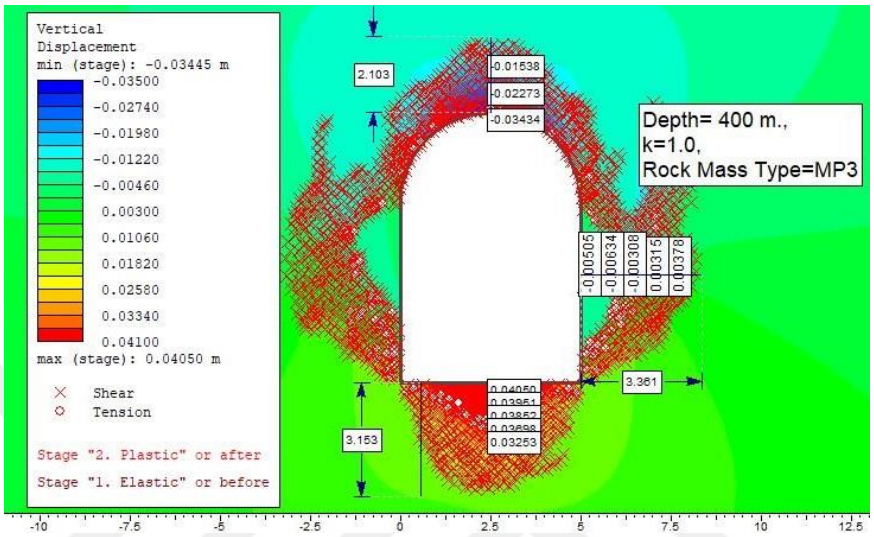


Figure G.1 Results after computation and interpretation of the unsupported model in terms of vertical displacement (m)

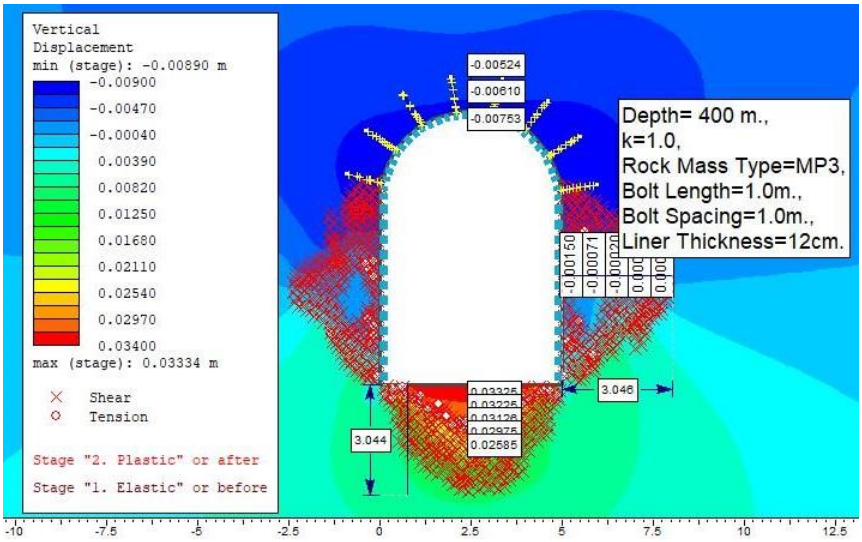


Figure G.2 Results after computation and interpretation of the supported model in terms of vertical displacement (m)

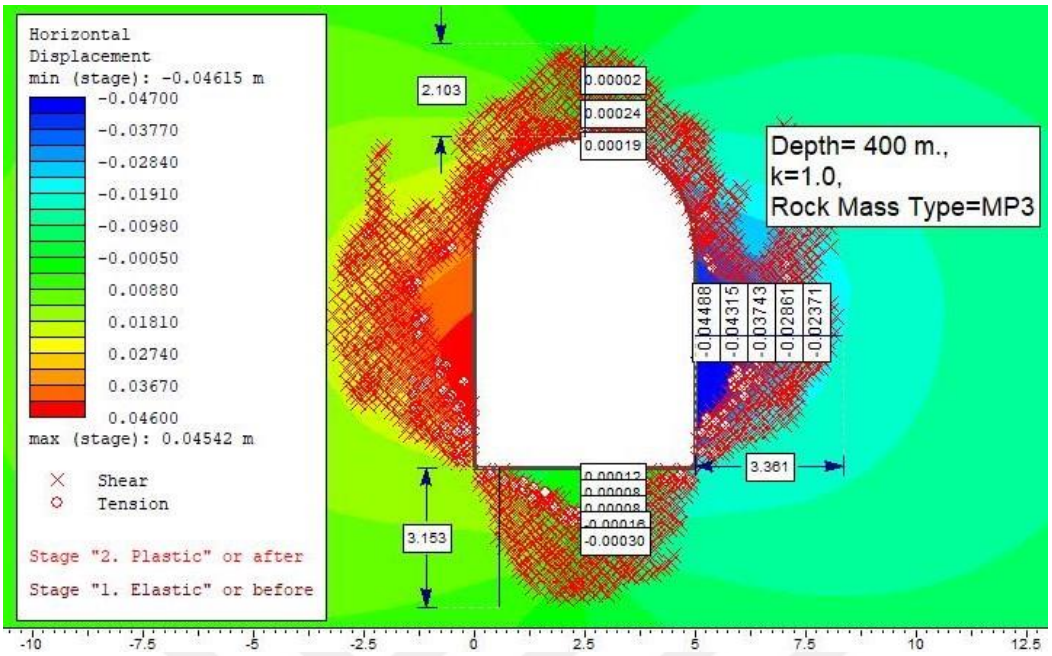


Figure G.3 Results after computation and interpretation of the unsupported model in terms of horizontal displacement (m)

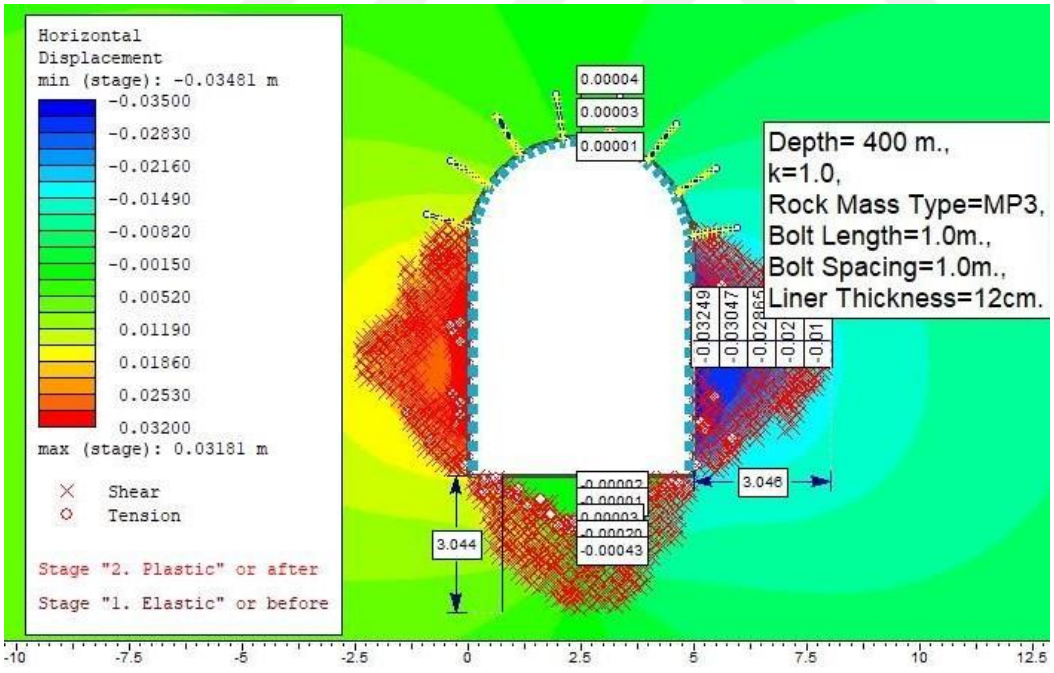


Figure G.4 Results after computation and interpretation of the supported model in terms of horizontal displacement (m)

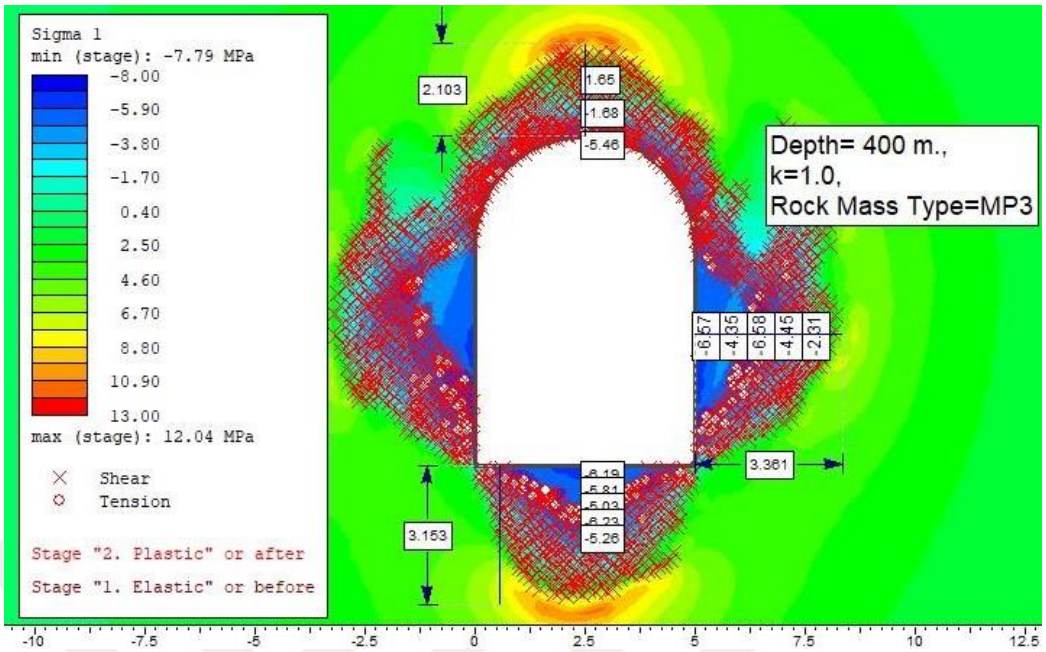


Figure G.5 Results after computation and interpretation of the unsupported model in terms of maximum principal stress ($\sigma_1$)

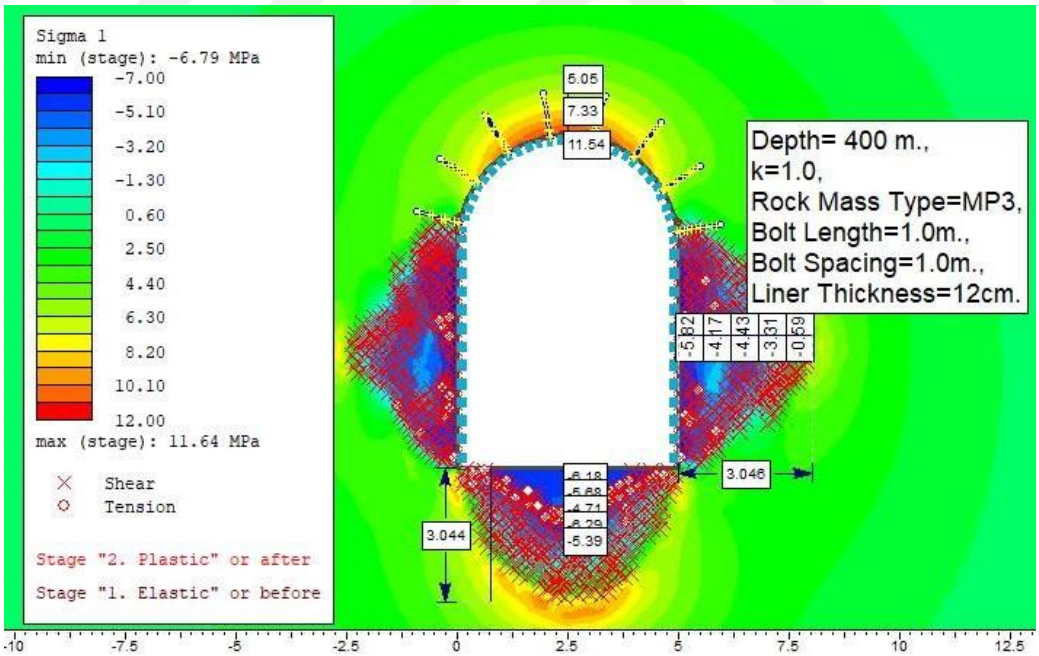


Figure G.6 Results after computation and interpretation of the supported model in terms of Maximum Principal Stress ($\sigma_1$)

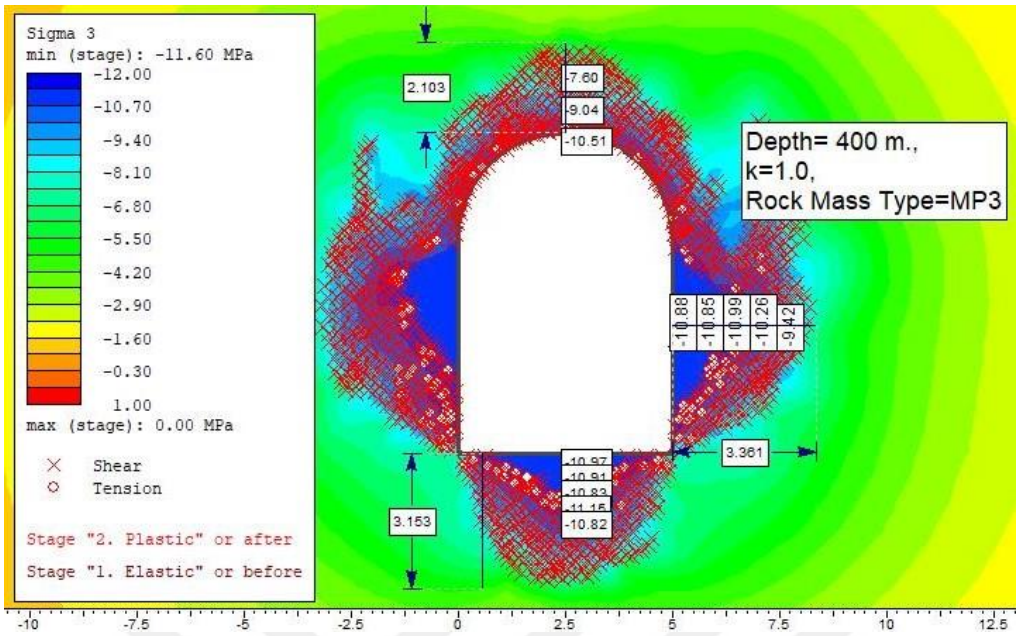


Figure G.7 Results after computation and interpretation of the unsupported model in terms of minimum principal stress ($\sigma_3$)

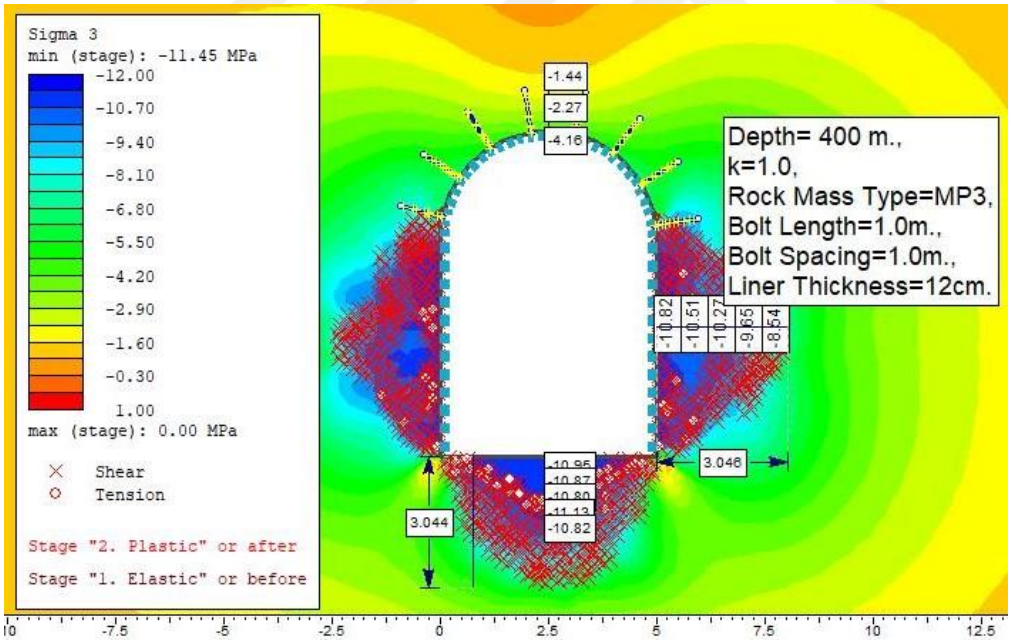


Figure G.8 Results after computation and interpretation of the supported model in terms of minimum principal stress ($\sigma_3$)